



THE UNIVERSITY
of ADELAIDE

CENTRE FOR PERSONALISED
CANCER MEDICINE

Targeted therapies for the treatment of solid cancers

Alaknanda Alaknanda

Bachelor of Medical Biotechnology (Hons)

This thesis is submitted in fulfilment of the requirement for the

Doctor of Philosophy

Adelaide Medical School

The University of Adelaide

Adelaide SA, Australia

July 2017

Table of Contents

Table of Contents	II
Publications.....	V
Presentations.....	VI
Grants & Awards.....	VI
Acknowledgements	VII
Declaration.....	IX
Overview	1
SECTION I.....	4
Proteasome as a therapeutic target for the treatment of solid cancers.....	4
Chapter 1	5
Proteasome as a therapeutic target.....	5
Introduction.....	6
Ubiquitin-Proteasome System.....	6
26S Proteasome Structure	7
Immuno-proteasome in antigen presentation	11
The role of the Immuno-proteasome in protein homeostasis.....	16
Proteasomes and Cancer	18
Proteasome Inhibitors in Cancer.....	20
Clinical Significance	23
References	25
CHAPTER 2	30
Proteasome addiction in breast cancers defines new therapeutic targets	30
Statement of Authorship.....	31
Prelude.....	33
Abstract	34
Introduction.....	35
Results	37
Comparison of expression of the c-proteasome in breast cancer subgroups	37
Co-expression of genes with i-proteasome expression	39
The interferon-gamma mediated signaling pathway.....	43
Relationship of proteasome expression with breast cancer patient survival.....	46
Basal-like breast cancers are addicted to the immuno-proteasome.....	49
Unfolded protein response in basal-like breast cancers that have i-proteasome addiction.....	54
Discussion.....	56
Materials and Methods	60
References	65
Supplementary Material.....	72

CHAPTER 3	84
New Peptidomimetic Boronates for Selective Inhibition of the Chymotrypsin-like Activity of the 26S Proteasome	84
Statement of Authorship	85
Prelude.....	87
Abstract	88
Introduction.....	89
Results and Discussion	90
References	101
Methods and Materials	105
Supplementary Data	109
CHAPTER 4	118
Investigation into the S2 and S3 binding sites of proteasome using light-controlled inhibitors.....	118
Statement of Authorship.....	119
Prelude.....	121
Abstract	122
Introduction.....	123
Results and Discussion	126
Chemistry.....	126
Proteasome inhibitory activities	128
Effect of compounds on cells	132
Conclusions.....	135
References	136
Supplementary material	139
CHAPTER 5	178
P2-extended D- peptides as novel proteasome inhibitors	178
Statement of Authorship.....	179
Prelude.....	181
Introduction.....	182
Synthesis.....	186
Biology	187
Conclusion	191
References	192
Methods and materials.....	194
SECTION II.....	196
Exploiting the p53 pathway as a targeted therapy to treat Ewing Sarcoma.....	196
Chapter 6	197
Exploiting the p53 pathway as a targeted therapy to treat Ewing Sarcoma.....	197
Introduction.....	198
Tumour Suppressor p53.....	199

History of Ewing sarcoma treatment	200
Ribosomal RNA Polymerase as a therapeutic target	202
Nucleolus in cancer	203
CX-5461: a potent and selective rRNA polymerase inhibitor	207
Summary.....	209
Clinical Significance	211
References	212
CHAPTER 7	218
Dysregulating ribosomal biogenesis to treat Ewing sarcoma.....	218
Statement of Authorship.....	219
Prelude.....	221
Introduction.....	222
Methods.....	224
Results	228
Ewing sarcoma cells are hypersensitive to RNA Pol I inhibition	228
CX-5461 induces cell death and cell cycle arrest in Ewing sarcoma cell lines	232
CX-5461 induced cell death in Ewing sarcoma cell lines is p53 dependent	234
CX-5461 induced ATM/ATR dependent G2/M arrest in resistant Ewing sarcoma cell lines	236
E2F1 protein levels predict response to CX-5461	238
Discussion.....	240
References	243
Supplementary material.....	247
Chapter 8	252
XI-006 induces potent p53-independent apoptosis in Ewing sarcoma	252
Statement of Authorship.....	253
Prelude.....	256
Abstract	257
Introduction.....	258
Results	261
MDM4 protein is overexpressed in sarcomas	261
MDM4 mRNA and protein levels do not confer sensitivity to XI-006.....	270
XI-006 cytotoxicity occurs independently of TP53	271
Low micro-molar concentrations of XI-006 do not induce DNA damage.....	272
Discussion.....	283
Methods.....	289
References	295
Supplementary materials.....	301
Conclusion.....	321

Publications

Original Research Papers

(Published as Alaknanda Adwal)

Zhang XZ, Adwal A, Turner AG, Callen DF, Abell AD. New Peptidomimetic Boronates for Selective Inhibition of the Chymotrypsin-like Activity of the 26S Proteasome. *ACS Med Chem Lett.* 2016; 7(12): 1039-1043.

(Zhang XZ and Adwal A contributed equally to this work.)

Blanco B, Palais KA, Adwal A, Callen DF, Abell AD. Azobenzene-containing photoswitchable proteasome inhibitors with selective activity and cellular toxicity. *Bioorg Med Chem.* 2017; S0968-0896(17)31211-7

Pishas KI, Adwal A, Neuhaus SJ, Clayer MT, Farshid G, Staudacher AH and Callen DF. XI-006 induces potent p53-independent apoptosis in Ewing sarcoma. *Sci Rep.* 2015; 5(13328)

The following publication incorporated work that was completed before my candidature.

Pishas KI, Neuhaus SJ, Clayer MT, Adwal A, Callen DF and Neilsen PM. Pre-activation of the p53 pathway through Nutlin-3a sensitizes sarcomas to drozitumab therapy. *Oncol Rep.* 2013 30:471-7

Presentations

Oral: Alaknanda A, Zhang XZ, Pishas KI, Abell AD and Callen DF. Can Proteasome inhibitors treat solid cancers? ASMR, Adelaide, South Australia.

Poster: Alaknanda A, Zhang XZ, Abell AD and Callen DF. Pre-clinical investigation into treating solid tumours with proteasome inhibitors. Lorne Cancer Conference, Lorne, Victoria

Poster: Alaknanda A, Zhang XZ, Pishas KI, Abell AD and Callen DF. 2nd generation proteasome inhibitors for treatment of solid tumours. Florey Postgraduate Research Conference, Adelaide, South Australia.

Grants & Awards

IPAS Pilot Project- First Steps Towards a Cancer Biosensor 2013

Institute of Photonics and Advanced Sensing (IPAS)

As a co-applicant, I provided preliminary data to support the application, 2015

Co-applicants: Dr. John Bruning, Dr. Niels Krosggaard, Dr. Michelle Zhang,
Prof. David Callen, Prof. Andrew Abell.

Beat Cancer Project Travel Grant 2015, Cancer Council, South Australia 2014

Novel proteasome inhibitors for treatment of sarcoma 2014

Sarcoma and Bone Cancer Research Foundation

Co- applicant: Prof. David Callen

Outstanding Poster Presentation, Florey Postgraduate Research Conference 2014

Acknowledgements

Firstly, I would like to express my sincere gratitude to my supervisor Professor David F. Callen for giving me this opportunity and for the continuous financial support of my PhD study. David, your passion for science, patience, motivation, and immense knowledge has helped and guided me throughout my candidature. I could not have imagined having a better advisor and mentor for my PhD study. I am eternally grateful.

I would like to thank my co-supervisor Professor Andrew D. Abell for giving me the opportunity to collaborate in a number of interdisciplinary projects, and his continuous guidance and support. I would also like to thank Dr. Andrew Turner not only for his insightful comments and encouragement, but also for answering the litany of daily question which incited me to think outside the box.

A special thanks goes to Dr. Paul M Neilsen who provided me an opportunity to join this team as an intern, and who gave me access to the laboratory and research facilities. Without his precious support it would not be possible to conduct this research.

To Dr. Kathleen Pishas, my mentor and dearest of friends, I am forever grateful for your friendship and your unwavering support in both scientific and non-scientific matters. Also, I thank my fellow lab mates and friends Sheng Lei, Feng Yu, Reshma Shakya and Qing Qing Wang for the fun times, stimulating discussions, for the late nights we were working together before

deadlines and tuesday lab meetings. My chemistry team in the Department of Chemistry- Beatrice Rodriquez, Borja Lopez Perez, and XiaoZhou Zhang, it was fantastic to have the opportunity to work with all of you. To Tim, thank you for pulling me away from work time to time and preserving my sanity.

Special thanks to the University of Adelaide for providing me with a full-fee scholarship and a comfortable research environment during my work towards this thesis.

And last but by no means least, I would like to thank and dedicate this thesis to my parents and brothers for their patience, unconditional financial and emotional support and indefinite love that they have given me throughout my PhD and my life in general.

Declaration

I, Alaknanda Alaknanda/Adwal, certify that this work contains no material which has been accepted for the award of any other degree or diploma in any university or other tertiary institution and, to the best of my knowledge and belief, contains no material previously published or written by another person, except where due reference has been made in the text. In addition, I certify that no part of this work will in the future be used in a submission for any other degree or diploma in any university or other tertiary institution without the prior approval for the University of Adelaide and where applicable, any partner institution for the joint-award of this degree.

I give consent to this copy of my thesis, when deposited in the University Library, being made available for loan and photography, subject to the provisions of the Copyright Act 1968. I acknowledge that copyright of published works contained within this thesis resides with the copyright holder(s) of those works.

I also give permission for digital version of my thesis to be made available on the web, via University's digital research repository, the Library catalogue, the Australasian Digital Thesis Program (ADTP) and also through search engines, unless permission has been granted by the University to restrict Access for a period of time.

Signed:.....

Date:.....

Overview

Cancer is the leading cause of the burden of disease and injury in Australia, accounting for approximately 19 percent of the total disease burden. In 2010, the risk of developing cancer before the age of 85 years was 1 in 2 in men and 1 in 3 in women and as such, its burden on society as a whole is immense. In recent years, considerable advances have been made in developing new therapeutics for cancer, particularly therapies targeted to specific molecular subtypes, which have resulted in significantly improved patient survival. However, for some types of solid cancers there have been no significant recent improvements in patient survival or development of targeted therapies. Examples are the triple negative (estrogen and progesterone receptor, and human epidermal growth factor receptor 2 negative) subgroup of breast carcinomas and Ewing sarcomas. Herein, we explore two biological pathways that are frequently dysregulated in these cancers and thus provide opportunity for therapeutic intervention.

Section I of this thesis explores the proteasome as a therapeutic target and the potential use of proteasome inhibitors in the treatment of solid cancers and in particular triple negative breast cancers. In general, cancer is associated with increased proteasome activity, and is therefore an attractive target for therapy. Bortezomib, carfilzomib and ixazomib are proteasome inhibitors with FDA approval, but their current use is limited to multiple myeloma and mantle cell lymphoma. Chapter 1 summarizes our current understanding of the structure and function of proteasome variants, their dysregulation in solid cancers, as well as the rationale for

proteasome inhibitor based therapy. Chapter 2 assesses the potential for the use of proteasome inhibitors for the treatment of breast cancers. Initially, the proteasome of breast cancer subgroups was characterized in detail by analysis of the The Cancer Genome Atlas breast cancer RNA-sequencing database. Analysis of these data revealed biologically meaningful insights which were subsequently confirmed by experiments in breast cancer cell lines. These results revealed that patients with basal-like and HER2⁺ breast cancer subgroups express significantly higher levels of the immuno-proteasome variant compared to luminal subgroups. Based on the presented data, it was concluded that this subgroup of breast cancers are likely to respond to proteasome inhibitor based therapy.

Proteasome inhibitors in clinical use have several shortcomings including side-effects and lack of efficacy for treatment of solid cancers. In chapter 3, 4 and 5, by exploiting a cross-disciplinary collaboration with Chemistry, we explore the efficacy of new synthesized compounds which can inhibit the proteasome and novel strategies to improve efficacy and/or decrease side effects associated with the current clinical used FDA approved proteasome inhibitors.

Section II of this thesis explores the potential of new therapeutic approaches for the treatment of Ewing sarcoma. Chapter 6 evaluates the potential of exploiting the p53 pathway as a targeted therapy for Ewing sarcoma. p53 is a critical tumour suppressor that is involved in a multitude of cellular processes including cell cycle regulation and apoptosis. It is frequently deactivated in the majority of cancers by either direct mutation or by up-regulation of its negative regulators MDM2 and MDM4. Ewing sarcoma is atypical among cancer types as the

more than 90% of cases retain a wild-type p53 with functionally intact downstream pathways. Chapter 7 and 8 assess two drugs that engage p53 signaling to elicit their anti-tumourigenic effects. Chapter 7 explores whether the RNA polymerase I inhibitor, CX-5461, has potential for treatment of Ewing sarcoma. RNA Polymerase I is a cellular enzyme that regulates ribosomal synthesis and thus controls the rate of cellular growth and proliferation. To attain accelerated growth, cancer cells up-regulate RNA Polymerase I activity and therefore it is an attractive therapeutic target. It has previously been shown that inhibition of RNA Polymerase I by CX-5461 causes cell death or cell cycle arrest in a variety of cancers both *in vitro* and *in vivo* in a p53-dependent manner. Our results reveal that Ewing sarcoma cell lines are acutely sensitive to RNA Polymerase I inhibition by CX-5461, with cell lines with wild-type p53 exhibiting cytotoxic LD₅₀ values in low nanomolar figures (<3nM). This study provides encouraging pre-clinical results for the application of CX-5461 for Ewing sarcoma treatment and warrants further *in vivo* evaluation. Chapter 8 assesses the potential of XI-006, a pharmacological inhibitor of MDM2, a p53 antagonist, for the treatment of Ewing sarcoma. While results were not consistent with targeting the activity of p53, XI-006 was found to be a potent inducer of apoptosis in Ewing sarcoma.

SECTION I

Proteasome as a therapeutic target for the treatment of solid cancers

Chapter 1
Proteasome as a therapeutic target

Introduction

This chapter discusses the diverse functions of the proteasome that have been characterized and the potential utility of proteasome inhibitors for treatment of solid cancers.

Ubiquitin-Proteasome System

Protein degradation by the ubiquitin-proteasome system is a highly selective and efficient process. For a protein to be recognized by the proteasome, a small peptide (ubiquitin) must first be attached to the target protein. This process is controlled by a group of enzymes (E1, E2 and E3) collectively referred to as ubiquitin ligases. E1 activates ubiquitin and transfers it to the carrier protein E2. E2 presents ubiquitin to E3. E3 recognizes and binds the target protein and interacts with E2 to covalently attach ubiquitin to the target protein (Figure 1). This process is reiterated a number of times to create a polyubiquitin chain that can be subsequently recognized by the proteasome. To date, there is only one known E1, 50 E2 and over 500 E3 ubiquitin ligases (reviewed in [1, 2]) providing a highly protein specific and controlled process of poly-ubiquitination and therefore degradation.

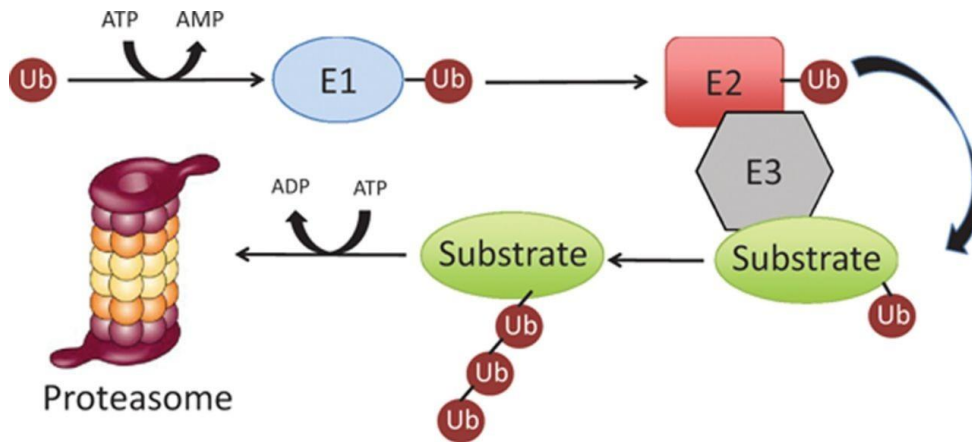


Figure 1. The Ubiquitin-Proteasome System. In step 1, ubiquitin is activated by an ubiquitin activating enzyme, E1. In step 2, activated ubiquitin is transferred to an ubiquitin conjugating enzyme, E2. In step 3, ubiquitin is subsequently conjugated to target proteins in a process mediated by an E3 ubiquitin ligase. In step 4, the polyubiquitinated substrate protein is degraded by the 26S proteasome.

26S Proteasome Structure

The constitutive proteasome (c-proteasome), generally referred to as 26S, is composed of a 20S catalytic core (~700kDa) capped with 19S regulatory structures at one or both ends (Figure 2). The 20S core is made up of four stacked rings, creating a central chamber where proteolysis occurs. The outer two rings, which are predominantly structural, each contain seven α subunits. Two inner rings each consist of seven β subunits. The proteolytic sites of the proteasome are located on three of the β -subunits on each of the two of inner rings, in the central cavity, resulting in a total of six proteolytic sites (reviewed in [3]). Catalytic activities of the proteasome are based upon preference to cleave a peptide bond after a particular amino acid residue. These activities are referred to as chymotrypsin-like (CT-L) activity, that cleaves after hydrophobic residues; trypsin-like (T-L) activity, that cleaves after basic residues; and caspase-

like (C-L) activity, that cleaves after acidic residues [4, 5]. The CT-L, T-L and C-L activities are associated with the β_5 , β_2 and β_1 subunits respectively [6].

Entry into the proteolytic chamber is controlled by binding to the 19S ATP-dependent regulatory particle. Polyubiquitin-tagged proteins are recognized by the 19S particle, the ubiquitin molecules are cleaved, the target protein is unfolded, and then can enter the 20S central catalytic chamber to be cleaved into short polypeptide fragments [5].

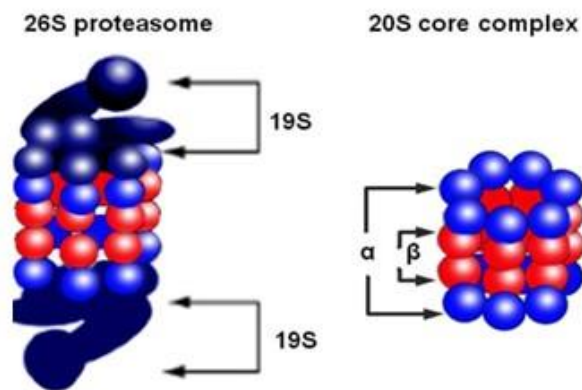


Figure 2. The Structure of the 26S Proteasome. The proteasome is a 26S enzyme complex that is comprised of a core 20S catalytic complex and a 19S regulatory complex. The 20S proteasome core has chymotrypsin-like, trypsin-like, and caspase-like activities that are associated with three distinct units: β_5 , β_2 , β_1 , respectively. Chymotrypsin-like activity at proteasome β_5 subunit is associated with the rate-limiting step of proteolysis.

There are two other known variants of the 20S in eukaryotes. In cells of the immune system, the β_{1i} , β_{2i} and β_{5i} subunits replace the corresponding constitutive subunits β_1 , β_2 and β_5 to

form an alternative 20Si core [7, 8]. The resulting proteasome is referred to as the immuno-proteasome (i-proteasome). Upon exposure to inflammatory cytokines (e.g. interferon- γ), many solid tissues and cancers are also capable of expressing the i-proteasome variant. In the context of catalytic activities, β 5i has CT-L activity, equivalent to β 5, and β 2i has T-L activity, equivalent to β 2. However, β 1i displays CT-L activity rather than the β 1-associated C-L activity (Figure 3). The i-proteasome variant also contains a different regulatory subunit PA28 (also known as 11S cap).

There is a third proteasome variant expressed by the cortical thymic epithelium in which the β 5t replaces β 5i in i-proteasomes to form the thymo-proteasome [7]. In addition to the variants described above, cells are also capable of expressing mixed proteasomes that contain varying combinations of thymo-, immuno- and constitutive- subunits [9]. Theoretically, combination of these different catalytic subunits can generate up to 36 different 20S core complexes that differ in their proteolytic specificity, although only a small subset have been demonstrated *in vivo*. The complexity of proteasome subtypes is further enhanced by association with different regulatory caps that can associate with 20S cores on one or both ends to form PA700 or PA28 bound, or one molecule each of PA700 and PA28 hybrid proteasomes.

The nomenclature of the various proteasome subunits used in this thesis is quite confusing due in part to the multitude of subunits, often with multiple symbols for the same subunit and proteasome variants. In addition, the same gene is referred to by different symbols in humans and mice. For ease of reading, Table 1 provides a list of names for the different catalytic subunits in humans and mice. The remainder of this chapter focuses on the critical differences between the functions of the c- and i-proteasome with emphasis on the roles of i-proteasome.

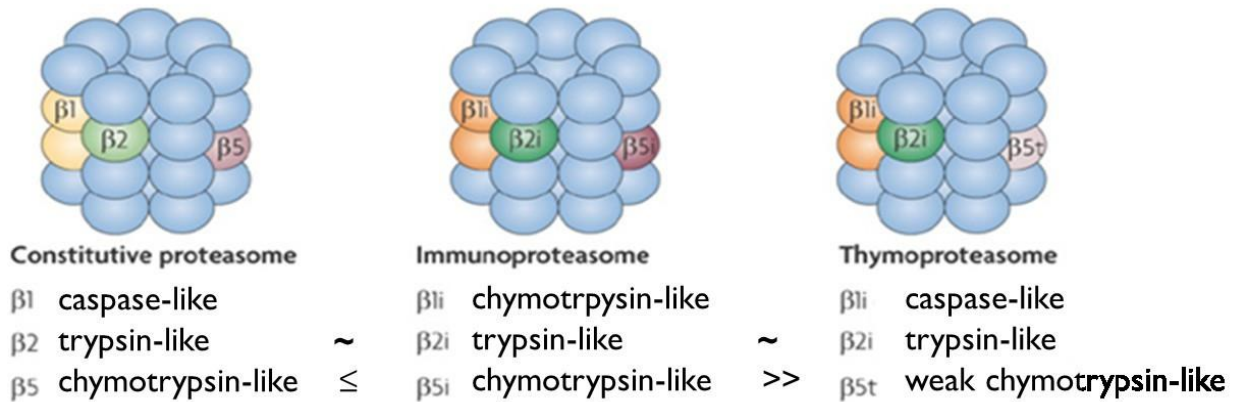


Figure 3. Subunit composition of the active sites of the constitutive, immuno- and thymo- proteasomes. The proteolytic subunits of the 20S constitutive, immuno- and thymo- proteasomes. Compared with the c-proteasome, the i-proteasome has a strongly decreased caspase-like activity and an increased chymotrypsin-like activity, whereas the thymoproteasome has a decreased chymotrypsin-like activity.

Table 1. Nomenclature of proteasomes.

Protein subunit	Homo sapiens gene symbol	Mus musculus gene symbol
$\beta 1$	<i>PSMB6</i>	-
$\beta 2$	<i>PSMB7</i>	-
$\beta 5$	<i>PSMB5</i>	-
$\beta 1i$	<i>PSMB9</i>	<i>Lmp2</i>
$\beta 2i$	<i>PSMB10</i>	<i>Mecl1</i>
$\beta 5i$	<i>PSMB8</i>	<i>Lmp7</i>

Immuno-proteasome in antigen presentation

The majority of proteasome generated peptide fragments from intracellular proteins are further degraded into shorter amino acid sequences and recycled for the synthesis of new proteins. However, a very small fraction of the cleaved peptides are delivered by the Transporter associated with antigen processing proteins (TAPs) to the endoplasmic reticulum, where these peptides act as ligands to nascent MHC class I molecules [10]. These MHC I bound peptides egress to the surface of the cell and can be recognized by naive CD8 T cells for routine immune surveillance. In addition, proteasomes also generate peptides for MHC I presentation from exogenous proteins that are internalised by endocytosis and or phagocytosis, a phenomenon called cross-presentation [11].

As mentioned previously, c-proteasome and i-proteasome possess different catalytic subunits. Compared to the c-proteasomes, i-proteasomes cleave more rapidly after hydrophobic and basic amino acid residues and less rapidly after acidic ones. As substrates with hydrophobic and basic C-termini are favored for uptake by TAP transporters [12] and are essential for tight binding to MHC class I molecules [13], it has long been suggested that i-proteasomes have a specialized role in creating peptides that are antigenic. Initial *in vivo* studies used single gene knockouts of the immuno-subunits to analyse phenotypic and CD8 T cell cytotoxic responses. Mecl-1-deficient mice infected with lymphocytic choriomeningitis virus (LCMV) had a slightly reduced number of CD8 T cells, and a decreased response to LCMV GP276 and NP205, but normal responses to NP396, GP33 and several other LCMV epitopes [14]. Mice lacking the Lmp2 subunit of the i-proteasome generate normal cytotoxic responses to Sendai virus and LCMV but show reduced capacity to generate CD8 T cells against the nucleoprotein epitope of influenza A [15]. Knockdown of Mecl1 or Lmp2 does not alter the cell surface expression of the class MHC I molecules in the above singly-deficient mice. In contrast, Fehling et al. observed that splenocytes from mice lacking Lmp7 subunit ($\beta 5i$) had a modest (~50%) reduction in MHC class I cell surface expression as well as decreased number of CD8 T cells specific to the male minor antigen HY [16]. Contrary to this study, Basler et al. did not observe any difference in the clearance of LCMV virus epitopes in Lmp7 deficient and wild-type mice. Overall, these studies suggest that mice lacking one i-proteasome subunit can substantially alter the production of some epitopes. However, these studies have only examined the presentation of a selective group of epitopes.

To rule out the possibility that functional overlap in peptide generation by the three i-proteasome subunits could compensate for the loss of one subunit, Kinciad et al. generated triple knockout-mice that were deficient in all three i-proteasome subunits [17]. Kinciad et al. showed that class I MHC antigenic presentation in these triple deficient mice was both qualitatively and quantitatively different from that of single knockout mice. In their analysis of 11 MHC class I antigens expressed on dendritic cells, expression of 8 antigens was significantly reduced. For Smyc antigen, compared to single-deficient mice that expressed this antigen without any defects, expression was substantially reduced in triple-deficient dendritic cells. Similarly, there were substantial defects in the expression of LCMV antigens GP33 and GP118, influenza antigen NP366-374 and antigen OVA257–264 presentation not seen in single-deficient mice in previous studies. This study substantiates that the i-proteasome is a major contributor to the MHC class I antigen presentation.

However, it should be noted that that while many antigens are efficiently produced by the i-proteasome, some are preferentially generated by the c-proteasome and their generation by the i-proteasome is highly inefficient. For example, the HLA-A2-binding antigenic peptide [18] ITDQVPFSV (gp100 209-217) derived from melanocytic protein gp100PMEL17, and the peptide YMDGTMSQV from melanocytic protein tyrosinase, are produced by the c-proteasome, but not by the i-proteasome. As a consequence, cells exclusively expressing c-proteasomes can efficiently stimulate gp100-specific and tyrosinase-specific cytotoxic T lymphocytes respectively. Overall, the changed subunit composition of i-proteasomes, relative to c-

proteasomes, contributes to altered protease activities that results in the generation of different antigenic peptides by these two types of proteasomes.

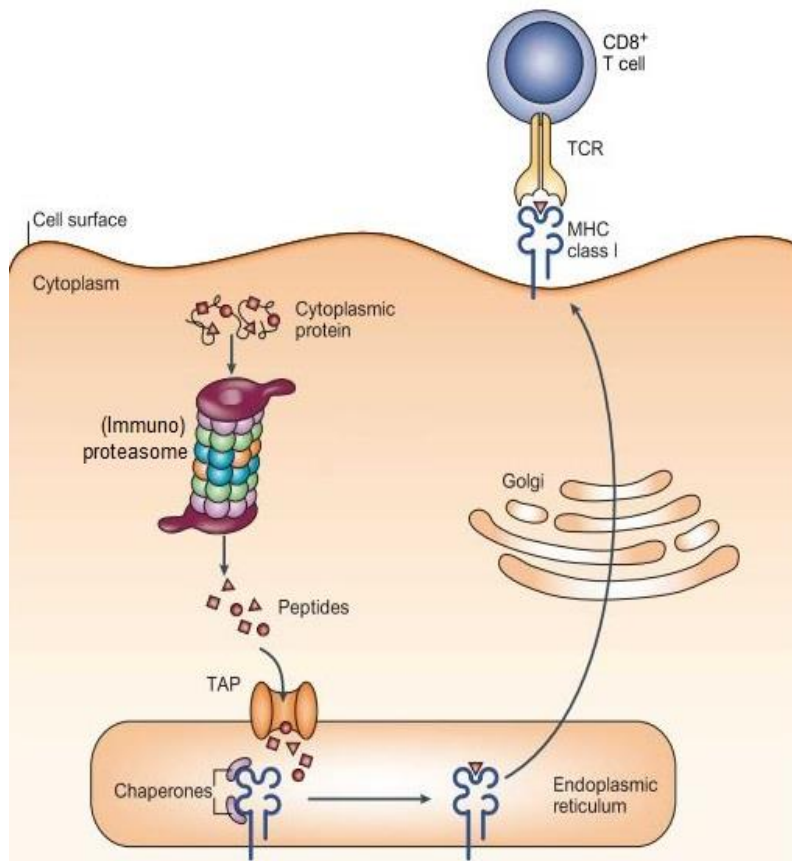


Figure 4. The role of the i-proteasome in antigen presentation. Poly-ubiquitinated cytoplasmic proteins are recognized and degraded by either c- or i-proteasome. The peptides are transported into the endoplasmic reticulum by a complex called TAP and attached to MHC class I molecules. Peptide-MHC complexes then egress---

The diversity of antigenic peptides may be further increased by the expression of intermediate proteasomes that contain combinations of c- and i-proteasome subunits and therefore different protease activities. The presence of proteasome complexes with different types and

contributions of activating caps has the potential to further modify and alter the peptidome. This can influence CD8+ T cell responses by increasing the diversity of antigenic peptides presented on MHC class I molecules [19].

The role of the Immuno-proteasome in protein homeostasis

In addition to being involved in antigen presentation, the i-proteasome has been shown to have roles in the cellular response to stress and injury. This idea was initially based on the observation that following stress, i-proteasome expression was substantially up-regulated in cells that do not typically present antigens [20]. For example, i-proteasome is significantly up-regulated in immune-privileged sites like retina [21-26] and brain [21, 27] in response to acute injury. It is also up-regulated in cultured cells exposed to cytokines like IFN γ and TNF α [22, 25, 26]. Since mice deficient in subunit Lmp2 of the i-proteasome express increased levels of oxidized proteins [21, 28] and those double deficient in Lmp7 and Mecl1 show greater sensitivity to oxidative challenge [22], this suggests that the i-proteasome may provide a protective role against oxidative stress.

Seifert et al. suggest that the primary role of the i-proteasome is to limit inflammatory damage, potentially by eliminating from the cell proteins damaged from inflammatory responses [29]. Data from Seifert and colleagues suggest that the i-proteasome is more efficient at degrading the “defective ribosomal products” (DRiPs), which are misfolded and /or oxidized proteins produced during protein synthesis. They observed that cytokine-induced oxidative stress in murine fibroblasts and human HeLa cells results in an initial increase in the levels of poly-ubiquitylated peptides, but was then followed by a decline after 24 hours, and a return to normal levels. The decrease observed after 24 hours coincided with induction of i-proteasomes and increase in proteasome CT-L activity, suggesting that i-proteasomes can function in the removal of poly-ubiquitinated peptides. In i-proteasome deficient cells, challenges with either

lipopolysaccharide or IFN γ induced aggresome and increased levels of oxidized and ubiquitylated proteins by 2-fold compared to control cells. *In vivo* experiments supported these observations, with Lmp7 knockout mice exhibiting a more severe clinical score and higher levels of oxidized proteins and protein aggregates in the inflamed liver and brain compared to mice with wild-type Lmp7. Another study by Opitz et al. in a murine model of acute enterovirus myocarditis, showed that mice deficient in Lmp7 i-proteasome subunit exhibit severe myocardial destruction and large inflammatory foci in cardiac cells. These Lmp7 deficient cardiomyocytes also had substantially more oxidized and poly-ubiquitylated protein accumulation compared to wild-type cells following exposure to IFN γ . The authors hypothesize that cytokine (e.g. IFN γ) induced inflammation significantly up-regulates protein synthesis, and therefore production of DRiPs leading to toxic protein aggregates, and as a consequence, the i-proteasome is up-regulated to protect cellular homeostasis. The significance of i-proteasomes in protein homeostasis upon stress induction has also been observed by various other studies [30].

Contrary to these studies, Nathan et al. did not observe either up-regulation of poly-ubiquitylated peptide or formation of toxic aggregates in mouse embryonic fibroblasts and B8 fibroblasts treated with 200 U/ml of IFN γ [31]. They also did not observe any difference in processing of the substrate ubiquitinated dihydrofolate reductase (Ub5DHFR) between two proteasome variants. Based on these results, the authors concluded that i-proteasomes are not more important in protein homeostasis than c-proteasomes. Discrepancies between both reports, however, might be explained by distinct experimental procedures [32].

Proteasomes and Cancer

The role of the proteasome in cancer was first considered when a number of oncogene and tumour suppressor gene products were found to be targets of ubiquitin and proteasome mediated degradation. Subsequent studies revealed that proteasome inhibitors induced apoptosis in leukemic cell lines and were also active in an *in vivo* model of Burkitt's lymphoma [21, 29, 33, 34]. The proteasome controls cellular growth and division by controlling the degradation of all misfolded, damaged and short lived proteins, for example those involved in cell cycle regulation and apoptosis. Dysregulated proteolysis contributes to malignant transformation either by enhancing the degradation of negative cell cycle regulators or by causing a defect in proteolysis of positive cell cycle regulators [35]. This can occur when mutations in substrates result in their evasion of normal ubiquitination that controls their abundance, or when there are specific defects of the ubiquitin-proteasome system [36, 37].

Cancer cells are generally associated with increased proteasome activity compared to non-malignant cells, likely due to factors including rapid cell proliferation, increased oxidative stress, and elevated cytokine levels [37]. With regard to i-proteasome expression levels in cancer, apparent differences exist across the various cancer types. For example, up-regulation of i-proteasome has been observed in multiple myeloma, prostate cancer, and lung cancer [38, 39]. On the other hand, i-proteasome is reported to be down-regulated in esophageal, renal, skin, and head and neck cancers [40-42]. Most of these studies did not further investigate the functional consequences of i-proteasome down-regulation. Therefore, it remains unclear

whether these changes in i-proteasome expression levels have any functional significance in terms of cancer cell survival and proliferation.

Several studies have also assessed the clinical significance of i-proteasome expression. In lung cancer, a study by Tripathi et al. observed that patients treated with surgery alone showed significantly reduced disease-free survival with low PSMB8 expressing tumours ($P = 0.004$) [43-46]. PSMB8 levels also emerged as an independent significant prognostic factor for disease-free survival [$P = 0.005$; hazard ratio (HR): 2.5; 95% confidence interval (CI): 1.3–5.0]. Notably, the reduced i-proteasome expression led to fewer peptides presented on HLA class I molecules (Tripathi et al., 2016). The authors observed that in NSCLS cell lines of mesenchymal origin (H1299 and DFCI024) displayed a markedly reduced diversity of peptides compared to epithelial cell lines (DFCI032 and HCC2935). The authors predict that due to NSCLS having high mutations, i-proteasomes are likely able to generate high levels and more diverse neo-epitopes, which can be recognized by tumour infiltrating T cells and trigger host immune responses.

In breast cancer, a study reported by Rouette et al. shows that i-proteasome gene expression correlates with survival in breast cancer, with high i-proteasome levels associated with a decreased risk of death (hazard ratio = 0.53) [47]. Survival at ten years was $61.9\% \pm 11.7\%$ for patients whose i-proteasome gene expression ranked in the top third of the cohort relative to $36.1\% \pm 8.0\%$ for those in the bottom third. Furthermore, expression of individual i-proteasome genes PSMB8 and PSMB10 were associated with a decreased risk of death.

Overall, these studies suggest that in certain cancers, i-proteasome expression is up-regulated and this is presumably required to facilitate increased availability of growth-promoting proteins to sustain accelerated cancer growth. The up-regulated i-proteasome, since they are also intimately connected with the MHC class I antigen-processing machinery, causes increased levels and diversity of antigens, their presentation and subsequent immune responses. Given this i-proteasome addiction for certain cancers, it is likely that disrupting proteasome function will have drastic effect on rapidly dividing cancer cells, which can be therapeutically exploited with pharmacological inhibitors.

Proteasome Inhibitors in Cancer

The first proteasome inhibitors were simple peptide aldehydes designed to study the rate of proteolytic activity of proteasomes in muscle atrophy. With increasing evidence for the role of the proteasome in cancer progression, the possibility that proteasome inhibitors may have potential as therapeutic agents was considered. Early studies showed that proteasome inhibitors displayed a broad spectrum of anti-proliferative and pro-apoptotic activity against hematological and solid tumours. However, these initial compounds were rudimentary and lacked the potency, specificity, or stability required for clinical use, which led to the design of new inhibitors with more potent and selective activity. Bortezomib (PS-341), a dipeptide boronic acid, was the first proteasome inhibitor that showed high *in vitro* and *in vivo* anti-proliferative activity against a range of cancer types by blocking CT-L activity [48]. It was approved by the FDA for treatment of patients with multiple myeloma, and mantle cell lymphoma and is in advanced stage clinical trials for many other tumour types as a combination

therapy [49-51]. However, there are limitations to the use of this inhibitor, including partial to no response in some patients, and dose limiting toxicities, particularly peripheral neuropathy. Furthermore, as single agents none of these inhibitors show efficacy in solid tumours.

Despite initial clinical activity in hematological malignancies, some develop resistance. In limited early studies of bortezomib in advanced stage solid tumours, development of resistance was also observed. Busse et al. demonstrated that bortezomib resistant cell-lines originating from refractory myeloma (U266), lymphomas (KARPAS422) and solid tumour (8505C) had either reduced expression, or reduced catalytic activity, of i-proteasome subunits. Given that bortezomib specific IC₅₀ for c- ($\beta 5 \sim 7.5 \text{ nM}$) or i- ($\beta 5 \text{ i} \sim 3.5 \text{ nM}$) proteasome subunits are almost identical, the authors suggested that sensitivity of proteasome inhibition was due to higher i-proteasome levels. Furthermore, induction of i-proteasome assembly by IFN γ exposure restored (40-60%) the sensitivity of such resistant cells to bortezomib with a concomitant decrease in the expression of the c-proteasome, suggesting that i-proteasomes are more sensitive to bortezomib than c-proteasomes [52, 53]. This observation is further complemented by various *in vitro* studies that indicate that increased levels of the constitutive subunits are associated with decreased bortezomib sensitivity [54]. It is likely that the overall effect of proteasome inhibition will vary greatly between tumour types [55-58] since different organ/cell types can express mixed and hybrid proteasomes where individual proteasomes contain both c- and i-subunits.

In cancer, the functional roles of the three proteasome activities (CT-L, C-L, and T-L) and their relative inhibition by proteasome inhibitors have not been fully elucidated. The majority of proteasome inhibitors are directed against CT-L activity, traditionally considered the rate-limiting step in protein degradation. Consequently, inhibitor potency has often only been measured against this activity for most proteasomes. More recently, it has been shown that all three catalytic activities contribute significantly to protein degradation and that their relative contributions are dependent on the cell type and protein substrate [30]. Furthermore, it has been shown that inhibition of CT-L sites alone correlates poorly with cytotoxicity and that either C-L or T-L sites need to be co-inhibited to achieve maximum cytotoxicity in cells [59].

These findings suggest that depending on tumour type, catalytic T-L and C-L sites become integral to proteasome dysfunction and need to be considered as co-targets of anticancer drugs. There is a paucity of data on the effect of proteasome inhibition in solid cancers, but a few preclinical studies reveal that bortezomib is cytotoxic to breast cancer and sarcoma-derived cell lines. However, these *in vitro* responses could not be translated into a therapeutic benefit in patients with breast cancer or metastatic/recurrent Ewing sarcoma [41, 60, 61]. Currently, there are extremely few solid tumours that respond to bortezomib in patient trials. Whether this poor response in solid tumours is related to their lack of i-proteasomes exemplifies the apparent limitation of bortezomib and will extend to all proteasome inhibitors as a class, is as yet unknown.

Most current and second generation proteasome inhibitors under development and in clinical trials pre-dominantly target the CT-L site and fail to account for the importance of C-L and T-L activities. Even though the second generation inhibitors that have now been developed (eg. carfilzomib and ixazomib) offer the potential for more specificity and potency, they may have only limited success in solid tumours that predominantly express the c-proteasomes. These observations highlight an urgent need to continue development of more cancer-specific proteasome inhibitors, as well as characterizing proteasomes in solid cancers.

Clinical Significance

Dysregulated and up-regulated activity of the proteasome is a universal feature of malignant cells. Up-regulated proteasome CT-L activity is characteristic in many malignancies, which makes this an attractive target for cancer therapy. Bortezomib and other proteasome inhibitors have been highly effective in liquid tumours such as multiple myeloma and refractory mantle cell lymphoma, which predominantly express the i-proteasome. However, these inhibitors have several shortcomings including toxicity and lack of efficacy in solid cancers. However, this maybe considered to be due to a lack of i-proteasome expression in solid cancers. Recent studies suggest that many solid cancers can also express the i-proteasome and therefore may be sensitive to proteasome inhibition. As such, further characterization of the proteasomes in solid cancers is crucial. In addition, the major proteasome inhibitor in current use, bortezomib, has limitations due to toxicity. There is scope to develop new proteasome inhibitors that can target different proteasome subunits and that have reduced overall toxicity.

The following four chapters highlight the potential of using proteasome inhibitors in solid cancer treatment. Chapter 2 demonstrates that the i-proteasome plays a crucial role in some subgroups of breast cancer. Chapter 3, 4, and 5 explore novel approaches in inhibitor design and synthesis that may increase efficacy and reduce toxicities associated with current proteasome inhibitors. The studies outlined here are essential for the further development of these cancer-specific proteasome inhibitors, which may serve as therapeutically active agents (alone or in combination with existing therapy) for hard to treat solid cancers.

References

1. Nath, D. and S. Shadan, The ubiquitin system. *Nature*, 2009. 458(7237): p. 421.
2. Shen, M., et al., Targeting the ubiquitin-proteasome system for cancer therapy. *Expert Opin Ther Targets*, 2013. 17(9): p. 1091-108.
3. Adams, J., The proteasome: structure, function, and role in the cell. *Cancer Treat Rev*, 2003. 29 Suppl 1: p. 3-9.
4. Borissenko, L. and M. Groll, 20S proteasome and its inhibitors: crystallographic knowledge for drug development. *Chem Rev*, 2007. 107(3): p. 687-717.
5. Coux, O., K. Tanaka, and A.L. Goldberg, Structure and functions of the 20S and 26S proteasomes. *Annu Rev Biochem*, 1996. 65: p. 801-47.
6. Marques, A.J., et al., Catalytic mechanism and assembly of the proteasome. *Chem Rev*, 2009. 109(4): p. 1509-36.
7. Groettrup, M., C.J. Kirk, and M. Basler, Proteasomes in immune cells: more than peptide producers? *Nat Rev Immunol*, 2010. 10(1): p. 73-8.
8. Yewdell, J.W., Immunoproteasomes: Regulating the regulator. *Proceedings of the National Academy of Sciences of the United States of America*, 2005. 102(26): p. 9089-9090.
9. Tanahashi, N., et al., Hybrid proteasomes. Induction by interferon-gamma and contribution to ATP-dependent proteolysis. *J Biol Chem*, 2000. 275(19): p. 14336-45.
10. Sijts, E.J.A.M. and P.M. Kloetzel, The role of the proteasome in the generation of MHC class I ligands and immune responses. *Cellular and Molecular Life Sciences*, 2011. 68(9): p. 1491-1502.
11. Blum, J.S., P.A. Wearsch, and P. Cresswell, Pathways of Antigen Processing. *Annual review of immunology*, 2013. 31: p. 443-473.
12. Bhasin, M. and G.P.S. Raghava, Analysis and prediction of affinity of TAP binding peptides using cascade SVM. *Protein Science : A Publication of the Protein Society*, 2004. 13(3): p. 596-607.
13. Schueler-Furman, O., et al., Structure-based prediction of binding peptides to MHC class I molecules: application to a broad range of MHC alleles. *Protein Science : A Publication of the Protein Society*, 2000. 9(9): p. 1838-1846.
14. Basler, M., et al., An altered T cell repertoire in MECL-1-deficient mice. *J Immunol*, 2006. 176(11): p. 6665-72.

15. Van Kaer, L., et al., Altered peptidase and viral-specific T cell response in LMP2 mutant mice. *Immunity*, 1994. 1(7): p. 533-41.
16. Fehling, H.J., et al., MHC class I expression in mice lacking the proteasome subunit LMP-7. *Science*, 1994. 265(5176): p. 1234-7.
17. Kincaid, E.Z., et al., Mice completely lacking immunoproteasomes display major alterations in antigen presentation. *Nature immunology*, 2012. 13(2): p. 129-135.
18. Chapiro, J., et al., Destructive cleavage of antigenic peptides either by the immunoproteasome or by the standard proteasome results in differential antigen presentation. *J Immunol*, 2006. 176(2): p. 1053-61.
19. Dalet, A., et al., An antigenic peptide produced by reverse splicing and double asparagine deamidation. *Proceedings of the National Academy of Sciences of the United States of America*, 2011. 108(29): p. E323-E331.
20. Zanker, D., et al., Mixed proteasomes function to increase viral peptide diversity and broaden antiviral CD8+ T cell responses. *J Immunol*, 2013. 191(1): p. 52-9.
21. Hussong, S.A., et al., Immunoproteasome deficiency alters retinal proteasome's response to stress. *Journal of Neurochemistry*, 2010. 113(6): p. 1481-1490.
22. Ferrington, D.A., et al., Immunoproteasome responds to injury in the retina and brain. *Journal of Neurochemistry*, 2008. 106(1): p. 158-169.
23. Hussong, S.A., et al., A Novel Role for the Immunoproteasome in Retinal Function. *Investigative Ophthalmology & Visual Science*, 2011. 52(2): p. 714-723.
24. Kapphahn, R.J., E.J. Bigelow, and D.A. Ferrington, Age-dependent inhibition of proteasome chymotrypsin-like activity in the retina. *Experimental Eye Research*, 2007. 84(4): p. 646-654.
25. Díaz-Hernández, M., et al., Neuronal Induction of the Immunoproteasome in Huntington's Disease. *Journal of Neuroscience*, 2003. 23(37): p. 11653-11661.
26. Mishto, M., et al., Immunoproteasome and LMP2 polymorphism in aged and Alzheimer's disease brains. *Neurobiology of Aging*, 2006. 27(1): p. 54-66.
27. Ethen, C.M., et al., Transformation of the proteasome with age-related macular degeneration. *FEBS Letters*, 2007. 581(5): p. 885-890.
28. Ding, Q., et al., Role of the proteasome in protein oxidation and neural viability following low-level oxidative stress. *FEBS Letters*, 2003. 546(2-3): p. 228-232.

29. Ding, Q., et al., LMP2 knock-out mice have reduced proteasome activities and increased levels of oxidatively damaged proteins. *Antioxid Redox Signal*, 2006. 8(1-2): p. 130-5.
30. Seifert, U., et al., Immunoproteasomes preserve protein homeostasis upon interferon-induced oxidative stress. *Cell*, 2010. 142(4): p. 613-24.
31. Nathan, James A., et al., Immuno- and Constitutive Proteasomes Do Not Differ in Their Abilities to Degrade Ubiquitinated Proteins. *Cell*, 2013. 152(5): p. 1184-1194.
32. Ebstein, F., et al., Immunoproteasomes Are Important for Proteostasis in Immune Responses. *Cell*, 2013. 152(5): p. 935-937.
33. Pickering, A.M., et al., THE IMMUNOPROTEASOME, THE 20S PROTEASOME, AND THE PA28 $\alpha\beta$ PROTEASOME REGULATOR ARE OXIDATIVE-STRESS-ADAPTIVE PROTEOLYTIC COMPLEXES. *The Biochemical journal*, 2010. 432(3): p. 585-594.
34. Kotamraju, S., et al., Upregulation of immunoproteasomes by nitric oxide: potential antioxidative mechanism in endothelial cells. *Free Radic Biol Med*, 2006. 40(6): p. 1034-44.
35. Crawford, L.J., B. Walker, and A.E. Irvine, Proteasome inhibitors in cancer therapy. *Journal of Cell Communication and Signaling*, 2011. 5(2): p. 101-110.
36. Bashir, T. and M. Pagano, Aberrant ubiquitin-mediated proteolysis of cell cycle regulatory proteins and oncogenesis. *Adv Cancer Res*, 2003. 88: p. 101-44.
37. Nakayama, K.I. and K. Nakayama, Ubiquitin ligases: cell-cycle control and cancer. *Nat Rev Cancer*, 2006. 6(5): p. 369-81.
38. Crawford, L.J., et al., Proteasome proteolytic profile is linked to Bcr-Abl expression. *Exp Hematol*, 2009. 37(3): p. 357-66.
39. Bossola, M., et al., Increased muscle proteasome activity correlates with disease severity in gastric cancer patients. *Ann Surg*, 2003. 237(3): p. 384-9.
40. Wehenkel, M., et al., A selective inhibitor of the immunoproteasome subunit LMP2 induces apoptosis in PC-3 cells and suppresses tumour growth in nude mice. *Br J Cancer*, 2012. 107(1): p. 53-62.
41. Altun, M., et al., Effects of PS-341 on the activity and composition of proteasomes in multiple myeloma cells. *Cancer Res*, 2005. 65(17): p. 7896-901.
42. Ho, Y.K., et al., LMP2-specific inhibitors: chemical genetic tools for proteasome biology. *Chem Biol*, 2007. 14(4): p. 419-30.

43. Liu, Q., et al., Down-regulation of HLA class I antigen-processing machinery components in esophageal squamous cell carcinomas: association with disease progression. *Scand J Gastroenterol*, 2009. 44(8): p. 960-9.
44. Murakami, Y., et al., Prognostic significance of immuno-proteasome subunit expression in patients with renal-cell carcinoma: a preliminary study. *Mol Urol*, 2001. 5(3): p. 113-9.
45. Meidenbauer, N., et al., High frequency of functionally active Melan-a-specific T cells in a patient with progressive immunoproteasome-deficient melanoma. *Cancer Res*, 2004. 64(17): p. 6319-26.
46. Ritz, U., et al., Deficient expression of components of the MHC class I antigen processing machinery in human cervical carcinoma. *Int J Oncol*, 2001. 19(6): p. 1211-20.
47. Rouette, A., et al., Expression of immunoproteasome genes is regulated by cell-intrinsic and -extrinsic factors in human cancers. *Sci Rep*, 2016. 6: p. 34019.
48. Tripathi, S.C., et al., Immunoproteasome deficiency is a feature of non-small cell lung cancer with a mesenchymal phenotype and is associated with a poor outcome. *Proceedings of the National Academy of Sciences*, 2016. 113(11): p. E1555-E1564.
49. Shahshahan, M.A., M.N. Beckley, and A.R. Jazirehi, Potential usage of proteasome inhibitor bortezomib (Velcade, PS-341) in the treatment of metastatic melanoma: basic and clinical aspects. *American Journal of Cancer Research*, 2011. 1(7): p. 913-924.
50. Lightcap, E.S., et al., Proteasome Inhibition Measurements: Clinical Application. *Clinical Chemistry*, 2000. 46(5): p. 673-683.
51. Hideshima, T., et al., The proteasome inhibitor PS-341 inhibits growth, induces apoptosis, and overcomes drug resistance in human multiple myeloma cells. *Cancer Res*, 2001. 61(7): p. 3071-6.
52. Field-Smith, A., G.J. Morgan, and F.E. Davies, Bortezomib (Velcade™) in the Treatment of Multiple Myeloma. *Therapeutics and Clinical Risk Management*, 2006. 2(3): p. 271-279.
53. Kane, R.C., et al., Bortezomib for the Treatment of Mantle Cell Lymphoma. *Clinical Cancer Research*, 2007. 13(18): p. 5291-5294.
54. Busse, A., et al., Sensitivity of tumour cells to proteasome inhibitors is associated with expression levels and composition of proteasome subunits. *Cancer*, 2008. 112(3): p. 659-70.
55. Franke, N.E., et al., Impaired bortezomib binding to mutant $\beta 5$ subunit is the underlying basis for bortezomib resistance in leukemia cells. *Leukemia*, 2012. 26(4): p. 757-68.
56. Oerlemans, R., et al., Molecular basis of bortezomib resistance: proteasome subunit beta5 (PSMB5) gene mutation and overexpression of PSMB5 protein. *Blood*, 2008. 112(6): p. 2489-99.

57. Balsas, P., et al., Bortezomib resistance in a myeloma cell line is associated to PSMbeta5 overexpression and polyploidy. *Leuk Res*, 2012. 36(2): p. 212-8.
58. Ruckrich, T., et al., Characterization of the ubiquitin-proteasome system in bortezomib-adapted cells. *Leukemia*, 2009. 23(6): p. 1098-105.
59. Kisselev, A.F., A. Callard, and A.L. Goldberg, Importance of the different proteolytic sites of the proteasome and the efficacy of inhibitors varies with the protein substrate. *J Biol Chem*, 2006. 281(13): p. 8582-90.
60. Berkers, C.R., et al., Activity probe for in vivo profiling of the specificity of proteasome inhibitor bortezomib. *Nat Meth*, 2005. 2(5): p. 357-362.
61. Adams, J., Development of the proteasome inhibitor PS-341. *Oncologist*, 2002. 7(1): p. 9-16.

CHAPTER 2

Proteasome addiction in breast cancers defines new therapeutic targets

Alaknanda Adwal and David F Callen

Centre for Personalised Cancer Medicine, Adelaide Medical School, University of Adelaide,
South Australia, Australia

Statement of Authorship

Statement of Authorship

Title of Paper	Proteasome addiction in breast cancers defines new therapeutic targets	
Publication Status	<input type="checkbox"/> Published <input checked="" type="checkbox"/> Submitted for Publication	<input type="checkbox"/> Accepted for Publication <input type="checkbox"/> Unpublished and Unsubmitted work written in manuscript style
Publication Details	eLIFE	

Principal Author

Name of Principal Author (Candidate)	Alaknanda Adwal	
Contribution to the Paper	Performed majority of experimental work (biological assessment), interpreted data and co-wrote manuscript. Also, acted as corresponding author.	
Overall percentage (%)	50%	
Certification:	This paper reports on original research I conducted during the period of my Higher Degree by Research candidature and is not subject to any obligations or contractual agreements with a third party that would constrain its inclusion in this thesis. I am the primary author of this paper.	
Signature		Date 6/3/2017

Co-Author Contributions

By signing the Statement of Authorship, each author certifies that:

- i. the candidate's stated contribution to the publication is accurate (as detailed above);
- ii. permission is granted for the candidate to include the publication in the thesis; and
- iii. the sum of all co-author contributions is equal to 100% less the candidate's stated contribution.



Name of Co-Author	David F Callen		
Contribution to the Paper	Contributed to conception, design and overall supervision of project, data analysis. Also co-wrote manuscript.		
Signature		Date	6/3/2017



Prelude

This chapter summarizes key highlights from analysis of RNA-sequencing data of breast cancers generated from the TCGA initiative. These analyses revealed biologically meaningful insights into the expression of immuno-proteasome variants in basal-like and HER2⁺ breast cancer subgroups that were confirmed by subsequent experimentation in cell line models.

This research has been submitted to eLIFE journal (March, 2017) and this chapter is the submitted version of the manuscript.

Contribution by the candidate: All experimental work and manuscript writing.

Abstract

The success of proteasome inhibitors in hematological cancers is attributed to up-regulated proteasome activity. Although breast cancers were resistant to this therapy in early clinical trials, proteasome activity was not assessed. Since patient stratification based on proteasome activity may provide a targeted approach, we interrogated proteasome expression in cell line and patient derived RNAseq breast cancer data. In basal-like and HER2⁺ tumours, immunoproteasome levels were significantly up-regulated compared to luminal A and B tumours. High expression of the immuno-proteasome was associated with improved patient survival in basal-like and HER2⁺ breast cancers, but not in luminal A or B. Bortezomib sensitivity was significantly correlated with increasing levels of immuno-proteasome expression in breast cancer cell lines. Bortezomib caused apoptosis in basal-like cell lines via unfolded protein response pathways. Overall, our findings provide an overarching hypothesis that integrates immunoproteasome expression and improved outcome in basal-like and HER2⁺ cancers.

Introduction

The proteasome is the major recycling centre for the cell with the c-proteasome degrading poly-ubiquitinated proteins via an ATP-driven protein complex consisting of a 20S core and 19S cap (Sorokin, Kim, & Ovchinnikov, 2009). Three protein components of the 20S core provide the critical proteolytic activities of β 1 caspase-like (encoded by the PSMB6 gene), β 2 trypsin-like (encoded by PSMB7) and β 5 chymotrypsin-like (encoded by PSMB5). In addition, there is an alternative form of the 20S core termed the immuno-proteasome (i-proteasome) with alternative active sites, β 1i (encoded by PSMB9), β 2i (encoded by PSMB10) and β 5i (encoded by PSMB8), together with a specialised 11S cap. The i-proteasome degrades unfolded and oxidised proteins and does not require ATP-driven unfolding of proteins (Shringarpure, Grune, Mehlhase, & Davies, 2003). The i-proteasome is predominantly expressed in haematopoietic cells and drives the major histocompatibility complex (MHC) class I response. Interferon- γ is a major inducer of i-proteasome expression (Aki et al., 1994).

Compared to normal cells, cancers are typically associated with an enhanced proteasome activity and this provides a potential therapeutic target (J. Adams, 2004). The proteasome inhibitors bortezomib, carfilzomib, and more recently ixazomib, are FDA approved and used clinically for treatment of multiple myeloma and mantle cell lymphoma. Disappointing results from early phase clinical trials using bortezomib for treatment of solid tumours such as breast cancer (Engel et al., 2007; Yang et al., 2006) refocused the use and development of new generation inhibitors primarily for multiple myeloma treatment. However, recently there has

been developing interest in the use of bortezomib in solid cancers in conjunction with other systemic treatments.

Although the proteasome is a potential therapeutic target in solid cancer, there has been limited characterisation of the proteasome in such cancers. The availability of next generation RNA sequencing data from a large number of breast cancers provides the opportunity to investigate the expression of the proteasome and its components in detail. This analysis was undertaken to determine if a proteasome inhibitor based therapy could target particular subgroups of breast cancer. Supporting data was then determined from analysis of appropriate breast cancer cell lines.

Results

Comparison of expression of the c-proteasome in breast cancer subgroups

This analysis is based on the breast cancer subgroups basal-like, luminal A, luminal B and HER2⁺ enriched as defined by PAM50, a well-characterized qRT-PCR intrinsic subtyping classifier that measures expression of 50 genes selected as characteristic of these five breast cancer intrinsic subtypes ([Parker et al., 2009](#)). The breast cancer RNAseq data is sourced from the TCGA initiative available from cBioPortal ([Cerami et al., 2012](#); [Gao et al., 2013](#)). It should be noted that levels of message do not necessarily reflect that of protein, and the levels of individual proteins of the complex may not reflect a functional proteasome as this requires assembly of a multi-protein complex. Despite these caveats, analysis of RNAseq data reveals biologically meaningful insights that are then confirmed by subsequent experimentation.

The level of expression of c-proteasome subunits (19S cap genes PSMC1 and PSMD1, and PSMB5, PSMB6 and PSMB7 encoding respectively the c-proteasome activities β 5c, β 1c and β 2c) are compared across the subtypes of breast cancers (Figure 1A; Supplementary Table 1). The differences in expression of these subunits are similarly maintained across the different subtypes with HER2⁺ enriched tumours having an average expression 33.7% higher than luminal A cancers. The maintenance of these differences does suggest that these comparative gene expressions are representative measures of the levels of proteasome proteins. From these data the different subgroups of breast cancer are likely to have inherently different levels of the c-

proteasome and this likely reflects the characteristic inherent physiological states of the different subtypes.

It was of interest to compare expression levels of i-proteasome in the breast cancer subgroups as recent evidence suggests that solid tissues can express i-proteasome ([Altun et al., 2005](#); [Ho, Bargagna-Mohan, Wehenkel, Mohan, & Kim, 2007](#); [Wehenkel et al., 2012](#)). The expression of the i-proteasome chymotrypsin-like activity (PSMB8) was compared (Figure 1B) as this activity is considered to be the major activity of the proteasome ([Kisselev, Callard, & Goldberg, 2006](#)). The basal-like cancers had the highest proportion of tumours with high levels of the i-proteasome (38% between 2000-4000 RSEM proteasome expression) while the luminal A cancers had significantly lower proportion (only 18% of cancers with greater than 2000 RSEM of the i-proteasome expression). It is apparent that breast cancers, in particular the basal-like cancers, can express levels of i-proteasome greater than that of the c-proteasome. Typically, the i-proteasome is highly expressed in hematopoietic cells, where it functions to generate peptide fragments for the MHC class I response ([Aki et al., 1994](#)).

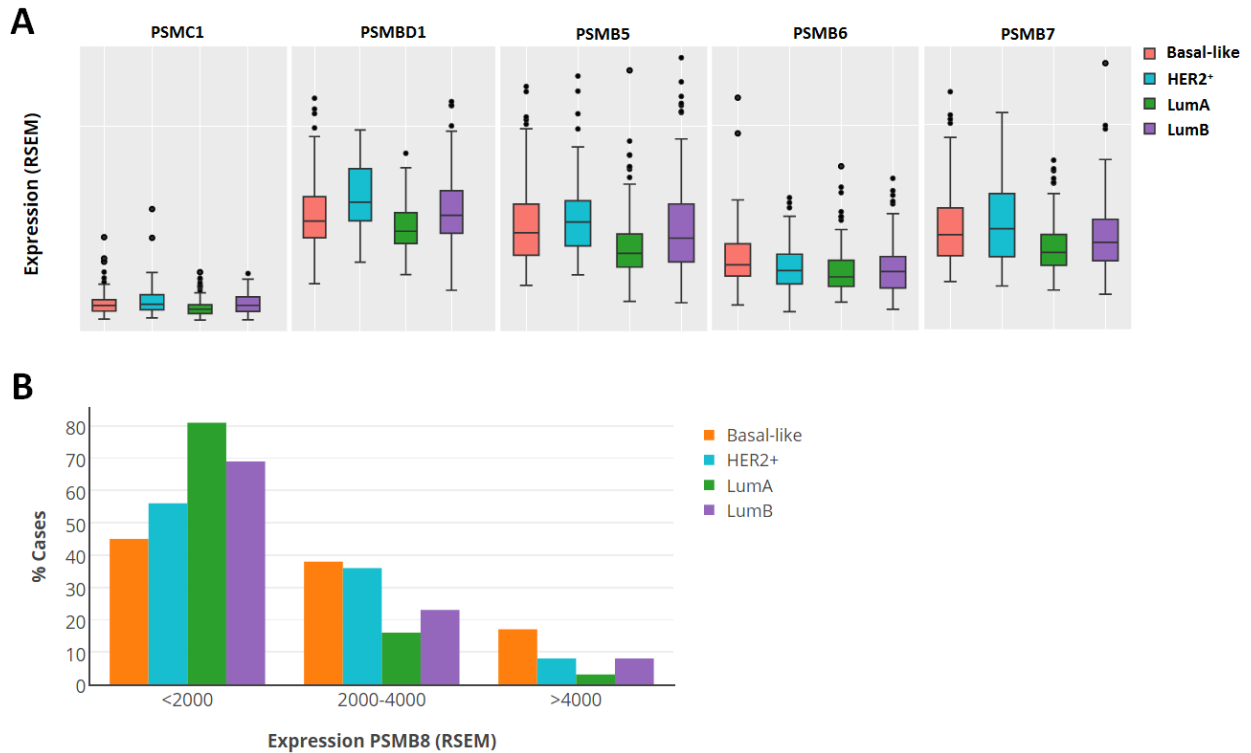


Figure 1. Comparison of relative expression of proteasome across breast cancer subtypes. A. PSMB5, PSMB6 and PSMB7 encode the c-proteasome activities of the 20S core; PSMC1 and PSMD1 are constant proteins of the 19S cap. LumA: Luminal A; LumB: Luminal B. **B. (left)** The relative i-proteasome (PSMB8) expression is presented in groupings from < 2000 RSEM, between 2000-4000 RSEM and >4000 RSEM. **B. (right)** I-proteasome expression presented in the percentage cases in the four intrinsic breast cancer subgroups.

Co-expression of genes with i-proteasome expression

Co-expression, as determined by the level of correlation between the expressions of two genes, can provide evidence for their involvement in the same pathway. In an approach to further investigate the roles of the proteasome in breast cancer, genes significantly co-expressed with the variable genes of the 20S core were determined. All genes were analysed, irrespective of

their relative expression. A conservative cut-off using $r=0.5$ was used which was equivalent to a Bonferroni corrected probability of <0.001 .

Correlation analysis revealed that the basal-like and luminal A breast cancer subgroups had distinct gene signatures. There were 84 genes in luminal A breast cancers where expression was correlated greater than 0.5 with PSMB8, PSMB9 and PSMB10 (Figure 2A). In contrast, in the 107 basal-like cancers there were 171 genes with correlated co-expression greater than 0.5 with each of PSMB8, PSMB9 and PSMB10 (Supplementary Tables 2 and 3). Notably, the basal-like tumours expressed higher levels of several MHC class I (TAP1, TAP2, B2M, HLA-A, -B and -C) and various MHC class II genes compared to luminal A tumours (Figure 2B; Supplementary Tables 3 and 4). The two subgroups also showed difference in the expression of transcription factors and cytokine/chemokines. Overlapping the lists of correlated genes, we obtained a 91-gene signature exclusive to basal-like tumours. Pathway and GO-term enrichment analysis of this signature suggested that the IFN γ -mediated immune response pathways were the most significantly up-regulated process (Figure 2C).

The genes co-expressed with the i-proteasome were divided into two groups of low and high average expression. Half of these co-expressed genes had an average expression in the 107 basal-like breast cancers less than 500 RSEM and were considered as low expressing. Comparison of the site of expression of the two groups demonstrated that the genes with lower expression were typically expressed in the lymphoid lineage rather than in breast cancer (e.g. the basal cell line MDA-MB-468) (Supplementary Figure 1). It is speculated that these

transcripts originate from infiltrating lymphoid cells in the tumour tissue samples that were processed for RNA sequencing and this infiltration was positively correlated with the presence of the i-proteasome.

The i-proteasome co-expressed genes with the highest expression include MHC class I and associated genes, such as TAP1 and TAP2, consistent with expression of i-proteasome driving this response. Unexpected was the high expression of the MHC class II genes that typically have expression in dendritic cells, mononuclear phagocytes and B cells and are induced by exposure to interferon gamma ([Ting & Trowsdale, 2002](#)). Possible sources of MHC class II expression are from breast cancer cells, stroma or from high levels of infiltrating hematopoietic cells within the tumour. To investigate the possible origin, MHC gene expression in breast cancer tissues was compared with breast cancer cell lines (Supplementary Table 4). In breast cancers, the MHC class I are highly expressed with the class II genes having an average expression of 23% of the class I. In breast cancer cell lines, although the MHC class I genes were expressed and were also correlated with PSMB8 expression, the expression of MHC II genes was negligible. There were only three of 68 breast cell lines that had showed robust expression of MHC class II genes. These data are consistent with the findings of Forero et al ([Forero et al., 2016](#)) where analysis by immunohistochemistry, and of laser-captured micro-dissected breast tumours, demonstrated that while the MHC II pathway was associated with B-cell and T-cell infiltration in the tumour there was also possible aberrant expression in breast cancer cells.

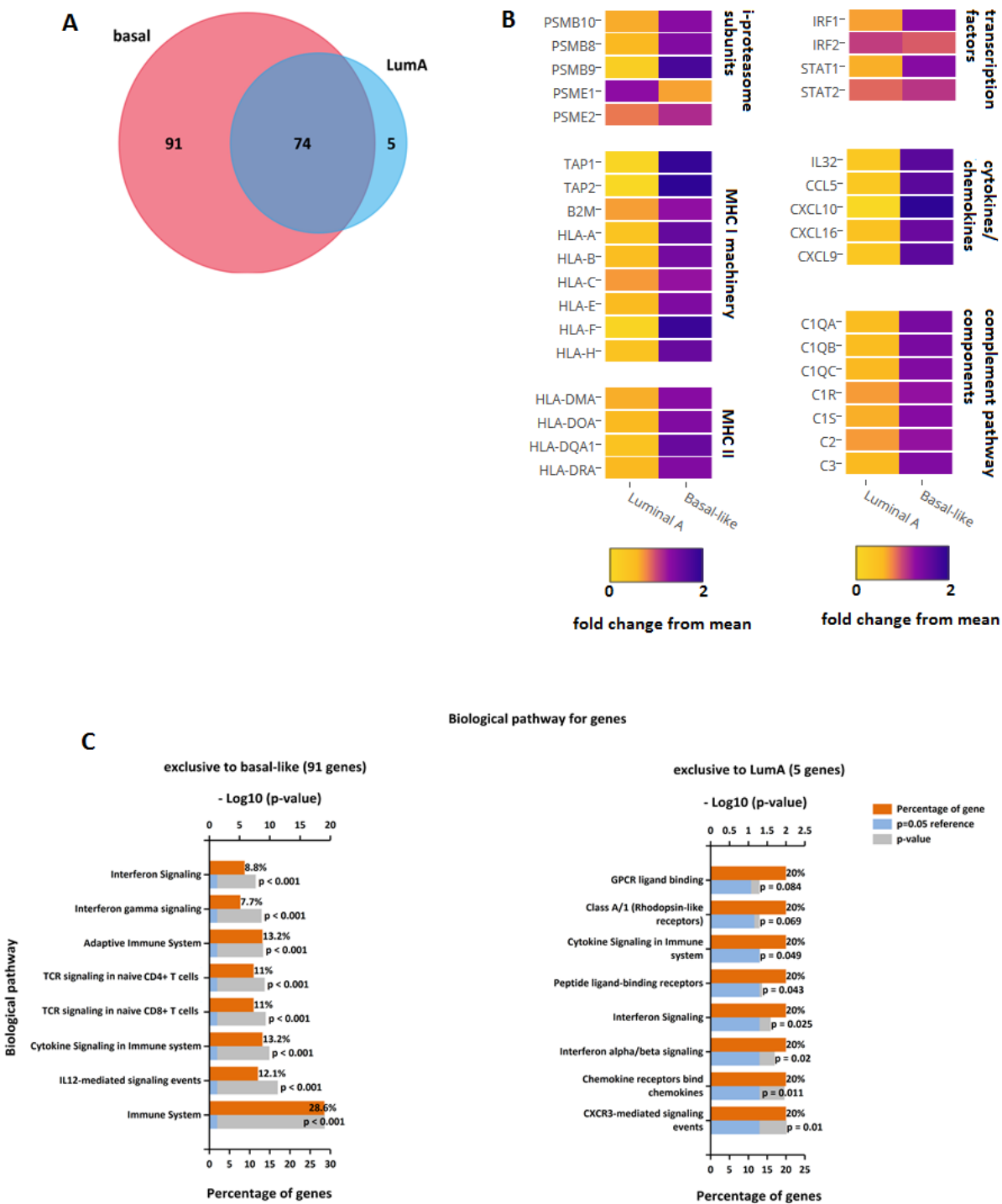


Figure 2. Analysis of i-proteasome co-expressed genes. A. Venn diagram demonstrating highly correlated genes with PSMB8 overlapping or exclusively expressed in the basal-like or luminal A

tumours. **B.** Heat map demonstrating the relative expression of highly correlated genes with PSMB8 in luminal and basal-like breast tumours. **C.** Major biological functional classification of immuno-proteasome co-expressed genes exclusive to either basal-like or luminal A breast tumours using the FunRich analysis software (<http://www.funrich.org>). (Pathan et al., 2015)

The interferon-gamma mediated signaling pathway

The interferon gamma mediated signaling pathway was highly represented in the i-proteasome co-expressed gene set (Figure 2C). Interferon- γ (IFNG) is a major inducer of the immuno-proteasome (Aki et al., 1994). Although the relative expression of IFNG was low among the basal-like breast samples (median expression 6.5 RSEM) this expression was significantly correlated with the levels of the i-proteasome expression (correlation expression levels IFNG and PSMB8, $r=0.62$). There was no significant correlation of IFNG with the expression of the c-proteasome (correlation of IFNG and PSMB5 expression, $r=-0.08$, ns). In addition, the levels of interferon gamma were strongly correlated with levels of TBX21 ($r=0.80$, median expression 26.8 RSEM) and CIITA ($r=0.69$, median expression 286.2 RSEM). TBX21 protein (T-bet) is a T-cell (Th1)-specific transcription factor that controls the expression of the cytokine interferon-gamma (IFN γ) (Oh & Hwang, 2014) and CIITA is the master controller of the MHC class II response (Downs, Vijayan, Sidiq, & Kobayashi, 2016). These data suggest that interferon- γ originates from infiltrating hematopoietic cells in the breast cancers. Interferon- γ can drive the expression of i-proteasome via the transcription factor IRF1 resulting in expression of MHC class I (Namiki et al., 2005). IRF1 expression was significantly correlated with i-proteasome expression in basal-like breast cancers ($r=0.81$). We speculate that a subset of basal-like breast

cancers are characterized by IFN- γ secreting hematopoietic cells, which as a consequence, drives IRF1 expression and i-proteasome in breast cancer cells. High levels of i-proteasome are associated with increased expression of the MHC I pathway and also expression of the MHC II pathway. It is speculated that in basal-like cancers, high levels of i-proteasome will activate an innate immune response via MHC expression.

We sought to validate this IFN- γ axis in basal and luminal cancer cell lines. As expected, treatment with interferon gamma significantly up-regulated mRNA expression of this axis in both cell lines. In MDA-MB-468, a basal cell line, both IRF1 and PSMB8 were up-regulated >10 fold while STAT1, TAP1 and TAP2 were up-regulated >7 and >3-fold respectively. In MCF7, a luminal cell line, baseline transcript levels of the IFN- γ axis were significantly lower compared to MDA-MB-468. Upon treatment with IFN- γ , IRF1 and PSMB8 levels were up-regulated >20 and 110 fold respectively. These up-regulated PSMB8 levels in treated MCF7 were comparable to that observed for MDA-MB-468 without any IFN- γ treatment. STAT1, TAP1 and TAP2 were also significantly up-regulated. There was no observable effect on the constitutive proteasome since there were only marginal changes in PSMB5 levels in both cell lines.

Silencing-rescue experiments in MDA-MB-468 and MCF7 cells demonstrated that in both cell lines silencing the IFN- γ driven transcription factor IRF1 (>90% silencing achieved with RNAi) significantly down-regulated the majority of its tested targets (Figure 3). In MDA-MB-468, PSMB8 levels decreased over 3-fold, while there was a 50% reduction in STAT1 and TAP2 levels. In MCF7, the effect of IRF1 silencing was more pronounced, with over 5-fold and 14-fold

reduction in PSMB8 and STAT1 mRNA expression and 3-fold reduction of TAP1 and TAP2 levels. Together, the evidence confirms that the IFN- γ -IRF1-STAT1-PSMB8 axis is intact in breast cancer cell lines.

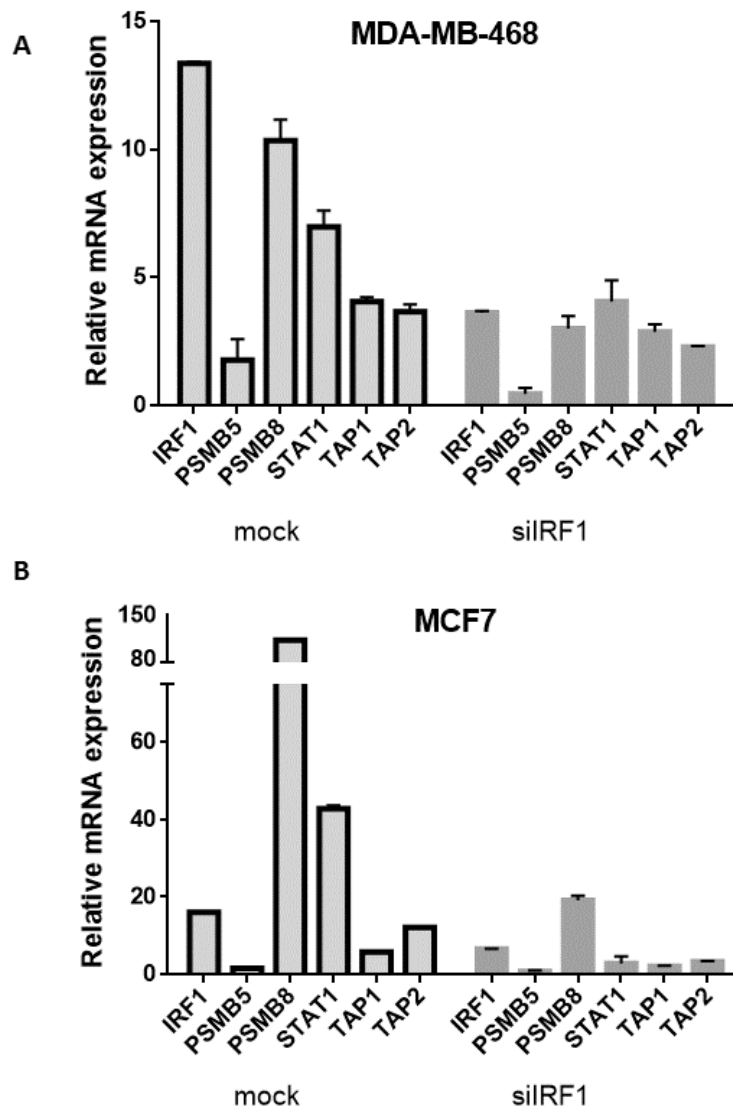


Figure 3. Interferon- γ induced IRF1 signaling axis is intact in both **A.** basal-like MDA-MB-468 and **B.** luminal MCF-7 cells. RT-qPCR analysis of mRNA expression of IFN- γ induced genes in cells transfected with siIRF1 or mock siRNA in the presence or absence of 100U/ml IFN- γ .

Relationship of proteasome expression with breast cancer patient survival

The proteasome is reported to be frequently up-regulated in cancer and therefore it was determined if expression of the proteasome was related to patient survival. As before, PSMB5 and PSMB8 were used as representative of the expression of the c- and i--proteasome respectively as they encode the $\beta 5$ chymotrypsin-like activity, considered to be the predominant activity of the proteasome ([Kisselev et al., 2006](#)). Kaplan Meier analyses of PSMB5 and PSMB8 in the four intrinsic subtypes of breast cancer are summarised in Supplementary Table 5 (Kaplan Meir graphs in Supplementary Figure 2). Low expression of the c-proteasome in luminal A and B cancers was significantly associated with improved survival, while this was non-significant or marginally significant for basal-like and HER2⁺cancers respectively. PSMB8 expression was significantly associated with improved survival in basal-like cancers but was not significantly associated with survival in the luminal or HER2⁺ subgroups (although patient numbers in the latter were limited), Figure 4. Similar results were found for PSMB9 and PSMB10, the other two i-proteasome genes, and also with IRF1. This was not unexpected as these three genes are significantly co-expressed with PSMB8.

High i-proteasome expression (greater than 1.5 times the expression of the c-proteasome, Supplementary Figure 3) is found in 23.1% of basal-like cancers but only 6.5% of luminal A cancers. It is intriguing that expression of the i-proteasome in luminal A cancers does not apparently influence patient survival (Supplementary Table 5). It is possible that in basal-like breast cancers there are specific circulating effector proteins and cytokines that allow a more

efficient initiation and maintenance of the innate immune response than in luminal A cancers. In an approach to identify such basal specific factors, genes with expression highly correlated with PSMB8 message were compared between those basal and luminal A cancers that expressed greater than 2500 RSEM of PSMB8 (Supplementary Table 3). In these high i-proteasome expressing cancers, expression of the classical complement pathway components C1S, C1R, C1Q and C2, is reduced by 43% in luminal A compared with basal-like cancers and in luminal A cancers is not correlated with the presence of the i-proteasome (correlation of C1S with PSMB8 in luminal A: $r=-0.16$, ns; basal: $r=0.57$, $p<0.005$). The classical complement pathway is an effector arm of the immune system and contributes to the destruction of cancer cells in conjunction with antibodies produced by B-cells (Pio, Ajona, & Lambris, 2013). Notably, the alternative complement pathway component C3 is also reduced by 54% in the luminal A compared to basal-like cancers. Interestingly, of 33 breast cancer cell lines that have been clearly defined as basal or ductal-like (Neve et al., 2006) only the basal-like cell lines express high levels of C1S (Supplementary Figure 4). This is significant as several studies suggest that the complement system has the ability to recognise malignant cells and is activated in response to the expression of tumour-associated antigens, with the subsequent deposition of complement components on tumour tissue (Corrales et al., 2012; Gminski, Mykala-Ciesla, Machalski, Drozd, & Najda, 1992; Nishioka, Kawamura, Hirayama, Kawashima, & Shimada, 1976).

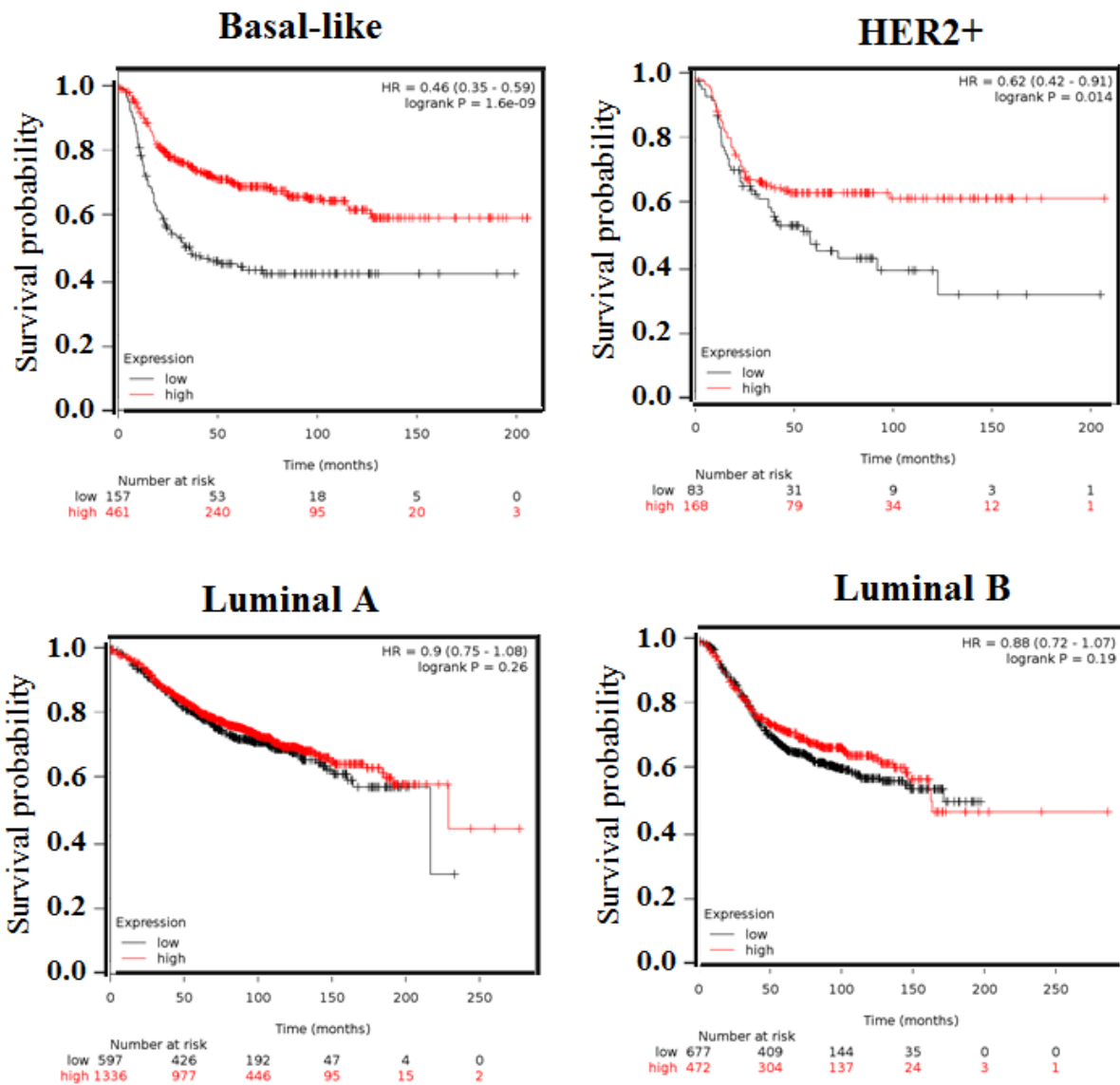


Figure 4. Kaplan Meier survival curves of breast cancer patients are stratified by PSMB8 expression. Survival data derived from Kaplan-Meier plotter (Gyorffy et al., 2010) using “Jetset” best probe set and auto-selection of best cut-off. P values are corrected for multiple testing using Bonferroni correction.

Basal-like breast cancers are addicted to the immuno-proteasome

High levels of the i-proteasome in basal-type breast cancers are associated with increased expression of HLA type I and type II genes and it is speculated that this results in increased host-immune surveillance and consequently a better patient prognosis. Within a basal breast cancer, those cells with high levels of i-proteasome will be expected to be eliminated by immune surveillance, resulting in overall suppression of i-proteasome expression. The persistence of basal-type cancers with high levels of i-proteasome suggests that increased activity of i-proteasome has a function that is essential for survival of these cancer cells. It is suggested that basal-like cancers can become “addicted” to high levels of i-proteasome. The likely basis for this addiction is the role of the i-proteasome in degrading oxidised and misfolded proteins in an ATP independent mechanism ([Sorokin et al., 2009](#)). In rapidly dividing cancer cells with a general breakdown in cellular homeostasis, oxidised and misfolded proteins would be expected to accumulate and have the potential to trigger a persistent “unfolded protein response” resulting in cell apoptosis ([M. Wang & R. J. Kaufman, 2014](#)). Thus we speculate that basal-type breast cancers express i-proteasome genes to enable cell survival by ameliorating the potential to trigger an unfolded protein response. In such cancers, as a consequence of this i-proteasome expression, there is also triggered a host-immune surveillance resulting in superior patient survival.

We next set out to determine if breast cancer cell lines demonstrated i-proteasome addiction. The expectation would be that cancers would vary in their addiction, with the levels of increasing addiction reflected in higher expression of i-proteasome and increasing sensitivity to a proteasome inhibitor such as bortezomib. Accordingly, bortezomib LD₅₀ was determined for each of the breast cancer cell lines (Figure 5A; Supplementary Table 6; Supplementary Figure 5) and the expression of *PSMB5* or *PSMB8* assessed from RNAseq data ([Klijn et al., 2015](#)). The breast cell line bortezomib LD₅₀s were significantly negatively correlated with the expression of *PSMB8* ($r=-0.86$, $p<0.0014$) but not with levels of *PSMB5* ($r=0.59$, $p=0.06$). Basal cell lines together with SKBR3, an ER⁻ PR⁻ HER2⁺ cell line, were on average greater than 25 fold more sensitive to bortezomib compared with the cell lines classified as luminal. Western data further confirmed the variation in i-proteasome in these breast cancer cell lines (Supplementary Figure 6).

These findings were not the consequence of bortezomib preferentially inhibiting the i-proteasome as native in-gel proteasome activity assay showed similar inhibition of total proteasome activity by 0.037 μ M bortezomib in MDA-MB-468 (high levels of i-proteasome and bortezomib LD₅₀ of 0.037 μ M) and MCF-7 (low levels of i-proteasome and bortezomib LD₅₀ of 1 μ M), Figure 5B. While this bortezomib dose was lethal for MDA-MB-468 (>90% cell death), there was minimal effect on MCF7 survival (Figure 5C). However, prolonged monitoring of MCF7 growth following exposure to 0.037 μ M bortezomib showed gradual cessation of cell proliferation

and eventually increasing cell death (Supplementary Figure 7). Therefore, inhibition of the c-proteasome causes cell cycle arrest and increasing cell death only after prolonged treatment. This is consistent with the major role of the c-proteasome in degradation of poly-ubiquitinated proteins that is required for the maintenance of cell homeostasis, in particular, cell division (Julian Adams, 2004; Koepp, 2014). In breast cancer cell lines with high levels of i-proteasome, bortezomib treatment causes rapid cell death and this is suggested to reflect the addiction of such cancers to a unique function provided by the i-proteasome.

To confirm that the observed sensitivity of basal breast cancer cell lines to bortezomib was due to direct i-proteasome inhibition and was not associated with an off-target effects of bortezomib, si-RNAs were used to silence PSMB8 expression in six breast cancer cell lines with varying i-proteasome expression. We predicted that this would have lethal consequences where cell lines were addicted to i-proteasome. This was indeed observed (Figure 5D), with si-RNA knockdown (>80% knockdown achieved in all cell lines) of PSMB8 resulting in induction of 45%, 48% and 39% apoptosis in MDA-MB468, BT-20 and Hs578T respectively. In contrast, ZR751 and MCF7 did not show any significant increase in cell death. The MDA-MB-231 cell line was an exception as although expressing high levels of PSMB8 and being sensitive to bortezomib, knock-down of PSMB8 did not markedly induce apoptosis.

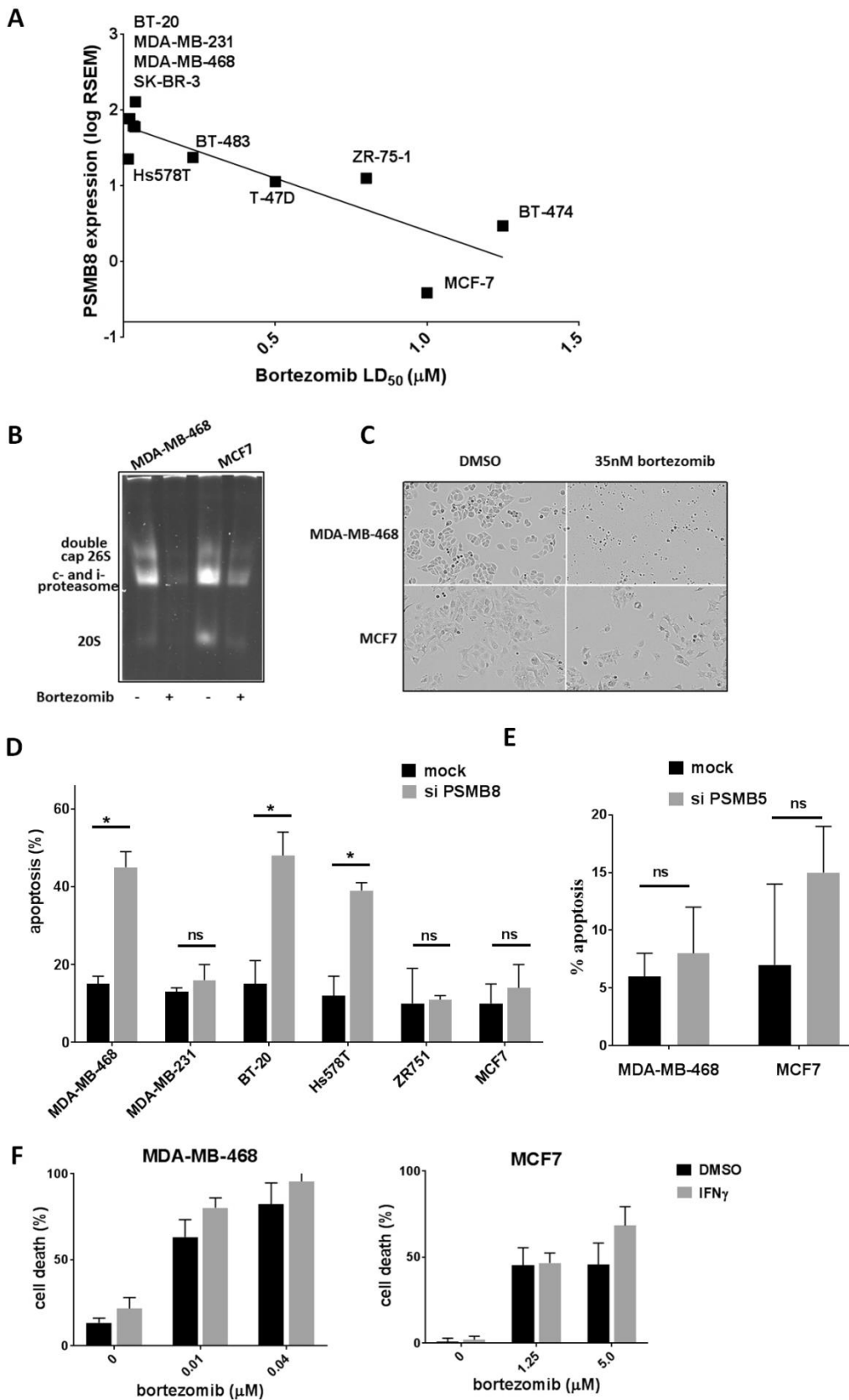


Figure 5. A. The bortezomib sensitivity of breast cancer cells lines is highly correlated with expression of i-proteasome. Bortezomib sensitivity from Table S6 expressed as log base 10, expression of i-proteasome as PSMB8 expression from RNAseq ([Klijn et al., 2015](#)). Cancer subtype as in ([Neve et al., 2006](#)). Bortezomib LD₅₀s determined from dose response graphs presented in Supplementary Figure S4 . **B.** Native in-gel proteasome assay of bortezomib treated breast cancer cell lines. MDA-MB-468 and MCF7 were untreated or treated with 0.037 μ M bortezomib for 2h. Whole cell lysates without detergents together with ATP were electrophoresed on 3.5% acrylamide gels. UV image following incubation with the fluorogenic peptide Suc-LLVY-AMC, a chymotrypsin-like specific substrate. **C.** Incucyte images demonstrating effect of 0.037 μ M bortezomib on MDA-MB-468 and MCF-7 cells after 48h. **D** and **E.** RNAi silencing of PSMB8 for 56h causes apoptosis in basal-like and HER2⁺but not luminal cell lines. PSMB5 silencing has no apoptotic effect on either MDA-MB-468 or MCF-7 cells under the same conditions. **F.** Pre-treatment with IFN- γ treatment (100U/ml) for 24h does not significantly affect sensitivity to bortezomib.

As the sensitivity of breast cancer cells to both bortezomib treatment and RNA interference was related to the levels of the i-proteasome, we next investigated whether treatment with IFN- γ can alter the sensitivity of cell lines to bortezomib. While treatment with 100 U/ml IFN- γ increased PSMB8 levels by 3-fold and 100-fold respectively in MDA-MB-468 and MCF7 (Supplementary Figure 8), sensitivity to bortezomib was not significantly altered (Figure 5F). Thus, i-proteasome levels per se do not determine the sensitivity to bortezomib.

Unfolded protein response in basal-like breast cancers that have i-proteasome addiction

We propose addiction of breast cancers to high levels of the i-proteasome with suppression of proteasome activity triggering ER stress and the unfolded response pathway (UPR). Three signalling pathways responsible for mediating the UPR have been described (Miao Wang & Randal J. Kaufman, 2014). These can be assessed by increased expression of ATF4 while activation of the PERK and IRE1 branches culminate in a spliced form of the X-box transcription factor, XBP1s. XBP1s is a key downstream transcription factor that activates the expression of a wide variety of genes required for protein folding and secretion, as well as clearance of misfolded proteins from ER. To test the effect of proteasome dysfunction on UPR activation, two basal-like and two luminal cell lines were treated with the bortezomib. Bortezomib treatment significantly increased the ATF4 levels by 4-fold and 2-fold in MDA-MB-468 and Hs578T cell lines while in luminal cells, ATF4 increase was only observed for MCF7 cells (Figure 6A).

We also tested whether treatment of MDA-MB-468 cells with bortezomib increased the XBP1s in a time dependent manner. This was indeed observed, with in addition, concomitant with up-regulation of pro-apoptotic genes FOXO3, NOXA, BIM, CASP3 and CASP7. We also observed a significant decrease in NFkB and BCL2 mRNA levels. This is consistent with previous studies in multiple myeloma that show bortezomib has pleotropic anti-cancer effects and causes suppression of anti-apoptotic target genes(Obeng et al., 2006).

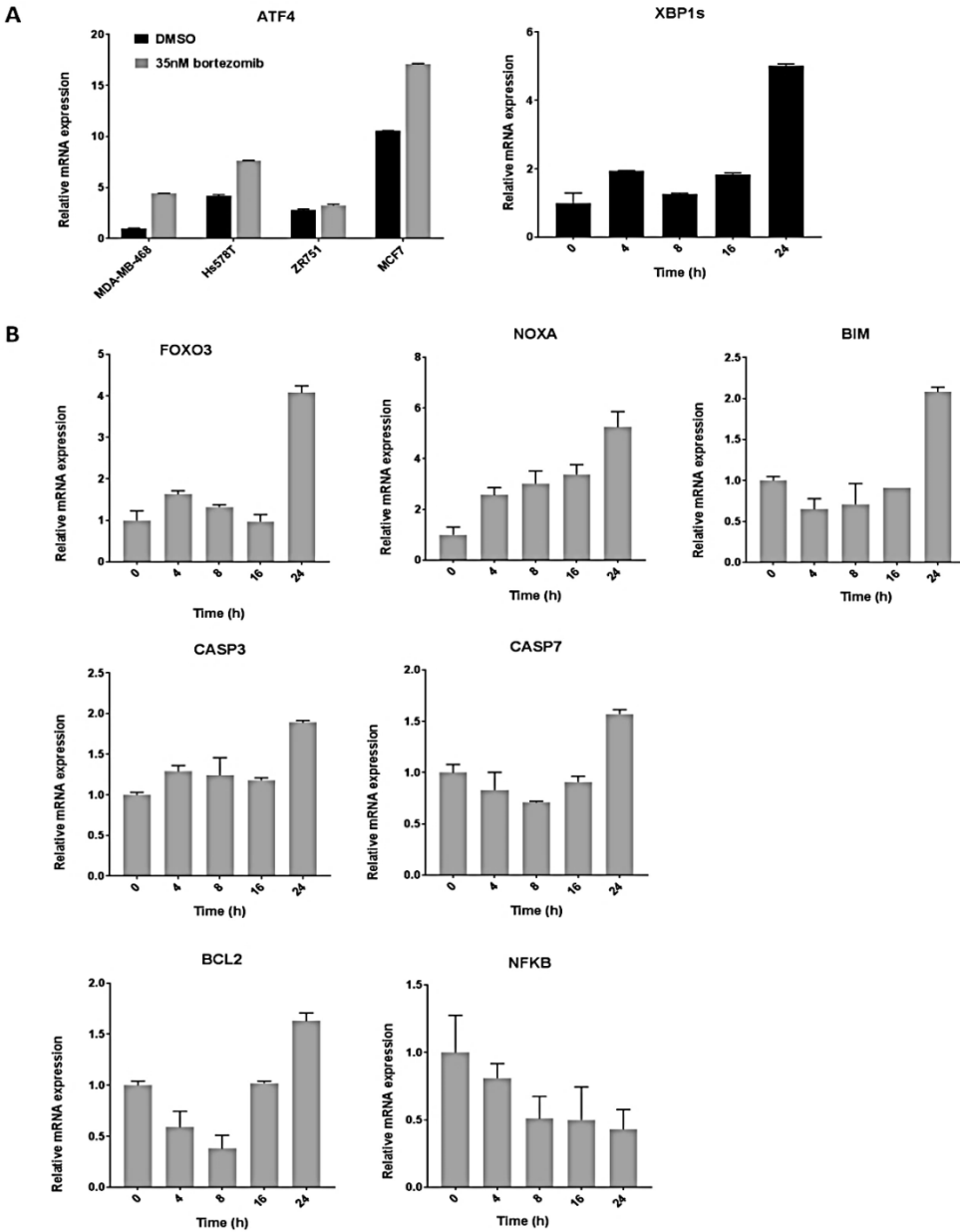


Figure 6. Unfolded protein response pathway in breast cancer cells. A. Cells were treated with 35nM bortezomib or vehicle control for 4h and total mRNA was extracted. ATF4 transcript levels were calculated via qRT-PCR. **B.** MDA-MB-468 cells were treated with 35nM bortezomib and the mRNA expression levels for the FOXO3, NOXA, BIM, CASP3, CASP7, BCL2 and NFkB were calculated.

Discussion

The proteasome has been successfully targeted for the treatment of multiple myeloma, with clinical responses to proteasome inhibitors have been correlated with increased proteasome activity ([Kuhn & Orłowski, 2012](#); [Niewerth et al., 2013](#)). Therefore, in an attempt to address whether proteasome inhibition can be a viable treatment for breast cancer, we analysed mRNA expression data from the TCGA breast cancer cohort. Unexpected was the observed variation in i-proteasome expression, with particularly high levels in a proportion of basal-like and HER2⁺ breast cancers. Based on our finding that the bortezomib LD₅₀ of breast cancer cell lines closely parallels the levels of i-proteasome, we propose that high levels of the i-proteasome are required for a critical function in these breast cancers. It has been previously proposed from siRNA lethality screens of breast epithelial cell lines that basal-like breast cancer cells have a proteasome addiction ([Petrocca et al., 2013](#)), although this was not specifically attributed to the i-proteasome. We propose that the basis for the i-proteasome addiction is its role in the maintenance of protein homeostasis ([Seifert et al., 2010](#)) rather than its specific role in production of class I antigens.

Our data are consistent with addiction specifically restricted to expression of the i-proteasome. Specific RNA interference of the i-proteasome subunit PSMB8 causes rapid cell death in basal-like and HER2⁺ but not in luminal cancer cells, whereas under the same conditions, silencing of the PSMB5 subunit of the c-proteasome does not have any cytotoxic effects. Since the half-life of the c-proteasome is >120h ([Heink, Ludwig, Kloetzel, & Krüger, 2005](#)), it is possible that

prolonged silencing of PSMB5 is required to induce cell death. However, although blanket inhibition of total proteasome activity by the same concentration of bortezomib is observed by native in-gel activity assays (Figure 5B) in both a basal-like and luminal cell line, there is no effect on the viability of the luminal cell line. In addition, treatment with 100u/ml IFN- γ does not increase the cytotoxic sensitivity of breast cancer cell lines to bortezomib despite increasing total i-proteasome levels. The latter observation provides a distinction between the intrinsically up-regulated i-proteasome levels that are observed in basal-like and HER2⁺ cells that are critical for survival and the up-regulation by extrinsic means, for example IFN- γ treatment, that has little or no effect on this addiction.

This has notable implications for therapeutic intervention, as tumours possessing high levels of i-proteasome are predicted to be responsive to clinically available proteasome inhibitors. We observed substantial heterogeneity in mRNA and protein expression of i-proteasome subunits among breast cancer subtypes, with basal-like and HER2⁺ cancers having higher levels of i-proteasome expression than luminal cancers. Up-regulation of i-proteasome activity in these cancers is likely to be dependent on an interplay between their genetic instability, metabolic demands and requirement for degradative capacity of oxidised and unfolded proteins. As both basal-like and HER2⁺ breast cancers are generally associated with high rates of cancer cell proliferation and genomic instability ([Shaver et al., 2016](#)), this is likely to drive high levels of oxidised and misfolded proteins. To accommodate this, there is an increase in their degradative capacity by up-regulating the i-proteasome. The i-proteasome is labile and also has the capacity to degrade proteins without the requirement for ATP. This is consistent with the observation

that while the c-proteasome levels remain constant in most cancers, i-proteasome levels are highly heterogeneous. If i-proteasome function is inhibited in such cancers, for example with bortezomib treatment, the endoplasmic reticulum stress and the UPR response will be triggered. We show that bortezomib treatment of a basal breast cancer cell line activates multiple branches of the IRE-1-XBP1 axis and consequently leads to cell death consistent with the up-regulation of NOXA, FOXO, BIM and down-regulation of NFκB. These results are consistent with studies in multiple myeloma where treatment with bortezomib initiates the UPR stress pathways ([Dong et al., 2009](#); [Obeng et al., 2006](#)).

An immune response gene expression module has been shown to identify a good prognosis subtype in estrogen receptor negative breast cancer ([Teschendorff, Miremadi, Pinder, Ellis, & Caldas, 2007](#)). In this context, recognition of tumour-associated antigens by TILs is a significant contributor to the detection and ultimate destruction of tumour cells ([del Campo, Carretero, Aptsiauri, & Garrido, 2012](#)). In our analysis, i-proteasome subunit PSMB8 was significantly correlated with good outcome in basal-like and HER2⁺ cases but not in luminal A and luminal B patients. It is expected that the up-regulated i-proteasomes in the presence of intact HLA expression and IFN-γ signaling pathways contribute to a more efficient and robust immune signal that is recognised by circulating TILs. However, it is unlikely to be the whole story as only a very small fraction of all antigens, even in the context of small cell lung cancer with extremely high mutation rates, are able to evoke a T cell response ([Tripathi et al., 2016](#)). A possible explanation is that the immunogenicity of a tumour is determined by both the uniqueness and adequate levels of that antigen. Genome sequencing studies show that most tumours have

point mutations in protein coding sequences, however only a small proportion will elicit an innate immune response via HLA mediated display of the i-proteasome degraded peptides. Although the mutation rates in basal-like cancers are not high, they are associated with high levels of genomic instability, which would be predicted to generate high levels of novel proteins. Recent developments in the analysis of RNAseq data have identified high rates of hybrid and novel transcripts in basal breast cancer ([Shaver et al., 2016](#)) and it would be predicted that these are potentially immunogenic. This may provide the basis for the improved prognosis of basal breast cancers expressing high levels of the i-proteasome.

In conclusion, we propose that to alleviate the UPR driven consequences of high mutational load and metabolic demands, cancers preferentially up-regulate i-proteasome activity. By appropriate screening with i-proteasome as a marker, cancers can be identified with i-proteasome addiction which can then be therapeutically exploited by treatment with proteasome inhibitors. In such cancers, there is a secondary, unintentional consequence of i-proteasome up-regulation. Due to its optimal peptide cleave specificity and enhanced degradative capacity, this up-regulated activity of the i-proteasome leads to an increased and diverse peptide pool and capacity to display antigenic peptide-MHCI repertoires on the surface of the cancer cells. This results in more efficient detection of cancer cells by the circulating TILs. Such incoming TILs release cytokines such as IFN- γ which has two effects in the in tumour microenvironment, upregulation of the i-proteasome-MHC axis and release of cytokines to further reinforce TIL recruitment. This positive feedback loop increases the efficiency of host anti-cancer surveillance which translates into an improved patient prognosis.

Materials and Methods

In silico analysis

Breast cancer RNA sequencing data was accessed from cBioPortal ([Cerami et al., 2012](#); [Gao et al., 2013](#)). The mRNA expression (RNA Seq V2 RSEM) was from TCGA as cited in [Ciriello et al. \(Ciriello et al., 2015\)](#). Intrinsic breast cancer subgroups categorised as basal-like, luminal A, luminal B and HER2⁺ were used. Gene expression data in cell lines were from the cancer cell line Encyclopaedia ([Barretina et al., 2012](#)) accessed via cBioPortal. Kaplan Meier analyses used the online Kaplan-Meier Plotter ([Szasz et al., 2016](#)).

Cell lines

All human breast carcinoma cancer cell lines were purchased from the American Type Culture Collection (ATCC, Manassas, VA, USA). MDA-MB-468, MDA-MB-231, BT-20 and Hs578T were cultured in DMEM. SKBR3 and BT-474 were cultured in RPMI. BT483 was cultured in RPMI with 20% FBS, 0.01mg/ml Insulin (Sigma-Aldrich, MO, USA). T47D was cultured in RPMI, 1mM sodium pyruvate (GIBCO, Grand Island, NY) and 0.01mg/ml insulin. ZR751 were cultured in RPMI and 1mM sodium pyruvate. MCF7 was cultured in RPMI with 0.01mg/ml insulin. MCF10A was cultured in DMEM/F12: (1:1) (Invitrogen) with 5% horse serum (Invitrogen), 10 µg/ml insulin, 20 ng/ml human epidermal growth factor (Sigma-Aldrich, MO, USA), 100 ng/ml cholera toxin, and 500 ng/ml hydrocortisone (Sigma-Aldrich, MO, USA). All cell lines were supplemented with 10% (v/v) fetal bovine serum (FBS, Sigma-Aldrich, MO,USA) unless stated otherwise, as well as 1% (vol/vol) penicillin (100 U/mL), streptomycin (100 U/mL), and 1%

(vol/vol) L-glutamine (PSG, all from GIBCO-BRL, Grand Island, NY). Cells were regularly screened for Mycoplasma (Lonza, Basel, Switzerland).

Western blot

Cells were trypsinised, centrifuged at 300g for 5min and washed twice with PBS. Cell were lysed using cell culture lysis buffer (100 mmol/L HEPES, pH 7.5, 2 mmol/L EDTA, 100 mmol/L NaF, 500 mmol/L sodium chloride, 50 µg/mL trypsin inhibitor) (Promega) containing cOmplete Mini Protease Inhibitor (Roche). The supernatant was collected and protein concentration was determined using the BCA protein assay (ThermoFisher Scientific, MA, USA). Whole protein lysates (5–20 µg) were resolved using SDS PAGE electrophoresis, and probed overnight at 4 °C with the following primary antibodies: PSMB5 (Cell signalling, 1:1000), PSMB6 (Cell Signalling, 1:1000), PSMB7 (Cell Signalling, 1:1000), PSMB8 (Cell Signalling, 1:1000), β-tubulin (Sigma-Aldrich, 1:200). Chemiluminescent detection of protein was done using appropriate secondary antibodies conjugated with horseradish peroxidase (Amersham) and the enhanced chemiluminescence kit according to the manufacturer's instructions (Amersham).

Native in gel activity assay

Total chymotrypsin-like activity of the proteasome was measured in freshly prepared cell lysates as described previously, with some minor modifications to the protocol. In brief, a total of 5×10^6 cells were washed 3 times with ice-cold PBS and spun down by centrifugation (5 minutes, 250g, 4°C). Cell pellets were then resuspended in an ATP-containing lysis buffer (10 mM Tris-HCl buffer (pH 7.8) containing 5 mM ATP, and 5 mM MgCl₂) and kept on ice for 10

minutes. For complete lysis, cells were sonicated (MSE sonicator, amplitude 15, for 10 seconds at 4°C) followed by centrifugation (5 minutes, 16 000g, 4°C) to remove cell debris. Forty microlitres of whole cell lysate from each of the cell lines were run on a 3.5% non-denaturing polyacrylamide gel (BIO-RAD, CA, USA) in 10mM Tris-HCl buffer supplemented with 0.5mM ATP (Sigma-Aldrich, MO, USA), 5mM MgCl₂, 10% (v/v) glycerol, 0.5 mM DTT). The gel was run at 35 V for 30 min in a 4°C cold cabinet, thereafter the voltage was increased to 75 V for four hours. Peptidolytic activity of proteasomes was detected after incubating the gels in a Suc-LLVY-MCA substrate dissolved in 50 mM Tris pH 8.0, 5 mM MgCl₂, 1 mM DTT, 2 mM ATP, and 0.02% SDS for 10 min at 37°C. Proteasome bands were identified by the release of highly fluorescent, free AMC under UV light (ChemiDoc, BIO-RAD). Fluorescence was quantitated using ImageJ software (<http://imagej.nih.gov/ij/>).

Determination of LD₅₀

Cells were seeded in 96-well microtiter plates at a density of 2×10^4 cells/well with varying concentrations of bortezomib. Cells were harvested 48 hours post-treatment, centrifuged at $1,300 \times g$, washed in phosphate buffered saline (PBS) and stained with 7-amino-actinomycin-D solution ($2 \mu\text{g}/\text{mL}$) (7AAD, Invitrogen) for 10 minutes at room temperature. Viable cells were determined with the use of a FACS Calibur flow cytometer (Becton Dickinson Immunocytometry Systems), and analyzed with the use of FLOWJO (Tree Star Inc.) and GraphPad Prism (GraphPad Software Inc. version 6).

RNA interference (RNAi)

For RNA inhibition studies, approximately 3×10^5 cells/well were seeded in six-well plates. Cells were transfected with 50 nM of the following siRNAs (GenePharma): PSMB8 - CCACUCACAGAGACAGCUAAU; IRF1- GAAAGUUGGCCUCCACGUCU; PSMB5- AAGCUCAUAGAUUCGACAUUG; non-coding RNA- UUCUCCGAACGUGUCACGUTT using Lipofectamine RNAiMAX reagent (Invitrogen) following the manufacturer's instructions. Cells were harvested 72 hours post-transfection for further experiments. The RNA interference efficiency for interference of PSMB8 was determined using qPCR.

Real-time Cell attachment

Cells were seeded in 24 well plates (50,000 cells/wells in triplicate) with cell attachment monitored qualitatively over a 24h period using IncuCyte live-cell imaging system (Essen BioScience, Ann Arbor, MI). Phase-contrast images were taken every hour.

qPCR

Total RNA was extracted from cultured cells using RNeasy mini kit (Qiagen). One microgram of total RNA was reverse transcribed using MMLV reverse transcriptase (Life Technologies). qPCR was performed using SYBR Green mastermix and run on a CFX96 Bio-Rad real time PCR machine. Primer sequences are presented in Table 1. Experiments were repeated three times. For each sample results were normalized to expression of GAPDH .

PSMB5	CCGCGCTCTACCTTACCTACCT GCATGGCTTAATCTTTGAGACAAG	PSMB6	CAAGCTGACACCTATTACAGAC CGGTATCGGTAACACATCTCCT
PSMB8	CGTCACCAACTGGGACGACA CTTCTCGCGTTGGCCTTGG	PSMB7	ATCGCTGGGGTGGTCTATAAG AAGAAATGAGCTGGTTGTCAT
IRF1	AGCTCAGCTGTGCGAGTGTA TAGCTGCTGTGGTCATCAGG	FOXO3	TCTTCAGGTCCTCCTGTTCTG GGAAGCACCAAAGAAGAGAGAAG
STAT1	CGGGCTCCTTCTTCGGATTC CAGAGGTAGACAGACCACC	NOXA	AGAGCTGGAAGTCGAGTGT GCACCTTACATTCTCTC
XBP1	TCCTGTTGGGCATTCTGGAC GGCTGGTAAGGAACTGGGTC	BIM	GTATTCGGTTCGCTGCGTTC GCGTTTCTCAGTCCGAGAGT
TAP1	TAGTCTGGGCAGGCCACTTT CTCGGAAAGTCCCAGGAACA	CASP3	TGCTATTGTGAGGCGGTTGT TCACGGCCTGGGATTTCAAG
TAP2	AGTGCTGGTGATTGCTCACA GAACCAGGCGGGAATAGAGG	CASP 7	GTGGGAACGATGGCAGATGA GAGGGACGGTACAAACGAGG
ATF4	CTTGATGTCCCCCTTCGACC GAAGGCATCCTCCTTGCTGT	BCL2	GTGAAGTCAACATGCCTGCC ACAGCCTGCAGCTTTGTTTC
		NFKB	CGCGCCGCTTAGGAGGGAGA GGGCCATCTGCTGTTGGCAGT

References

1. Adams, J. (2004). The Proteasome in Cell-Cycle Regulation. In J. Adams (Ed.), *Proteasome Inhibitors in Cancer Therapy* (pp. 77-84). Totowa, NJ: Humana Press.
2. Adams, J. (2004). The proteasome: a suitable antineoplastic target. *Nat Rev Cancer*, 4(5), 349-360. doi: 10.1038/nrc1361
3. Aki, M., Shimbara, N., Takashina, M., Akiyama, K., Kagawa, S., Tamura, T., . . . Ichihara, A. (1994). Interferon-gamma induces different subunit organizations and functional diversity of proteasomes. *J Biochem*, 115(2), 257-269.
4. Altun, M., Galardy, P. J., Shringarpure, R., Hideshima, T., LeBlanc, R., Anderson, K. C., . . . Kessler, B. M. (2005). Effects of PS-341 on the activity and composition of proteasomes in multiple myeloma cells. *Cancer Res*, 65(17), 7896-7901. doi: 10.1158/0008-5472.can-05-0506
5. Barretina, J., Caponigro, G., Stransky, N., Venkatesan, K., Margolin, A. A., Kim, S., . . . Garraway, L. A. (2012). The Cancer Cell Line Encyclopedia enables predictive modelling of anticancer drug sensitivity. *Nature*, 483(7391), 603-607. doi: 10.1038/nature11003
6. Cerami, E., Gao, J., Dogrusoz, U., Gross, B. E., Sumer, S. O., Aksoy, B. A., . . . Schultz, N. (2012). The cBio cancer genomics portal: an open platform for exploring multidimensional cancer genomics data. *Cancer Discov*, 2(5), 401-404. doi: 10.1158/2159-8290.CD-12-0095
7. Ciriello, G., Gatza, M. L., Beck, A. H., Wilkerson, M. D., Rhie, S. K., Pastore, A., . . . Perou, C. M. (2015). Comprehensive Molecular Portraits of Invasive Lobular Breast Cancer. *Cell*, 163(2), 506-519. doi: 10.1016/j.cell.2015.09.033

8. Corrales, L., Ajona, D., Rafail, S., Lasarte, J. J., Riezu-Boj, J. I., Lambris, J. D., . . . Pio, R. (2012). Anaphylatoxin C5a creates a favorable microenvironment for lung cancer progression. *J Immunol*, 189(9), 4674-4683. doi: 10.4049/jimmunol.1201654
9. del Campo, A. B., Carretero, J., Aptsiauri, N., & Garrido, F. (2012). Targeting HLA class I expression to increase tumour immunogenicity. *Tissue Antigens*, 79(3), 147-154. doi: 10.1111/j.1399-0039.2011.01831.x
10. Dong, H., Chen, L., Chen, X., Gu, H., Gao, G., Gao, Y., & Dong, B. (2009). Dysregulation of unfolded protein response partially underlies proapoptotic activity of bortezomib in multiple myeloma cells. *Leukemia & Lymphoma*, 50(6), 974-984. doi: 10.1080/10428190902895780
11. Downs, I., Vijayan, S., Sidiq, T., & Kobayashi, K. S. (2016). CITA/NLRC5: A critical transcriptional regulator of MHC class I gene expression. *Biofactors*, 42(4), 349-357. doi: 10.1002/biof.1285
12. Engel, R. H., Brown, J. A., Von Roenn, J. H., O'Regan, R. M., Bergan, R., Badve, S., . . . Gradishar, W. J. (2007). A phase II study of single agent bortezomib in patients with metastatic breast cancer: a single institution experience. *Cancer Invest*, 25(8), 733-737. doi: 10.1080/07357900701506573
13. Forero, A., Li, Y., Chen, D., Grizzle, W. E., Updike, K. L., Merz, N. D., . . . Varley, K. E. (2016). Expression of the MHC Class II Pathway in Triple-Negative Breast Cancer Tumour Cells Is Associated with a Good Prognosis and Infiltrating Lymphocytes. *Cancer Immunol Res*, 4(5), 390-399. doi: 10.1158/2326-6066.CIR-15-0243

14. Gao, J., Aksoy, B. A., Dogrusoz, U., Dresdner, G., Gross, B., Sumer, S. O., . . . Schultz, N. (2013). Integrative analysis of complex cancer genomics and clinical profiles using the cBioPortal. *Sci Signal*, 6(269), pl1. doi: 10.1126/scisignal.2004088
15. Gminski, J., Mykala-Ciesla, J., Machalski, M., Drozd, M., & Najda, J. (1992). Immunoglobulins and complement components levels in patients with lung cancer. *Rom J Intern Med*, 30(1), 39-44.
16. Gyorfyy, B., Lanczky, A., Eklund, A. C., Denkert, C., Budczies, J., Li, Q., & Szallasi, Z. (2010). An online survival analysis tool to rapidly assess the effect of 22,277 genes on breast cancer prognosis using microarray data of 1,809 patients. *Breast Cancer Res Treat*, 123(3), 725-731. doi: 10.1007/s10549-009-0674-9
17. Heink, S., Ludwig, D., Kloetzel, P.-M., & Krüger, E. (2005). IFN- γ -induced immune adaptation of the proteasome system is an accelerated and transient response. *Proceedings of the National Academy of Sciences of the United States of America*, 102(26), 9241-9246. doi: 10.1073/pnas.0501711102
18. Ho, Y. K., Bargagna-Mohan, P., Wehenkel, M., Mohan, R., & Kim, K. B. (2007). LMP2-specific inhibitors: chemical genetic tools for proteasome biology. *Chem Biol*, 14(4), 419-430. doi: 10.1016/j.chembiol.2007.03.008
19. Kisselev, A. F., Callard, A., & Goldberg, A. L. (2006). Importance of the different proteolytic sites of the proteasome and the efficacy of inhibitors varies with the protein substrate. *J Biol Chem*, 281(13), 8582-8590. doi: 10.1074/jbc.M509043200

20. Klijn, C., Durinck, S., Stawiski, E. W., Haverty, P. M., Jiang, Z., Liu, H., . . . Zhang, Z. (2015). A comprehensive transcriptional portrait of human cancer cell lines. *Nat Biotechnol*, 33(3), 306-312. doi: 10.1038/nbt.3080
21. Koepp, D. M. (2014). Cell cycle regulation by protein degradation. *Methods Mol Biol*, 1170, 61-73. doi: 10.1007/978-1-4939-0888-2_4
22. Kuhn, D. J., & Orlowski, R. Z. (2012). The Immunoproteasome as a Target in Hematologic Malignancies. *Seminars in hematology*, 49(3), 10.1053/j.seminhematol.2012.1004.1003. doi: 10.1053/j.seminhematol.2012.04.003
23. Namiki, S., Nakamura, T., Oshima, S., Yamazaki, M., Sekine, Y., Tsuchiya, K., . . . Watanabe, M. (2005). IRF-1 mediates upregulation of LMP7 by IFN-gamma and concerted expression of immunosubunits of the proteasome. *FEBS Lett*, 579(13), 2781-2787. doi: 10.1016/j.febslet.2005.04.012
24. Neve, R. M., Chin, K., Fridlyand, J., Yeh, J., Baehner, F. L., Fevr, T., . . . Gray, J. W. (2006). A collection of breast cancer cell lines for the study of functionally distinct cancer subtypes. *Cancer Cell*, 10(6), 515-527. doi: 10.1016/j.ccr.2006.10.008
25. Niewerth, D., Franke, N. E., Jansen, G., Assaraf, Y. G., van Meerloo, J., Kirk, C. J., . . . Cloos, J. (2013). Higher ratio immune versus constitutive proteasome level as novel indicator of sensitivity of pediatric acute leukemia cells to proteasome inhibitors. *Haematologica*, 98(12), 1896-1904. doi: 10.3324/haematol.2013.092411
26. Nishioka, K., Kawamura, K., Hirayama, T., Kawashima, T., & Shimada, K. (1976). The complement system in tumour immunity: significance of elevated levels of complement in tumour bearing hosts. *Ann N Y Acad Sci*, 276, 303-315.

27. Obeng, E. A., Carlson, L. M., Gutman, D. M., Harrington, W. J., Lee, K. P., & Boise, L. H. (2006). Proteasome inhibitors induce a terminal unfolded protein response in multiple myeloma cells. *Blood*, 107(12), 4907-4916. doi: 10.1182/blood-2005-08-3531
28. Oh, S., & Hwang, E. S. (2014). The role of protein modifications of T-bet in cytokine production and differentiation of T helper cells. *J Immunol Res*, 2014, 589672. doi: 10.1155/2014/589672
29. Parker, J. S., Mullins, M., Cheang, M. C., Leung, S., Voduc, D., Vickery, T., . . . Bernard, P. S. (2009). Supervised risk predictor of breast cancer based on intrinsic subtypes. *J Clin Oncol*, 27(8), 1160-1167. doi: 10.1200/JCO.2008.18.1370
30. Pathan, M., Keerthikumar, S., Ang, C.-S., Gangoda, L., Quek, C. Y. J., Williamson, N. A., . . . Mathivanan, S. (2015). FunRich: An open access standalone functional enrichment and interaction network analysis tool. *PROTEOMICS*, 15(15), 2597-2601. doi: 10.1002/pmic.201400515
31. Petrocca, F., Altschuler, G., Tan, S. M., Mendillo, M. L., Yan, H., Jerry, D. J., . . . Lieberman, J. (2013). A genome-wide siRNA screen identifies proteasome addiction as a vulnerability of basal-like triple-negative breast cancer cells. *Cancer Cell*, 24(2), 182-196. doi: 10.1016/j.ccr.2013.07.008
32. Pio, R., Ajona, D., & Lambris, J. D. (2013). Complement inhibition in cancer therapy. *Semin Immunol*, 25(1), 54-64. doi: 10.1016/j.smim.2013.04.001
33. Seifert, U., Bialy, L. P., Ebstein, F., Bech-Otschir, D., Voigt, A., Schroter, F., . . . Kruger, E. (2010). Immunoproteasomes preserve protein homeostasis upon interferon-induced oxidative stress. *Cell*, 142(4), 613-624. doi: 10.1016/j.cell.2010.07.036

34. Shaver, T. M., Lehmann, B. D., Beeler, J. S., Li, C.-I., Li, Z., Jin, H., . . . Pietenpol, J. A. (2016). Diverse, Biologically Relevant, and Targetable Gene Rearrangements in Triple-Negative Breast Cancer and Other Malignancies. *Cancer Res*, 76(16), 4850-4860. doi: 10.1158/0008-5472.can-16-0058
35. Shringarpure, R., Grune, T., Mehlhase, J., & Davies, K. J. (2003). Ubiquitin conjugation is not required for the degradation of oxidized proteins by proteasome. *J Biol Chem*, 278(1), 311-318. doi: 10.1074/jbc.M206279200
36. Sorokin, A. V., Kim, E. R., & Ovchinnikov, L. P. (2009). Proteasome system of protein degradation and processing. *Biochemistry (Mosc)*, 74(13), 1411-1442.
37. Szasz, A. M., Lanczky, A., Nagy, A., Forster, S., Hark, K., Green, J. E., . . . Gyorffy, B. (2016). Cross-validation of survival associated biomarkers in gastric cancer using transcriptomic data of 1,065 patients. *Oncotarget*. doi: 10.18632/oncotarget.10337
38. Teschendorff, A. E., Miremadi, A., Pinder, S. E., Ellis, I. O., & Caldas, C. (2007). An immune response gene expression module identifies a good prognosis subtype in estrogen receptor negative breast cancer. *Genome Biol*, 8(8), R157. doi: 10.1186/gb-2007-8-8-r157
39. Ting, J. P., & Trowsdale, J. (2002). Genetic control of MHC class II expression. *Cell*, 109 Suppl, S21-33.
40. Tripathi, S. C., Peters, H. L., Taguchi, A., Katayama, H., Wang, H., Momin, A., . . . Ostrin, E. J. (2016). Immunoproteasome deficiency is a feature of non-small cell lung cancer with a mesenchymal phenotype and is associated with a poor outcome. *Proceedings of the National Academy of Sciences*, 113(11), E1555-E1564. doi: 10.1073/pnas.1521812113

41. Wang, M., & Kaufman, R. J. (2014). The impact of the endoplasmic reticulum protein-folding environment on cancer development. *Nat Rev Cancer*, 14(9), 581-597. doi: 10.1038/nrc3800
42. Wang, M., & Kaufman, R. J. (2014). The impact of the endoplasmic reticulum protein-folding environment on cancer development. *Nat Rev Cancer*, 14(9), 581-597. doi: 10.1038/nrc3800
43. Wehenkel, M., Ban, J. O., Ho, Y. K., Carmony, K. C., Hong, J. T., & Kim, K. B. (2012). A selective inhibitor of the immunoproteasome subunit LMP2 induces apoptosis in PC-3 cells and suppresses tumour growth in nude mice. *Br J Cancer*, 107(1), 53-62. doi: 10.1038/bjc.2012.243
44. Yang, C. H., Gonzalez-Angulo, A. M., Reuben, J. M., Booser, D. J., Puztai, L., Krishnamurthy, S., Cristofanilli, M. (2006). Bortezomib (VELCADE) in metastatic breast cancer: pharmacodynamics, biological effects, and prediction of clinical benefits. *Ann Oncol*, 17(5), 813-817. doi: 10.1093/annonc/mdj131

Supplementary Material

Supplementary Table 1. Expression of proteasome subunits across different breast cancer subtypes.

		c-proteasome					i-proteasome				
		19S cap		β 5c	β 1c	β 2c	11S (PA28) cap		β 5i	β 1i	β 2i
		PSMC 1	PSMD1	PSM B5	PSMB 6	PSM B7	PSME1	PSME2	PSMB8	PSMB 9	PSMB10
BASAL-like	Mean	670	2865	2631	1754	2584	2875	2716	2324	1142	1133
	SEM	28	87	101	70	128	163	182	154	106	82
HER2	Mean	801	3298	2937	1609	2740	4148	3304	2121	791	1090
	SEM	65	116	174	90	191	403	331	256	100	142
LumA	Mean	555	2522	2061	1433	1972	3960	2306	1536	463	780
	SEM	13	39	52	37	41	103	87	69	29	39
LumB	Mean	666	2984	2610	1511	2273	4551	3033	1795	680	759
	SEM	22	80	114	56	78	201	169	115	68	51

Expression expressed as RSEM derived from RNAseq data (Ciriello et al., 2015); SEM: Standard error of mean.

Supplementary Table 2. Correlations between expressions of c- and i-proteasome subunits in breast cancer subtypes.

Breast cancer subgroup	PSMB5 vs PSMB6	PSMB5 vs PSMB7	PSMB6 vs PSMB7	PSMB8 vs PSMB9	PSMB8 vs PSMB10	PSMB9 vs PSMB10	PSMB5 vs PSMB8
Basal-like	0.46	0.29 ns	0.30 ns	0.91	0.77	0.79	0.01 ns
HER2	0.63	0.50	0.54	0.95	0.48	0.50	0.17 ns
Lum A	0.42	0.56	0.48	0.86	0.82	0.79	0.27
Lum B	0.45	0.37	0.35	0.84	0.67	0.54	0.29 ns

Correlation coefficients statistically significant ($p < 0.01$ with Bonferroni correction) unless indicated. ns-not significant.

Supplementary Table 3. Basal-like and luminal A breast cancer cases with expression of >2500

RSEM PSMB8.

Gene	Basal-like breast cancer			Luminal A breast cancer		
	Co-expression with PSMB8	Average expression	RSEM	Co-expression with PSMB8	Average expression	RSEM
ACSL5	0.36	1048.03		0.13	640.32	
APOL1	0.35	3407.02		0.43	2843.47	
APOL2	0.60	1394.49		0.42	1418.60	
APOL3	0.53	1529.15		0.44	1248.63	
B2M	0.24	86320.13		0.60	73047.57	
BTN3A2	0.38	2386.53		0.53	1996.33	
C1QA	0.28	4719.39		0.56	2381.88	
C1S	0.57	18930.23		-0.16	8117.87	
CCL5	0.30	3366.94		0.56	1416.05	
CD2	0.37	897.83		0.45	571.72	
CD74	0.59	86455.96		0.52	68460.55	
CIITA	0.38	967.43		0.35	433.81	
CORO1A	0.47	2140.68		0.60	1815.36	
CXCL9	0.22	8159.66		0.28	3565.02	
FCER1G	0.27	1191.62		0.16	606.02	
FERMT3	0.39	856.66		0.54	603.90	
FMNL1	0.37	1047.33		0.37	778.95	
GBP1	0.36	7916.98		0.22	1749.36	
GBP2	0.21	4394.59		0.13	2488.62	
GBP4	0.21	4211.08		0.35	1653.19	
GBP5	0.23	3474.53		0.29	599.90	
HCLS1	0.29	1550.66		0.37	1078.15	
HLA-A	0.55	47843.13		0.77	39174.51	
HLA-B	0.51	72681.09		0.84	69223.83	
HLA-C	0.37	40223.73		0.78	42023.00	
HLA-DMA	0.58	2980.80		0.35	2087.84	
HLA-DMB	0.38	2207.65		0.27	1481.64	
HLA-DPA1	0.40	12075.63		0.31	9016.45	
HLA-DPB1	0.57	7200.12		0.54	5498.39	
HLA-DQA1	0.42	6231.44		0.34	3076.99	
HLA-DQB1	0.45	5280.92		0.59	3694.48	
HLA-DRA	0.46	35077.89		0.39	21567.79	
HLA-DRB1	0.53	11666.09		0.69	8506.56	
HLA-DRB5	0.50	4462.02		0.71	2962.90	

HLA-E	0.49	14271.52	0.70	11422.87
HLA-F	0.75	5238.08	0.74	2846.93
HLA-H	0.59	4631.20	0.69	3696.58
IFI35	0.46	969.00	0.28	1675.83
IL2RB	0.29	986.55	0.40	640.19
IL2RG	0.39	1904.72	0.54	952.76
IRF1	0.56	3231.79	0.54	1974.15
ITGB2	0.25	3734.61	0.35	2204.41
LAP3	0.30	4887.38	0.37	3320.59
LGALS9	0.48	2716.08	0.51	2032.64
MVP	0.52	3162.78	0.04	5446.77
NFKB2	0.38	2008.49	0.41	1251.15
NLRC5	0.28	2020.48	0.28	1012.90
PML	0.04	3206.75	0.31	1961.82
PSMB8	1.00	4030.34	1.00	3602.91
PSME1	0.34	4298.28	0.52	5915.11
PSME2	0.40	4266.86	0.46	4002.40
PTPN6	0.49	1541.36	0.48	1337.84
RAC2	0.34	1541.22	0.61	1245.61
RARRES3	0.34	2125.79	0.41	6345.87
SPI1	0.32	844.55	0.52	547.76
TAP1	0.57	12942.36	0.84	5870.72
TAP2	0.57	5474.91	0.74	2245.24
TAPBP	0.61	11090.77	0.81	8159.85
TCIRG1	0.50	1592.64	0.43	1324.59
TNFRSF14	0.45	1052.90	0.50	1111.30
TNFRSF1B	0.46	1626.59	0.40	1003.91
TYMP	0.46	4108.39	0.55	2683.15
TYROBP	0.29	1442.54	0.54	1026.17
UBA7	0.52	1045.64	0.18	1312.04
UBD	0.40	9537.38	0.51	2368.57
UBE2L6	0.36	4611.63	0.52	4036.45
WARS	0.29	12689.24	0.62	3206.70

Note: Number cases basal-like with expression of PSMB8>2500 is 42. R values >0.483 have

P<0.05 with Bonferroni correction for multiple testing. Number of cases luminal A with expression of PSMB8>2500 is 23. R values>0.647 have P<0.05 with Bonferroni correction for multiple testing.

Supplementary Table 4. Comparison of MHC expression between breast cancer tissues and breast cancer cell lines

		MHC class I				MHC class II					
		PSM B8	HLA-A	HLA-B	HLA-C	HLA-DMA	HLA-DPA1	HLA -	HLA -	HLA -	HLA -
								DPB1	DQA1	DQB1	DRA
Breast cancer	Average expression*	0.8	8.5	13.3	9.1	0.6	2.8	1.7	1.1	1.1	7.0
	Correlation with PSMB8		0.80	0.80	0.72	0.62	0.50	0.51	0.44	0.44	0.55
Breast cell lines	Average expression*	0.2	2.1	1.8	2.3	0.07	0.03	0.007	0.01	0.03	0.1
	Correlation with PSMB8		0.56	0.63	0.64	0.34	0.16	0.22	0.14	0.001	0.30

*Expression given as relative to expression of PSMB5 since breast cancer data calculated as RSEM and cell line as RPKM (Reads Per Kilobase of transcript per Million mapped reads). Breast cancer RNA seq expression from cell 2015 TCGA, breast cell line expression from Klijn et al.

Supplementary Table 5. Summary of the effect of PSMB5 and PSMB8 expression on the survival of breast cancer patients.

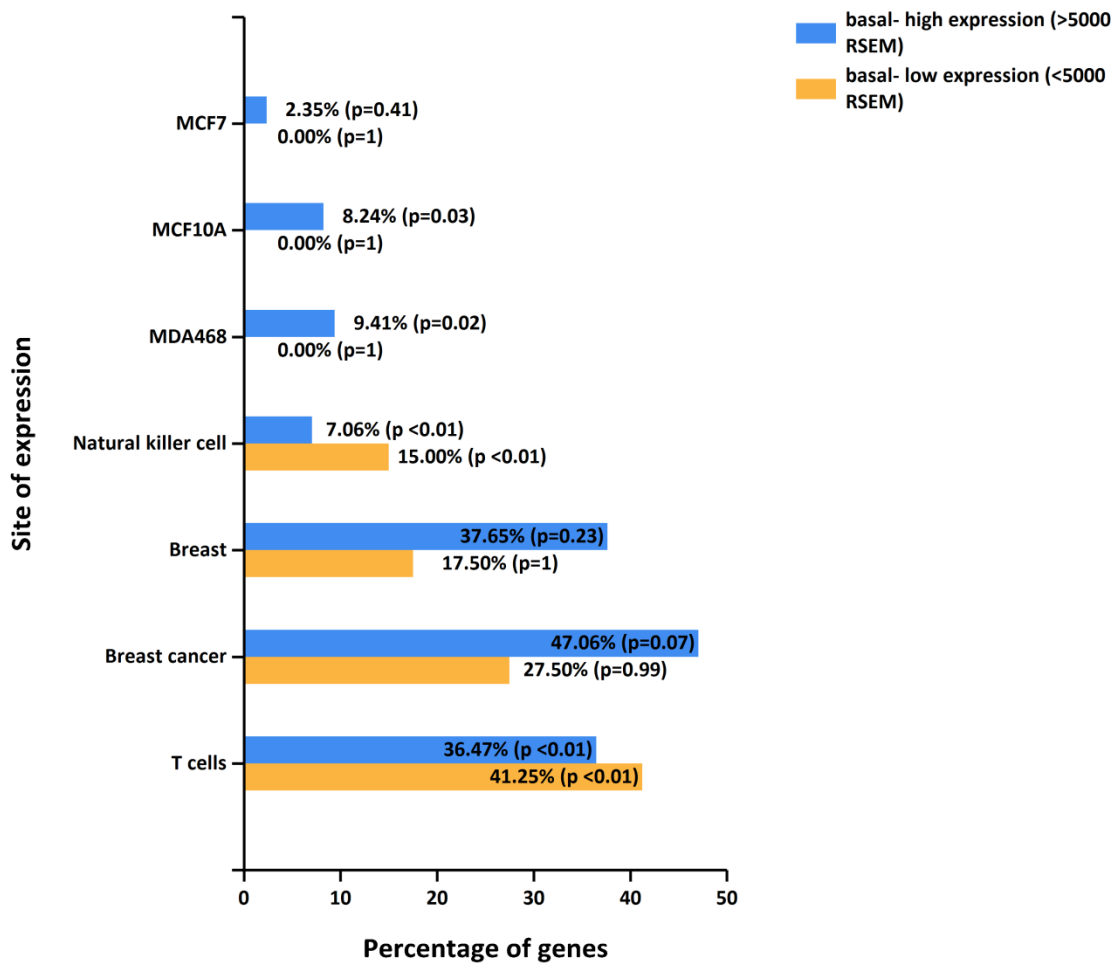
		PSMB5 c-proteasome			PSMB8 i-proteasome		
Intrinsic subtype	Number cases	Number cases high expression	Expression level with best prognosis	p value	Number cases high expression	Expression level with best prognosis	p value
Basal	580	428		ns	223	high	1.3e-06
Luminal A	1764	491	low	8e-09	1205		ns
Luminal B	1002	388	low	0.0015	418		ns
HER2 ⁺	208	24		ns	142		ns

Supplementary Table 6. Relative expression of PSMB8 in breast cancer cell lines and cytotoxic sensitivity to bortezomib.

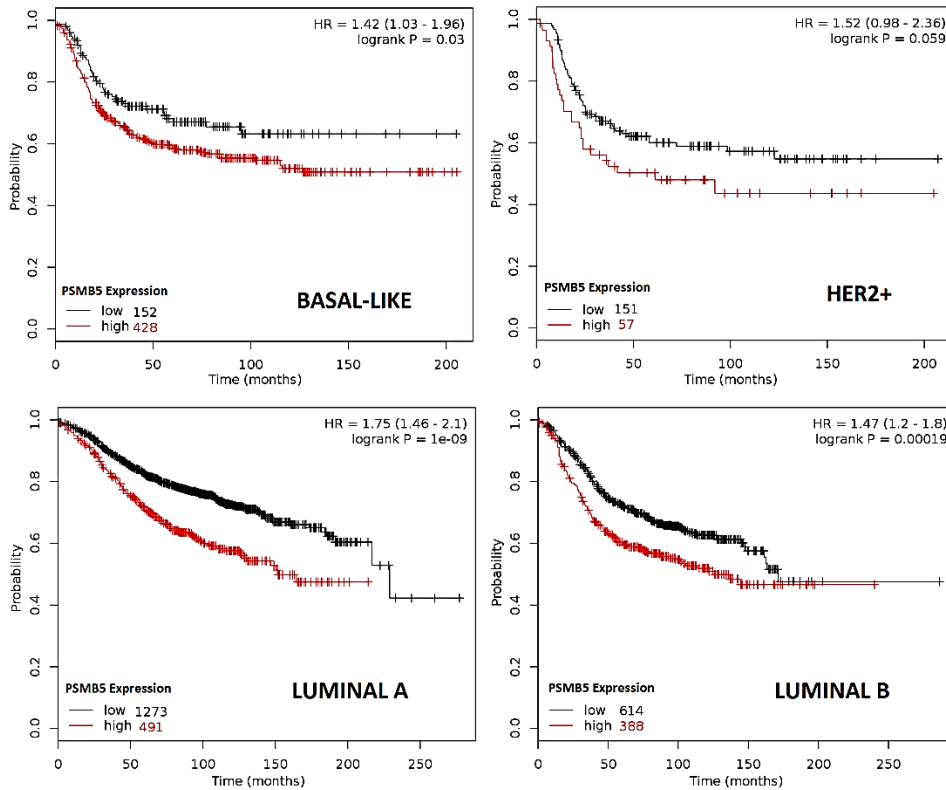
Cell line	Cancer subtype	Bortezomib LD ₅₀ (μM) ± S.D	message (PSMB8)
Hs578T	Basal	0.015 (0.014)	11.40
SKBR3	HER2 ⁺	0.020 (0.04)	12.66
MDA-MB-468	Basal	0.032 (0.018)	12.19
MDA-MB-231	Basal	0.037 (0.02)	12.09
BT-20	Basal	0.039 (0.01)	13.18
BT483	Luminal	0.228 (0.27)	11.27
T47-D	Luminal	0.5 (0.14)	10.57
ZR75-1	Luminal	0.8 (0.45)	10.71
MCF7	Luminal	1.0 (0.72)	9.35
BT474	Luminal	> 1.25 (0.18)	9.92

Supplementary Figure 1. Site of expression of the genes highly correlated (>0.5) with PSMB8 expression divided into high and low expressing groups according to whether the expression of the candidate genes was greater or smaller than 5000 RSEM..

Site of expression for basal- high expression (>5000 RSEM) and basal- low expression (<5000 RSEM)

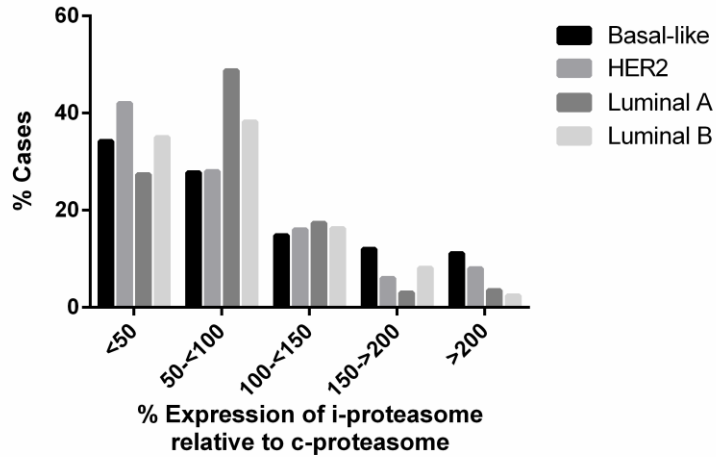


Supplementary Figure 2. Relative survival of sub-types of breast cancer classified by expression of c-proteasome gene PSMB5. Plots generated by Kaplan-Meier plotter ([Gyorffy et al., 2010](#)) using “Jetset” best probe set and auto-selection of best cut-off for classifying high and low expression. Logrank P values not corrected for multiple testing.



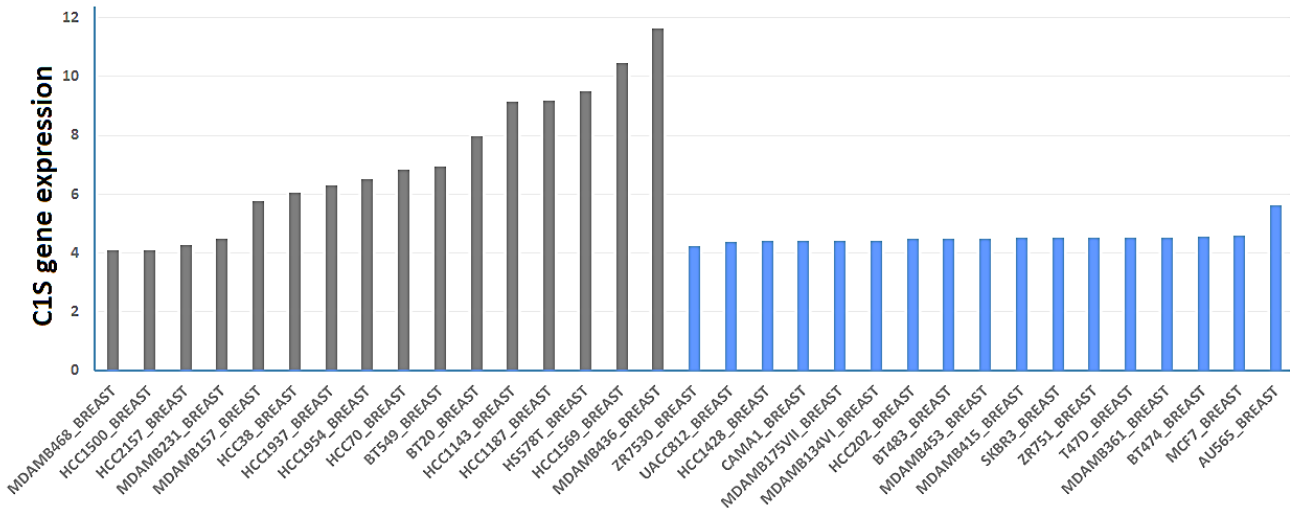
Supplementary Figure 3. Relative expression of i-proteasome in breast cancer subgroups.

The relative i-proteasome (PSMB8) expression is presented in groupings from <50% to greater than 200% relative to the c-proteasome (PSMB5) expression. Presented is the percentage cases in each of the four intrinsic breast cancer subgroups.

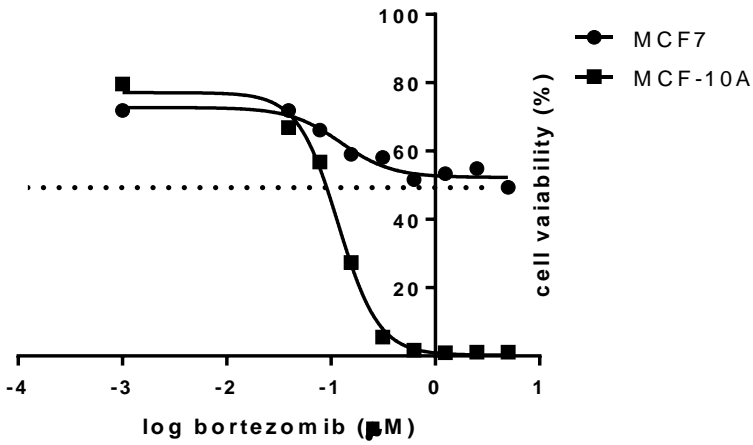
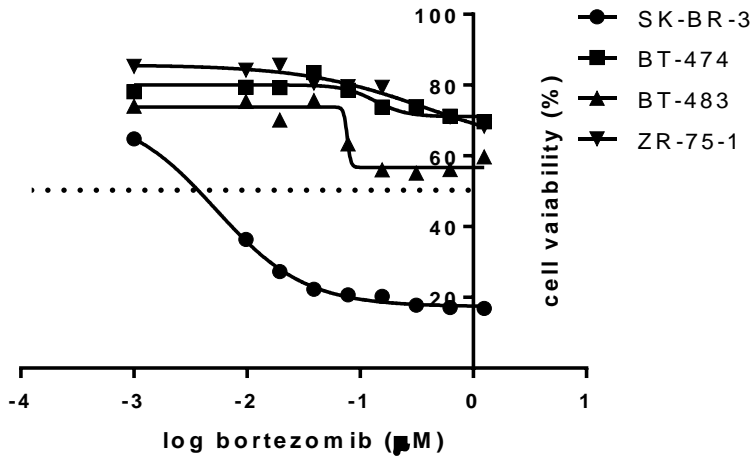
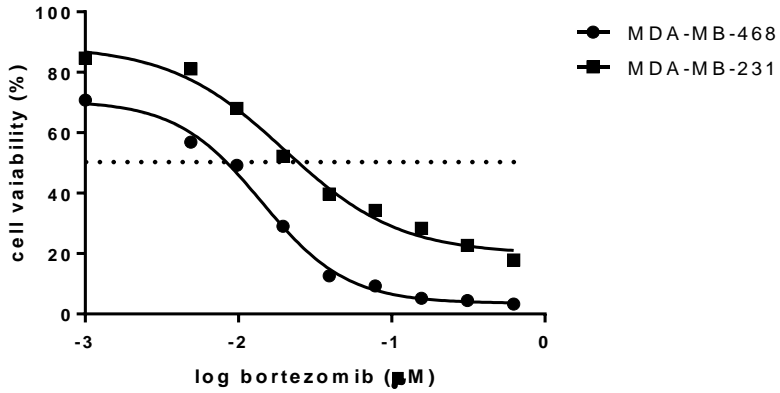


Supplementary Figure 4. Expression of C1S in breast cancer cell lines.

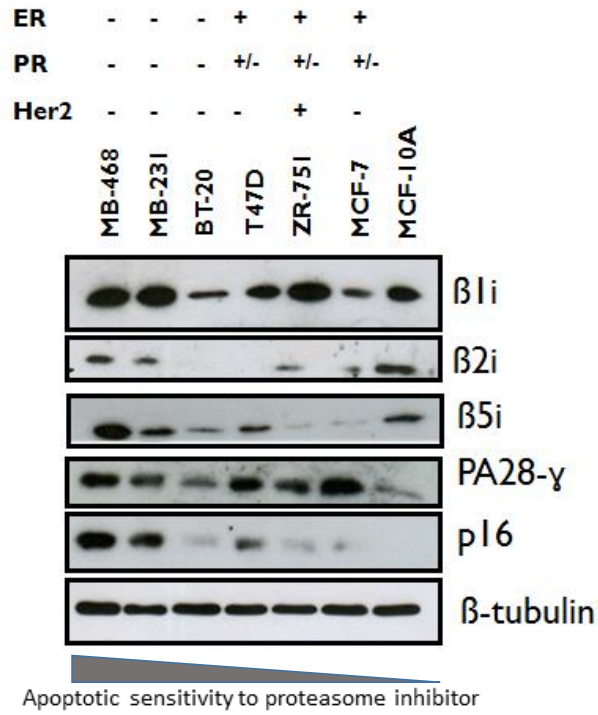
Expression levels of C1S from Affymetrix expression arrays ([Barretina et al., 2012](#)). Black bars are basal type cell lines, blue bars luminal type cell lines ([Neve et al., 2006](#)).



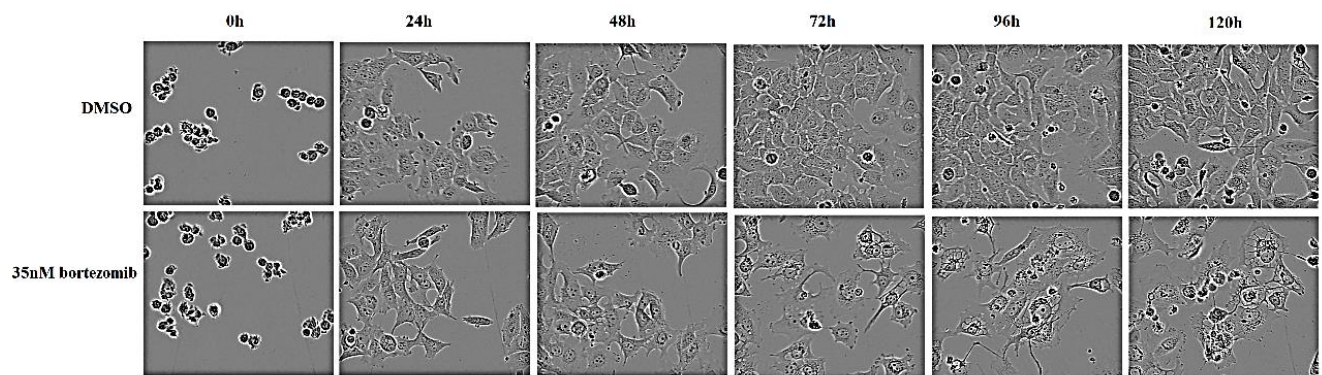
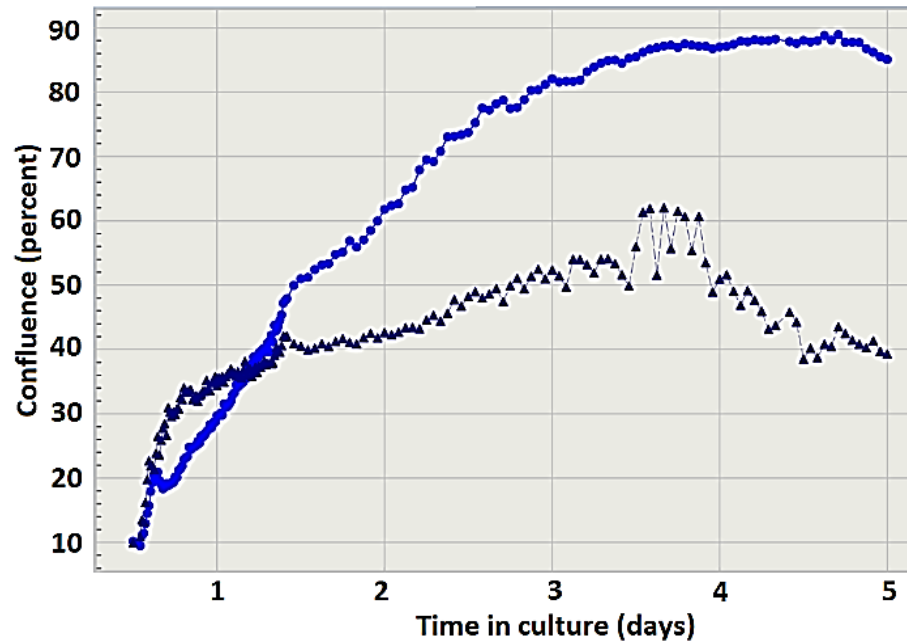
Supplementary Figure 5. Representative LD₅₀ graphs.



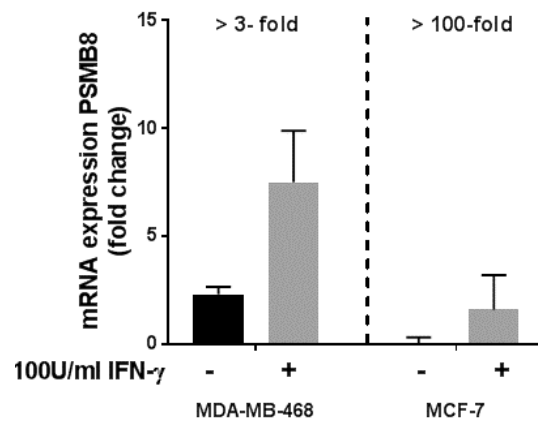
Supplementary Figure 6. Basal-like breast cancer cell lines have higher i-proteasome subunits expression compared to luminal breast cancer cell lines.



Supplementary Figure 7. Bortezomib induces growth arrest in MCF7. A. Breast cancer cell line MCF7 was grown in absence (blue line) or presence of 35nM bortezomib (black line). Proliferation was inhibited and cell death occurred after 4 days of culture. B. Proliferation curves were calculated from Incucyte images.



Supplementary Figure 8. Treatment with IFN- γ induces i-proteasome expression. Cell were treated with 100U/ml IFN- γ for 24h. RT-qPCR analysis was done on mRNA expression of the PSMB8 subunit of the i-proteasome. In MDA-MB-468 cells, PSMB8 expression was induced over 3-fold compared to untreated cells. In MCF-7 cells, IFN- γ treatment caused over 100-fold induction in the PSMB8 levels. These induced mRNA levels were comparative to that observed for MDA-MB-468 cells basally.



CHAPTER 3

New Peptidomimetic Boronates for Selective Inhibition of the Chymotrypsin-like Activity of the 26S Proteasome

Xiaozhou Zhang^{1,2}, **Alaknanda Adwal**³, Andrew G. Turner³, David F. Callen³, Andrew D. Abell^{1,3}

¹Department of Chemistry, The University of Adelaide, North Terrace, Adelaide SA, Australia.

²ARC Centre of Excellence for Nanoscale BioPhotonics, Institute of Photonics and Advanced Sensing, Department of Chemistry, The University of Adelaide, South Australia, 5005

³Centre for Personalised Cancer Medicine, Adelaide Medical School, The University of Adelaide, North Terrace, Adelaide SA, Australia

Statement of Authorship

Statement of Authorship

Title of Paper	New Peptidomimetic Boronates for Selective Inhibition of the Chymotrypsin-like Activity of the 26S Proteasome
Publication Status	<input checked="" type="checkbox"/> Published <input type="checkbox"/> Accepted for Publication <input type="checkbox"/> Submitted for Publication <input type="checkbox"/> Unpublished and Unsubmitted work written in manuscript style
Publication Details	ACS Med Chem Lett. 2016 Sep 13;7(12):1039-1043

Principal Author

Name of Principal Author (Candidate)	Alaknanda Adyal		
Contribution to the Paper	Conducted all biological experiments, analysed and interpreted data and wrote manuscript. Also, acted as the corresponding author.		
Overall percentage (%)	30%		
Certification:	This paper reports on original research I conducted during the period of my Higher Degree by Research candidature and is not subject to any obligations or contractual agreements with a third party that would constrain its inclusion in this thesis. I am the primary author of this paper.		
Signature		Date	6/3/2017

Co-Author Contributions

By signing the Statement of Authorship, each author certifies that:

- the candidate's stated contribution to the publication is accurate (as detailed above);
- permission is granted for the candidate to include the publication in the thesis; and
- the sum of all co-author contributions is equal to 100% less the candidate's stated contribution.

Name of Co-Author	Xiaozhou Zhang		
Contribution to the Paper	Synthesized chemical compounds and conducted chemistry experiments, interpreted data and co-wrote manuscript.		
Signature		Date	3/4/2017

Name of Co-Author	Andrew G Turner		
Contribution to the Paper	Contributed to overall design and manuscript preparation.		
Signature		Date	29/3/17

Name of Co-Author	David F Callen		
Contribution to the Paper	Contributed to conception, design and manuscript preparation, and overall supervision of project.		
Signature		Date	10/03/17

Name of Co-Author	Andrew D Abell		
Contribution to the Paper	Contributed to conception, design and manuscript preparation, and overall supervision of project.		
Signature		Date	1/4/2017

Prelude

The 26S proteasome has emerged over the past decade as an attractive therapeutic target in the treatment of many cancers, in particular hematological malignancies. Here, we report new peptidomimetic boronates that demonstrate superior *in vivo* activity and less toxicity compared to benchmark proteasome inhibitors Bortezomib and Carfilzomib.

This research has been published in ACS Med. Chem. Lett. (Dec, 2016) and this chapter is the published version of the manuscript.

Contribution by the candidate: All biological/cell line experimental work and manuscript writing pertaining to biology.

Abstract

Proteasome is a large proteinase complex that degrades proteins via its three catalytic activities. Among these activities, the 'chymotrypsin-like' activity has emerged as the focus of drug discovery in cancer therapy. Here, we report new peptidomimetic boronates that are highly specific for the chymotrypsin-like catalytic activity of the proteasome. These new specific proteasome inhibitors demonstrated high *in vitro* potency and selective cytotoxicity for cancer cells, with therapeutic windows superior to those observed for the benchmark proteasome inhibitors, bortezomib and carfilzomib. Treatment with the new inhibitors induced accumulation of high molecular weight polyubiquitinated proteins in the cancer cell lines, indicative of inhibition of 26S proteasome and subsequent cancer cell death due to unfolded proteins due to proteasome inhibition.

Introduction

Inhibition of the 26S proteasome is a recognised therapy for the treatment of certain haematological cancers, with bortezomib and carfilzomib (Figure 1) being FDA approved for the treatment of multiple myeloma. Several other proteasome inhibitors are currently in clinical trials.¹ These proteasome inhibitors share some common structural features, with a linear peptide backbone and a C-terminal electrophile that forms a covalent bond with N-terminal threonine of β 1, β 2, or β 5 catalytic subunits of the 26S proteasome. Bortezomib is a dipeptide boronic acid that reversibly inhibits chymotrypsin-like (CT-L) activity of the 26S proteasome by preferentially binding to the active site of the β 5 subunit.² However, at higher doses it also inhibits the caspase-like (C-L) and trypsin-like (T-L) activities associated with the β 1 and β 2 subunits respectively. Studies have shown that bortezomib has broad off-target inhibitory effect on other proteases, which are likely to contribute to its multiple clinical side effects.³ In comparison, the C-terminal epoxyketone of carfilzomib is highly selective for β 5 and β 5i subunits with minimal cross reactivity to other proteases, allowing more sustained and specific inhibition of the 20S proteasome.⁴ While carfilzomib has reduced side effects compared to bortezomib, its C-terminal epoxyketone is highly unstable *in vivo*, resulting in a short plasma half-life (5-20 minutes) and, therefore, low tissue distribution.⁵ These shortcomings restrict the use of bortezomib and carfilzomib in treating multiple myeloma and mantle cell lymphoma. Despite excellent *in vitro* efficacy in preclinical models, these inhibitors have so far failed to show a similar clinical benefit in patients with solid tumours.⁶ This is likely associated with the low bio-stability and selectivity of carfilzomib and bortezomib.^{7,8} Thus, new proteasome

inhibitors are required with improved overall anti-cancer efficacy, especially for the treatment of solid cancers.

Results and Discussion

Here we report new peptidomimetic boronate-based 26S proteasome inhibitors (see 1a,b and 2a,b in Figure 1) that have high specificity for $\beta 5$ catalytic subunit and low toxicity to non-malignant cells. Compounds 1a and 2a induced robust accumulation of high molecular weight proteins by inhibiting the 26S proteasome. Compared to bortezomib and carfilzomib, compound 1a was significantly more toxic towards many cancer cell lines tested. Importantly, both compounds displayed less toxicity towards non-malignant cell lines. The combination of high cancer cell cytotoxicity and low non-malignant cytotoxicity endows compounds 1a and 2a with excellent therapeutic potential.

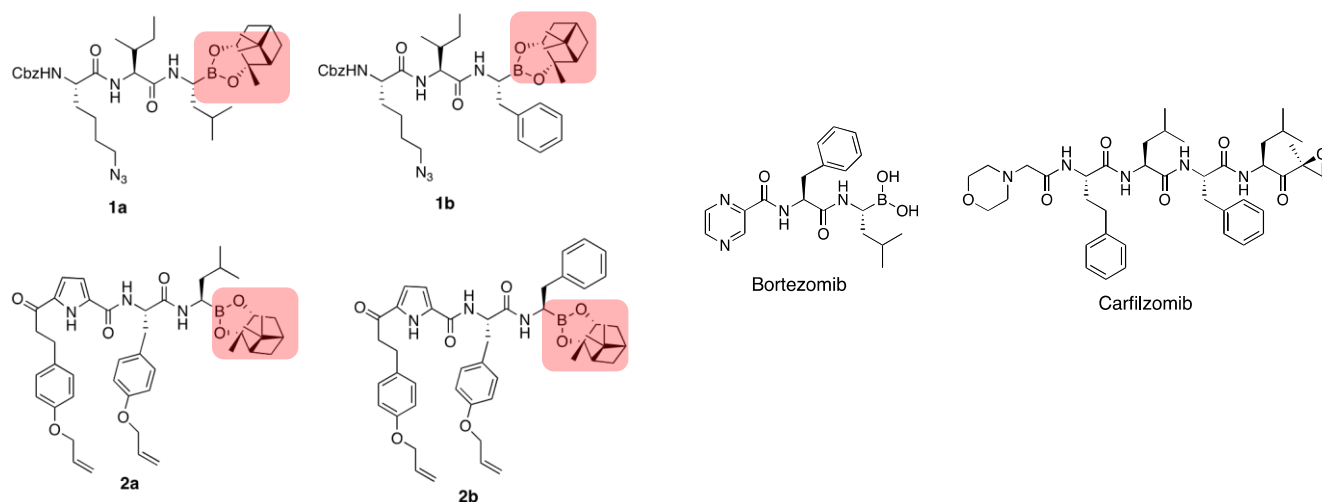


Figure 1. Structures of FDA-approved proteasome inhibitors bortezomib and carfilzomib and the target peptidomimetic boronate inhibitors 1a,b, 2a,b.

Previous reports^{9,10} have shown that the incorporation of a hydrophobic substituent, such as isoleucine, at P2 of peptidic aldehydes enhances selectivity for the CT-L activity over the T-L and C-L activities of the 20S proteasome. One such example (compound 3, Figure 2) shows an excellent *in vitro* activity of 21 nM for CT-L. This peptidic aldehyde also bears a unique aliphatic azide at P3 to provide additional opportunities for hydrogen bonding interactions with the active site. Compound 4, (Figure 2), with an O-allylated tyrosine at P2 and a pyrrole replacing the P3 residue and an associated peptide bond, also shows selectivity for the CT-L activity. The backbone pyrrole moiety reduces the peptide-like character of the inhibitor and defines the backbone into an extended conformation. However, C-terminal aldehyde-based peptidomimetics of type 3 and 4 are known to react with a variety of other proteases, e.g. chymotrypsin^{11,12}, calpains^{13,14} and cathepsins.^{15,16} Here we replace the aldehyde with a boronic pinanediol ester (highlighted in pink, Figure 1), a group reported to provide similar activity toward CT-L of the 26S proteasome compared to the corresponding boronic acid,¹⁷ while being easier to prepare and purify. The chiral ester also defines the absolute configuration of the P1 group introduced during synthesis and negates the need for a final and somewhat problematic deprotection to produce boronic acid. Target compounds 1a and 2a have a leucine at P1 as found in known proteasome inhibitors such as bortezomib and carfilzomib.¹⁸⁻²⁰ In comparison, compounds 1b and 2b have a phenylalanine at this position since the S1 binding pocket of the CT-L activity is known to favour the binding of a large hydrophobic group.²¹

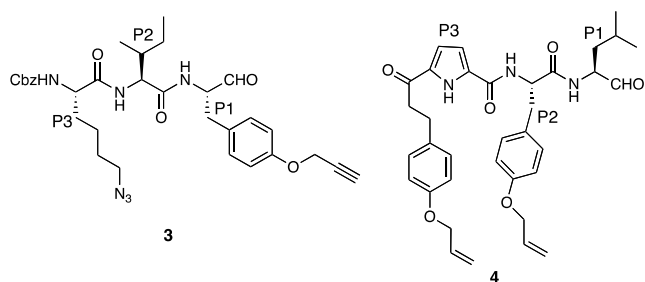
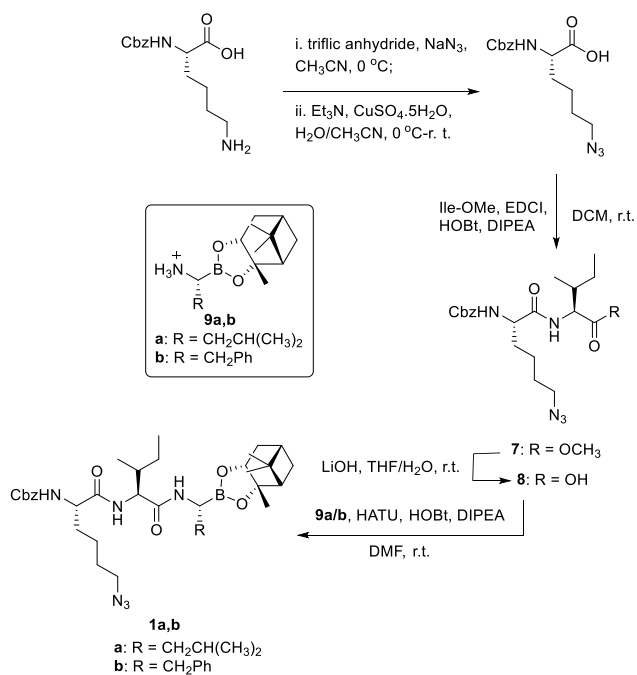


Figure 2. Structures of proteasome inhibitors reported by Abell et al. The amino acid residues of the inhibitors are defined according to nomenclature developed by Schechter and Berger.²²

The key azide **6** was prepared by reacting Cbz-Lys-OH (**5**) with triflic anhydride and sodium azide under basic conditions. Subsequent EDCI-mediated coupling of azide **6** to Ile-OMe gave the dipeptide **7**. Hydrolysis of the methyl ester of **7** in the presence of LiOH gave the free acid **8** in an excellent yield of 93%. This free acid was then coupled with amino boronate **9a,b** in the presence of HATU, HOBT and DIPEA to give the target inhibitors **1a,b**.

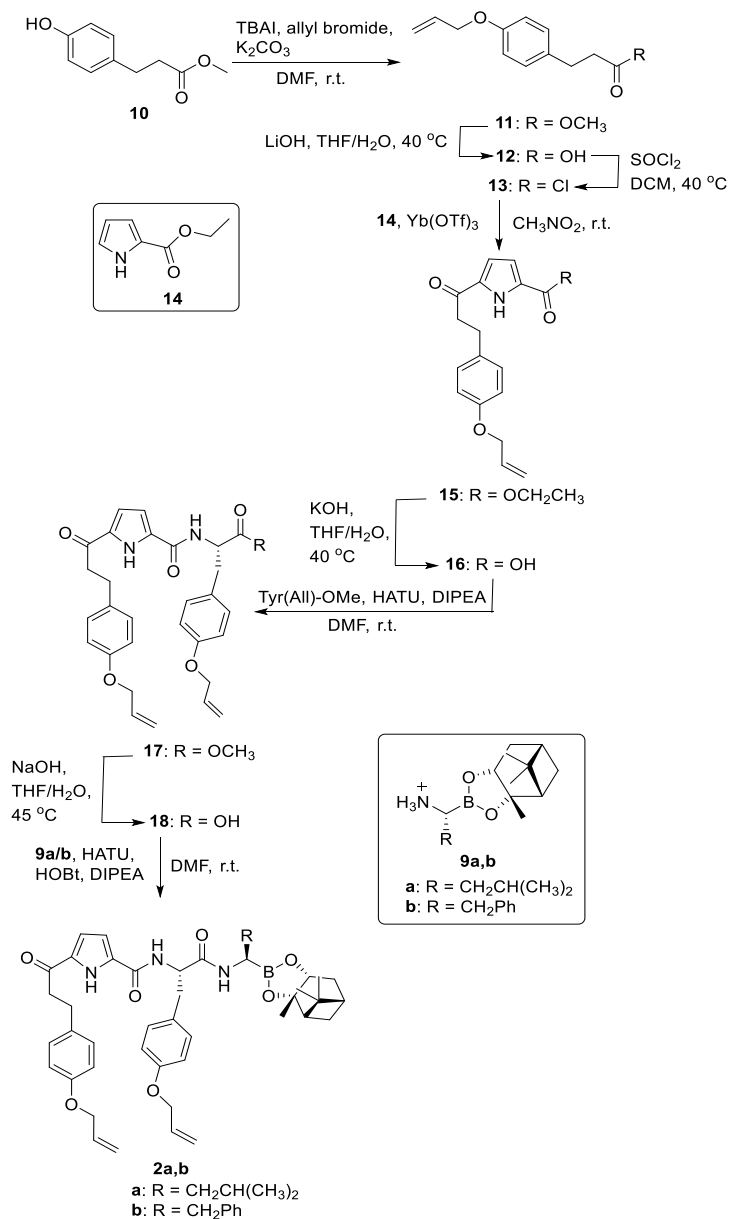


Scheme 1. Synthesis of compounds 1a,b.

The key acid chloride 12 was prepared from commercially available methyl 3-(4-hydroxyphenyl) propionate (10) in three steps in an overall yield of 86%. Specifically, reaction of 10 with allyl bromide gave 11, the ester of which was hydrolysed with LiOH to give carboxylic acid 12. Reaction with SOCl₂ gave the acid chloride 13, which was used in a Friedel-Crafts acylation of pyrrole 14,15 using Yb(OTf)₃, to give the key dipeptide-mimic 15. Subsequent hydrolysis of the ester of 15 with KOH gave carboxylic acid 16, which was subsequently coupled with Tyr(All)-OMe in the presence of HATU, HOBT and DIPEA to give diene 17 in 78% yield over two steps. The methyl ester of diene 17 was hydrolysed with NaOH to give free acid 18 in excellent yield. HATU-mediated coupling of 18 with amino boronates 9a,b gave the target inhibitors 2a,b.

The 20S proteasome exhibits T-L, C-L and CT-L protease activities. Of the three activities, the CT-L activity carries out the bulk of the proteolytic breakdown, and is the most common target of pharmacologically designed proteasome inhibitors.²³ Therefore, we first evaluated whether the compounds 1a,b and 2a,b were potent and selective for the CT-L activity.

As expected, both bortezomib and carfilzomib were highly potent inhibitors of CT-L activity in this assay with IC₅₀ values of 34.6 nM and 23.1 nM respectively. Bortezomib also significantly inhibited the C-L activity, which is consistent with a previous report.²⁴ The new peptidic boronates 1a,b and 2a,b were also highly active against the CT-L activity, with derivatives 1a,b and 2a proving to be more potent than bortezomib and carfilzomib. The most potent inhibitor in this series, 1a, has an IC₅₀ of 14.1 nM against the CT-L activity, which is more than 2-fold more potent than bortezomib. Interestingly, inhibitors with leucine residue at P1 (1a, 2a)



Scheme 2. Synthesis of compounds 2a,b.

inhibited the CT-L activity with higher potencies compared to the inhibitors bearing a P1 phenylalanine (1b, 2b), suggesting that the S1 subsite of $\beta 5$ subunit favours the binding of branched hydrophobic amino acids over planar aromatic residues. Unlike bortezomib, all of the compounds were at least 10-fold less active against the C-L activity compared to the CT-L activity. Compound 2a was the most selective inhibitor of CT-L over C-L, with a 200-fold

difference in activities. Following administration of carfilzomib, patients display less of the “typical” toxicities associated with bortezomib, and this has been attributed to its higher selectivity for inhibiting CT-L activity over T-L, C-L as well as other serine proteases’ activities. Therefore, the combination of excellent potency and high selectivity for the CT-L activity observed for the peptidic boronates 1a,b and 2a,b provides an opportunity to reduce side effects associated with the low subunit selectivity of bortezomib and limit drug resistance caused by the mutation in CT-L activity of the proteasome found in bortezomib-resistant cell lines.²⁵

Table 1. Inhibition of purified 20S proteasome from rabbit reticulocytes by compounds 1a,b, 2a,b, bortezomib and carfilzomib.

	IC ₅₀ (CT-L) (nM) ^a	IC ₅₀ (T-L) (nM) ^a	IC ₅₀ (C-L) (nM) ^a
1a	14.1 ± 4.2	>25000	1598.0 ± 98.3
1b	21.0 ± 4.4	>25000	2448.3 ± 73.2
2a	20.9 ± 7.7	>25000	4179.0 ± 341.4
2b	104.0 ± 15.9	>25000	3343.3 ± 416.1
bortezomib	34.6 ± 4.2	>25000	108.4 ± 34.0
carfilzomib	23.1 ± 4.4	>25000	>25000

a +/- Standard error of mean; n=3.

We next investigated whether the high potency and selectivity of 1a and 2a for CT-L activity translated into improved cytotoxic activity against cultured cancer cell lines. The cytotoxic LD₅₀ across a panel of sarcoma, ovarian, breast and myeloma cell lines was determined using 7AAD assays following a 48 h exposure to titrations (0-5000 nM) of 1a, 2a, bortezomib and carfilzomib. Viability studies were also performed with a non-malignant breast epithelial cell line MCF-10A, a primary human lung fibroblasts cell line IMR-90, a primary human skin fibroblast line NDF and a normal human immortalised lymphoblastoid cell line LCL, thus allowing us to determine if the cytotoxicity of these compounds was cancer cell-specific.

Compounds 1a and 2a were both potent cytotoxic agents and dose-dependently decreased cell viability. Of the two inhibitors, in both solid and liquid cancer cell lines, compound 1a consistently resulted in equal or greater cytotoxicity compared to bortezomib and carfilzomib. Myeloma cell lines are known to be highly sensitive to proteasome inhibitors. Consistent with this, the myeloma cell lines NCI-H929 and U266 showed the highest levels of sensitivity, with LD₅₀ values of 6.4 nM and 15 nM, respectively. Sensitivity to compound 1a varied considerably between solid cancer cell lines, with LD₅₀ values ranging from 35 nM in the RD-ES sarcoma cell line to 1500 nM in the MCF-7 breast carcinoma cell line. In particular, compound 1a induced cell death in the Ewing sarcoma cell line WE-68 (LD₅₀ 35 nM) and ovarian cancer cell line SK-OV-3 (LD₅₀ 370 nM) at significantly lower doses compared to bortezomib (100 nM; 1600 nM respectively, p<0.01; n=3). Importantly, the cytotoxicity of compounds 1a and 2a was more specific to cancer cells, compared to bortezomib and carfilzomib. Compound 1a was approximately 3-fold, and compound 2a 6-fold less toxic to non-malignant cells compared to

bortezomib. The relative sensitivity of the cell lines to each inhibitor was essentially identical, suggesting a common mechanism of cytotoxic action of each inhibitor in a particular cell line.

Table 2. Cytotoxicity of proteasome inhibitors against a panel of solid cancer cell lines or non-malignant cell lines.

Cell line	Histology/ origin	P53 status	LD ₅₀ (μ M)			
			1a	2a	Bortezomib	Carfilzomib
WE-68	Ewing sarcoma	wild-type	0.035* (\pm 0.001)	0.065 (\pm 0.007)	0.1 (\pm 0.01)	0.08 (\pm 0.02)
RDES	Ewing sarcoma	mutant	0.035 (\pm 0.005)	0.065 (\pm 0.01)	0.04 (\pm 0.002)	0.043 (\pm 0.012)
KGN	Ovarian cancer	wild-type	0.065 (\pm 0.02)	0.18 (\pm 0.11)	0.18 (\pm 0.09)	0.45 (\pm 0.15)
SKOV3	Ovarian cancer	null	0.37* (\pm 0.15)	1.5 (\pm 0.3)	1.6 (\pm 0.4)	0.32 (\pm 0.11)
MCF7	Breast cancer	wild-type	1.5* (\pm 0.5)	3* (\pm 0.05)	9.8 (\pm 5.5)	4.5 (\pm 3.5)
MDAMB468	Breast cancer	mutant	0.03 (\pm 0.004)	0.05 (\pm 0.003)	0.037 (\pm 0.013)	0.33 (\pm 0.11)
NCI-H929	Multiple myeloma	wild-type	0.0064 (\pm 0.0002)	0.009 (\pm 0.003)	0.0066 (\pm 0.0011)	ND
U266	Multiple myeloma	mutant	0.015 (\pm 0.001)	0.029 (\pm 0.002)	0.018 (\pm 0.001)	0.06 (\pm 0.01)
MCF10A	Breast carcinoma	wild-type	5 (\pm 1.5)	9* (\pm 3)	1.5 (\pm 0.6)	0.32 (\pm 0.09)
IMR-90	Normal primary lung fibroblast	wild-type	0.2 (\pm 0.1)	0.15 (\pm 0.1)	0.13 (\pm 0.09)	0.13 (\pm 0.02)
DSF	Normal skin fibroblast	Wild-type	0.5 (\pm 0.1)	1.08* (\pm 0.12)	0.48 (\pm 0.2)	0.35 (\pm 0.11)
LCL	B-cell lymphoblastoid	wild-type	0.03* (\pm 0.001)	0.09* (\pm 0.003)	0.02 (\pm 0.002)	0.03 (\pm 0.006)

^aDose-response curves are provided in Supporting Information. *indicates statistical significance (<0.05) compared to bortezomib. ND-not determined.

Previous studies report that inhibition of the proteasome causes stabilisation of the tumour suppressor p53, leading to activation of downstream pathways and as a consequence cancer cell cycle arrest or cell death.^{26,27} Therefore, to determine if the cell death observed upon treatment with 1a and 2a was influenced by p53 signalling, a pair of p53 wild-type and p53 mutant/null cell lines were used for each cancer type. There was no significant difference between the average LD₅₀ values of the p53 wild-type and p53 mutant/null cell lines (Figure S2, supporting information), albeit there was considerable variation within each cancer type. In multiple myeloma and ovarian cancer, p53-proficient cell lines NCI-H929 and KGN were approximately 2-fold and 5-fold more sensitive than U266 and SKOV-3 cell lines in which p53 was mutated or null. However, in breast cancer cell lines the trend was reversed, with p53 mutated cell line MDAMB-468 being markedly more sensitive than MCF7 with wild-type p53. As the overall pattern of sensitivity of the cell lines was individually consistent across a small library of proteasome inhibitors (bortezomib, carfilzomib, 1a and 2a), it is possible that stabilization of p53 may mediate cytotoxic effects in a cancer or tissue dependent manner.

Next, the accumulation of polyubiquitinated proteins in intact cells was analysed to verify that the observed cell death was a result of proteasome inhibition by compounds 1a/2a. Cellular proteins destined for degradation are first “tagged” with multiple ubiquitin molecules to be recognised by the 26S proteasome. Therefore, inhibition of the proteasome results in rapid accumulation of high molecular weight polyubiquitin-conjugated proteins, which can be detected with an anti-ubiquitin antibody. Western blot analyses revealed that treatment with 35 nM of compounds 1a and 2a for 4 h substantially increased high molecular weight

polyubiquitinated proteins in both MDA-MB-468 and MCF7 cell lines (Figure 3). This observation excludes the possibility that reduced uptake of proteasome inhibitors by MCF7 is responsible for the cytotoxic insensitivity of this cell line. For both 1a and 2a, the extent of polyubiquitin accumulation was quantitatively similar to that observed using bortezomib. This is largely consistent with cytotoxic efficacies observed for these compounds. Defects or mutations in downstream signalling pathways that drive proteasome inhibitor mediated cell death are likely responsible for the variation in sensitivity seen across cell lines. However, the mechanism that drives cell death requires further assessment and falls outside the scope of this study.

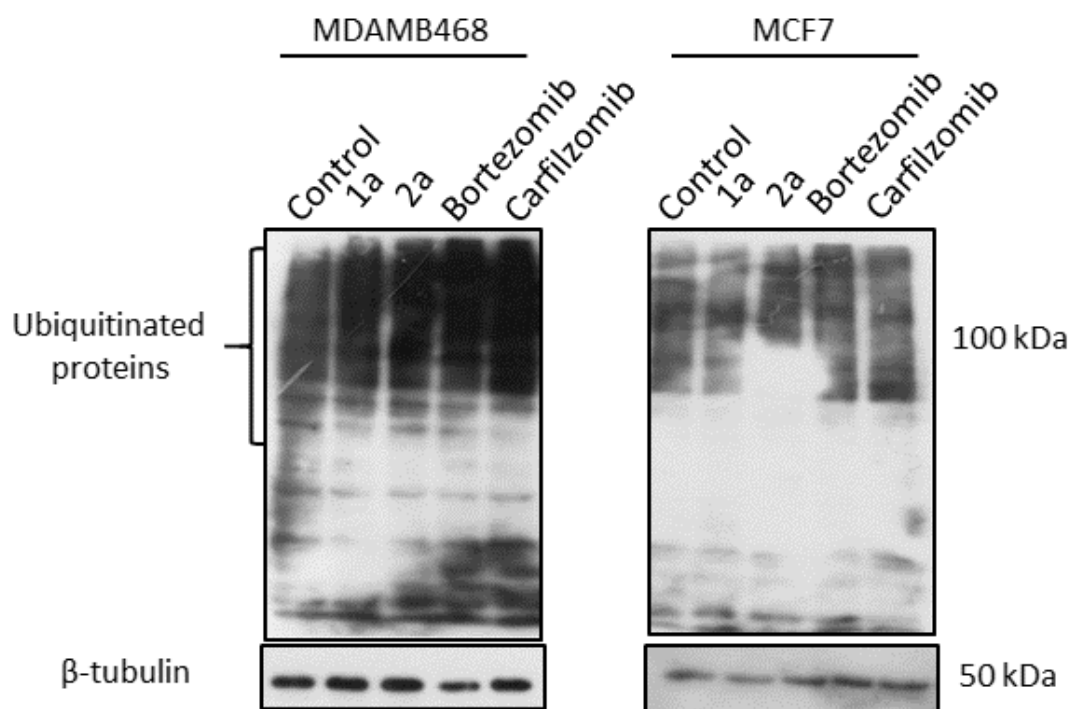


Figure 3. Compounds 1a and 2a induce accumulation of high molecular weight ubiquitin conjugates. MDAMB468 and MCF7 were treated with 35 nM of compounds 1a, 2a, bortezomib

or carfilzomib for 4 h, and Western blots of cell homogenates hybridised to an anti-ubiquitin antibody. β -tubulin was used as a loading control.

In summary, we report examples of a new class of proteasome inhibitor 1a,b and 2a,b with improved *in vitro* activity against the purified enzyme and higher specificity for the CT-L activity compared to bortezomib. Inhibitor 1a was shown to be significantly more cytotoxic against solid tumour cells compared to both bortezomib and carfilzomib. More importantly, 1a provides a larger therapeutic window than the benchmarks for all tested tumour types including myeloma. We also demonstrate that the observed cytotoxicity of compounds 1a and 2a was due to inhibition of the 26S as Western blot analysis of the cell lines treated with these compounds showed a significant accumulation of polyubiquitinated proteins as a result of decreased proteasome function. Thus compound 1a is an attractive drug candidate that offers potential benefits as it is predicted to possess reduced clinical side effects compared to the current chemotherapy agents bortezomib and carfilzomib.

References

1. Teicher, B. A.; Tomaszewski, J. E., Proteasome inhibitors. *Biochemical Pharmacology* 2015, 96 (1), 1-9.
2. Chen, D.; Frezza, M.; Schmitt, S.; Kanwar, J.; Dou, Q. P., Bortezomib as the first proteasome inhibitor anticancer drug: current status and future perspectives. *Current cancer drug targets* 2011, 11 (3), 239-53.
3. Arastu-Kapur, S.; Anderl, J. L.; Kraus, M.; Parlati, F.; Shenk, K. D.; Lee, S. J.; Muchamuel, T.; Bennett, M. K.; Driessen, C.; Ball, A. J.; Kirk, C. J., Nonproteasomal targets of the proteasome inhibitors bortezomib and carfilzomib: a link to clinical adverse events. *Clin Cancer Res* 2011, 17 (9), 2734-43.
4. Kuhn, D. J.; Orlowski, R. Z.; Bjorklund, C. C., Second generation proteasome inhibitors: carfilzomib and immunoproteasome-specific inhibitors (IPSIs). *Curr Cancer Drug Targets* 2011, 11 (3), 285-95.
5. Wang, Z.; Yang, J.; Kirk, C.; Fang, Y.; Alsina, M.; Badros, A.; Papadopoulos, K.; Wong, A.; Woo, T.; Bomba, D.; Li, J.; Infante, J. R., Clinical pharmacokinetics, metabolism, and drug-drug interaction of carfilzomib. *Drug Metab Dispos* 2013, 41 (1), 230-7.
6. Huang, Z.; Wu, Y.; Zhou, X.; Xu, J.; Zhu, W.; Shu, Y.; Liu, P., Efficacy of therapy with bortezomib in solid tumours: a review based on 32 clinical trials. *Future Oncol* 2014, 10 (10), 1795-807.
7. Arastu-Kapur, S.; Anderl, J. L.; Kraus, M.; Parlati, F.; Shenk, K. D.; Lee, S. J.; Muchamuel, T.; Bennett, M. K.; Driessen, C.; Ball, A. J.; Kirk, C. J., Nonproteasomal Targets of the Proteasome

Inhibitors Bortezomib and Carfilzomib: a Link to Clinical Adverse Events. *Clinical Cancer Research* 2011, 17 (9), 2734-2743.

8. Bennett, M. K.; Kirk, C. J., Development of proteasome inhibitors in oncology and autoimmune diseases. *Current Opinion in Drug Discovery & Development* 2008, 11 (5), 616-625.

9. Neilsen, P. M.; Pehere, A. D.; Pishas, K. I.; Callen, D. F.; Abell, A. D., New 26S Proteasome Inhibitors with High Selectivity for Chymotrypsin-Like Activity and p53-Dependent Cytotoxicity. *ACS Chemical Biology* 2012, 8 (2), 353-359.

10. Braun, H. A.; Umbreen, S.; Groll, M.; Kuckelkorn, U.; Mlynarczuk, I.; Wigand, M. E.; Drung, I.; Kloetzel, P.-M.; Schmidt, B., Tripeptide Mimetics Inhibit the 20 S Proteasome by Covalent Bonding to the Active Threonines. *J. Biol. Chem.* 2005, 280 (31), 28394-28401.

11. Ito, A.; Tokawa, K.; Shimizu, B., Peptide aldehydes inhibiting chymotrypsin. *Biochem. Biophys. Res. Commun.* 1972, 49 (2), 343-349.

12. Stein, R. L.; Strimpler, A. M., Slow-binding inhibition of chymotrypsin and cathepsin G by the peptide aldehyde chymostatin. *Biochemistry* 1987, 26 (9), 2611-2615.

13. Fukiage, C.; Azuma, M.; Nakamura, Y.; Tamada, Y.; Nakamura, M.; Shearer, T. R., SJA6017, a newly synthesized peptide aldehyde inhibitor of calpain: amelioration of cataract in cultured rat lenses. *Biochim. Biophys. Acta, Mol. Basis Dis.* 1997, 1361 (Copyright (C) 2011 American Chemical Society (ACS). All Rights Reserved.), 304-312.

14. Abell, A. D.; Jones, M. A.; Coxon, J. M.; Morton, J. D.; Aitken, S. G.; McNabb, S. B.; Lee, H. Y. Y.; Mehrtens, J. M.; Alexander, N. A.; Stuart, B. G.; Neffe, A. T.; Bickerstaffe, R., Molecular modeling, synthesis, and biological evaluation of macrocyclic calpain inhibitors. *Angew. Chem.,*

Int. Ed. 2009, 48 (Copyright (C) 2011 American Chemical Society (ACS). All Rights Reserved.), 1455-1458, S1455/1-S1455/38.

15. Chua, K. C. H.; Pietsch, M.; Zhang, X.; Hautmann, S.; Chan, H. Y.; Bruning, J. B.; Gütschow, M.; Abell, A. D., Macrocyclic Protease Inhibitors with Reduced Peptide Character. *Angew. Chem. Int. Ed.* 2014, 53 (30), 7828-7831.

16. Boros, E. E.; Deaton, D. N.; Hassell, A. M.; McFadyen, R. B.; Miller, A. B.; Miller, L. R.; Paulick, M. G.; Shewchuk, L. M.; Thompson, J. B.; Willard Jr, D. H.; Wright, L. L., Exploration of the P2–P3 SAR of aldehyde cathepsin K inhibitors. *Bioorg. Med. Chem. Lett.* 2004, 14 (13), 3425-3429.

17. Zhu, Y.; Zhao, X.; Zhu, X.; Wu, G.; Li, Y.; Ma, Y.; Yuan, Y.; Yang, J.; Hu, Y.; Ai, L.; Gao, Q., Design, Synthesis, Biological Evaluation, and Structure,àActivity Relationship (SAR) Discussion of Dipeptidyl Boronate Proteasome Inhibitors, Part I: Comprehensive Understanding of the SAR of α -Amino Acid Boronates. *J. Med. Chem.* 2009, 52 (14), 4192-4199.

18. Mroczkiewicz, M.; Winkler, K.; Nowis, D.; Placha, G.; Golab, J.; Ostaszewski, R., Studies of the synthesis of all stereoisomers of MG-132 proteasome inhibitors in the tumour targeting approach. *J. Med. Chem.* 2010, 53 (Copyright (C) 2012 American Chemical Society (ACS). All Rights Reserved.), 1509-1518.

19. Demo, S. D.; Kirk, C. J.; Aujay, M. A.; Buchholz, T. J.; Dajee, M.; Ho, M. N.; Jiang, J.; Laidig, G. J.; Lewis, E. R.; Parlati, F.; Shenk, K. D.; Smyth, M. S.; Sun, C. M.; Vallone, M. K.; Woo, T. M.; Molineaux, C. J.; Bennett, M. K., Antitumour Activity of PR-171, a Novel Irreversible Inhibitor of the Proteasome. *Cancer Research* 2007, 67 (13), 6383-6391.

20. Hideshima, T.; Richardson, P.; Chauhan, D.; Palombella, V. J.; Elliott, P. J.; Adams, J.; Anderson, K. C., The proteasome inhibitor PS-341 inhibits growth, induces apoptosis, and

overcomes drug resistance in human multiple myeloma cells. *Cancer Res.* 2001, 61 (Copyright (C) 2011 American Chemical Society (ACS). All Rights Reserved.), 3071-3076.

21. Borissenko, L.; Groll, M., 20S Proteasome and Its Inhibitors: Crystallographic Knowledge for Drug Development. *Chem. Rev.* 2007, 107 (3), 687-717.

22. Schechter, I.; Berger, A., On the size of the active site in proteases. I. Papain. *Biochem. Biophys. Res. Commun.* 1967, 27 (Copyright (C) 2012 American Chemical Society (ACS). All Rights Reserved.), 157-62.

23. Kisselev, A. F.; Callard, A.; Goldberg, A. L., Importance of the different proteolytic sites of the proteasome and the efficacy of inhibitors varies with the protein substrate. *The Journal of biological chemistry* 2006, 281 (13), 8582-90.

24. Bruning, A.; Vogel, M.; Mylonas, I.; Friese, K.; Burges, A., Bortezomib Targets the Caspase-Like Proteasome Activity in Cervical Cancer Cells, Triggering Apoptosis That Can be Enhanced by Nelfinavir. *Current Cancer Drug Targets* 2011, 11 (7), 799-809.

25. Lu, S.; Wang, J., The resistance mechanisms of proteasome inhibitor bortezomib. *Biomarker research* 2013, 1 (1), 13.

26. Neilsen, P. M.; Pehere, A. D.; Pishas, K. I.; Callen, D. F.; Abell, A. D., New 26S proteasome inhibitors with high selectivity for chymotrypsin-like activity and p53-dependent cytotoxicity. *ACS Chem Biol* 2013, 8 (2), 353-9.

27. Harris, G. F. t.; Anderson, M. E.; Lee, J. H., The effect of proteasome inhibition on p53 degradation and proliferation in tonsil epithelial cells. *Arch Otolaryngol Head Neck Surg* 2008, 134 (2), 157-63.

Methods and Materials

General Information

Bortezomib (Selleckchem, Houston, TX, USA), Carfilzomib (Selleckchem, Houston, TX, USA), or in-house generated derivatives were dissolved in 10 mM DMSO and stored at -20°C . Antibodies used for western blot analysis included a mouse anti-tubulin (Sigma), anti-ubiquitin (Cell Signalling), sheep anti-mouse IgG-HRP (GE, USA), or donkey anti-rabbit IgG-HRP (GE, USA). All human cell lines (WE-68, RD-ES, SKOV3, KGN, MCF7, MDA-MB-468, NCI-H929, U266, MCF-10A, and IMR-90) were purchased from American Type Tissue Culture. WE-68, NCI-H929, U266, MCF7 and LCL cell lines (established from a normal individual) were grown in RPMI-1640 media. RD-ES, MDA-MB-468, SKOV-3, KGN and a primary human embryonic fibroblast cell line were grown in Dulbecco's Modified Eagle's Medium (DMEM). The medium was supplemented with 10% FCS, 1% PSG and 10 mM HEPES. MCF-7 cells were supplemented with 1% insulin. All cells were maintained at 37°C in a humidified atmosphere of 5% CO_2 .

***In Vitro* Proteasome Activity Assay**

Proteasome CT-L, C-L and T-L activities were determined using hydrolysis of specific short peptide substrates conjugated to the fluorescent tag 7-amido-4-methylcoumarin (AMC). Purified rabbit 20S proteasome and fluorogenic CT-L substrate (Suc-Leu-Leu-Val-Tyr-AMC) were purchased from Boston Biochem (Cambridge, MA, USA). The T-L and C-L fluorogenic substrates (Bz-Val-Gly-Arg-AMC and Ac-nLPnLD-AMC) were purchased from Enzo Life Sciences

(Farmingdale, NY, USA). Purified 20S proteasome (Enzo Life Sciences, Farmingdale, NY, USA) (0-2 µg) was pre-incubated with the indicated concentrations of inhibitors at 37 °C for 15 minutes and subsequently added to the AMC-labelled substrate peptide (50 µM) in assay buffer (20 mM Tris-HCl, pH 7.5, 0.5 mM EDTA, and 0.001% SDS (w/v)) for a further 2 hours. Fluorescent substrate cleavage by the 20S proteasome was linear during this incubation period. Hydrolysed AMC was subsequently detected with the Synergy™ H4 Hybrid Multi-Mode Microplate Reader (BioTek, USA) at excitation/emission wavelengths of 390/460 nm. Hydrolysis activity was measured as relative fluorescence units allowing IC₅₀ values to be calculated that represented half of the maximal inhibitory activity of the proteasome. A minimum of three biological replicates was performed for each data point.

***In Vitro* α-chymotrypsin Activity Assay**

The activity of α-chymotrypsin was assayed spectrophotometrically at 25 °C using Synergy H4 Hybrid Multi-Mode Microplate Reader (Bio-Tek Instruments, Inc.). A solution of α-chymotrypsin (21.9 µg/mL) in 1 mM aqueous HCl was prepared fresh by a 1:40 dilution of a stock solution (874 µg/mL) in 1 mM aqueous HCl and kept on ice. A 1:100 dilution of the 21.9 µg/mL solution in ice-cold 1 mM aqueous HCl was prepared immediately before the start of each measurement. The assay was conducted in black 96-well plates as below: To each well were added Ala-Ala-Phe-7-AMC (Sigma Aldrich, Castle Hill, NSW) substrate in DMSO (5 µL, final concentrations = 0.25, 0.5 mM), α-chymotrypsin in 1 mM aqueous HCl (10 µL, final concentration = 4 nM), an inhibitor (0.25 nM-25 nM) in DMSO (10 µL) and N-

[Tris(hydroxymethyl)methyl]-2-aminoethanesulfonic acid (TES) buffer (50 mM, pH 8.0, adjusted with NaOH) (175 μ L). The excitation and emission wavelengths of the substrate were 380 nm and 460 nm respectively. Progress curves were monitored over 10 min for each concentration of every inhibitor. The K_i values of inhibitors were determined graphically according to Dixon 1 using mean values of relative rates obtained from triplicate measurements at two different concentrations.

Cell Viability Assays

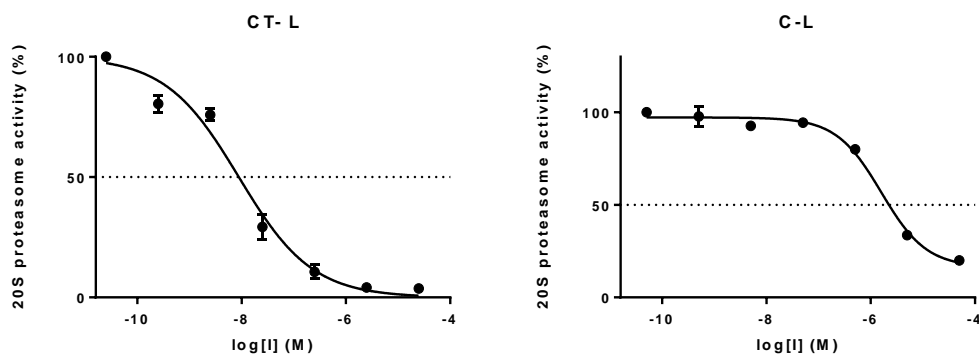
Cell viability assays were performed as previously described 2. Briefly, cells were seeded in 96-well microtiter plates at a density of 3×10^4 cells per well in the presence of the indicated proteasome inhibitor. Cells were harvested 48 hours post-treatment, centrifuged at $1,300 \times g$, washed in phosphate-buffered saline (PBS), and stained with 7AAD solution (2 μ g/mL) (7-amino-actinomycin-D, Invitrogen, Carlsbad, CA) for 10 minutes at RT. Viable cells were determined using a FACS Calibur flow cytometer (Becton Dickinson Immunocytometry Systems) and analyzed with FLOWJO (Tree Star, Inc.) and GraphPad Prism (GraphPad Software Inc.). For each experiment each data-point was in triplicate and the LD_{50} calculated from three biological replicates.

Western blot analysis

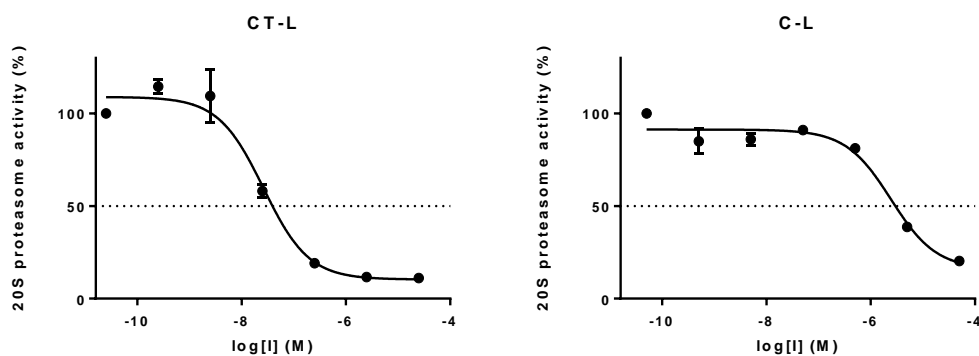
Western blot analysis was performed as previously described 3. Whole protein lysates (5–20 µg) were resolved using SDS PAGE electrophoresis, and probed overnight at 4 °C with the anti-Ubiquitin primary antibody (3933, 1:1000, Cell Signaling Technology). Chemiluminescent detection of protein was done using appropriate secondary antibody conjugated with horseradish peroxidase (Amersham) and the enhanced chemiluminescence kit according to the manufacturer's instructions (Amersham).

Supplementary Data

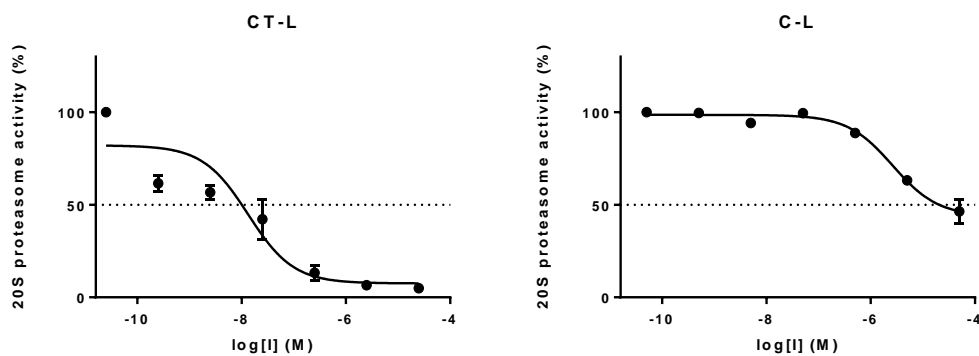
Supplementary Figure S1: Dose response curves- Compound 1a



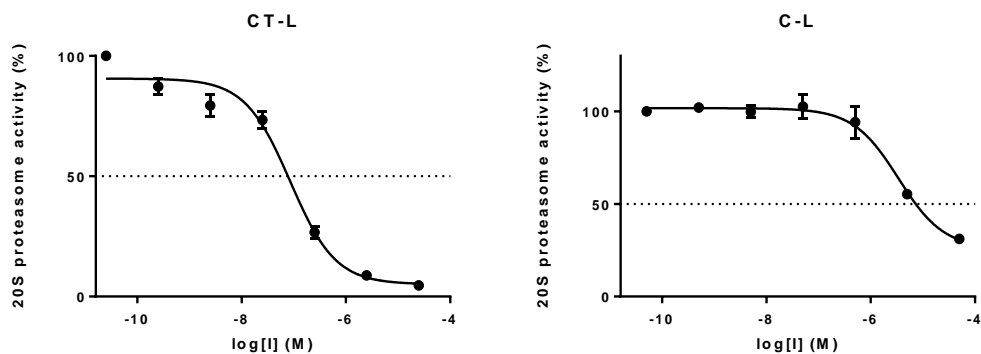
Supplementary Figure S1: Dose response curves- Compound 1b



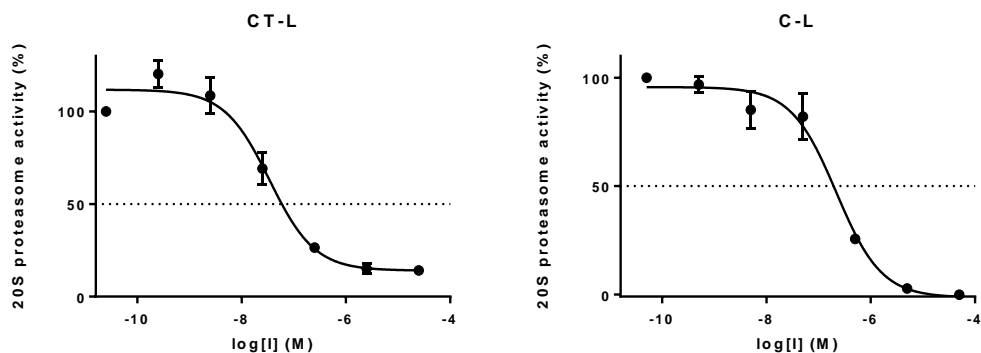
Supplementary Figure S1: Dose response curves- Compound 2a



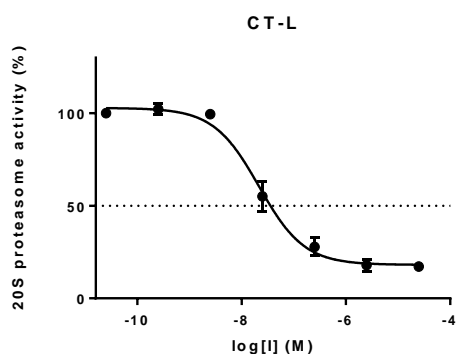
Supplementary Figure S1: Dose response curves- Compound 2b



Supplementary Figure S1: Dose response curves- Bortezomib



Supplementary Figure S1: Dose response curves- Carfilzomib

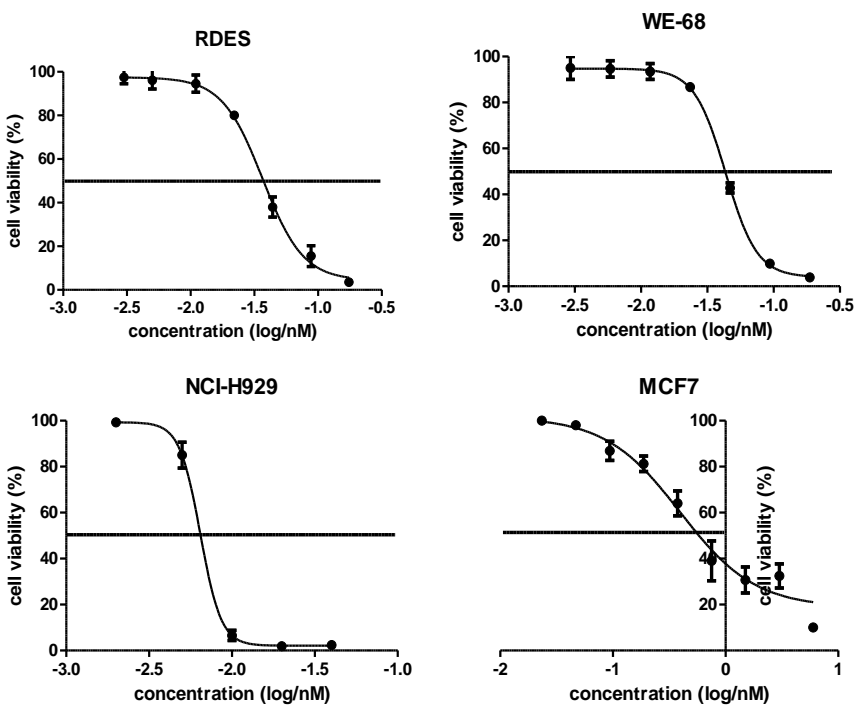


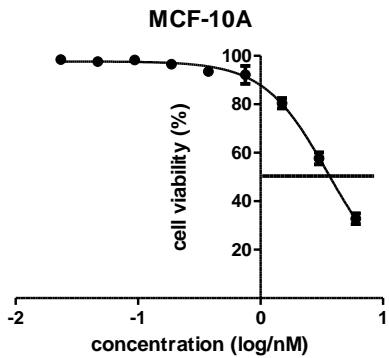
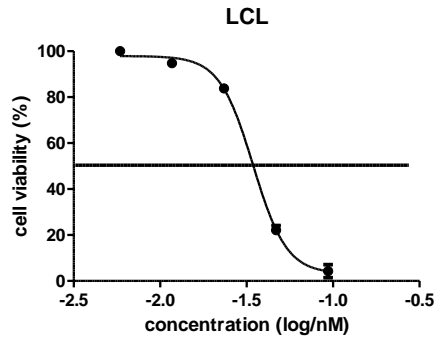
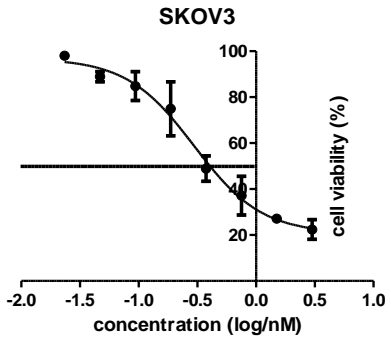
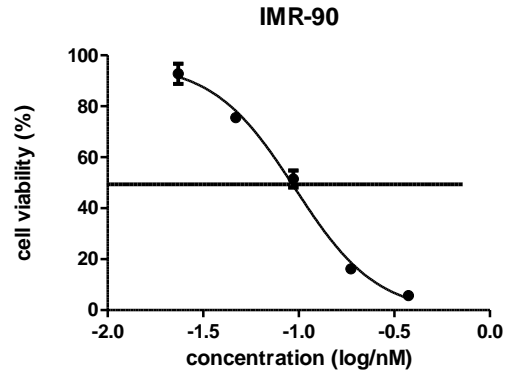
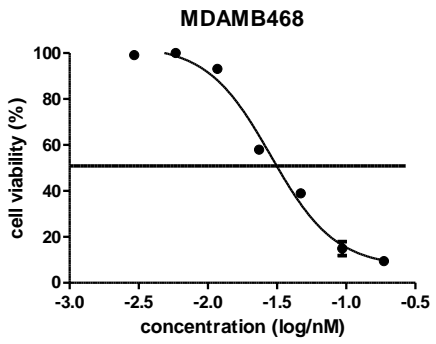
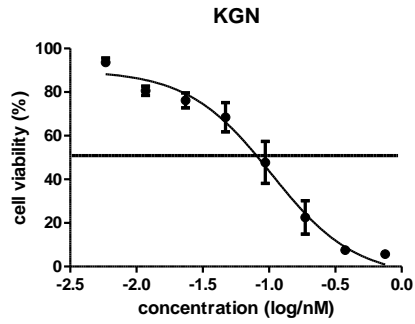
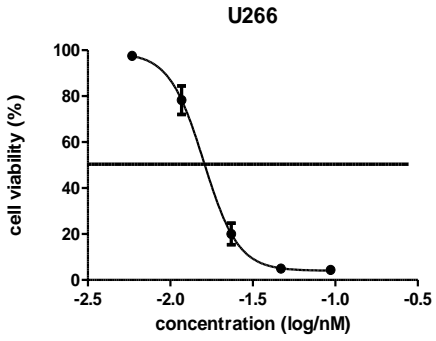
Supplementary Figure S1: Dose-response curves for proteasome inhibitors on purified rabbit 20S proteasome. The purified proteasome was incubated with the indicated concentrations of bortezomib, carfilzomib, compounds 1a,b and 2a,b and specific AMC-tagged peptide substrates

(Suc-Leu-Leu-Val-Tyr-AMC for CT-L, Bz-Val-Gly-Arg-AMC for T-L and Ac-nLPnLD-AMC for C-L) for 2 h. Hydrolysed AMC was subsequently detected with the Synergy™ H4 Hybrid Multi-Mode Microplate Reader (BioTek, USA) at excitation/emission wavelengths of 390/460 nm. Dose-response curves and IC₅₀ values (concentration of proteasome inhibitor required to inhibit 50% of enzyme activity) were calculated using GraphPad Prism software (GraphPad Software Inc).

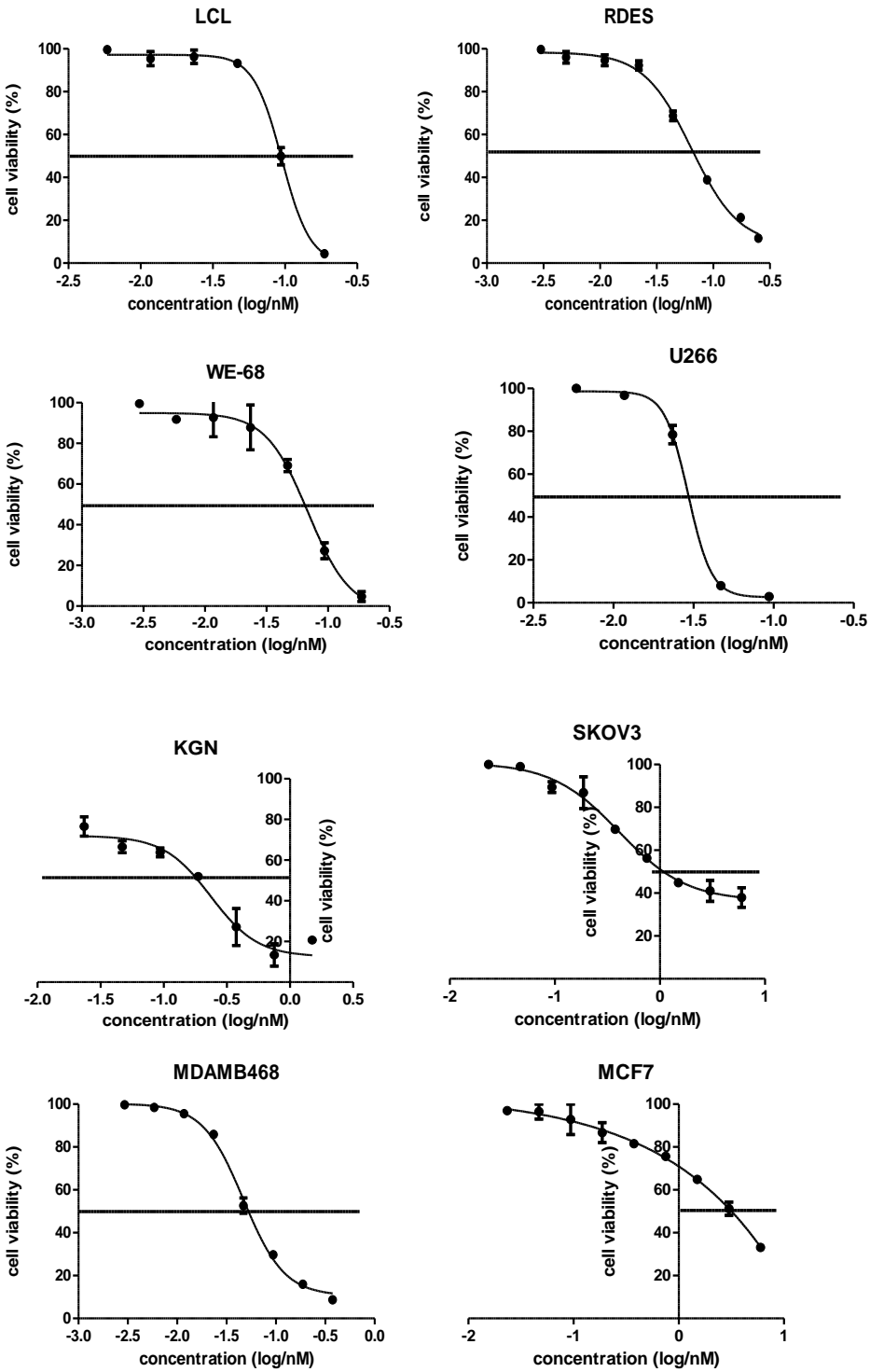
Dose-response Curves for Cell Cytotoxicity Experiments

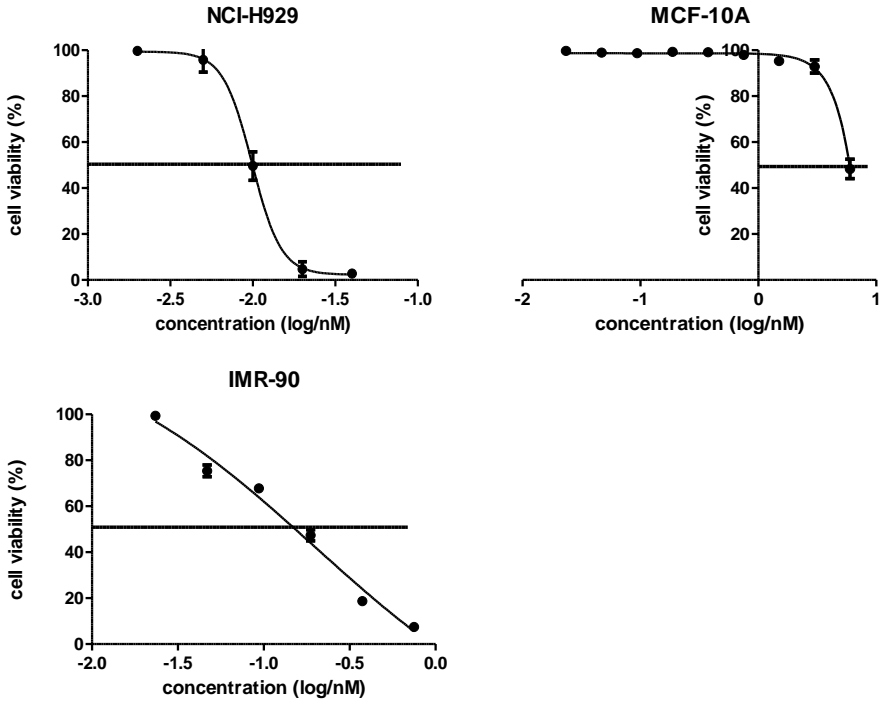
Supplementary Figure S2: Dose response curves- Compound 1a



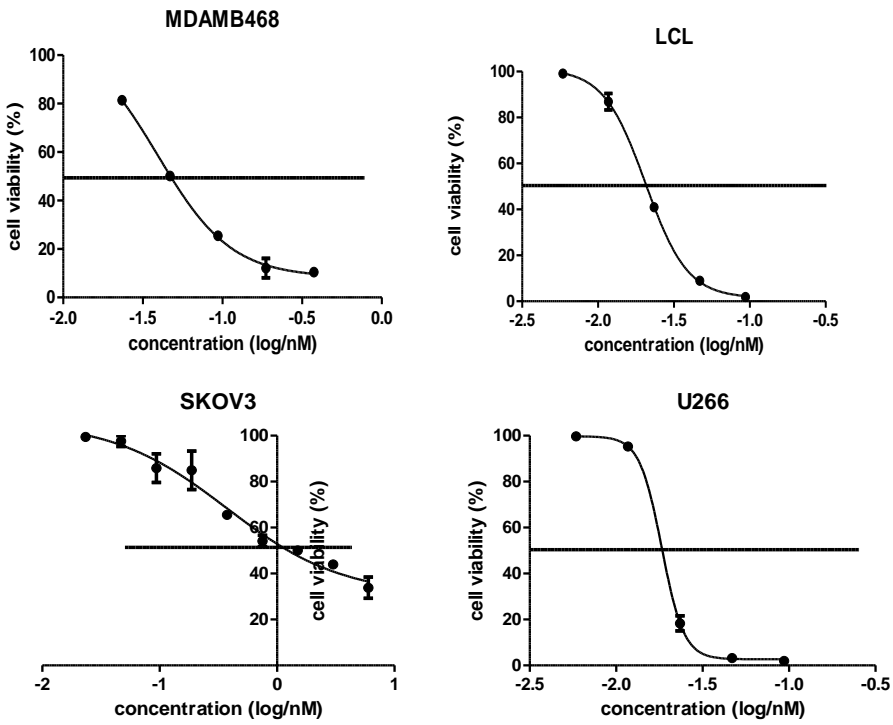


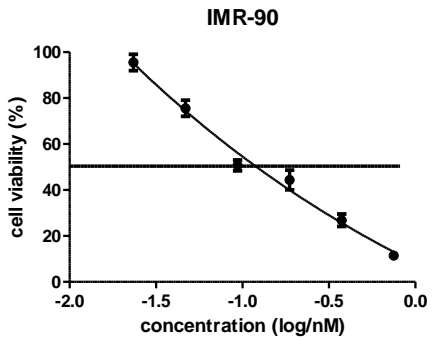
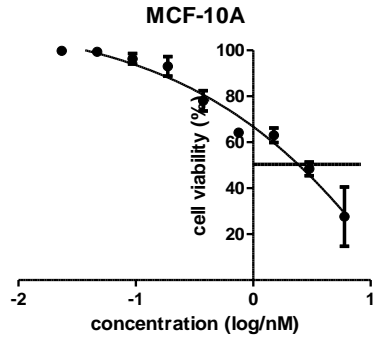
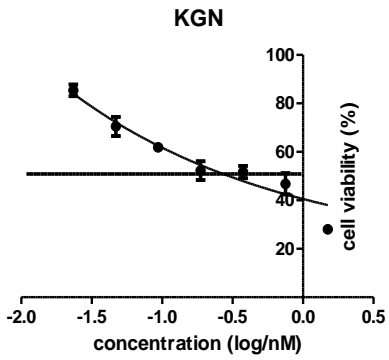
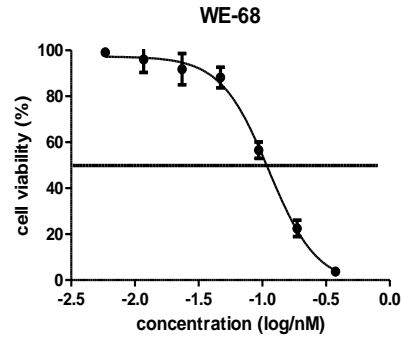
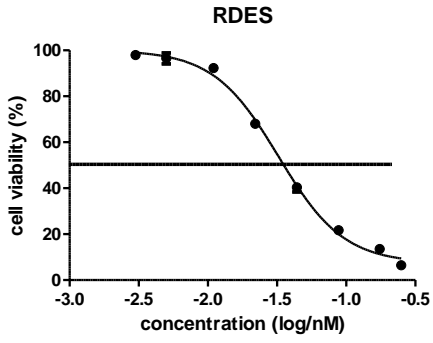
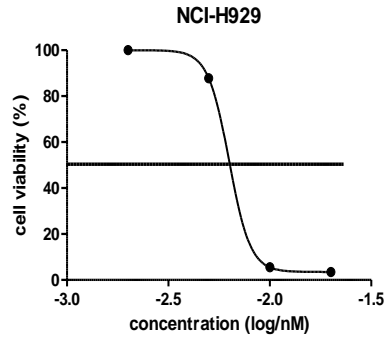
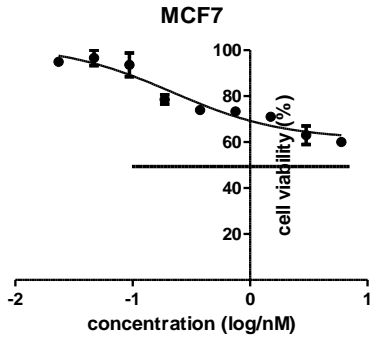
Supplementary Figure S2: Dose response curves- Compound 2a



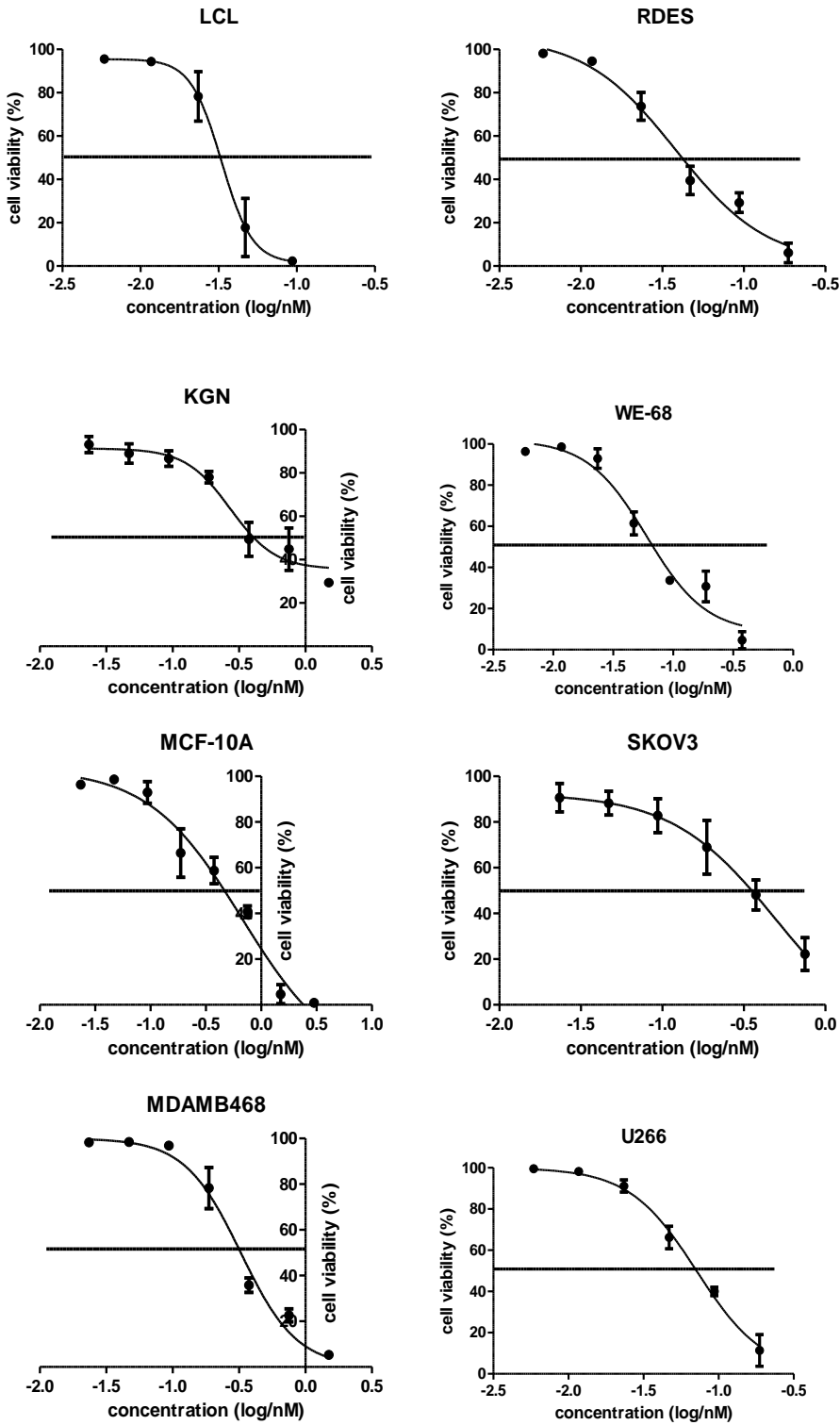


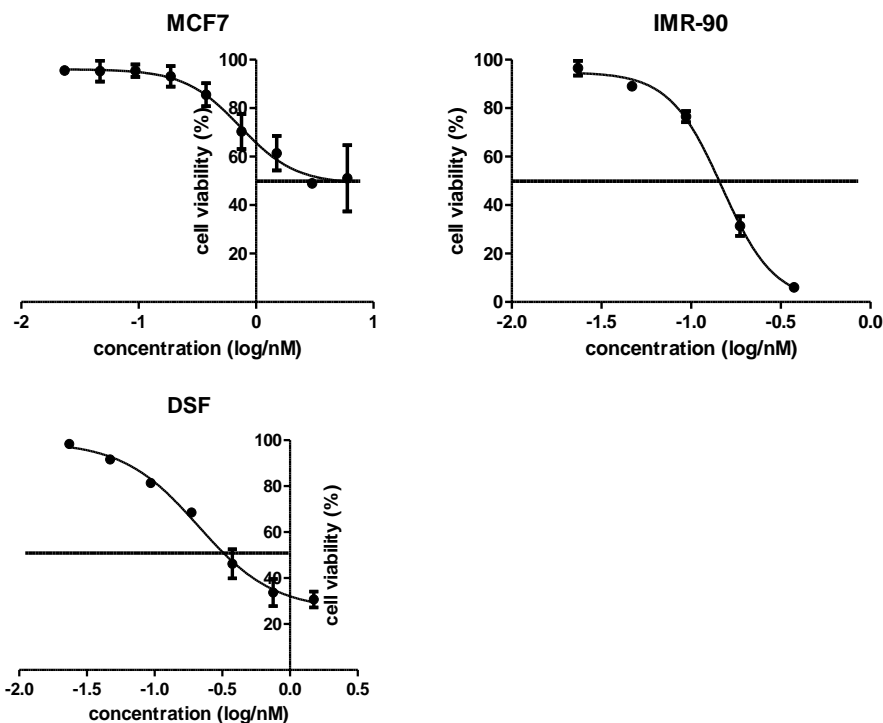
Supplementary Figure S2: Dose response curves- Bortezomib





Supplementary Figure S2: Dose response curves- Carfilzomib





Supplementary Figure S2: Dose-response curves for proteasome inhibitors on a panel of normal and cancer cell lines. WE-68 and RDES Ewings sarcoma cells, KGN and SKOV3 ovarian cancer cells, NCI-H929 and U266 multiple myeloma cells, MDAMB468 and MCF7 breast carcinoma cells (cancer cells) or primary lung and skin fibroblasts, immortalized non-malignant MCF10A or normal b-lymphoblastoids (normal cells) and were incubated with the indicated concentrations of bortezomib, carfilzomib, compounds 1a and 2a for 48 hours. The viability of the cell cultures was subsequently assessed following the protocol outlined in the Materials and Methods. Dose-response curves and IC₅₀ values (concentration of proteasome inhibitor required to kill 50% of cells) were calculated using GraphPad Prism software (GraphPad Software Inc).

CHAPTER 4

Investigation into the S2 and S3 binding sites of proteasome using light-controlled inhibitors

Beatriz Blanco¹, Kathryn Palasis¹, **Alaknanda Adwal**², David F. Callen² and Andrew D. Abell^{1,3}

¹Department of Chemistry, The University of Adelaide, North Terrace, Adelaide, South Australia 5005, Australia

²Centre for Personalised Cancer Medicine, Adelaide Medical School, The University of Adelaide, North Terrace, Adelaide, South Australia 5005,


³ARC Centre of Excellence for Nanoscale BioPhotonics, Institute of Photonics and Advanced Sensing, Department of Chemistry, The University of Adelaide, Adelaide, South Australia 5005

Statement of Authorship

Statement of Authorship

Title of Paper	Investigation into the S2 and S3 binding sites of proteasome using light-controlled inhibitors		
Publication Status	<input type="checkbox"/> Published	<input type="checkbox"/> Accepted for Publication	<input checked="" type="checkbox"/> Unpublished and Unsubmitted work written in manuscript style
Publication Details	<input type="checkbox"/> Submitted for Publication		

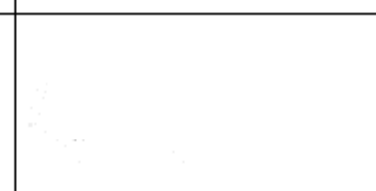
Principal Author

Name of Principal Author (Candidate)	Alaknanda Adyal		
Contribution to the Paper	Conducted all biological experiments, analysed and interpreted data and wrote manuscript.		
Overall percentage (%)	15%		
Certification:	This paper reports on original research I conducted during the period of my Higher Degree by Research candidature and is not subject to any obligations or contractual agreements with a third party that would constrain its inclusion in this thesis. I am the primary author of this paper.		
Signature		Date	6/3/2017

Co-Author Contributions

By signing the Statement of Authorship, each author certifies that:

- the candidate's stated contribution to the publication is accurate (as detailed above);
- permission is granted for the candidate to include the publication in the thesis; and
- the sum of all co-author contributions is equal to 100% less the candidate's stated contribution.

Name of Co-Author	Beatrice Blanco		
Contribution to the Paper	Synthesized chemical compounds and conducted chemistry experiments, interpreted data and co-wrote manuscript.		
Signature		Date	3/4/2017

Name of Co-Author	Kathryn Palasis		
Contribution to the Paper	Contributed to overall design and manuscript preparation.		
Signature		Date	3/4/17

Name of Co-Author	David F Callen		
Contribution to the Paper	Contributed to conception, design and manuscript preparation, and overall supervision of project.		
Signature		Date	10/03/17

Name of Co-Author	Andrew D Abell		
Contribution to the Paper	Contributed to conception, design and manuscript preparation, and overall supervision of project.		
Signature		Date	1/4/2017

Prelude

Although the FDA has approved the use of proteasome inhibitors for the treatment of multiple myeloma and refractory mantle cell lymphoma, their administration results in severe toxicities due to their non-specific damage to healthy tissue. Here, we have assessed whether a photopharmacological approach, using switchable moieties incorporated into the molecular structure of proteasome inhibitors can potentially be used to activate drugs specifically in cancerous tissue.

This chapter is presented as a manuscript in preparation for submission to a journal for publication.

Contribution by the candidate: All biological/cell line experimental work and manuscript writing pertaining to biology.

Abstract

A series of azobenzene-containing peptidic boronate esters was prepared and the activity of the thermally adapted states (TAS), enriched in *trans* isomer, and the photostationary states (PSS), enriched in *cis* isomer, for each compound were evaluated against $\beta 5$ and $\beta 1$ proteasome subunits. Compounds with a sterically demanding phenyl-substituted azobenzene at P2 (**4c**), and a less sterically demanding unsubstituted azobenzene at the *N*-terminus (**5a**), showed the greatest difference in activity between the two states. In both cases, the more active *trans*-enriched TAS had activity comparable to bortezomib and delanzomib. Furthermore, *cis*-enriched **4c** inhibited tumor growth in both breast and colorectal carcinoma cell lines. Significantly, the initial *trans*-enriched TAS of **4c** was not cytotoxic against the non-malignant MCF-10A cells.

Introduction

The 26S proteasome is a supramolecular protein assembly that plays a pivotal role in the degradation of proteins that regulate the cell cycle.¹ Its over activity is associated with the development and progression of some cancers and as such it has recently been identified as an attractive target for anticancer drugs, particularly for the treatment of multiple myeloma (MM).² Its substrates are degraded at three sites located within the inner cavity of the component 20S proteasome, i.e., chymotrypsin-like ($\beta 5$), trypsin-like ($\beta 2$), and caspase-like ($\beta 1$) subunits.³ ⁴ ⁵ ⁶ The clear link between the proteasome and the development of a number of human diseases has encouraged the development of a range of inhibitors and an evaluation of their therapeutic potential.⁷ ⁸ ⁹ ¹⁰ ¹¹ ¹² ¹³ ¹⁴ ¹⁵ In fact, the FDA has now approved three such inhibitors (bortezomib (**1**), carfilzomib and ixazomib) for the treatment of multiple myeloma and refractory mantle cell lymphoma, with others in development.¹⁶ ¹⁷ ¹⁸ Several other proteasome inhibitors have entered clinical trials, including delanzomib (**2**) and oprozomib.¹⁹ While delanzomib²⁰ is reported to overcome resistance reported for bortezomib *in vitro*,²¹ it shows limited efficacy in the treatment of other types of cancer. It also displays severe side effects due to non-specific cytotoxicity towards healthy tissue (Fig. 1).²² ²³

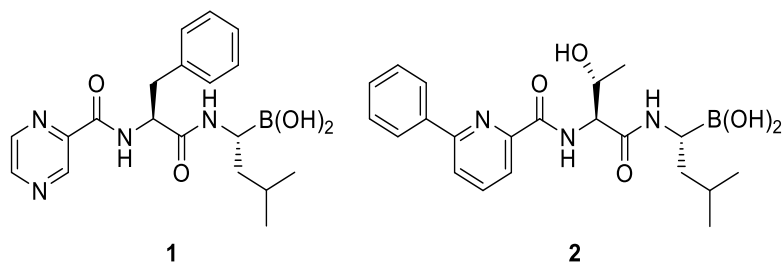
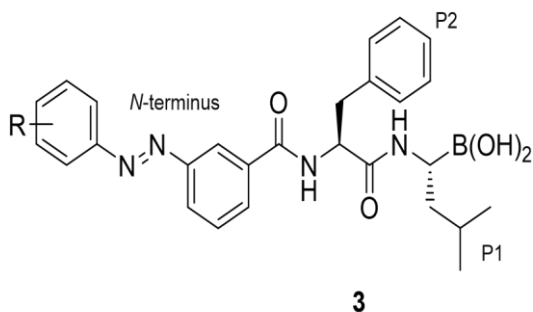


Figure 1. Chemical structures of proteasome inhibitors Bortezomid (**1**) and Delanzomib (**2**)

There is a clear need to develop new proteasome inhibitors with improved safety and efficacy profiles. One approach described herein is to develop inhibitors that undergo specific activation at the site of action, e.g., through the action of light.²⁴ Light is ideally suited to control the activity of a pharmacophore as it can be delivered with very high spatiotemporal precision.²⁵ With this in mind, Feringa et al.²⁶ recently reported an analogue of bortezomib containing an *N*-terminal azobenzene, see structure **3** in [Fig. 2](#). A photostationary state (PSS) of **3** enriched in the *cis* isomer proved to be moderately (two- to three-fold) more active than a thermally adapted state (TAS) enriched in the *trans* isomer, with the magnitude of difference showing some dependence on the nature of the component azobenzene. Related studies have been carried out on other proteases. [27](#); [28](#); [29](#) We now report studies on an extended series of photoswitchable proteasome inhibitors with a number of different azobenzenes at the *N*-terminus (see [5](#)) and at P2 (see [4](#)), to further investigate the effect of azobenzene substitution on activity and also to explore the S2 binding site [30](#); [31](#) as an alternative site for modification. All compounds contain a boronate ester, rather than the boronic acid of bortezomib and delanzomib, with this prodrug presenting similar potency while being easier to prepare. [32](#); [33](#) The P2 positioned azobenzene of **4** replaces the phenylalanine of bortezomib, where this site is known to accommodate larger groups.⁵ The *N*-terminal azobenzene-based peptide boronates **5** provide an opportunity to investigate the influence of an alternative backbone sequence with a threonine at P2 as found in delanzomib. Azobenzene substituents were chosen to investigate potential steric effects and to expand on earlier studies. Synthetic *trans*-enriched azobenzenes **4** and **5** were photochemically isomerized to give an

alternative PSS enriched in the *cis* isomer. All states were assayed against the $\beta 5$ and $\beta 1$ subunits of rabbit 20S proteasome (Fig. 3).



R = Ph, *o*-Me-Ph, *m*-Me-Ph, *p*-Me-Ph, *p*-OMe-Ph and 2,6-diMe-Ph

Figure 2. Photoswitchable proteasome inhibitors 3. Residues are designated P1, P2 etc from the boronic acid, where these groups interact with corresponding proteasomal specificity pockets according to the nomenclature of Schechter and Berger. 34.

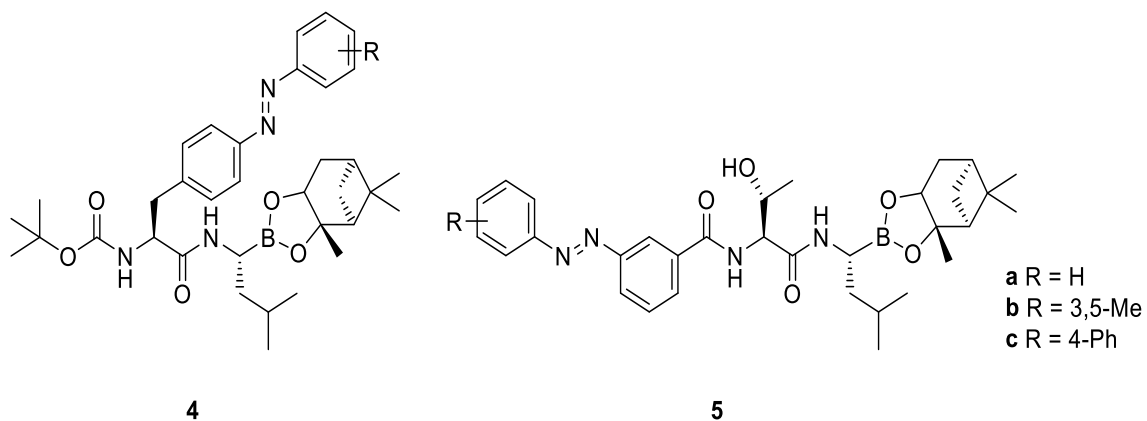
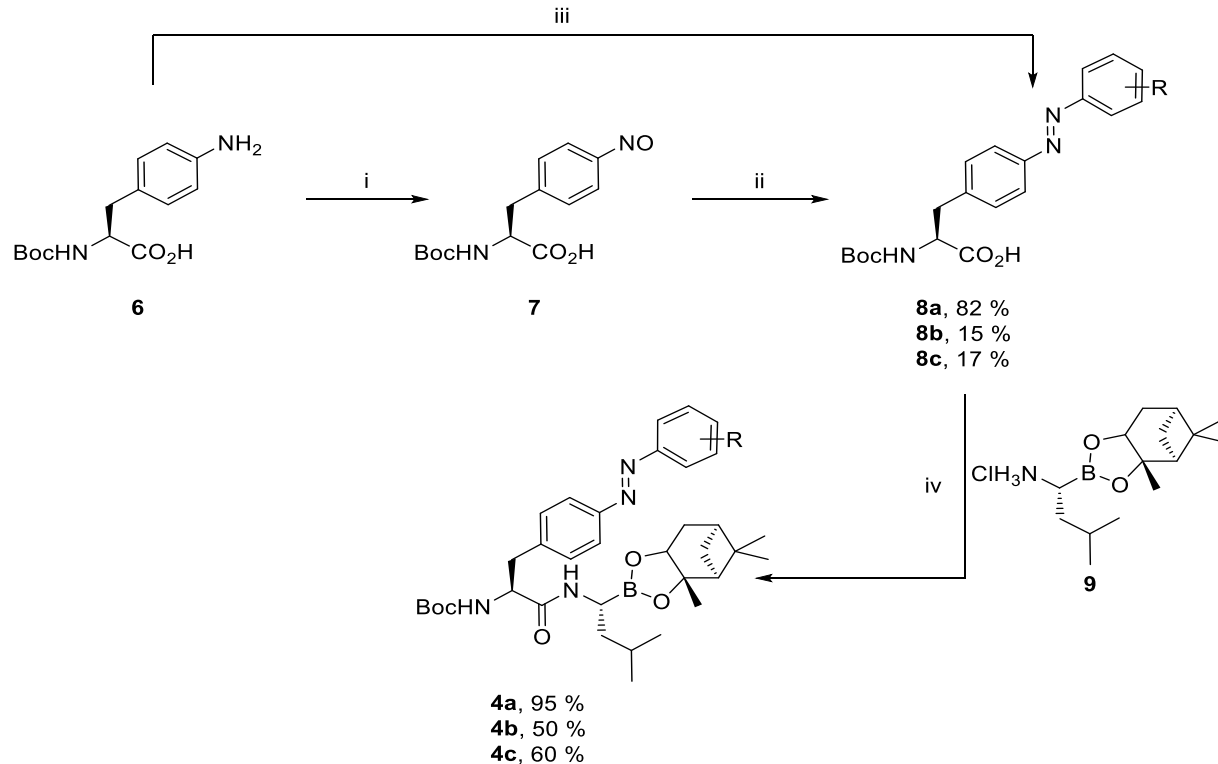


Figure 3. Photoswitchable target compounds 4 and 5.

Results and Discussion

Chemistry

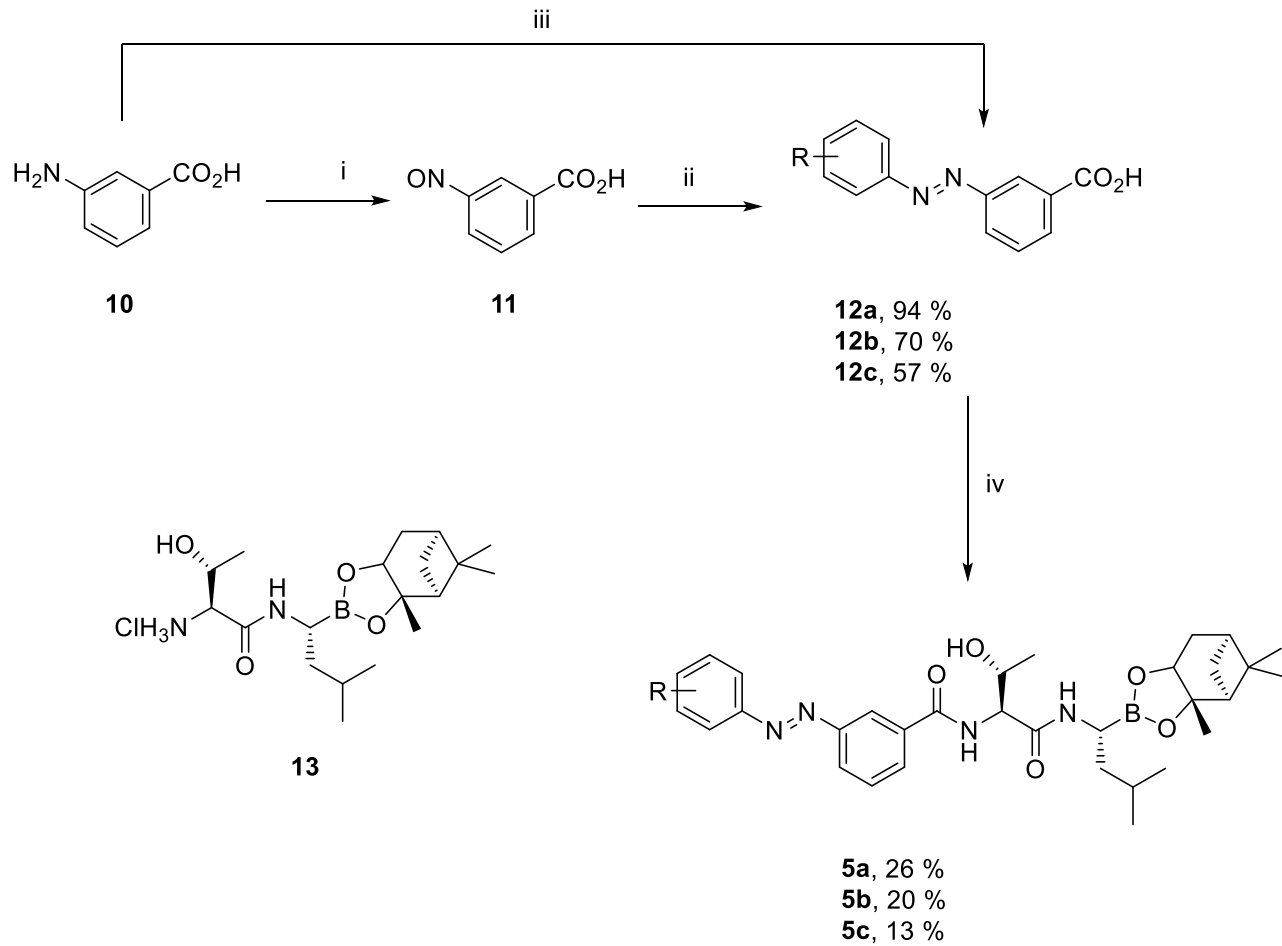
The bortezomib analogues **4a–c** were prepared as shown in Scheme 1. The key intermediates **8b** and **8c** were prepared by oxidation of the aniline **6** to the nitroso derivative **7** using Oxone[®] followed by condensation with the appropriate aniline. The other key intermediate **8a** was synthesized by condensation of **6** directly with commercially available nitrosobenzene. The proposed inhibitors **4a–c** were then prepared by coupling of **8a–c** with **935'**³⁶ using *N,N,N',N'*-tetramethyl-*O*-(benzotriazol-1-yl)uronium tetrafluoroborate (TBTU) as the coupling agent. The alternative delanzomib derivatives **5a–c**, containing an *N*-terminal azobenzene, were synthesized as outlined in Scheme 2. The key azobenzenes **12b** and **12c** were prepared by oxidation of the aniline **10** to the nitroso **11**³⁷ using Oxone[®] followed by condensation with the corresponding aniline. The remaining key azobenzene **12a** was prepared by condensation of **10** directly with commercially available nitrosobenzene. TBTU mediated coupling of **12a–c** with **13**³⁸ then gave the desired boronate esters **5a–c** as shown.



Scheme 1. Synthesis of photoswitchable inhibitors **4**. Reagents and conditions: i) Oxone[®], DCM:water, RT, 3 h; ii) ArNH₂, DMSO, HOAc, 60 °C, O/N; iii) Nitrosobenzene, HOAc, RT, O/N; iv) TBTU, DIPEA, DMF, 0 °C to RT, O/N.

Proteasome inhibitory activities

¹H NMR analysis of compounds **4–5** in DMSO-*d*₆ revealed an initial TAS strongly enriched in the *trans* isomer, with the results shown in [Table 1a](#). A solution of each compound in DMSO-*d*₆ (~1 mg/mL) was then irradiated with UV light using a UVP BL6SV lamp (λ = 365 nm) for 1 h to give the corresponding *cis*-enriched PSS of **4–5**. ¹H NMR again defined the *trans/cis* compositions, with the results also shown in [Table 1a](#). All compounds analysed after irradiation gave a PSS strongly enriched in the *cis* isomer (>76%), with the exception of **5a** with its relatively small *N*-terminal azobenzene (46% *cis*). Compound **5c**, with its sterically large *N*-terminal azobenzene, gave the highest enrichment of *cis* isomer (92%). In comparison, compounds with a less sterically demanding azobenzene substituent (as in **4a** and **5a**) give the highest isomer differential prior to UV irradiation, with the *trans* isomer being the major in this case.



Scheme 2. Synthesis of photoswitchable inhibitors **5**. Reagents and conditions: i) Oxone[®], DCM:water, RT, 4 h, (71 %); ii) ArNH₂, DMSO, HOAc, 60 °C, O/N; iii) Nitrosobenzene, HOAc, RT, O/N; iv) **13**, DMF, TBTU, NMM, 0 °C to RT, O/N.

Table 1. a) trans/cis ratios of compounds 4–5 before and after irradiation ($\lambda = 365$ nm, in DMSO-d6). b) IC₅₀(nM) values for compounds 4–5, bortezomib and delanzomib at β 5 and β 1 active sites before and after irradiation (365 nm

Active site	Compound	4a	4b	4c	Bort.	5a	5b	5c	Delanz.
a)	non-irradiated (trans/cis)	99:1	91:9	95:5	-	97:3	78:22	77:23	-
	irradiated (trans/cis)	17:83	11:89	16:84	-	54:46	24:76	8:92	-
b) β 5	trans	10	53	11	5.4	17	55	22	10
	cis	12	41	54	7.9	84	249	29	12
	fold	1.2	1.3	5	1.5	5	4.5	1.3	1.2
β 1	trans	107	211	460	76	868	1624	498	59
	cis	110	214	303	70	759	1633	1088	55
	fold	1.1	1	1.5	1	1.1	1	2	1.1

light).

Both states of **4** and **5** were then evaluated for inhibitory activity against $\beta 5$ and $\beta 1$ proteasome subunits and the results are shown in [Table 1b](#). IC_{50} values were determined graphically according to Dixon methodology and as detailed in [Supplementary data](#).³⁹ Potency data is also included in [Table 1b](#) for bortezomib and delanzomib for comparison. All azobenzene derivatives inhibited the $\beta 5$ and $\beta 1$ active sites, with IC_{50} values ranging from low nanomolar to micromolar. Compounds were generally more potent against $\beta 5$ than $\beta 1$, with critical $\beta 5$ potency⁵ being similar to that of bortezomib and delanzomib. The non-irradiated (*trans*-enriched) TASs of **4a**, **4c** and **5a** were the most potent, with IC_{50} values of 10, 11 and 17 nM, respectively. It is interesting to note that a large azobenzene is generally well tolerated in both series, with both **4c** and **5c** showing good $\beta 5$ potency. The incorporation of an azobenzene into the structures does somewhat compromise activity against $\beta 1$, especially for those derivatives containing an *N*-terminal azobenzene (**5**). The best photoswitching of activity was obtained with compounds **4c**, **5a** and **5b**, with an approximate 5-fold decrease in $\beta 5$ activity observed on irradiation in each case. The result for **5a** is particularly significant given that irradiation only gave modest isomerism to the *cis* isomer, see [Table 1a](#). A more hindered azobenzene at P2 (**4c**) but less hindered *N*-terminal azobenzene (**5a** and **5b**) gave the best photoswitching of activity. The effect on $\beta 1$ activity is both less pronounced and less predictable.

Effect of compounds on cells

The bortezomib analogue **4c**, with a combination of the most potent $\beta 5$ activity, good conversion to the *cis* isomer (84% *cis*) and the best differential in activity between the two states (5-fold), was investigated further to define global cytotoxicity against different cell lines. Colon colorectal (HCT-116) and breast carcinoma (MDA-MB-468) cancer cell lines were chosen for these studies as they are known to be sensitive to proteasome inhibitors. ⁴⁰; ⁴¹ Cytotoxic LD₅₀ values were determined using 7AAD assays following a 48 h exposure to titrations (0–5000 nM) with the results shown in [Fig. 3](#).

Interestingly, the *cis*-enriched PSS of **4c** proved to be more active against both cell lines, despite it being less active than the corresponding *trans*-TAS against the proteasome $\beta 5$ subunit (see [Table 1](#)). This is an important finding for potential photopharmacological applications that necessarily require photoactivation at the site of action. In particular, *cis*-enriched **4c** induced cell death in the colon colorectal cancer cell line HCT-116 with a LD₅₀ of 212 nM compared to 1.03 μ M for *trans*-enriched **4c**. Nearly full selectivity was observed at 310 nM, with *cis*-enriched **4c** killing almost all cells (cell viability = 27%), and *trans*-enriched **4c** having limited cytotoxicity (cell viability = 91%), see [Fig. 4a](#). While the *cis*-enriched PSS of **4c** is stable for >48 h in DMSO, it does undergo slow isomerism to the *trans* isomer in buffer without evidence of decomposition. The cytotoxicity of *cis*-enriched **4c** is thus likely evident well before the 48 h time-course of the assay, where the *trans*-enriched state of **4c** displays limited cytotoxicity. A diminished differential was observed between the two isomeric states against the MDA-MB-468 breast cancer cell line, with an LD₅₀ of 144 nM and 246 nM for *cis*-enriched and *trans*-enriched states respectively.

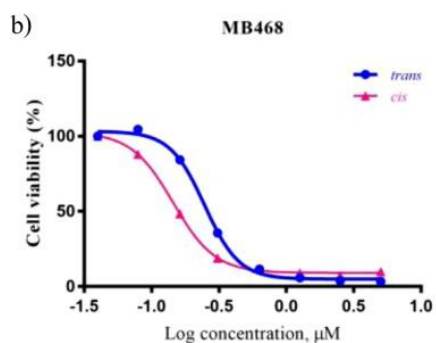
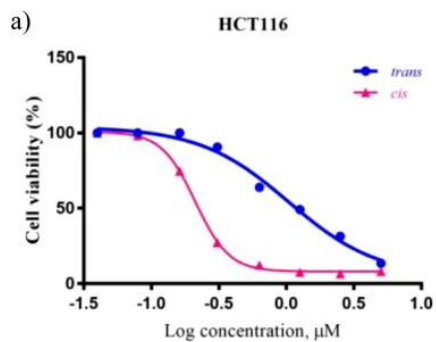


Fig. 4. **4c**-(*trans*)-TAS (blue) and **4c**-(*cis*)-PSS (pink) apoptotic dose response curves against (a) colon colorectal HCT-116 and (b) breast carcinoma MB-468 cancer cell lines following 48 h of treatment.

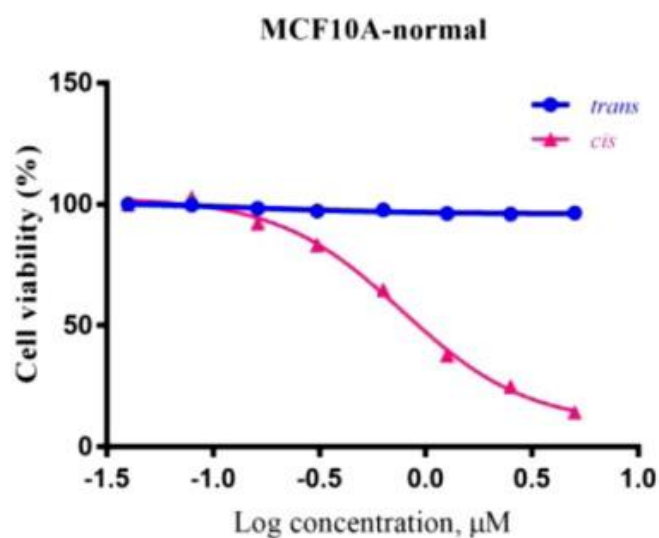


Fig. 5. 4c-(trans)-TAS (blue) and 4c-(cis)-PSS (pink) apoptotic dose response curves against normal cell line MDF-10A following 48 h of treatment.

Interestingly, the *cis*-enriched PSS of **4c** showed moderate cytotoxicity against the non-malignant MCF-10A cell line with an LD₅₀ of 683 nM. In comparison, the *trans*-enriched state of **4c** was inactive at the highest concentration tested (5000 nM) (Fig. 5). This suggests that the biological activity of the *trans*-TAS would be low in healthy tissue, to maximize any therapeutic benefit of the *cis* isomer.

Conclusions

In summary, a series of photoswitchable proteasome inhibitors was designed, synthesized and evaluated for activity against $\beta 5$ and $\beta 1$ proteasome subunits. The most active inhibitors displayed activity comparable to bortezomib and delanzomib. Derivatives **4c**, **5a** and **5b** gave the best photoswitching differential in activity against the $\beta 5$ subunit, with an approximate 5-fold lower activity observed for *cis*-enriched PSSs. This compares to a somewhat more modest two- to three- fold increase in activity observed for a *cis*-enriched PSS of bortezomib analogues **3**.²⁶ The sterically less demanding *N*-terminal azobenzene of **5a** appears to particularly favor photoswitching of activity, given that irradiation in this case only gave modest isomerism to the less active *cis* isomer. The *cis*-enriched PSS of bortezomib derivative **4c** displayed good cytotoxicity to proteasome inhibitor-sensitive cancer cell lines, with LD₅₀ values of 212 and 144 nM against the colon colorectal cancer HCT-116 and the breast carcinoma MB-468 cell lines, respectively. The corresponding *trans*-TAS displayed significantly lower cytotoxicity, particularly against the colon colorectal cancer cell line. Importantly, the *trans*-enriched TAS of **4c** was devoid of cytotoxicity against a non-malignant breast epithelial cell line MCF-10A. This suggests that the more stable *trans* isomer should have reduced side effects to facilitate and reinforce any potential therapeutic effect of the *cis* isomer. Further studies to investigate any off-target effects of the compounds reported are underway.

References

1. Gallastegui N, Groll M. *Trends Biochem Sci.* 2010;35:634–642.
2. Muz B, Ghazarian RN, Ou M, Luderer MJ, Kusdono HD, Azab AK. *Drug Des Dev Ther.* 2016;10:217–226; Hideshima T, Richardson P, Chauhan D, et al. *Cancer Res.* 2001;61:3071–3076.
3. Rechsteiner M, Hill CP. *Trends Cell Biol.* 2005;15:27–33.
4. Baumeister W, Walz J, Zühl F, Seemüller E. *Cell.* 1998;92:367–380.
5. Xin BT, de Bruin G, Huber EM, et al. *J Med Chem.* 2016;59:7177–7187; Huber EM, de Bruin G, Heinemeyer W, Soriano GP, Overkleeft HS, Groll M. *J Am Chem Soc.* 2015;137:7835–7842; Gräwert MA, Groll M. *Chem Commun.* 2012;48:1364–1378; Groll M, Heinemeyer W, Jäger S, et al. *Proc Natl Acad Sci USA.* 1999;96:10976–10983.
6. Berkens CR, Ovaas H. *Biochem Trans.* 2010;38:14–20.
7. Elliott PJ, Pien CS, McCormack TA, Chapman ID, Adams J. *J Allergy Clin Immunol.* 1999;104:294–300.
8. Koreth J, Alyea EP, Murphy WJ, Welniak LA. *Biol Blood Marrow Transplant.* 2009;15:1502–1512.
9. Pehere AD, Pietsch M, Gütschow M, et al. *Chem Eur J.* 2013;19:7975–7981; Pehere AD, Zhang X, Abell AD. *Aust J Chem.* 2017;70:138–151; Pehere AD, Abell AD. *Org Lett.* 2012;14:1330–1333.
10. Bennett MK, Kirk CJ. *Curr Opin Drug Discovery Dev.* 2008;11:616–625.
11. Kisselev AF, Van der Linden WA, Overkleeft HS. *Chem Biol.* 2012;19:99–115.
12. Terpos E, Sezer O, Croucher P, Dimopoulos M-A. *Blood.* 2007;110:1098–1104.
13. Mattingly LH, Gault RA, Murphy WJ. *Endocr Metab Immune Disord Drug Targets.* 2007;7:29–34.

14. Le Chapelain C, Groll M. *Angew Chem Int Ed*. 2016;55:2–5.
15. Totaro KA, Barthelme D, Simpson PT, et al. *ACS Infect Dis*. 2017;3:176–181.
16. Muz B, Ghazarian RN, Ou M, Luderer MJ, Kusdono HD, Azab AK. *Drug Des Dev Ther*. 2016;10:217–226.
17. Gallerani E, Zucchetti M, Brunelli D, et al. *Eur J Cancer*. 2013;49:290–296.
18. Steele JM. *J Oncol Pharm Pract*. 2013;19:348–354.
19. U.S. National Library of Medicine. U.S. National Institutes of Health, ClinicalTrials.gov.
20. Piva R, Ruggeri B, Williams M, et al. *Blood*. 2008;111:2765–2775.
21. Berkers CR, Leestemaker Y, Schuurman KG, et al. *Mol Pharmaceutics*. 2012;9:1126–1135.
22. Arastu-Kapur S, Anderl JL, Kraus M, et al. *Clin Cancer Res*. 2011;17:2734–2743.
23. Kubiczikova L, Pour L, Sedlarikova L, Hajek R, Sevcikova S. *J Cell Mol Med*. 2014;18:947–961.
24. Velema WA, Szymanski W, Feringa BL. *J Am Chem Soc*. 2014;136:2178–2191.
25. Szymanski W, Beierle JM, Kistemaker HAV, Velema WA, Feringa BL. *Chem Rev*. 2013;113:6114–6178.
26. Hansen MJ, Velema WA, de Bruin G, Overkleeft HS, Szymanski W, Feringa BL. *ChemBioChem*. 2014;15:2053–2057.
27. Abell AD, Jones M, Neffe A, et al. *J Med Chem*. 2007;12:2916–2920.
28. Pearson D, Alexander N, Abell AD. *Chem Eur J*. 2008;14:7358–7365.
29. Pearson D, Abell AD. *Org Biomol Chem*. 2006;4:3618–3625; Pearson D, Downard AJ, Muscroft-Taylor A, Abell AD. *J Am Chem Soc*. 2007;129:14862–14863.
30. Groll M, Berkers CR, Ploegh HL, Ovaa H. *Structure*. 2006;14:451–456.
31. Borissenko L, Groll M. *Chem Rev*. 2007;107:687–717.

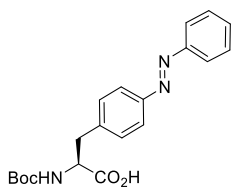
32. Kettner CA, Shenvi AB. *Biol Chem.* 1984;259:15106; Weber PC, Lee SL, Lewandowski FA, Schadt MC, Chang CH, Kettner CA. *Biochemistry.* 1995;34:3750.
33. Trippier PC, McGuigan C. *Med Chem Commun.* 2010;1:183–198; Venturelli A, Tondi D, Cancian L, et al. *J Med Chem.* 2007;50:5644–5654.
34. Schechter I, Berger A. *Biochem Biophys Res Commun.* 1967;27:157–162.
35. Elgendy S, Claeson G, Kakkar VV, et al. *Tetrahedron.* 1994;50:3803–3812.
36. Zhu Y, Zhao X, Zhu X, et al. *J Med Chem.* 2009;52:4192–4199.
37. Priewisch B, Ruck-Braun K. *J Org Chem.* 2005;70:2350–2352.
38. Dorsey BD, Iqbal M, Chatterjee S, et al. *J Med Chem.* 2008;51:1068–1072.
39. Dixon M. *Biochem J.* 1953;55:170–171.
40. Piva R, Ruggeri B, Williams M, et al. *Blood.* 2008;111:2765–2775.
41. Zhang X, Adwal A, Turner AG, Callen DF, Abell AD. *ACS Med Chem Lett.* 2016;7:1039–1043; Neilsen PM, Pehere AD, Pishas KI, Callen DF, Abell AD. *ACS Chem Biol.* 2013;8:353–359.

Supplementary material

a. Chemical Synthesis

General Information. Unless otherwise indicated, all starting materials and reagents were purchased from AK Scientific or Sigma-Aldrich and used without further purification. The boronic ester **13** was prepared following literature procedures.¹ TLC analysis was performed on 60 F₂₅₄ Silica gel TLC plates, and spots were visualised under UV light (254 nm) and using either CAM or KMnO₄ stains. LC60A 40-63 micron silica was used for flash chromatography purifications. ¹H and ¹³C NMR spectra were obtained using either an Agilent DD2 console 500 MHz or a Varian Inova 600 MHz spectrometer, at the indicated frequencies, using either CDCl₃, CD₃OD or DMSO-*d*₆. ¹H chemical shifts are reported in ppm (δ) to 2 decimal places and ¹³C chemical shifts are reported in ppm to 1 decimal place. ¹H coupling constants are reported to 1 decimal place. Infra-red spectra were obtained using a PerkinElmer FTIR 100 spectrometer (ATR), and all peaks are reported to 1 decimal place. HRMS (ESI) spectra were recorded using an Agilent QTOF HRMS and m/z masses are reported to 4 decimal places. Chemical structures and their systematic names were generated using ChemDraw Ultra 12.0. A UVP BL6SV lamp (358 nm) was used as the UV light source in photoswitching experiments.

Abbreviations used: NMM: *N*-methylmorpholine; TBTU: *N,N,N',N'*-tetramethyl-O-(benzotriazol-1-yl)uronium tetrafluoroborate; DCM: dichloromethane; MgSO₄: magnesium sulfate; DMSO: dimethyl sulfoxide; DIPEA: *N,N*-Diisopropylethylamine; EtOAc: ethyl acetate;



8a

Synthesis of (S,E)-2-((tert-butoxycarbonyl)amino)-3-(4-(phenyldiazenyl)phenyl)propanoic acid (8a)

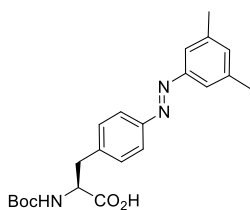
Nitrosobenzene (346 mg, 3.23 mmol, 1 eq) and 4-aminophenylalanine (500 mg, 1.78 mmol, 1.1 eq) were added to acetic acid (15 mL) and the mixture was stirred at room temperature for 12 h. The solution was diluted with water, extracted with DCM, dried over MgSO₄ and the solvent evaporated under reduced pressure. Purification by flash chromatography (20% EtOAc:Hexane) gave **8a** (537 mg, 82%) as an orange foam.

¹H NMR (500 MHz, CDCl₃) δ 7.90 (d, *J* = 7.3 Hz, 2H, 2xArH), 7.87 (d, *J* = 8.3 Hz, 2H, 2xArH), 7.53–7.44 (m, 3H, 3xArH), 7.34 (d, *J* = 8.2 Hz, 2H, 2xArH), 4.98 (d, *J* = 7.1 Hz, 1H, NH), 4.66 (dd, *J* = 12.8, 6.8 Hz, 1H, Tyr-α-H), 3.30 (dd, *J* = 13.7, 5.1 Hz, 1H, Tyr-β-CHH), 3.17 (dd, *J* = 13.7, 6.0 Hz, 1H, Tyr-β-CHH) and 1.43 (s, 9H, C(CH₃)₃) ppm.

¹³C NMR (126 MHz, CDCl₃) δ 176.1, 155.5, 152.8, 151.9, 139.4, 131.1, 130.3, 129.2, 123.1, 123.0, 80.6, 54.4, 38.0 and 28.4 ppm.

HRMS (ESI) calcd for C₂₀H₂₃NaN₃O₄ (M+Na)⁺ 392.1586, found 392.1584.

IR (ATR) ν: 2981 (O–H), 1710 and 1653 (C=O) and 1512 (N=O) cm⁻¹.



8b

Synthesis of (S,E)-2-((tert-butoxycarbonyl)amino)-3-(4-((3,5-dimethylphenyl)diazenyl)phenyl)propanoic acid (8b)

A biphasic mixture of 4-aminophenylalanine **6** (500 mg, 1.8 mmol, 1 eq) and Oxone® (1.6 g, 5.34 mmol, 3 eq) in DCM (25 mL) and water (13 mL) was stirred vigorously at room temperature for 3 h. The organic layer was separated and the aqueous layer was extracted with DCM (x2). The combined organic layers were washed with brine, dried over MgSO₄, filtered and evaporated under reduced pressure. Crude **7** was used immediately in the next step and without further purification.

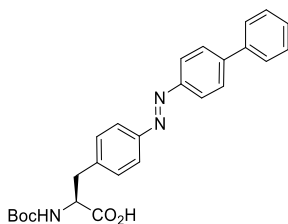
To a solution of **7** (524 mg, 1.8 mmol, 1 eq) and 3,5-dimethylaniline (0.17 mL, 1.42 mmol, 0.8 eq) in DMSO (4.5 mL) was added acetic acid (0.4 mL) and the mixture was stirred at room temperature for 18 h. The crude product was partitioned between water and EtOAc and the organic phase was washed with water (x2). The organic phase was dried over MgSO₄, filtered and evaporated under reduced pressure. Purification by flash chromatography (30-50% EtOAc:hexane) gave **8b** (103 mg, 15%) as an orange solid.

¹H NMR (500 MHz, CD₃OD): δ 7.80 (d, *J* = 8.1 Hz, 2H), 7.48 (s, 2H), 7.39 (d, *J* = 8.1 Hz, 2H), 7.12 (s, 1H), 4.42 (dd, *J* = 8.7, 5.0 Hz, 1H), 3.25 (dd, *J* = 13.8, 4.9 Hz, 1H), 3.00 (dd, *J* = 13.8, 9.0 Hz, 1H), 2.37 (s, 6H) and 1.38 (s, 9H) ppm.

¹³C NMR (125 MHz, CD₃OD): δ 175.4, 157.7, 154.1, 152.8, 142.3, 140.0, 133.6, 131.2, 123.7, 121.5, 80.5, 56.2, 38.6, 28.7 and 21.3 ppm.

HRMS (ESI) calculated for C₂₂H₂₈N₃O₄⁺ (M+H)⁺ 398.2074, found 398.2045.

IR (ATR): ν_{max} = 2922.1 and 2853.1 (N–H and O–H) and 1704.3 (C=O)cm⁻¹.



8c

Synthesis of (S,E)-3-(4-([1,1'-biphenyl]-4-ylidiazenyl)phenyl)-2-((tert-butoxycarbonyl)amino)propanoic acid (8c)

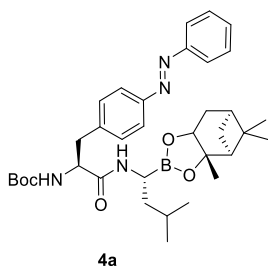
To a solution of **7** (524 mg, 1.8 mmol, 1 eq) and [1,1'-biphenyl]-4-amine (244 mg, 1.44 mmol, 0.8 eq) in DMSO (4.5 mL) was added acetic acid (0.4 mL) and the solution stirred at room temperature for 18 h. The crude product was partitioned between water and EtOAc and the organic phase was washed with water (x2). The organic phase was dried over MgSO₄, filtered and evaporated under reduced pressure. Purification by flash chromatography (30-50% EtOAc:hexane) gave **8c** (138 mg, 17%) as an orange solid.

¹H NMR (500 MHz, CD₃OD): δ 7.97 (d, *J* = 7.9 Hz, 2H), 7.85 (d, *J* = 7.7 Hz, 2H), 7.78 (d, *J* = 7.8 Hz, 2H), 7.69 (d, *J* = 7.8 Hz, 2H), 7.49–7.41 (m, 4H), 7.38 (t, *J* = 7.3 Hz, 1H), 4.44 (dd, *J* = 8.3, 4.9 Hz, 1H), 3.27 (dd, *J* = 13.8, 4.5 Hz, 1H), 3.01 (dd, *J* = 13.4, 9.6 Hz, 1H) and 1.39 (s, 9H) ppm.

^{13}C NMR (125 MHz, CD_3OD): δ 175.1, 157.8, 153.1, 152.9, 145.1, 142.5, 141.3, 131.3, 130.0, 129.0, 128.7, 128.1, 124.4, 123.8, 80.6, 56.1, 38.6 and 28.7 ppm.

HRMS (ESI) calculated for $\text{C}_{26}\text{H}_{28}\text{N}_3\text{O}_4^+$ ($\text{M}+\text{H}$) $^+$ 446.2074, found 446.2054.

IR (ATR): ν_{max} 3261.4 and 2923.1 (N–H and O–H) and 1719.8 and 1651.7 (C=O) cm^{-1} .



Synthesis of tert-butyl ((2S)-1-(((1R)-3-methyl-1-((3aS,4S,6S)-3a,5,5-trimethylhexahydro-4,6-methanobenzo[d][1,3,2]dioxaborol-2-yl)butyl)amino)-1-oxo-3-(4-((E)-phenyldiazenyl)phenyl)propan-2-yl)carbamate (4a)

A solution of **8a** (117 mg, 0.31 mmol, 1 eq) and **9** (100 mg, 0.33 mmol, 1.05 eq) in DCM (3 mL) was cooled in ice. TBTU (99 mg, 0.31 mmol, 1 eq) and DIPEA (0.21 mL, 1.24 mmol, 4 eq) were added, and the mixture was warmed to room temperature over 18 h. The mixture was diluted EtOAc, washed with saturated ammonium chloride solution (x3), dried over MgSO_4 , filtered and evaporated under reduced pressure. Purification by flash chromatography (40% diethyl ether:hexane) gave **4a** (76 mg, 95%) as an orange solid.

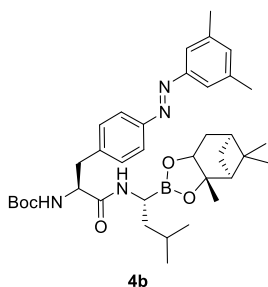
^1H NMR (500 MHz, CD_3OD) δ 7.87 (m, 4H, 2xArH), 7.51 (m, 3H, 3xArH), 7.44 (d, J = 8.1 Hz, 2H, ArH), 4.55 (t, J = 7.3 Hz, 1H, Tyr- α -H), 4.20 (d, J = 7.3 Hz, 1H, CH), 3.14 (dd, J = 13.5, 7.3 Hz, 1H, Tyr- β -CHH), 3.05 (d, J = 8.0 Hz, 1H, Tyr- β -CHH), 2.70 (t, J = 7.7 Hz, CH), 2.33 (d, J = 2.4 Hz, 1H, CH), 2.17–2.09 (m, 1H), 1.96 (t, J = 5.4 Hz, 1H, CH), 1.85 (br s,

1H, CH), 1.80 (d, $J = 14.1$ Hz, 1H, CH), 1.53–1.44 (m, 1H, CH), 1.41 (d, $J = 10.6$ Hz, 1H, CH), 1.39 (s, 3H, CH₃), 1.38 (s, 9H, 3xCH₃), 1.27 (s, 3H, CH₃), 1.24 (m, 2H, CH₂), 0.86 (s, 3H, CH₃), 0.85 (d, $J = 6.7$ Hz, 3H, CH₃) and 0.82 (d, $J = 6.5$ Hz, 3H, CH₃) ppm.

¹³C NMR (125 MHz, CD₃OD) δ 177.3, 157.2, 154.0, 152.9, 141.2, 132.2, 131.4, 130.2, 124.0, 123.7, 84.3, 80.8, 77.4, 54.2, 53.5, 41.6, 41.3, 39.1, 38.9, 37.6, 29.7, 28.6, 27.8, 27.4, 26.5, 24.6, 23.6 and 22.2 ppm.

IR (ATR) ν : 2931 (N–H), 2346 (N=N) and 1684 (C=O) cm⁻¹.

HRMS (ESI) calcd for C₃₅H₄₉BN₄NaO₅ (M+Na)⁺ 639.3688, found 639.3699.



Synthesis of tert-butyl ((2S)-3-(4-((E)-(3,5-dimethylphenyl)diazenyl)phenyl)-1-(((1R)-3-methyl-1-((3aS,4S,6S)-3a,5,5-trimethylhexahydro-4,6-methanobenzo[d][1,3,2]dioxaborol-2-yl)butyl)amino)-1-oxopropan-2-yl)carbamate (4b)

Compound **4b** was obtained as an orange solid (38 mg, 50%) using the above procedure.

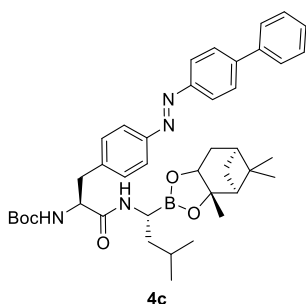
¹H NMR (500 MHz, CD₃OD): δ 7.84 (m, $J = 8.2$ Hz, 2H), 7.50 (s, 2H), 7.44 (d, $J = 8.2$ Hz, 2H), 7.17 (s, 1H), 4.57–4.51 (m, 1H), 4.21 (dd, $J = 8.4, 1.9$ Hz, 1H), 3.13 (dd, $J = 13.7, 7.3$ Hz, 1H), 3.04 (dd, $J = 13.5, 8.1$ Hz, 1H), 2.69 (t, $J = 7.7$ Hz, 1H), 2.40 (s, 6H, 2xCH₃), 2.39–2.31 (m, 1H), 2.17–2.09 (m, 1H), 1.96 (t, $J = 5.4$ Hz, 1H), 1.89–1.83 (m, 1H),

1.82–1.77 (m, 1H), 1.49 (dd, $J = 13.3, 6.3$ Hz, 1H), 1.44–1.36 (m, 9H, CH₃ + C(CH₃)₃), 1.29 (s, 4H), 0.88 (s, 3H, CH₃), 0.86 (d, $J = 6.3$ Hz, 3H, CH₃) and 0.83 (d, $J = 6.5$ Hz, 3H, CH₃) ppm.

¹³C NMR (150 MHz, CD₃OD): δ 177.4, 157.7, 154.6, 153.4, 141.8, 140.5, 134.0, 131.7, 124.2, 121.9, 85.2, 81.2, 78.0, 53.9, 41.7, 39.7, 37.7, 31.3, 30.0, 29.0, 28.1, 27.6, 27.1, 24.9, 24.0, 22.7 and 21.6 ppm.

HRMS (ESI) calculated for C₃₇H₅₄BN₄O₅⁺ (M+H)⁺ 645.4182, found 645.4141.

IR (ATR): $\nu_{\max} = 2961.8$ and 2923.6 (N–H), 1695.4 and 1646.5 (C=O) cm⁻¹.



Synthesis of tert-butyl ((2S)-3-(4-((E)-[1,1'-biphenyl]-4-yl)diazenyl)phenyl)-1-(((1R)-3-methyl-1-((3aS,4S,6S)-3a,5,5-trimethylhexahydro-4,6-methanobenzo[d][1,3,2]dioxaborol-2-yl)butyl)amino)-1-oxopropan-2-yl)carbamate (4c)

Compound **4c** was obtained as an orange solid (46 mg, 60%) using the above procedure.

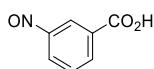
¹H NMR (500 MHz, CDCl₃) δ 7.98 (d, $J = 8.1$ Hz, 2H, 2xArH), 7.87 (d, $J = 7.8$ Hz, 2H, 2xArH), 7.74 (d, $J = 8.0$ Hz, 2H, 2xArH), 7.66 (d, $J = 7.9$ Hz, 2H, 2xArH), 7.47 (s, 3H, 3xArH), 7.39 (d, $J = 7.5$ Hz, 2H, 2xArH), 6.09 (s, 1H, NH), 5.17 (s, 1H, NH), 4.36 (s, 1H,

CH), 4.25 (d, $J = 8.4$ Hz, 1H, CH), 3.23–3.07 (m, 3H, 3xCH), 2.29 (s, 1H, CH), 2.21–2.12 (m, 1H, CH), 2.01 (t, $J = 5.2$ Hz, 1H, CH), 1.87 (s, 1H, CH), 1.80 (d, $J = 14.4$ Hz, 1H, CH), 1.50 (dd, $J = 13.1, 6.6$ Hz, 2H, 2xCH), 1.42 (s, 9H, C(CH₃)₃), 1.38 (s, 3H, CH₃), 1.28–1.22 (m, 3H, CH₃), 0.86 (d, $J = 6.4$ Hz, 6H, 2xCH₃) and 0.80 (s, 3H, CH₃) ppm.

¹³C NMR (126 MHz, CDCl₃) δ 173.9, 154.4, 146.3, 142.8, 132.9, 131.6, 130.6, 130.4, 129.8, 126.0, 125.8, 88.5, 80.4, 79.9, 54.0, 42.8, 42.2, 41.0, 40.8, 38.2, 31.2, 30.9, 29.8, 29.0, 28.0, 26.7, 25.7 and 24.6 ppm.

HRMS (ESI) calcd for calculated for C₂₇H₂₉N₃O₄Na⁺ (M+Na)⁺ 482.2050, found 482.2020.

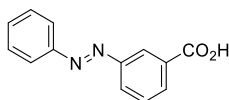
IR (ATR) ν : 3377.8 and 2982.8 (N–H), 1694.6 and 1515.8 (C=O) cm⁻¹.



11

Synthesis of 3-nitrosobenzoic acid (11)²

3-Aminobenzoic acid **10** (1 g, 7.2 mmol, 1 eq) was dissolved in DCM (18 mL). A solution of Oxone[®] (4.4 g, 14.4 mmol, 2 eq) in water (80 mL) was added and the solution stirred under nitrogen for 3 h. The precipitate was filtered and washed with water, to give **11** as a beige solid (1 g, 91%).

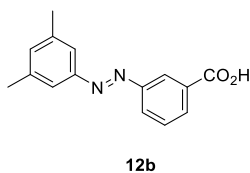


12a

Synthesis of (E)-3-(phenyldiazenyl)benzoic acid (12a)³

² Priewisch, B.; Rück-Braun, K. *Journal of Organic Chemistry* **2005** 70(6), 2350–2352.

A solution of nitrosobenzene (171 mg, 1.6 mmol, 1 eq) in glacial acetic acid (13 mL) was added to a suspension of *p*-aminobenzoic acid (263 mg, 2.24 mmol, 1.4 eq) in glacial acetic acid (13 mL) and the mixture was stirred at room temperature for 18 h. Excess water was added and the precipitate was filtered and washed with water, to give **12a** (341 mg, 94%) as an orange solid.



Synthesis of (*E*)-3-((3,5-dimethylphenyl)diazenyl)benzoic acid (12b**)**

A solution of **11** (150 mg, 1 mmol, 2.5 eq) in DMSO (2.5 mL) and 3,5-dimethylaniline (0.1 mL, 0.8 mmol, 1 eq) in acetic acid (0.23 mL) was stirred at room temperature for 18 h. Excess water was added and the precipitate was filtered and washed with water, to give **12b** (340 mg, 57%) as a brown solid.

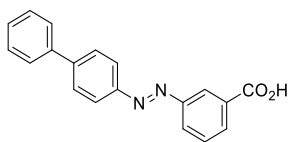
¹H NMR (500 MHz, DMSO-*d*₆) δ 13.25 (s, 1H, OH), 8.36 (s, 1H, ArH), 8.12 (t, *J* = 8.4 Hz, 2H, 2xArH), 7.74 (t, *J* = 7.8 Hz, 1H, ArH), 7.56 (s, 2H, 2xArH), 7.25 (s, 1H, ArH) and 2.39 (s, 6H, 2xCH₃) ppm.

¹³C NMR (125 MHz, DMSO-*d*₆) δ 166.7 (C), 152.0 (C), 151.9 (C), 138.8 (2xC), 133.3 (CH), 132.2 (C), 131.7 (CH), 129.9 (CH), 127.4 (CH), 122.0 (CH), 120.5 (2xCH) and 20.8 (2xCH₃) ppm.

HRMS (ESI) calcd for C₁₅H₁₅N₂O₂ (M+H)⁺ 255.1128, found 255.1135.

IR (ATR) ν: 3224 (O–H), 2345 (N=N) and 1683 (C=O) cm⁻¹.

³ Fatás, P., Longo, E., Rastrelli, F., Crisma, M., Toniolo, C., Jiménez, A. I., Cativiela, C. and Moretto, A. *Chemistry–A European Journal* **2011**, *17* (45), 12606–12611.



12c

Synthesis of (E)-3-([1,1'-biphenyl]-4-yl)diazenylbenzoic acid (12c)

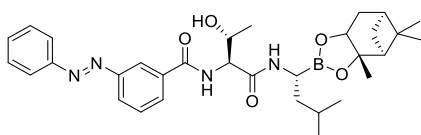
To a solution of **11** (300 mg, 2 mmol, 2.5 eq) in DMSO (5 mL) was added [1,1'-biphenyl]-4-amine (268 mg, 1.58 mmol, 1 eq) in acetic acid (0.5 mL) and the solution was stirred at room temperature for 18 h. Excess water was added and the precipitate was filtered and washed with water, to give **12c** (340 mg, 57%) as a brown solid.

¹H NMR (500 MHz, CDCl₃) δ 8.68 (s, 1H, ArH), 8.24 (d, *J* = 7.6 Hz, 1H, ArH), 8.20 (d, *J* = 7.8 Hz, 1H, ArH), 8.06 (d, *J* = 8.3 Hz, 2H, 2xArH), 7.79 (d, *J* = 8.4 Hz, 2H, 2xArH), 7.68 (dd, *J* = 17.5, 7.6 Hz, 3H, 3xArH), 7.50 (t, *J* = 7.6 Hz, 2H, 2xArH) and 7.42 (t, *J* = 7.3 Hz, 1H, ArH) ppm.

¹³C NMR (126 MHz, DMSO-*d*₆) δ 166.7 (C), 152.0 (2xC), 138.9 (2xC), 132.2 (C), 130.0 (2xCH), 129.1 (2xCH), 128.8 (2xCH), 127.8 (CH), 127.5 (2xCH), 126.9 (2xCH), 125.9 (CH) and 123.4 (CH) ppm.

HRMS (ESI) calcd for C₁₉H₁₅N₂NaO₂ (M+H)⁺ 303.1128, found 303.1151.

IR (ATR) ν: 3012 (O–H), 2343 (N=N) and 1678 (C=O) cm⁻¹.



5a

Synthesis of *N*-((2*S*,3*R*)-3-hydroxy-1-(((1*R*)-3-methyl-1-((3*aS*,4*S*,6*S*)-3*a*,5,5-trimethylhexahydro-4,6-methanobenzo[*d*][1,3,2]dioxaborol-2-yl)butyl)amino)-1-oxobutan-2-yl)-3-((*E*)-phenyldiazenyl)benzamide (5a)

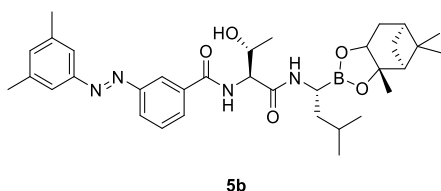
A solution of **12a** (35 mg, 0.15 mmol, 1.1 eq) and **13** (56 mg, 0.14 mmol, 1 eq) in *N,N*-dimethylformamide (0.2 mL) was cooled in ice and to this was added TBTU (53 mg, 0.16 mmol, 1.1 eq) and NMM (66 μ L, 0.6 mmol, 4 eq). The mixture was warmed to room temperature over 18 h. Excess EtOAc was added and the mixture washed with saturated ammonium chloride solution (x3), dried over MgSO₄, filtered and evaporated under reduced pressure. Purification by flash chromatography (30-40% EtOAc:hexane) gave **5a** (21 mg, 26%) as an orange solid.

¹H NMR (500 MHz, CDCl₃) δ 8.33 (s, 1H, ArH), 8.10 (d, *J* = 7.7 Hz, 1H, ArH), 7.96 (d, *J* = 6.9 Hz, 3H, 3xArH), 7.63 (t, *J* = 7.7 Hz, 1H, ArH), 7.58–7.51 (m, 3H, 3xArH), 4.59 (s, 1H, Thr- β -H), 4.53 (d, *J* = 21.7 Hz, 1H), 4.29 (d, *J* = 8.3 Hz, 1H, Leu- α -H), 3.34 (m, 2H, Thr- α -H + CHH), 2.31–2.23 (m, 1H), 2.16 (m, 1H), 1.97 (t, *J* = 5.5 Hz, 1H), 1.85 (m, 1H), 1.77 (dd, *J* = 14.5 Hz, 1H), 1.67 (m, 1H), 1.58–1.50 (m, 1H), 1.47 (m, 1H), 1.35 (s, 3H), 1.29 (m, 3H, CH₃), 1.23 (s, 3H), 1.20 (s, 3H), 0.92 (dd, *J* = 6.3, 3.2 Hz, 6H) and 0.79 (s, 3H) ppm.

¹³C NMR (125 MHz, CD₃OD) δ 167.8, 152.7, 152.5, 134.8, 131.6, 129.6, 129.6, 129.3, 126.2, 123.2, 121.6, 86.3, 78.1, 66.8, 56.8, 51.4, 39.8, 39.6, 38.3, 35.6, 28.6, 27.2, 26.4, 25.7, 24.1, 23.2 and 22.1 ppm.

IR (ATR) ν : 3311 and 2933 (O–H and N–H) and 1639 (C=O) cm⁻¹.

HRMS (ESI) calcd for C₃₂H₄₃BNa₄O₅ (M+Na)⁺ 597.3234, found 597.3247.



Synthesis of 3-((E)-(3,5-dimethylphenyl)diazenyl)-N-((2S,3R)-3-hydroxy-1-(((1R)-3-methyl-1-((3aS,4S,6S)-3a,5,5-trimethylhexahydro-4,6-methanobenzo[d][1,3,2]dioxaborol-2-yl)butyl)amino)-1-oxobutan-2-yl)benzamide (5b)

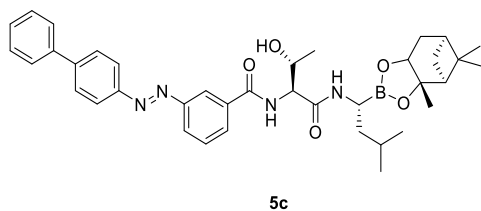
Compound **5b** was obtained as an orange solid (17 mg, 20%) using the above procedure.

¹H NMR (500 MHz, CD₃OD) δ 8.41 (s, 1H, ArH), 8.09 (d, *J* = 7.9 Hz, 1H, ArH), 8.03 (d, *J* = 7.7 Hz, 1H, ArH), 7.68 (t, *J* = 7.8 Hz, 1H, ArH), 7.57 (s, 2H, 2xArH), 7.20 (s, 1H, ArH), 4.82 (d, *J* = 3.5 Hz, 1H, Thr-β-H), 4.34 (s, 1H), 4.20 (d, *J* = 8.2 Hz, 1H, Leu-α-H), 2.86–2.81 (m, 1H, Thr-α-H), 2.42 (s, 2H, 2xCH₃), 2.37–2.30 (m, 1H), 2.16–2.11 (m, 1H), 1.97 (t, *J* = 5.3 Hz, 1H), 1.85 (s, 1H), 1.83–1.72 (m, 2H), 1.53 (d, *J* = 10.3 Hz, 1H), 1.43 (dd, *J* = 13.7, 6.5 Hz, 2H), 1.38 (s, 3H), 1.28 (d, *J* = 7.0 Hz, 6H), 0.93 (t, *J* = 6.3 Hz, 6H) and 0.86 (s, 3H) ppm.

¹³C NMR (125 MHz, CD₃OD) δ 177.5, 170.9, 155.3, 155.3, 141.5, 137.5, 135.4, 132.1, 131.8, 128.4, 123.8, 123.0, 86.0, 78.8, 69.4, 59.4, 54.8, 42.6, 42.3, 40.6, 38.6, 30.9, 29.0, 28.5, 28.1, 25.8, 24.8, 23.7, 22.5 and 21.5 ppm.

IR (ATR) ν: 3316 and 2933 (O–H and N–H) and 1651 (C=O) cm⁻¹.

HRMS (ESI) calcd for C₃₄H₄₇BNa₄O₅ (M+Na)⁺ 625.3537, found 625.3520.



Synthesis of 3-((E)-[1,1'-biphenyl]-4-yl diazenyl)-N-((2S,3R)-3-hydroxy-1-(((1R)-3-methyl-1-((3aS,4S,6S)-3a,5,5-trimethylhexahydro-4,6-methanobenzo[d][1,3,2]dioxaborol-2-yl)butyl)amino)-1-oxobutan-2-yl)benzamide (5c)

Compound **5c** was obtained as an orange solid (10 mg, 13%) using the above procedure.

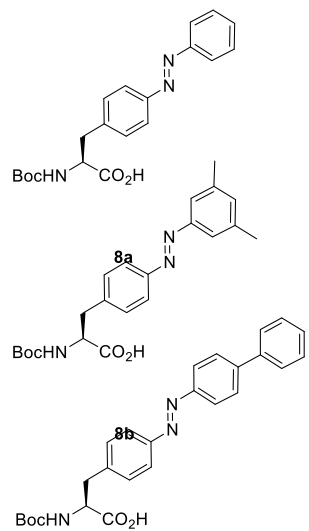
¹H NMR (500 MHz, CDCl₃) δ 8.35 (d, *J* = 1.7 Hz, 1H), 8.12–8.09 (m, 1H), 8.04 (d, *J* = 8.5 Hz, 2H), 7.96 (d, *J* = 7.8 Hz, 1H), 7.78 (d, *J* = 8.5 Hz, 2H), 7.71–7.67 (m, 2H), 7.64 (d, *J* = 7.8 Hz, 1H), 7.50 (t, *J* = 7.6 Hz, 2H), 7.42 (d, *J* = 7.4 Hz, 1H), 7.31 (d, *J* = 8.0 Hz, 1H), 6.91 (d, *J* = 5.7 Hz, 1H), 4.62 (dd, *J* = 7.9, 1.7 Hz, 1H, Thr-β-H), 4.54 (d, *J* = 21.1 Hz, 1H), 4.29 (d, *J* = 10.8 Hz, 1H, Thr-α-H), 3.34 (dd, *J* = 15.4, 6.0 Hz, 1H, Leu-α-H), 3.04 (s, 1H), 2.32–2.27 (m, 1H), 2.24 (d, *J* = 19.1 Hz, 2H), 2.16 (d, *J* = 22.4 Hz, 1H), 1.97 (t, *J* = 5.5 Hz, 1H), 1.85 (d, *J* = 16.8 Hz, 1H), 1.78 (d, *J* = 19.7 Hz, 1H), 1.68 (d, *J* = 26.6 Hz, 1H), 1.55 (d, *J* = 33.0 Hz, 1H), 1.45 (s, 1H), 1.36 (s, 3H), 1.27 (m, 6H), 1.24 (s, 3H) and 0.92 (dd, *J* = 6.5, 3.5 Hz, 6H) ppm.

¹³C NMR (125 MHz, CDCl₃) δ 171.6, 167.8, 152.8, 151.7, 144.4, 140.2, 134.8, 129.6, 129.6, 129.1, 128.2, 128.0, 127.4, 126.2, 123.7, 121.6, 86.3, 78.1, 66.8, 56.8, 51.4, 39.8, 39.6, 38.3, 35.6, 29.8, 28.6, 27.2, 26.4, 25.8, 24.1, 23.2, 22.1, 18.4 and 14.3 ppm.

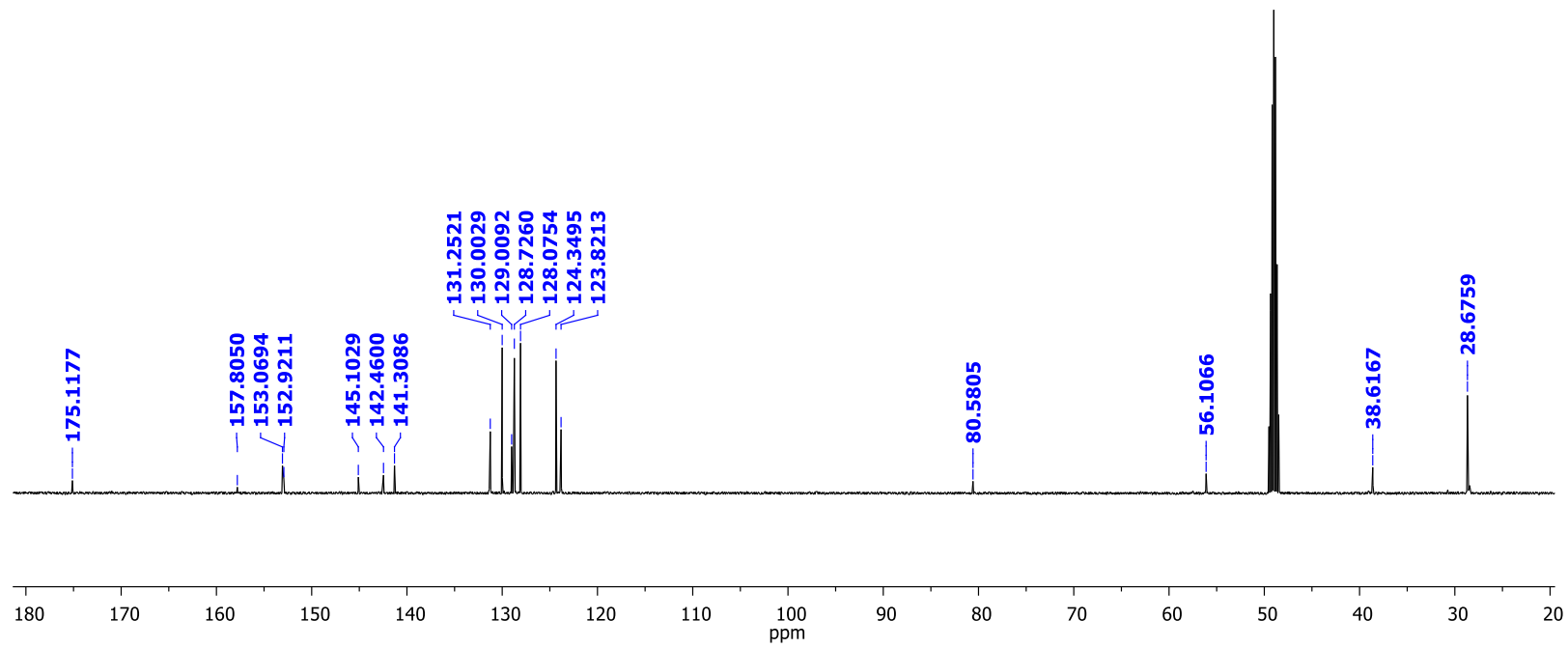
IR (ATR) ν: 3012 and 2923 (O–H and N–H) and 1641 (C=O) cm⁻¹.

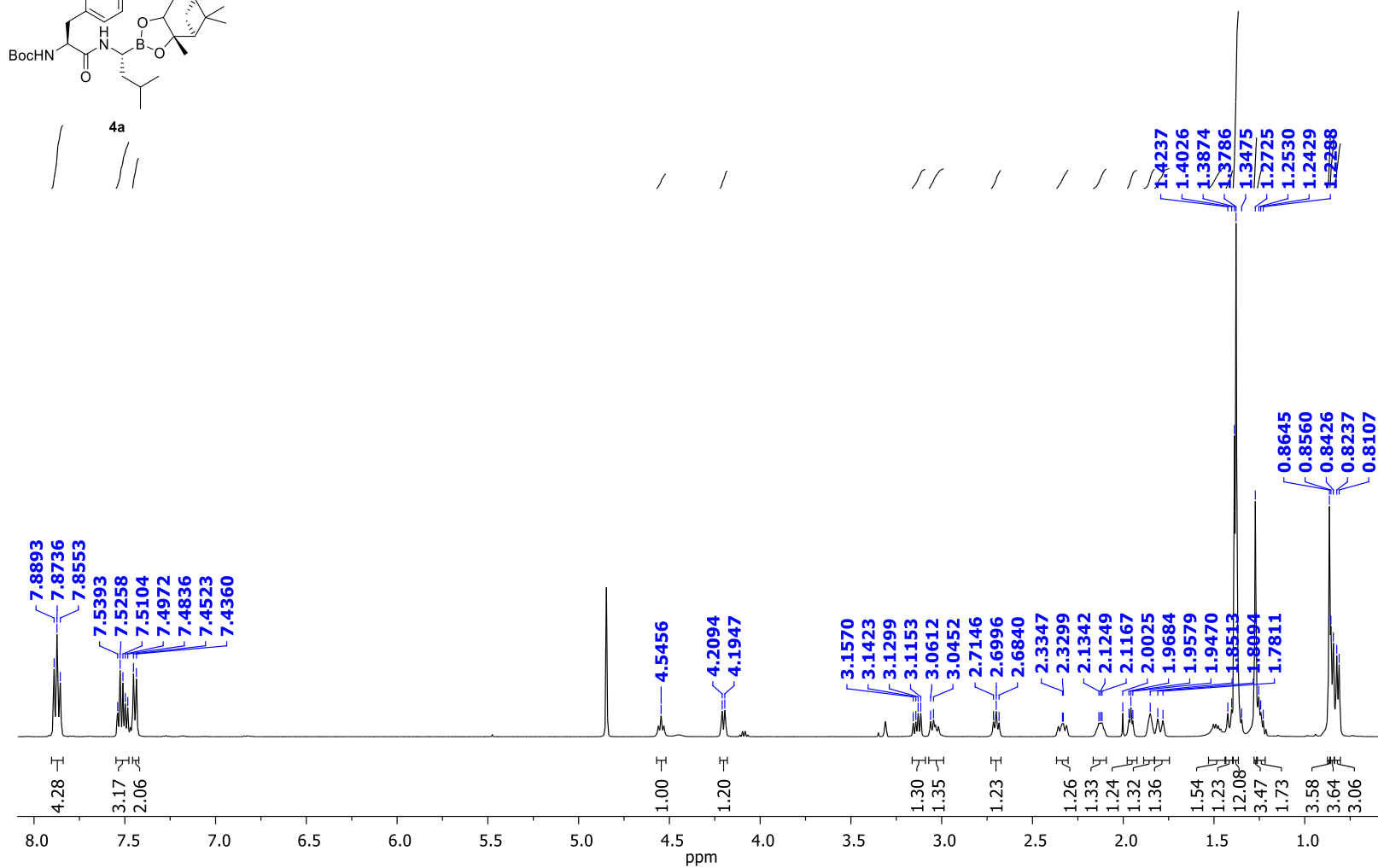
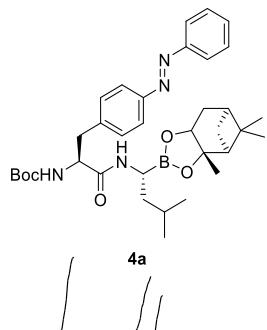
HRMS (ESI) calcd for $C_{38}H_{48}BN_4O_5$ (M+H)⁺ 351.3712, found 351.3749.

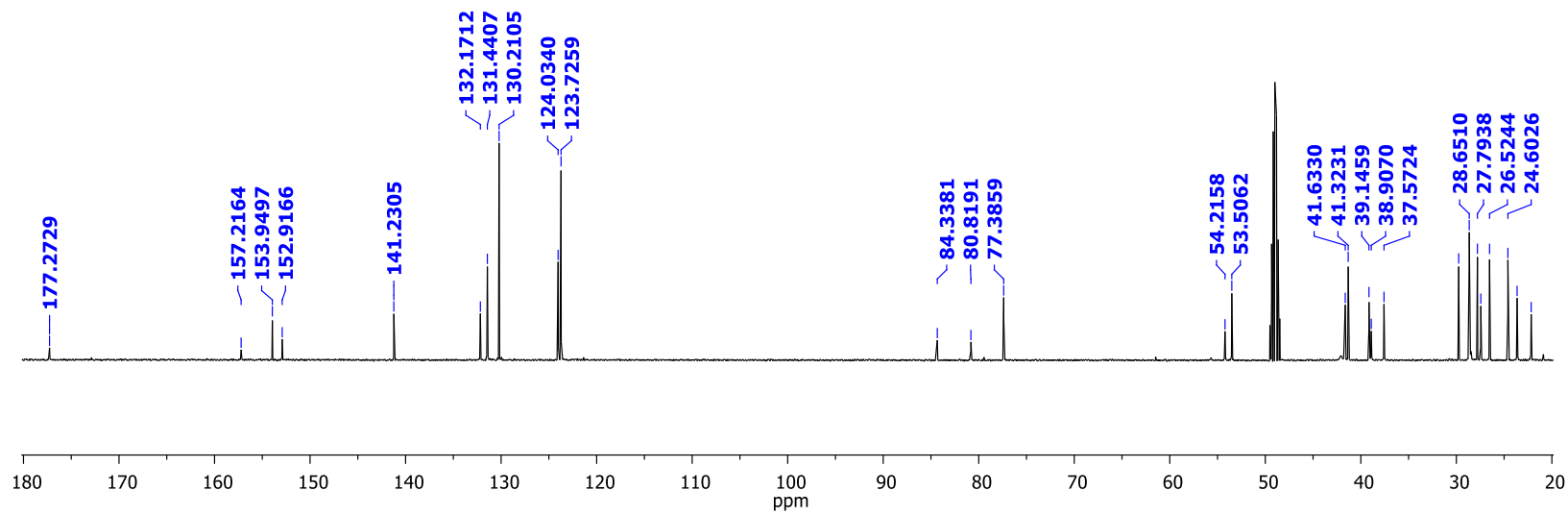
b. ^1H and ^{13}C NMR Spectra

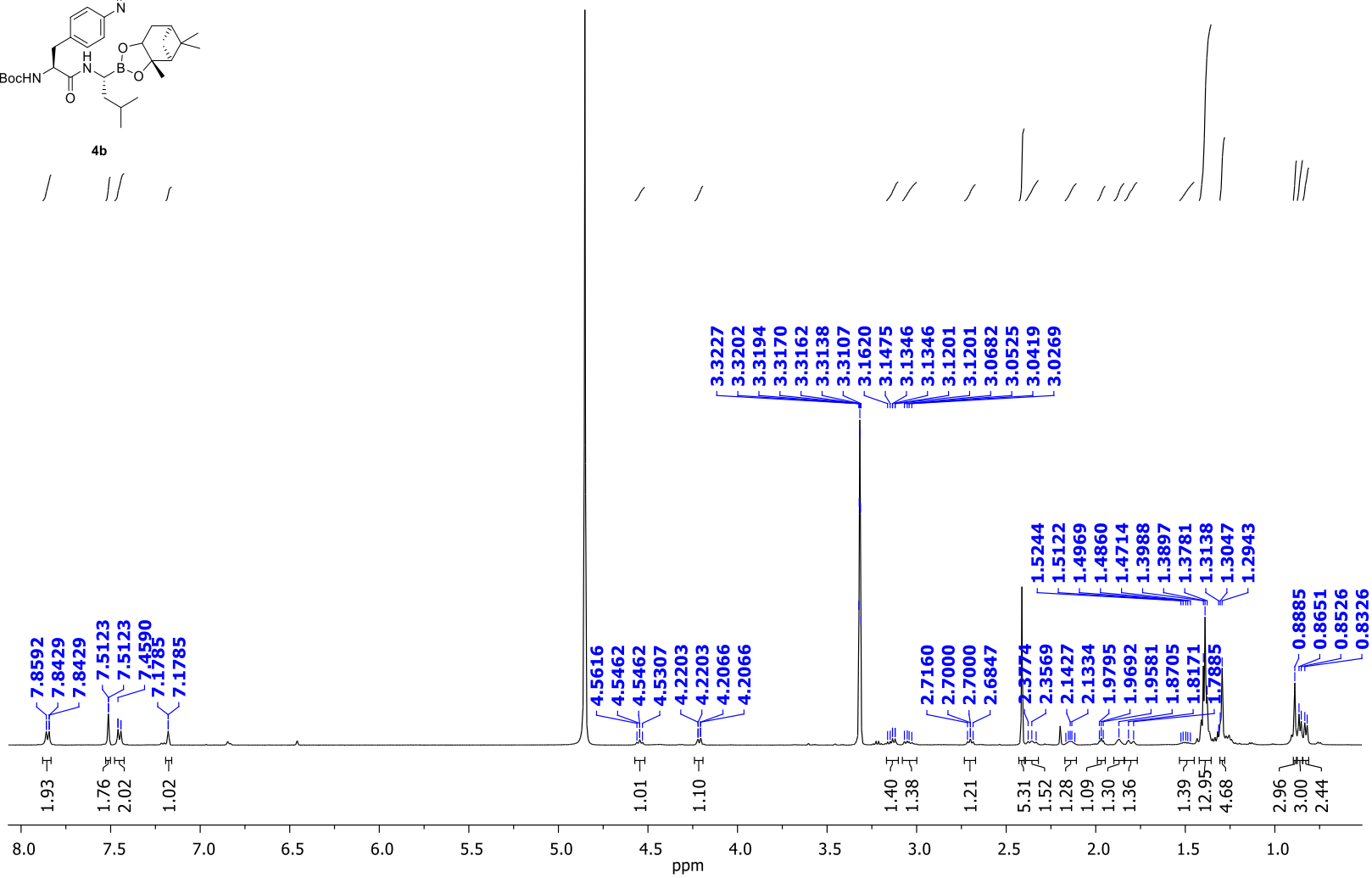
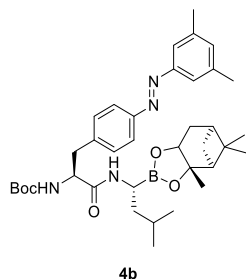


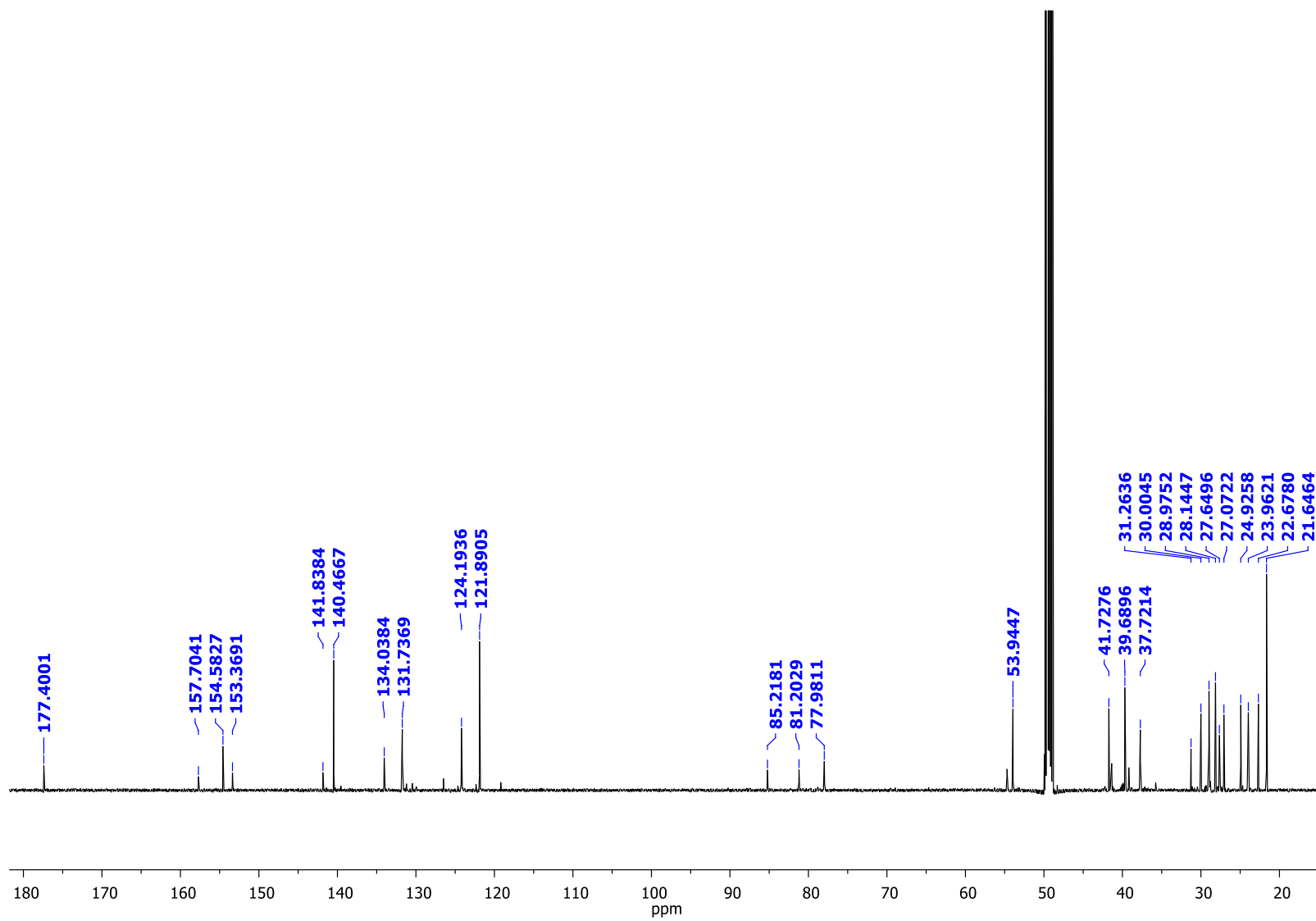
8c

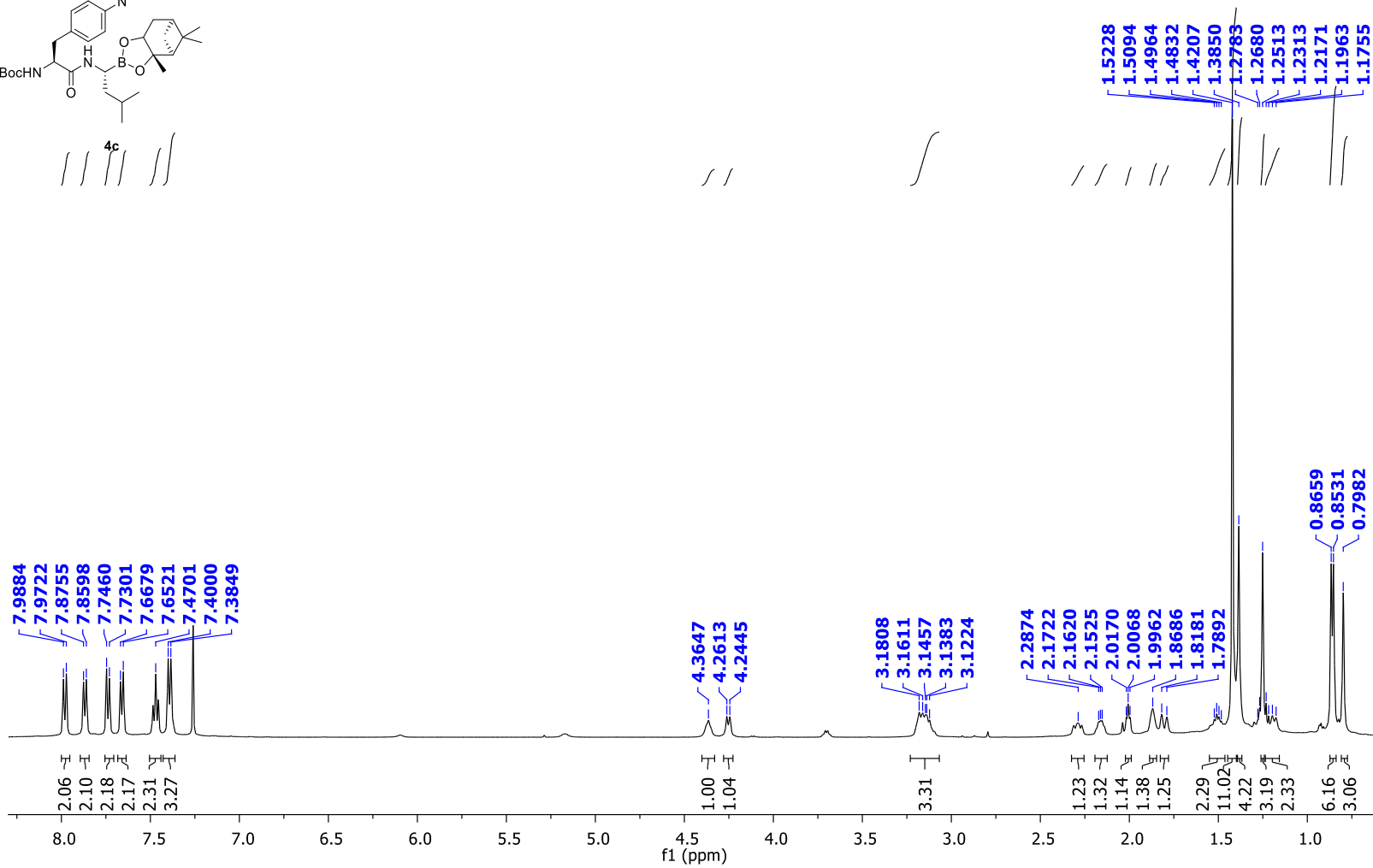
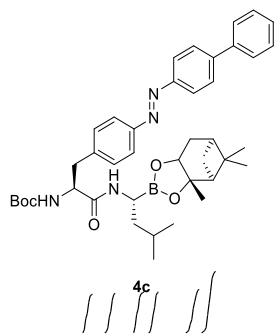


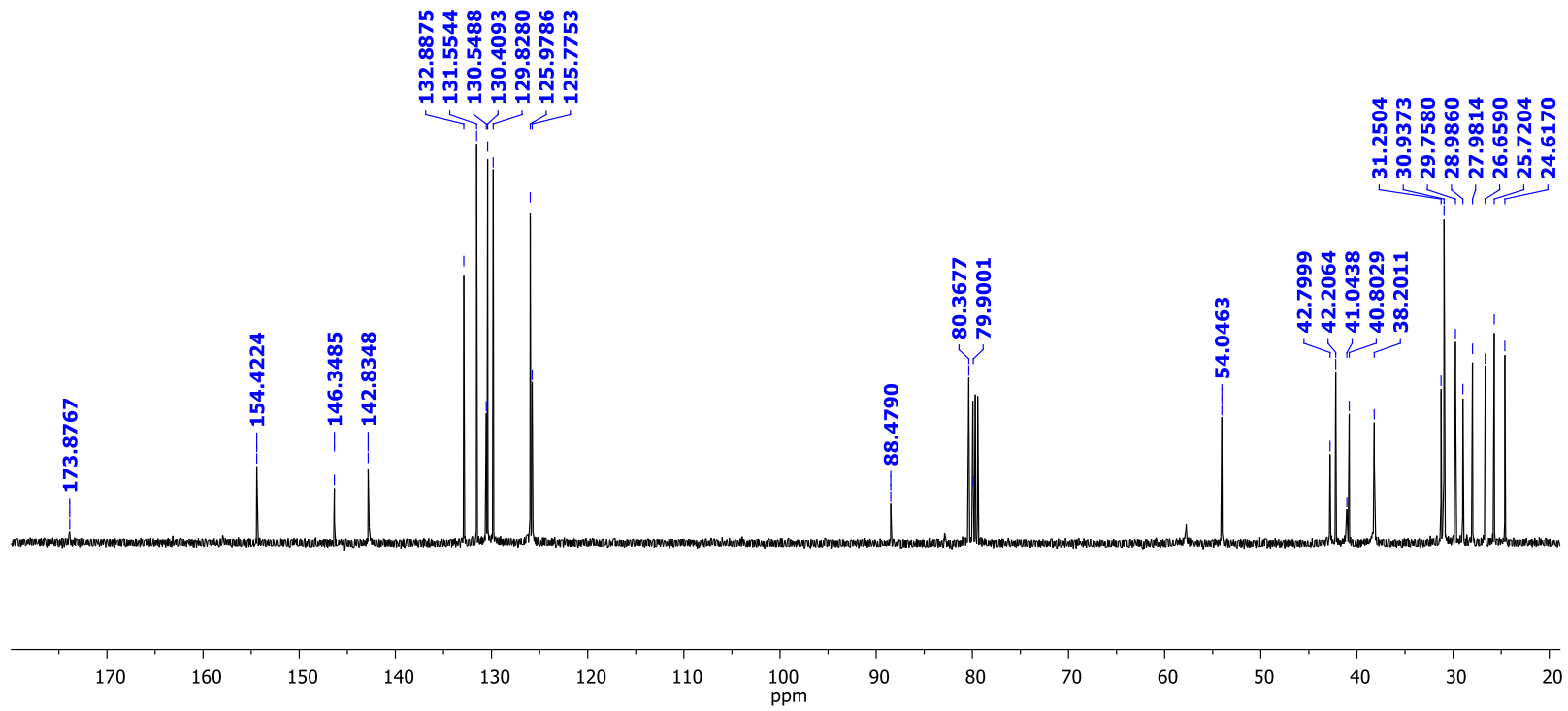


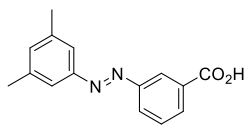




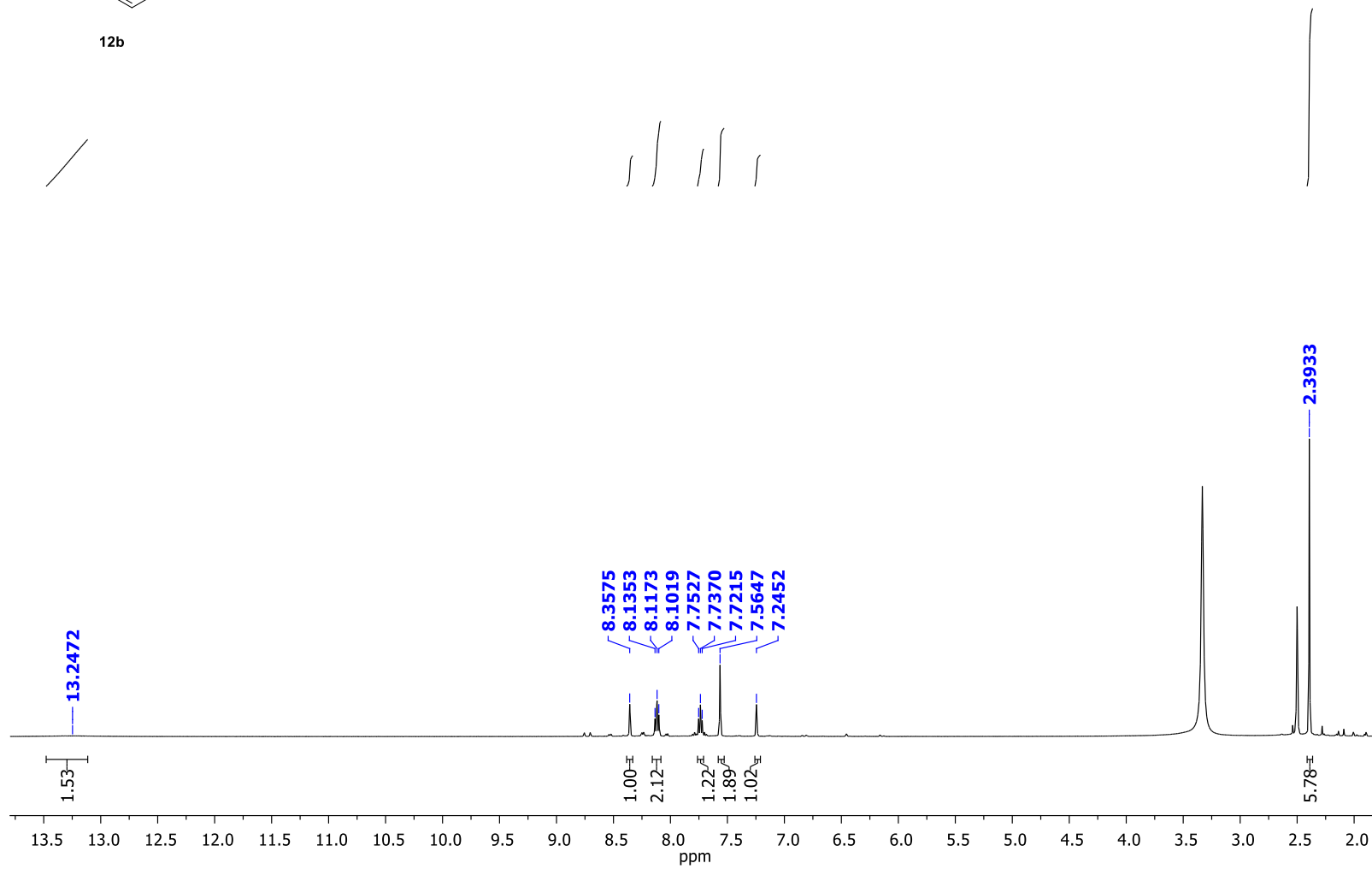


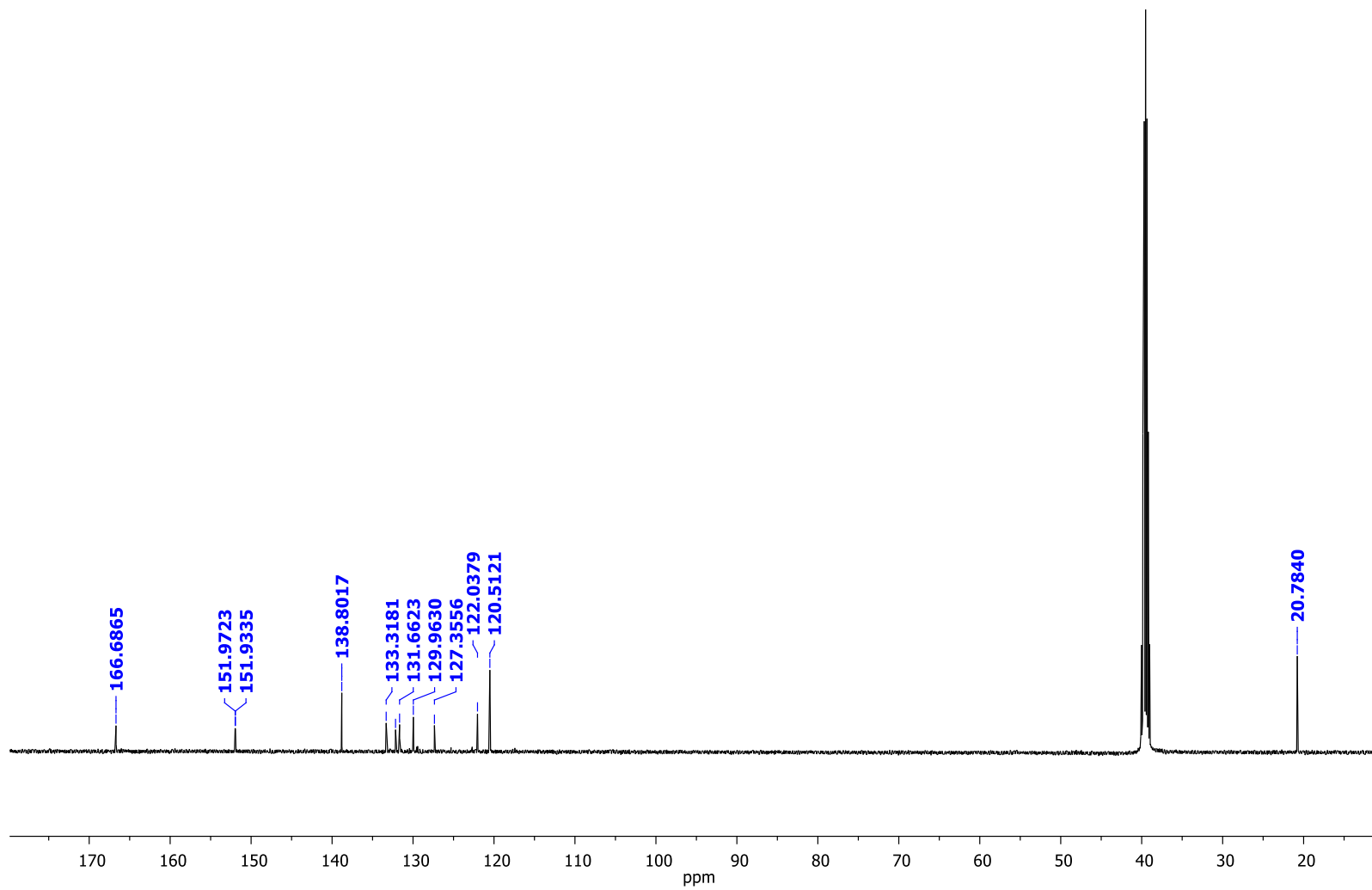


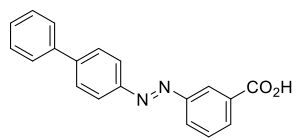




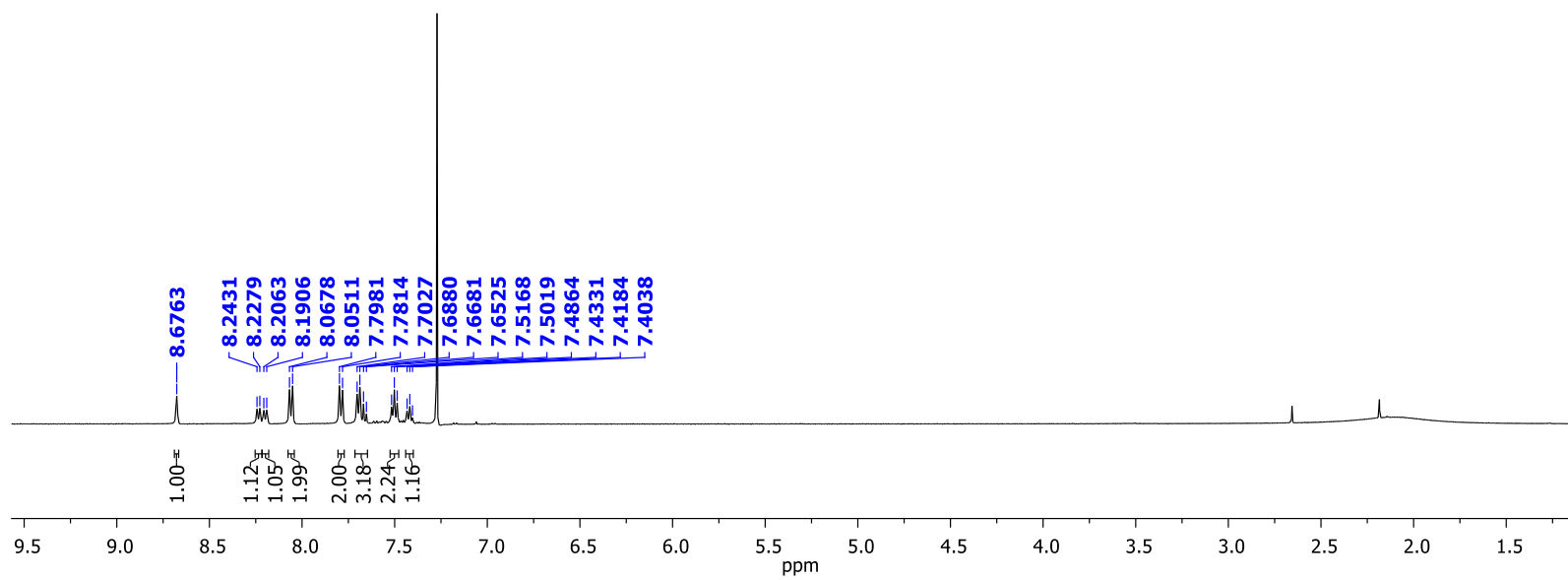
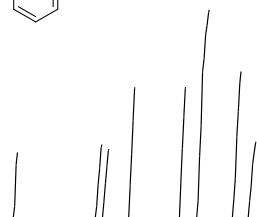
12b

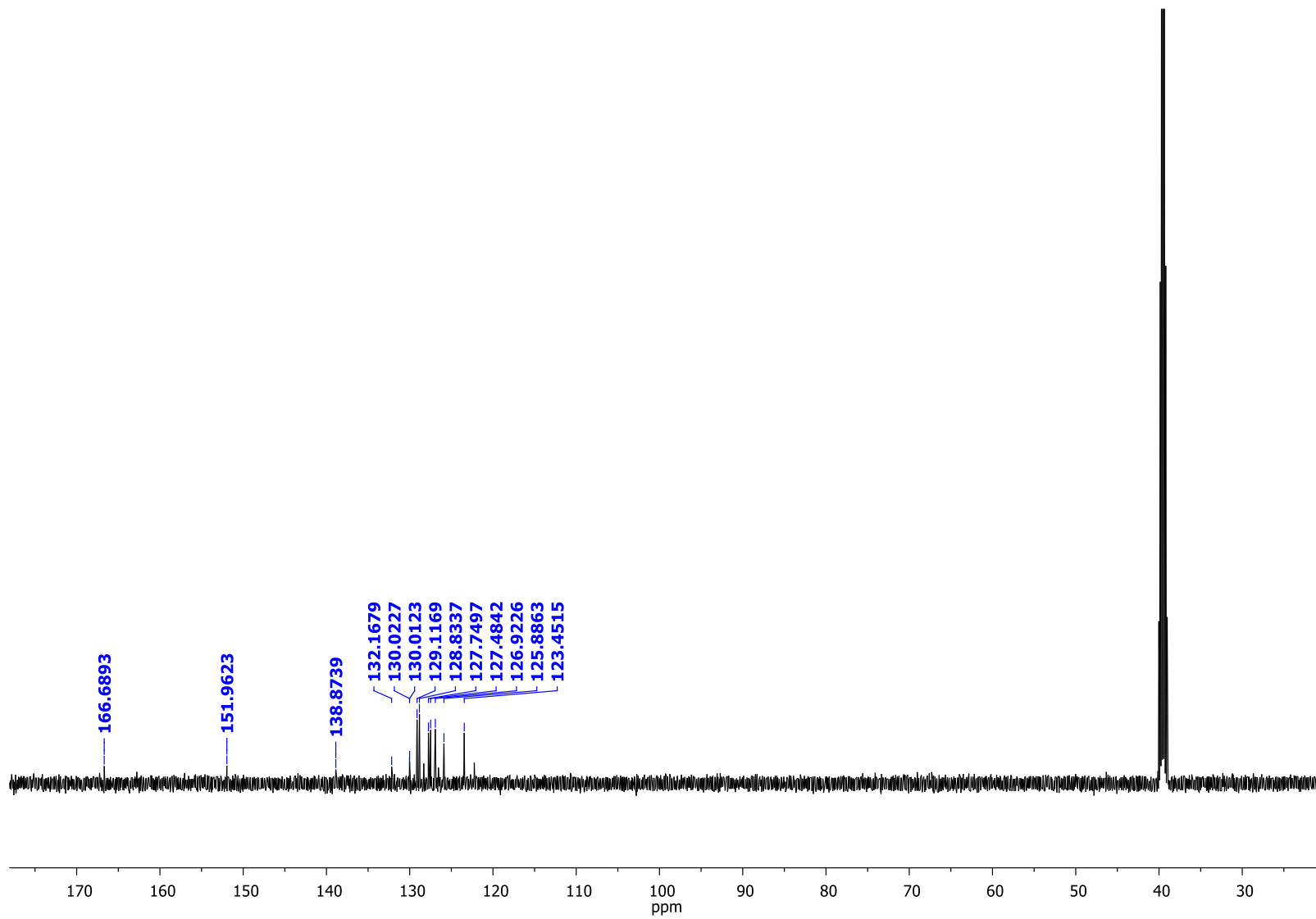


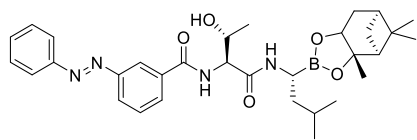




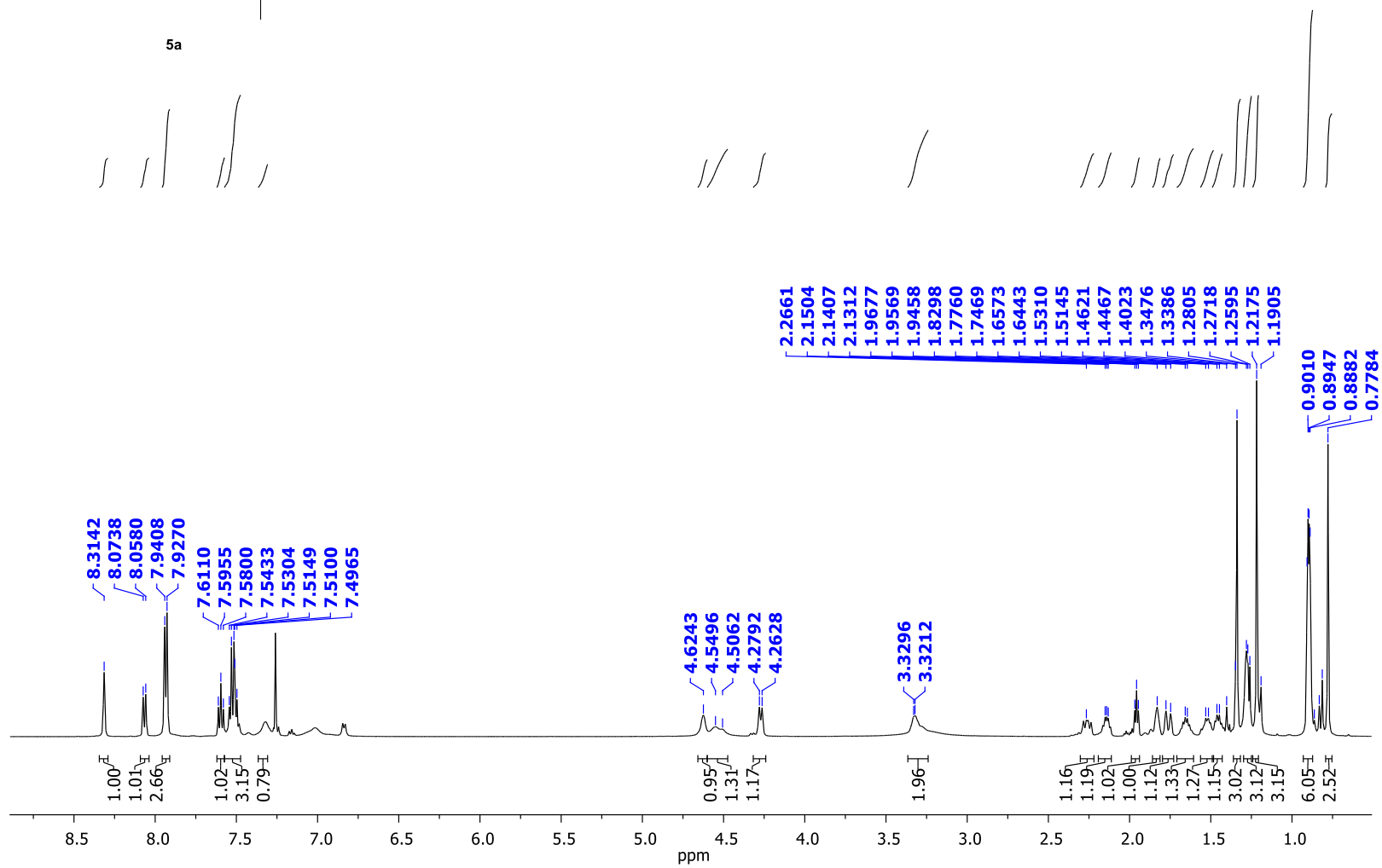
12c

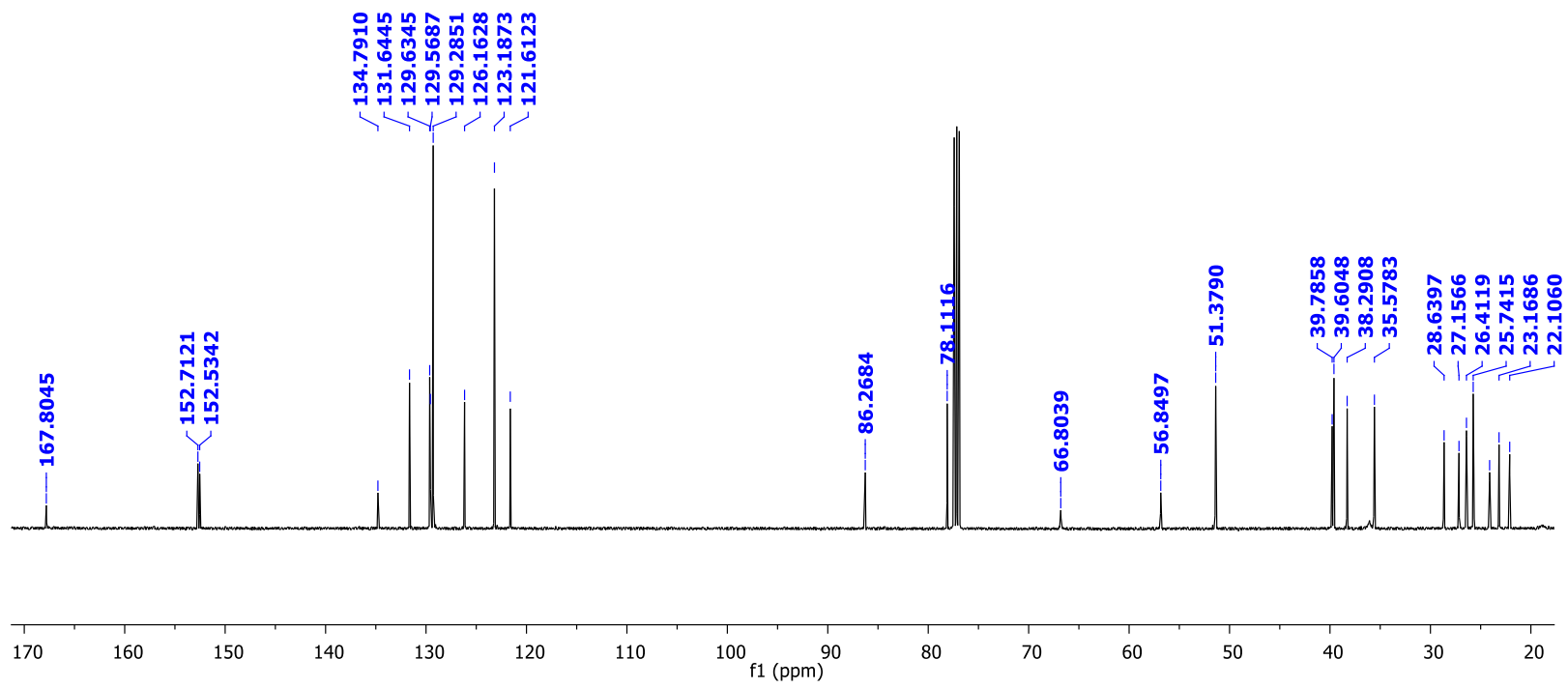


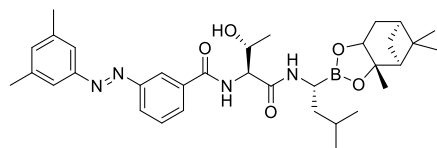




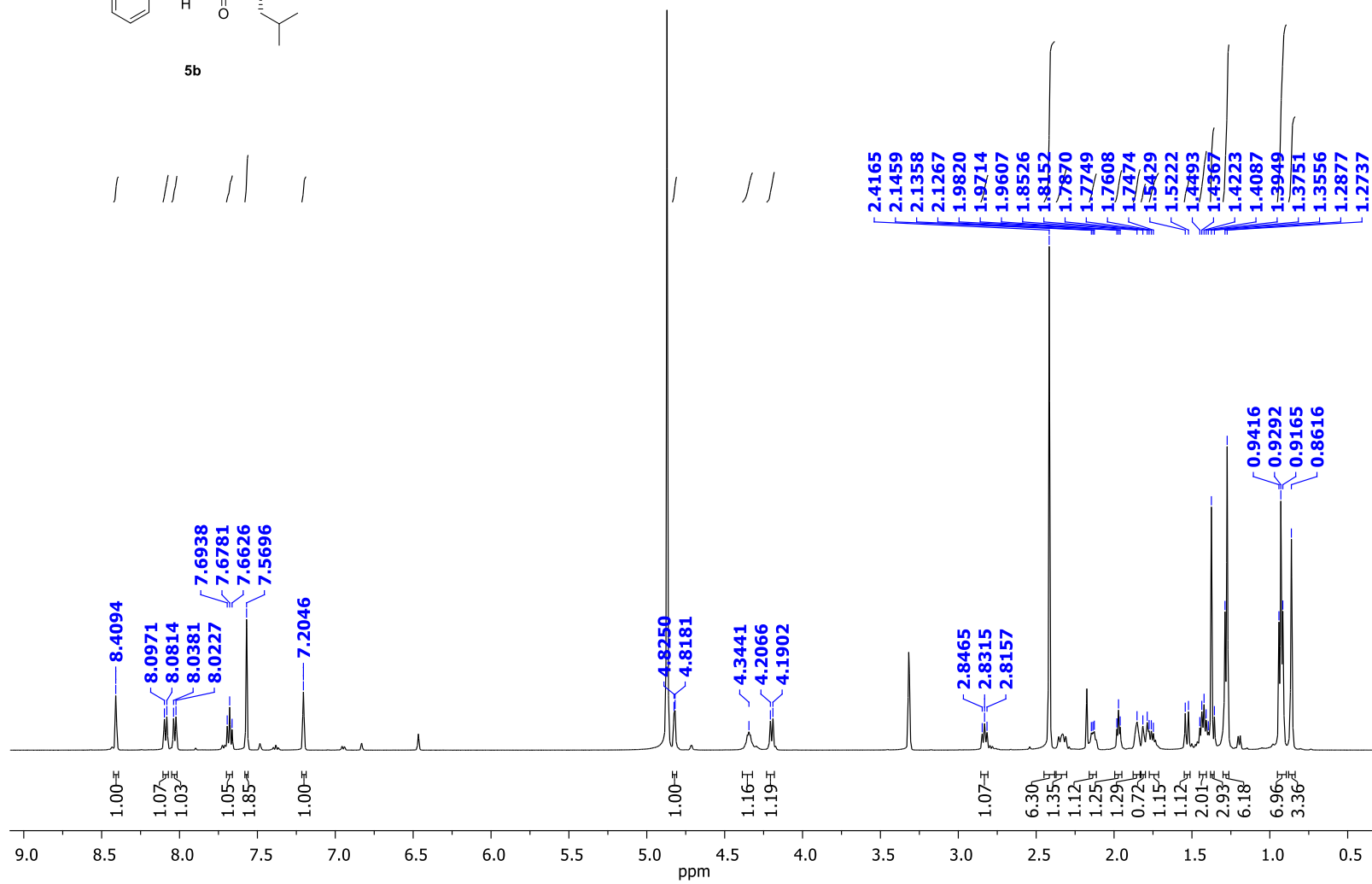
5a

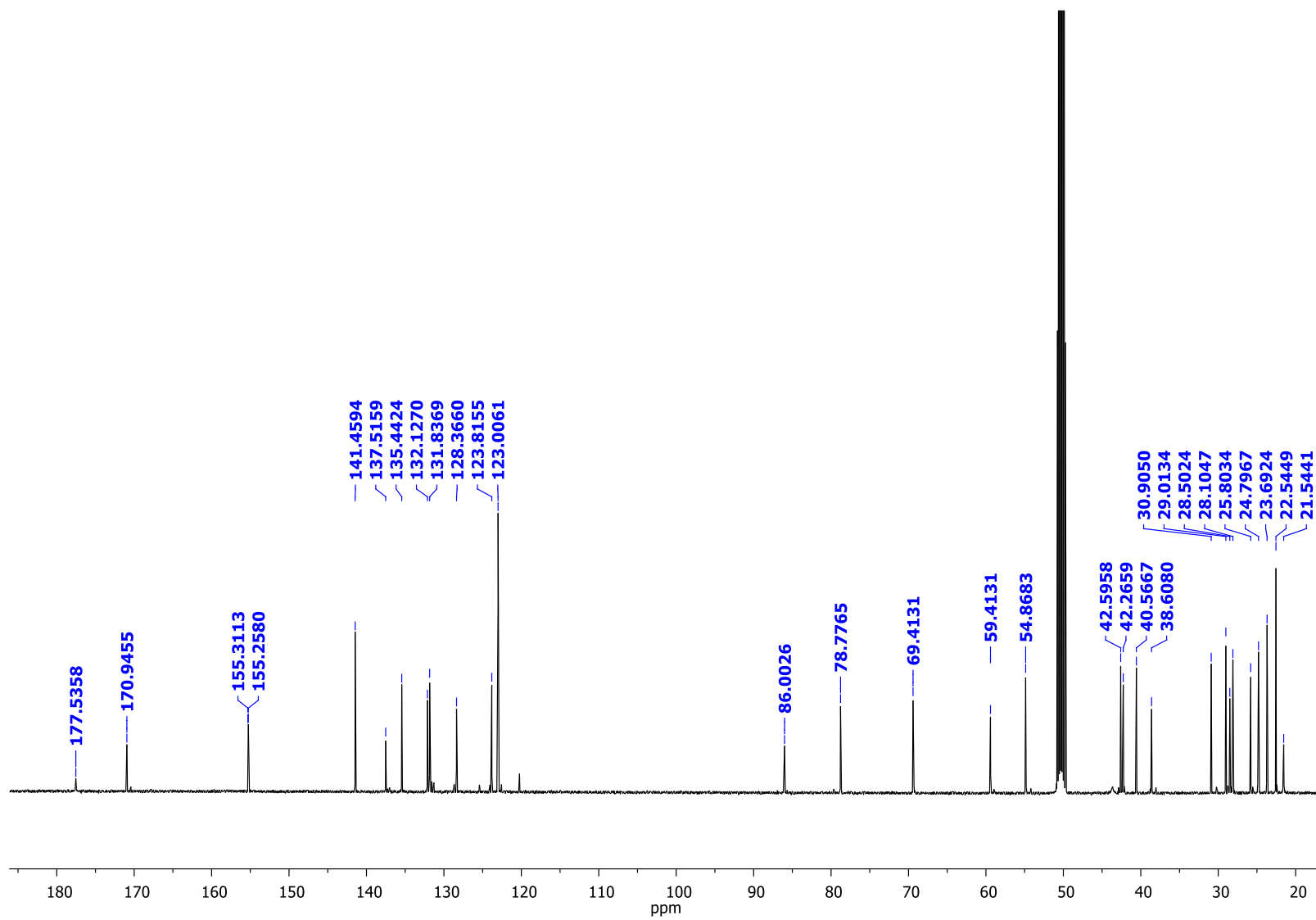


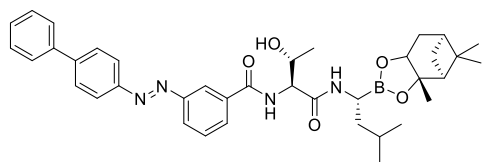




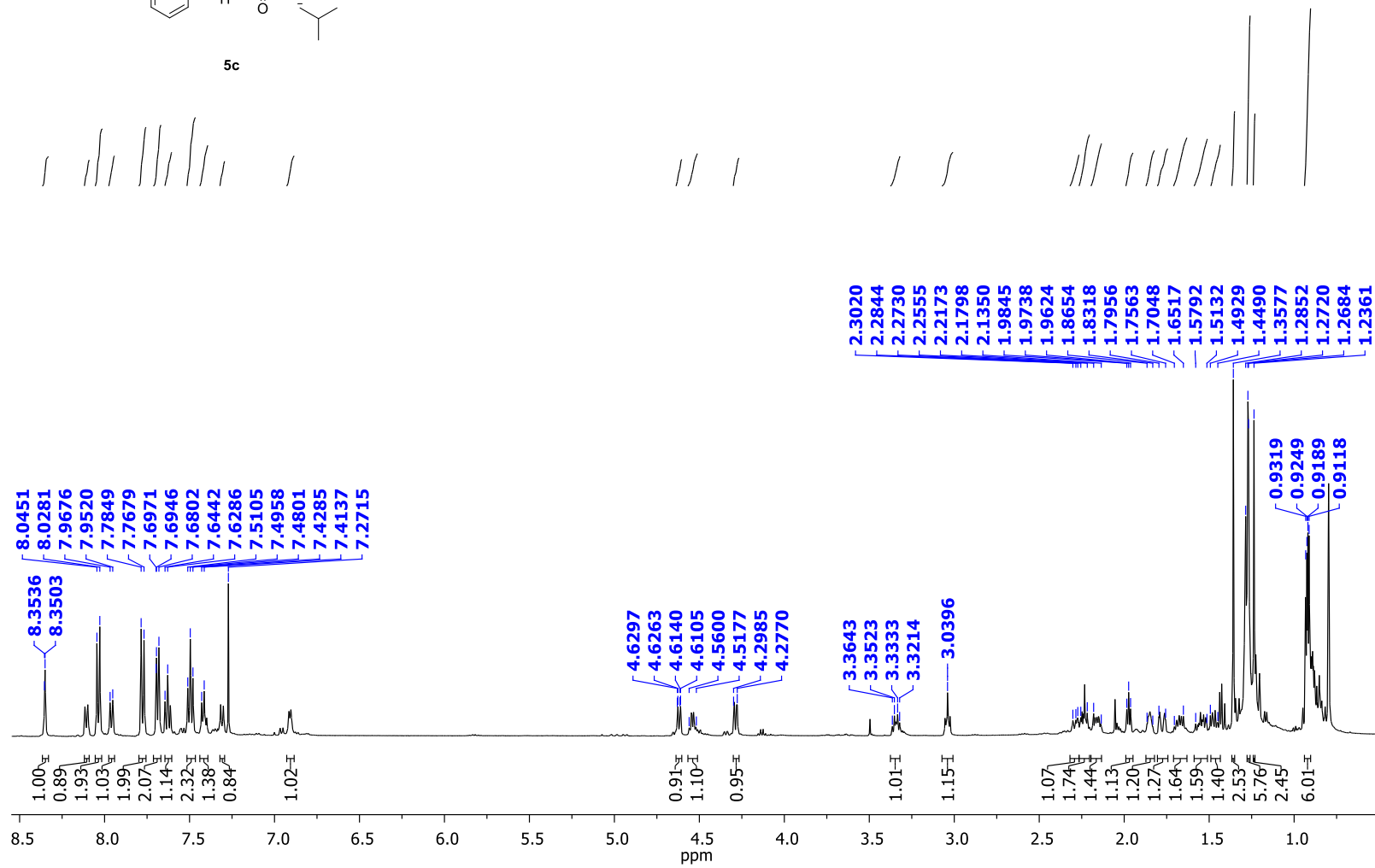
5b

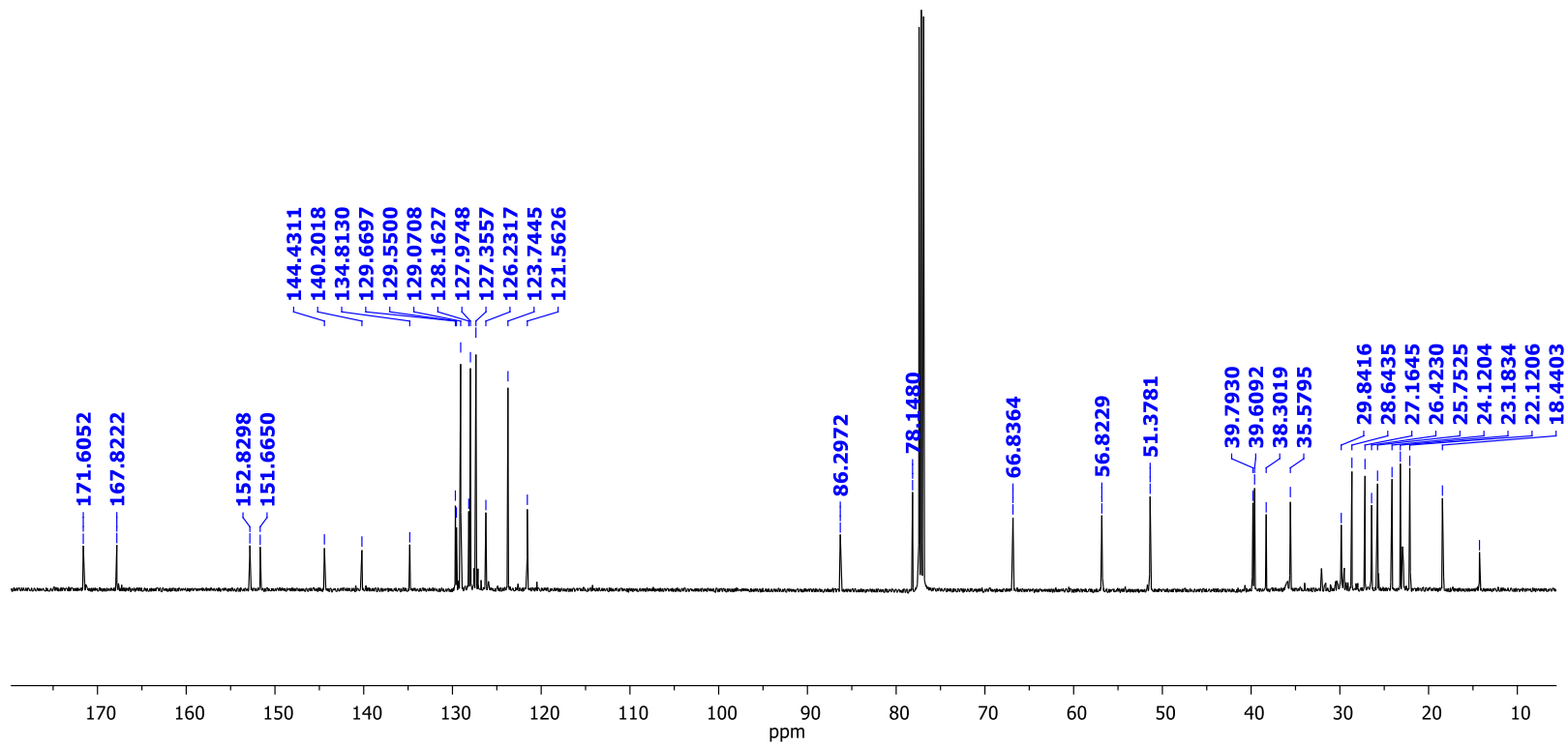






5c





c. *In Vitro* Proteasome Activity Assay

Proteasome inhibition assays were conducted following a modified literature procedure.⁴ In order to ensure that the assay was within the linear range, a standard curve was prepared in duplicate using 8 different concentrations (0-250 μ M). Rabbit 20S proteasome was used, at a concentration of 12.5 μ g/mL in Tris buffer (20 mM Tris-HCl, pH 7.5, 0.5 mM EDTA, and 0.001% SDS (w/v)). Proteasome CT-L (β 5) and C-L (β 1) activities were determined using hydrolysis of specific short peptide substrates conjugated to the fluorescent tag 7-amido-4-methylcoumarin (AMC). Fluorogenic CT-L substrate (Suc-Leu-Leu-Val-Tyr-AMC) was purchased from Boston Biochem (Cambridge, MA, USA) and C-L fluorogenic substrate (Ac-nLPnLDAMC) was purchased from Enzo Life Sciences (Farmingdale, NY, USA). Both substrates were made up to 62.5 μ M in Tris buffer (20 mM Tris-HCl, pH 7.5, 0.5 mM EDTA, and 0.001% SDS (w/v)). GraphPad Prism 5.0, GraphPad Software, Inc. GraphPad was used for the determination of kinetic values and of the half maximal inhibitory concentration (IC_{50}) of each inhibitor. The mean IC_{50} and standard error were determined by fitting the dose-response data to the built-in model- (inhibitor) vs. response- variable slope (without log transformation). IC_{50} with standard error for the key derivative: **4c** (thermally adapted state) β 5- 11 ± 5 nM, β 1- 460 ± 77 nM; **4c** (photostationary state) β 5- 54 ± 10 nM, β 1- 303 ± 40 nM

Assay procedure: 10 mM stock solutions of the test inhibitors in DMSO were diluted to 500 μ M in DMSO. 50 μ L of the 500 μ M stock solutions were transferred into a 96 clear well round-bottom plate (in duplicate) and each was diluted to 250 μ M by adding 50

⁴ a) K. C. H. Chua, M. Pietsch, X. Zhang, S. Hautmann, H. Y. Chan, J. B. Bruning, M. Gütschow, A. D. Abell, *Angew. Chem. Int. Ed.* **2014**, *53*, 7828–7831; b) S. J. Gendler, Z. A. Tökés, *Biochimica et Biophysica Acta (BBA) - General Subjects* **1986**, *882*, 242–253.

μL of DMSO. Serial ten-fold dilutions of the 250 μM inhibitor solutions with DMSO were performed within the next 7 wells, giving duplicates of each compound at 8 different concentrations (0-250 μM). The above dilutions were performed identically on another 96 clear well round-bottom plate, however this plate was then irradiated with UV light ($\lambda = 365 \text{ nm}$) for 1 h using a UVP BL6SV lamp, and the plate then concealed from light using aluminium foil. Compounds on the non-irradiated plate were used to test *trans*-enriched TAS of each inhibitor, while compounds on the irradiated plate were used to test *cis*-enriched PSS of each inhibitor. 10 μL of each non-irradiated compound at the 8 different concentrations was transferred into another 96 well round-bottom plate (in duplicate), followed by 10 μL of 20S proteasome (12.5 $\mu\text{g}/\text{mL}$ in Tris buffer) and the plate was left to incubate for 10 min at rt. 40 μL of the corresponding fluorogenic substrate (62.5 μM in Tris buffer) was added to each well, and the plate left to incubate for 2 h at 37°C. Similarly, 10 μL of each irradiated compound at the 8 different concentrations was transferred to another 96 well round-bottom plate (in duplicate), followed by 10 μL of 20S proteasome (12.5 $\mu\text{g}/\text{mL}$ in Tris buffer) and the plate was left to incubate (wrapped in aluminium foil) for 10 min at rt. 40 μL of the corresponding fluorogenic substrate (62.5 μM in Tris buffer) was added to each well, and the plate left to incubate for 2 h at 37°C (wrapped in aluminium foil). Fluorescence caused by the release of AMC was measured at $\lambda_{\text{em}} = 445 \text{ nm}$ and $\lambda_{\text{ex}} = 390 \text{ nm}$ on a *Synergy H4 Hybrid Multi-Mode Microplate Reader*, (Bio-Tek Instruments, Inc.). Proteasome activity was determined under conditions in which substrate hydrolysis increased linearly with time and the change in fluorescence signal was proportional to the concentration of free AMC.

d. Cell Viability Assay

Cell culture. Derivative **4c** was dissolved in DMSO (10 mM) and the solution stored at -20°C . Human cell lines (HCT116, MDA-MB-468, and MCF-10A) were purchased from American Type Tissue Culture. MDA-MB-468 and HCT116 cells were grown in Dulbecco's Modified Eagle's Medium (DMEM) and supplemented with 10% FCS, 1% PSG and 10 mM HEPES. MCF10A cells were cultured in DMEM/F12: (1:1) (Invitrogen) with 5% horse serum (Invitrogen), 10 $\mu\text{g}/\text{mL}$ insulin, 20 ng/mL human epidermal growth factor (Sigma-Aldrich, MO, USA), 100 ng/mL cholera toxin, and 500 ng/mL hydrocortisone (Sigma-Aldrich, MO, USA). All cells were maintained at 37°C in a humidified atmosphere of 5% CO_2 .

Determination of LD_{50} . Cells were seeded in 96-well microtiter plates at a density of 2×10^4 cells/well with varying concentrations of proteasome inhibitors. For **4c**-(*cis*)-enriched compound, cells were wrapped in aluminum foil and kept in the dark. Cells were harvested 48 hours post treatment, centrifuged at $1,300 \times g$, washed in phosphate buffered saline (PBS) and stained with 7-amino-actinomycin-D solution (2 $\mu\text{g}/\text{mL}$) (7AAD, Invitrogen) for 10 min at room temperature. Viable cells were determined with the use of a *FACS Calibur flow cytometer* (Becton Dickinson Immunocytometry Systems), and analyzed with the use of *FLOWJO* (Tree Star Inc.) and GraphPad Prism (GraphPad Software Inc. version6).

e. Photochemical data

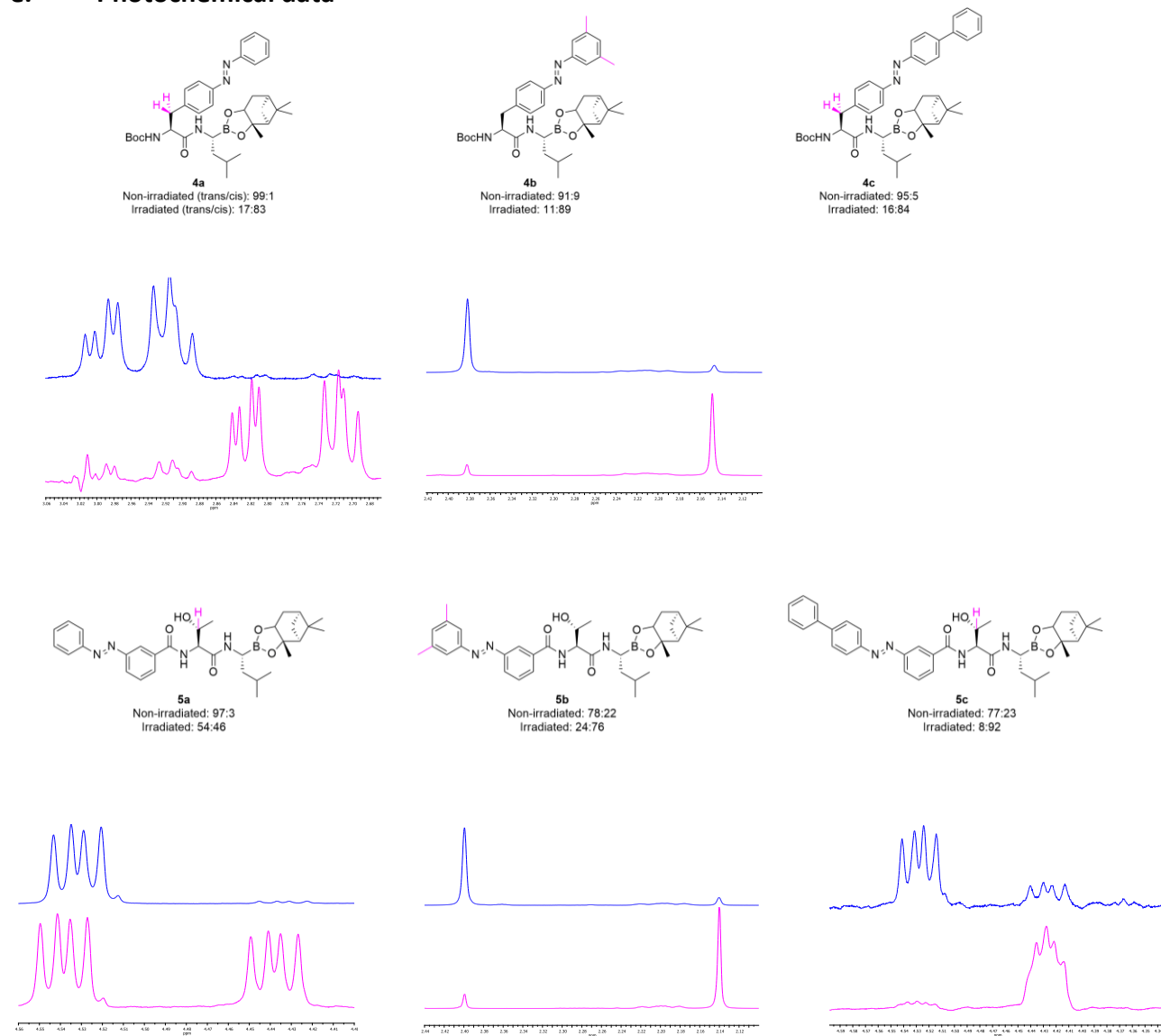


Figure S1. Determination of the ratio of *trans/cis* isomers for each state for each compound before and after irradiation ($\lambda = 365$ nm, 1 h) in $\text{DMSO-}d_6$ (~ 2 mg/mL), by ^1H NMR analysis. The figures show spectra of *trans*-enriched TAS (non-irradiated, blue line) and *cis*-enriched PSS (irradiated, pink line) for each compound. Protons for signals shown are highlighted.

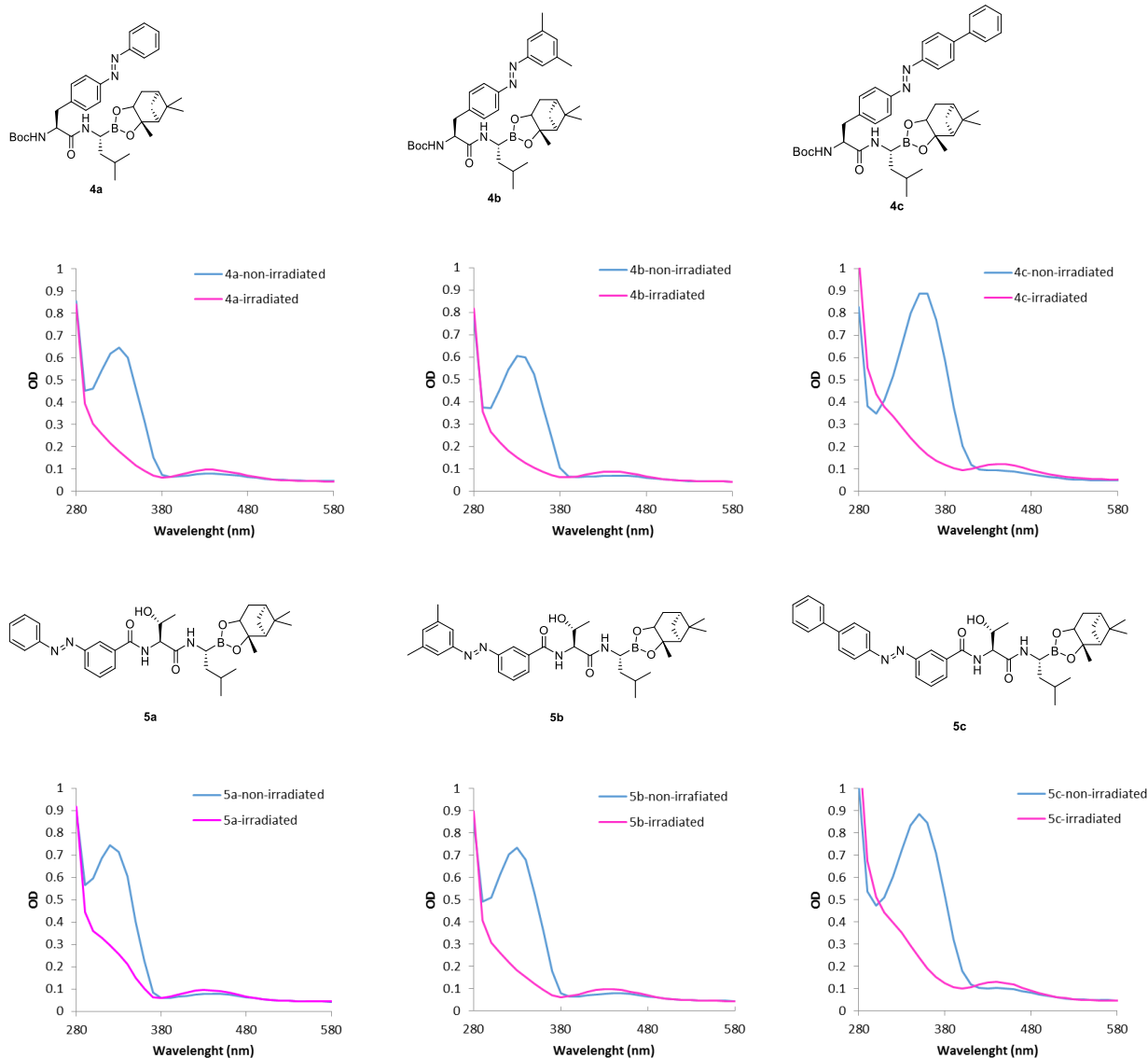


Figure S2. UV-Vis spectra of compounds **4-5** (250 μ M in DMSO). Non-irradiated (*trans*-enriched TAS) samples are shown in blue, and samples irradiated at 365 nm (*cis*-enriched PSS) are shown in pink.

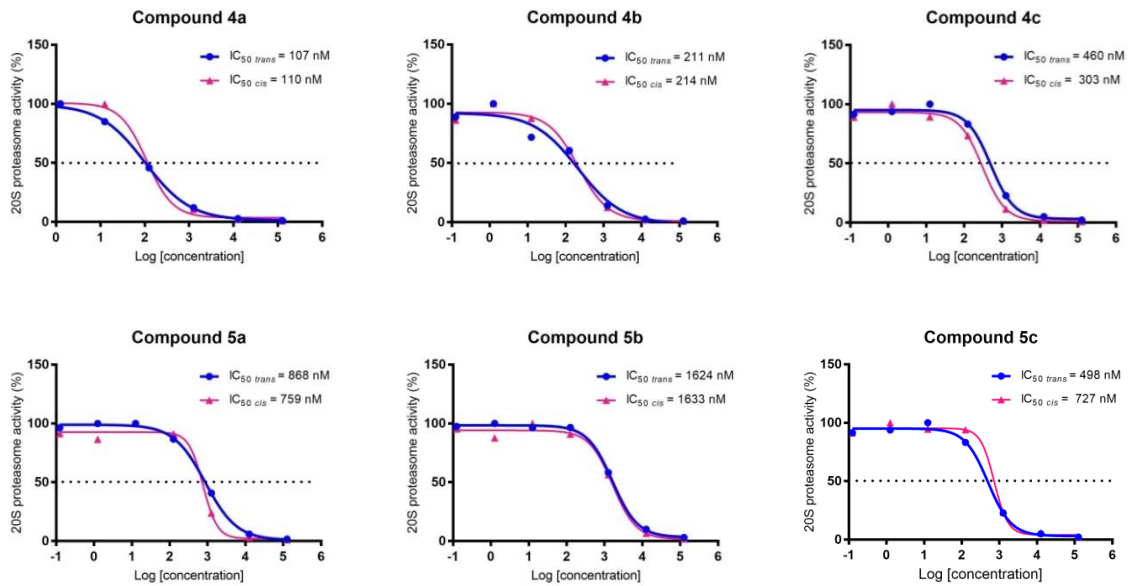


Figure 3. IC₅₀ curves of 4–5 against $\beta 1$ proteasome subunit before and after irradiation. The *trans* TAS is indicated in blue and the *cis*-PSS in pink.

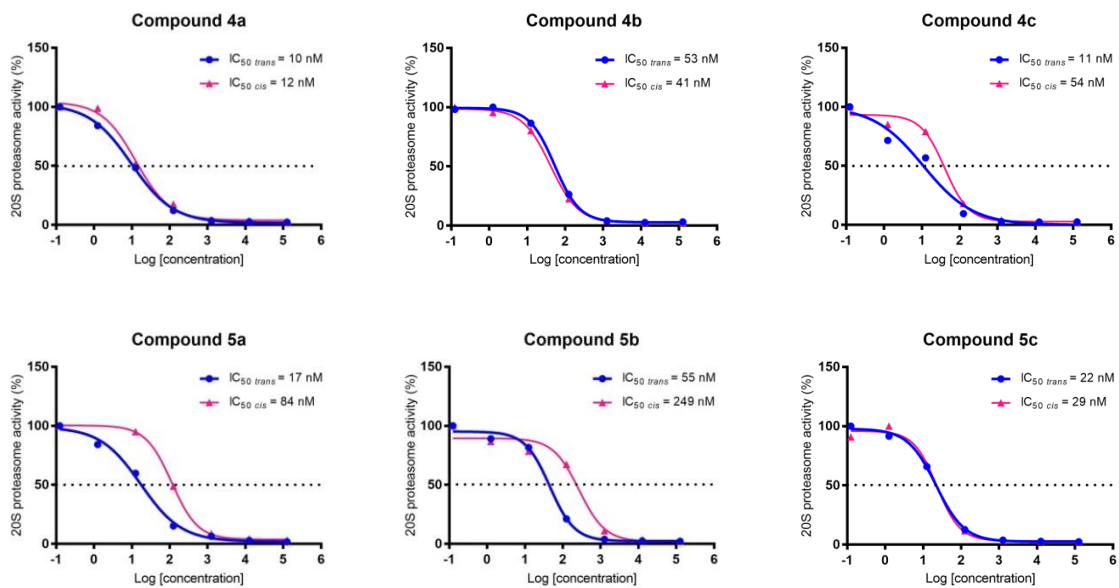
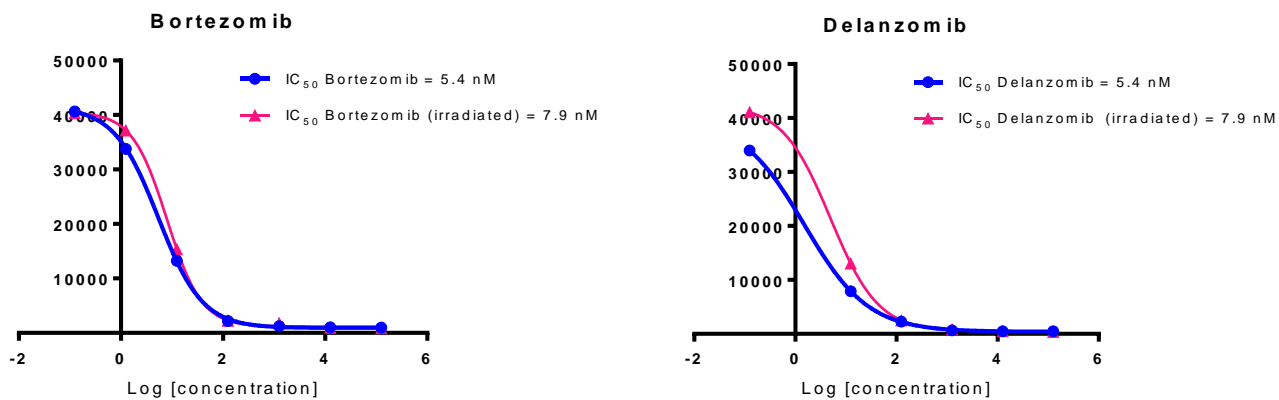


Figure 4. IC₅₀ curves of 4–5 against $\beta 5$ proteasome subunit before and after irradiation. The *trans*-TAS is indicated in blue and the *cis*-PSS in pink.



CHAPTER 5

P2-extended D- peptides as novel proteasome inhibitors

Borja Lopez^a, **Alaknanda Adwal**^b, David F. Callen^b and Andrew D. Abell^{a,c}

^a Department of Chemistry, The University of Adelaide, North Terrace, Adelaide, South Australia 5005, Australia

^b Centre for Personalised Cancer Medicine, Adelaide Medical School, The University of Adelaide, North Terrace, Adelaide, South Australia 5005, Australia

^c ARC Centre of Excellence for Nanoscale BioPhotonics, Institute of Photonics and Advanced Sensing, Department of Chemistry, The University of Adelaide, Adelaide, South Australia 5005, Australia

Statement of Authorship

Statement of Authorship

Title of Paper	P2-extended D- peptides as novel proteasome inhibitors
Publication Status	<input type="checkbox"/> Published <input type="checkbox"/> Accepted for Publication <input type="checkbox"/> Submitted for Publication <input checked="" type="checkbox"/> Unpublished and Unsubmitted work written in manuscript style
Publication Details	

Principal Author

Name of Principal Author (Candidate)	Alaknanda Adhya		
Contribution to the Paper	Conducted all biological experiments, analysed and interpreted data and co-wrote manuscript.		
Overall percentage (%)	10%		
Certification:	This paper reports on original research I conducted during the period of my Higher Degree by Research candidature and is not subject to any obligations or contractual agreements with a third party that would constrain its inclusion in this thesis. I am the primary author of this paper.		
Signature		Date	6/3/2017

Co-Author Contributions

By signing the Statement of Authorship, each author certifies that:

- i. the candidate's stated contribution to the publication is accurate (as detailed above);
- ii. permission is granted for the candidate to include the publication in the thesis; and
- iii. the sum of all co-author contributions is equal to 100% less the candidate's stated contribution.



Name of Co-Author	Borja Lopez Perez		
Contribution to the Paper	Synthesized chemical compounds and conducted chemistry experiments, interpreted data and co-wrote manuscript.		
Signature		Date	3/4/2017

Name of Co-Author	David F Callen		
Contribution to the Paper	Contributed to conception, design and manuscript preparation, and overall supervision of project.		
Signature		Date	10/03/17

Name of Co-Author	Andrew D Abell		
Contribution to the Paper	Contributed to conception, design and manuscript preparation, and overall supervision of project.		
Signature		Date	1/4/2017

Prelude

The dipeptide boronic acid bortezomib, is a FDA approved proteasome inhibitor now in use for the treatment of multiple myeloma and few other malignancies. The major drawback to bortezomib use is its dose-limiting toxicity that arises due to its cross-reactive peptidic structure. Here we have explored whether modification at P1 and P2 position of bortezomib based derivatives increases affinity, specificity and cytotoxicity.

This chapter is presented as a manuscript in preparation for submission to a journal for publication.

Contribution by the candidate: All biological/cell line experimental work and manuscript writing pertaining to biology.

Introduction

The 26S proteasome is a supramolecular protein complex that plays a pivotal role in the ubiquitin-dependent protein degradation pathway [1]. The proteins are degraded at three active sites located within the inner cavity of the 20S proteasome: chymotrypsin-like ($\beta 5$), trypsin-like ($\beta 2$), and caspase-like ($\beta 1$) [2]. The 19S regulatory particle is responsible for unfolding protein-substrates and stimulating proteolytic activity. In cancer cells, up-regulated proteasome activity is essential to the mechanisms underlying tumorigenesis, metastasis, and angiogenesis. Indeed, since the approval of Bortezomib (Velcade) for multiple myeloma in 2003 by the FDA (Figure 1), the proteasome has been validated as an important target for cancer therapy [3-5].

Most proteasome inhibitors, including bortezomib, inhibit proteasome activity by forming an antiparallel β -sheet with the substrate-binding channel of the active sites. The boron atom covalently interacts with the nucleophilic oxygen lone pair of Thr10 [6]. However, due to cross-reactivity [7], bortezomib also exhibits permanent abrogation of global protein degradation and severe off-target effects that result in low systemic tissue distribution.

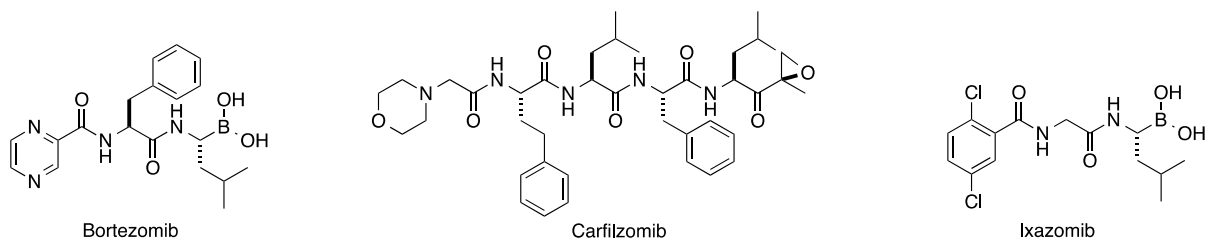


Figure 1. Structures of bortezomib, carfilzomib and ixazomib.

In this regard, it is imperative to develop proteasome inhibitors with different structural characteristics and, to explore new binding sites with the goal of achieving improved pharmacokinetic and pharmacodynamic profiles. Recent reports of non-peptidic proteasome inhibitors have widened the range of potential scaffolds as a way forward to address shortcomings associated with bortezomib non-specificity [8]. Therefore a plausible approach to improve proteolytic stability is to modify the chemical structure of the peptide backbone by introduction of L-amino acids or alkylated residues on the peptidic scaffold [8, 9]. The analysis of the crystal structure of bortezomib in complex with the yeast proteasome revealing an antiparallel beta sheet conformation and a spacious S2 pocket, in which the P2 phenylalanine of bortezomib lacked interactions with the protein (Figure 2)[6]. This observation presents an opportunity to introduce L-amino acids or alkylated residues at P2 without necessarily affecting binding properties. Although early structure-activity relationship studies on bortezomib at P2 indicated that bulky groups decrease potency (ref), recent reports have proven that inhibitors bearing sterically demanding moieties at P2 can show highly potent proteasome inhibition. In addition, the introduction of such sterically demanding moieties can provide new information about the composition of these poorly explored proteasomal primed substrate-binding sites.

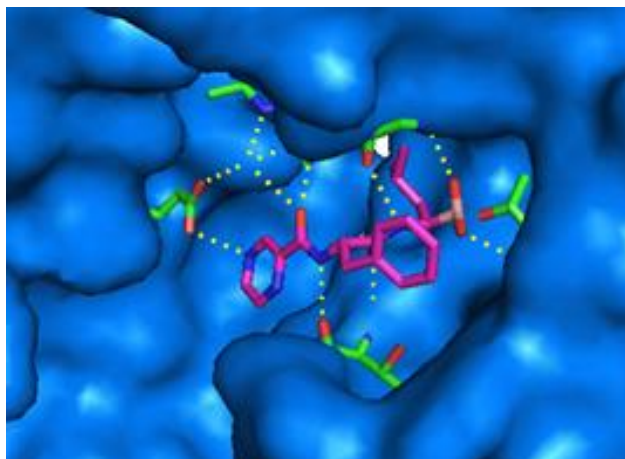
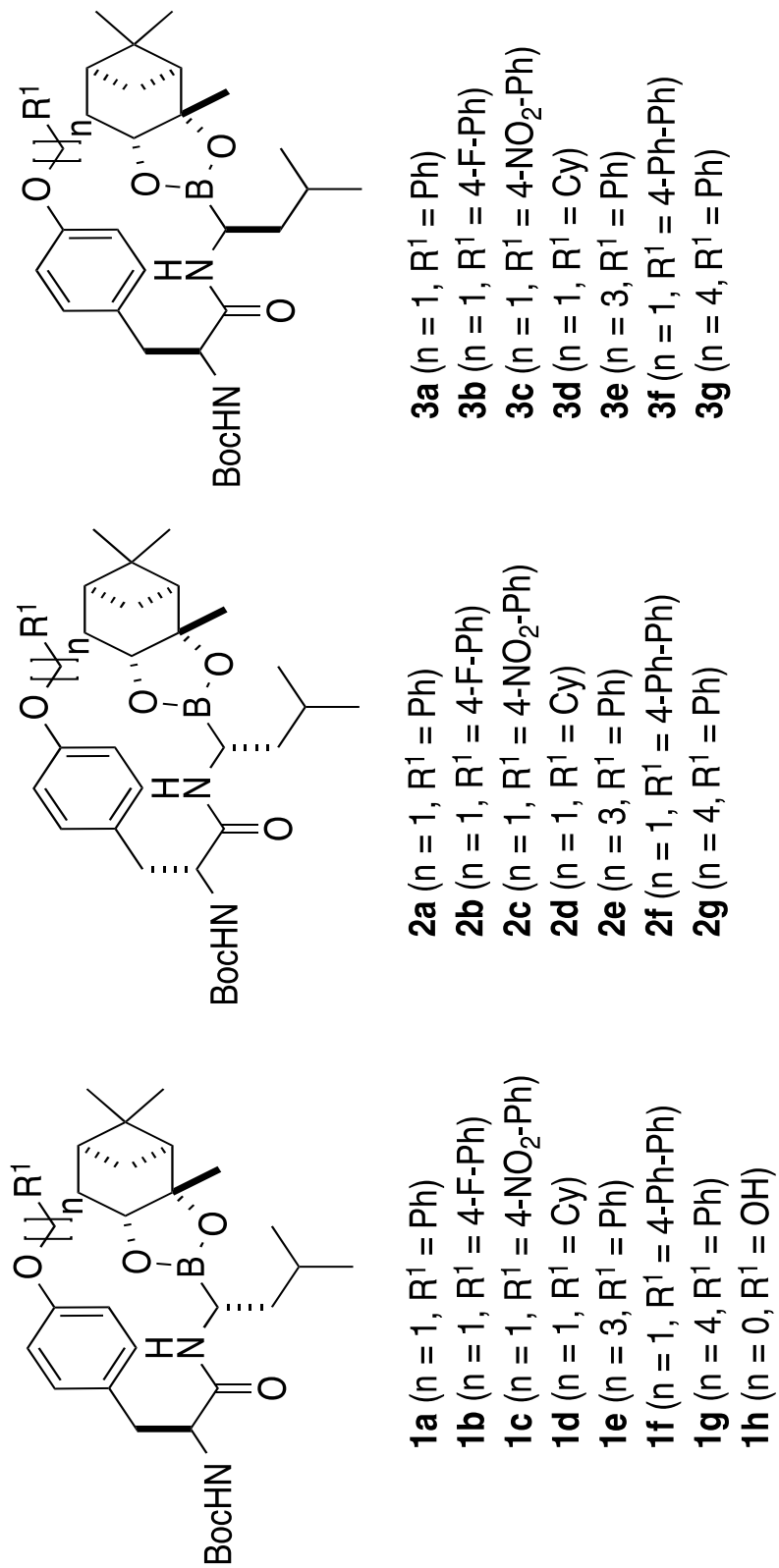


Figure 2. β 5 active site of the yeast proteasome in complex with bortezomib.

In this work, we investigate the biological profile of bortezomib-type inhibitors bearing side chains of different length, nature and configuration at P2 to obtain useful structural information for future design of proteasome inhibitors and with the aim to improve proteolytic sensitivity (Figure 3). Firstly, we studied the effect of the non-natural configuration on the binding properties at S1 (**2a-g**) and S2 (**3a-g**) pockets. Secondly, we explored the variation in the electron density of the aromatic system by introducing substituents at the para position of the phenyl moiety in P2. Both electron donating (**1-3h**, **1-3f**) and electron withdrawing groups (**1-3b**, **1-3c**) were analyzed. The influence of the pi interactions was also investigated by introducing a non- aromatic group as in compounds **1-3d**.

Figure 3. Inhibitors synthesized in this work.



Synthesis

Inhibitors **1**, **2** and **3** were prepared as depicted in Scheme 1. Commercially available Boc-L-tyrosine methyl ester (**4**) was first alkylated in the presence of K_2CO_3 and the corresponding bromide in DMF. Ester hydrolysis of **4** followed by coupling of the resulting acids **5** with (+)-pinanediol ester of leucineboronic ester **7**. in the presence of HATU and DIPEA gave the desired dipeptidic boronates **1**. During the purification process of boronic esters **1**, it was isolated the corresponding epimers at P1 (**3**) as well. This was caused by the partial loss of quiral integrity on the leucine alpha proton during the preparation of **7**.ⁱ To assign the absolute configuration of these two sets of boronic esters, one of the inhibitors was crystallized. The X-ray of **1e** confirms that the major epimer isolated possesses the natural configuration at P2 (Figure 4). Epi-P2 Boronic esters **2** were synthesized following the same synthetic pathway but starting with Boc-D-tyrosine methyl ester (**8**).

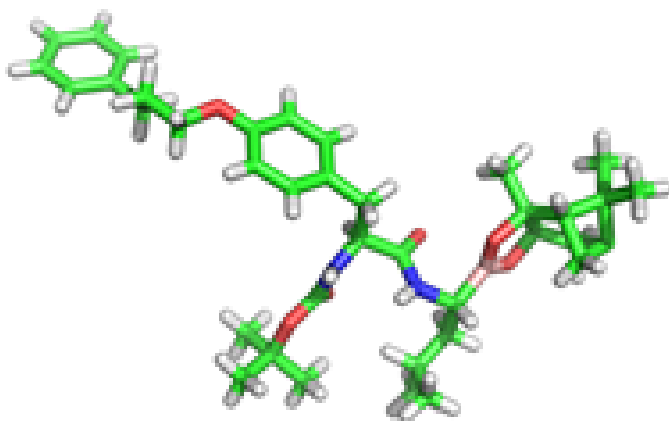
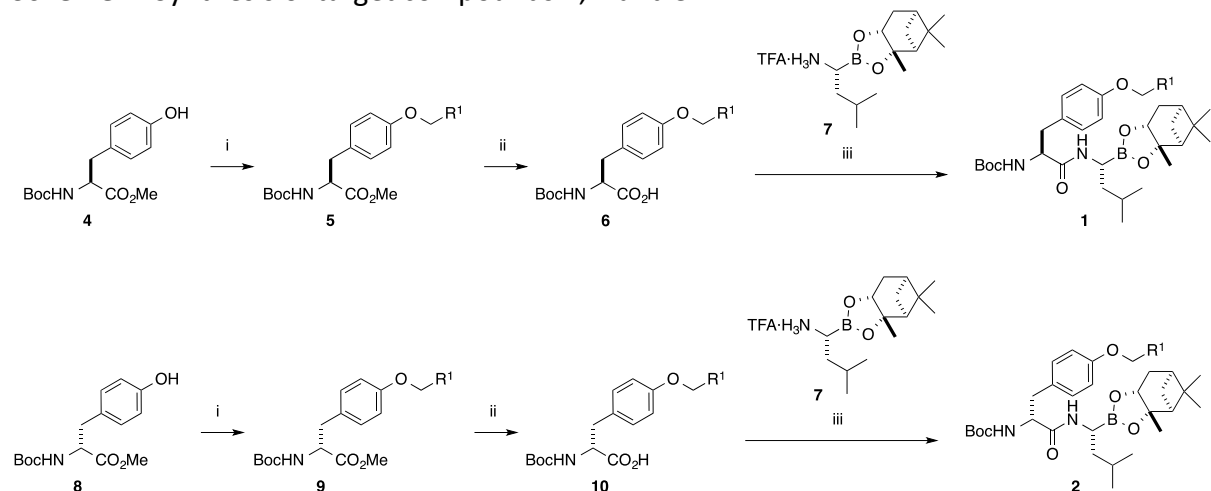


Figure 4. Crystal structure of boronic ester **1e**.

Scheme 1. Synthesis of target compounds **1**, **2** and **3**.



Reagents and conditions: (i) BrCH_2R^1 , K_2CO_3 , DMF, 60 °C, 16h; (ii) LiOH, 0 °C, 2h; (iii) HATU, DIPEA, DMF, 4h; (iv) $^i\text{BuB}(\text{OH})_2$, HCl (1M), MeOH, hexanes.

Biology

Compounds were tested against chymotrypsin-like ($\beta 5$), trypsin-like ($\beta 2$), and caspase-like ($\beta 1$) binding pockets of core particle (Table 1). Like bortezomib, all compounds were most active at inhibiting $\beta 5$ activity, while the inhibitory activity was reduced by approximately 10-fold when they were tested against $\beta 1$, and were depleted of activity on the $\beta 2$ binding pocket. In line with previous reports [10,11], the corresponding boronic acids of **3** showed similar activity to their boronic ester analogues. Stereochemistry at P1 proved to be crucial as compounds with the natural configuration (**1**) were 7 to 30 fold more active than their epimer counterparts (**3**). This indicates that the orientation of the D-alanine is not favorable for the interaction with the S1 pocket at the binding site. In contrast, the configuration at P2 has less impact on the IC_{50} values. The difference in activity between natural (**1**) and P2-epi inhibitors (**2**) only differ by 1 to 3 fold. These two observations confirm the specificity of the S1 pocket and the promiscuity of

the spacious S2 site. For natural inhibitors **1**, the nature of the ring had an effect on the inhibition. The S2 binding pocket seems to have a preference for aromatic rings (**1a**) over aliphatic rings (**1d**). Incorporation of an electro-withdrawing group in the para-position of phenyl ring such as in **1c** did not markedly change the inhibition, however, the presence of fluorine atom at the same position as in **1b** led to an increase of potency (36 nM). The presence of a free phenol (**1h**) led to a considerable loss of potency probably due to the lack of hydrogen bonding to stabilize it. In contrast, stereoisomers **2** did not show a clear pattern. Remarkably, all the activities for the inhibitors were below 250 nM even though they present a D-aminoacid at P2.

Table 1. Inhibition values for the compounds against the three binding sites of the 20S proteasome.

Compd	IC ₅₀ [μ M]		
	β 5	β 1	β 2
1a	0.088	0.43	>125
1b	0.036	0.28	>125
1c	0.074	0.26	>125
1d	0.11	0.42	>125
1e	0.091	0.40	>125
1f	0.099	0.78	>125
1g	0.044	0.48	>125
1h	4.28	17.31	>125
2a	0.141	0.98	>125
2b	0.117	0.50	>125
2c	0.126	0.67	>125
2d	0.186	1.40	>125
2e	0.240	1.25	>125
2f	0.112	1.57	>125
2g	0.132	1.45	>125
3a	1.63 (1.45)	9.25	>125
3b	1.05 (0.94)	3.00	>125

3c	3.45 (3.67)	7.68	>125
3d	2.04 (2.20)	15.19	>125
3e	1.13 (1.25)	4.88	>125
3f	0.711 (-)	2.81	>125
3g	0.70 (0.95)	2.81	>125
bortezomib	0.007	0.12	2

^aValue for boronic acid.

Next, cytotoxicities of the two most potent compounds emerging from this work (**1b** and **1g**) were assessed against a panel of 8 cell lines (Table 2), including 4 breast cancer cell lines (MDA-MB-468, MCF7, HS578T and MDAMB231), a colorectal cancer cell line (HCT-116), a Ewing sarcoma cell line (WE-68) and two non-malignant cell lines MCF-10A and normal dermal fibroblasts (NDF).

Compared to bortezomib, the cytotoxic potency of both compounds **1b** and **1g** was significantly reduced (between 5-10 fold) against all cell lines except for MDA-MB-468. For instance, in the breast carcinoma cell line Hs578T, boronic ester **1b** was 10-fold less potent compared to bortezomib with LD₅₀ values of 0.15 μ M and 0.015 μ M respectively. This 10 fold decrease in cytotoxic potency for **1b** is expected and consistent with its decreased inhibitory potency against the β 5 activity of the proteasome in *in vitro* assays (Table 1). As expected, compounds **1b** and **1g** did not differ in their relative cytotoxic potencies against all cell lines except MDA-MB-468. Unexpectedly, in the MDA-MB-468 breast carcinoma cell line, cytotoxic potencies for compound **1b** was comparable to bortezomib and significantly higher than **1g**. The basis for this result is unclear but may be attributed to the specific molecular characteristics of this cell line. Both **1b** and **1g** as well as bortezomib were significantly less cytotoxic against the non-

malignant cell lines. Overall, our results show that bortezomib-ester derivatives, despite having bulky P2 moieties, remain functionally active.

Table 2. Cytotoxicity of Compounds against Tumour Cell Lines (LD₅₀ (μM))

Compd	MDA- MB-468	MCF7	HS578T	MDA-MB- 231	HCT116	WE68	MCF- 10A	NDF
1b	0.05	>1.25	0.15	0.16	0.08	0.81	>1.25	0.14
1g	0.90	1.25	0.31	0.29	0.17	1.25	>1.25	0.41
Bortezomib	0.04	1.5	0.015	0.035	0.005	0.1	>1.25	0.48

Conclusion

A common motif on the three FDA-approved proteasome inhibitors is the presence of a peptidic scaffold with an electrophilic warhead for covalent binding to the catalytic Thr1 residues of the proteasome. Choosing peptidic backbones for inhibitor synthesis has both pros and cons. On the plus side, there is ease of synthesis, cost-effectiveness and derivatization. However, a major drawback is their cross-reactivity and drug delivery challenges. As other proteases can easily cleave these peptides, frequent dosing becomes necessary. Protease-resistant peptides would address many of these limitations.

Here, we have assessed how configuration at P1 and P2 position of bortezomib based inhibitors affects affinity, specificity and cytotoxic efficacy. Stereochemistry at P1 proved to be crucial as compounds with the natural configuration were 50 fold more active than their epimer counterparts. In contrast, the configuration at P2 has less impact on the IC_{50} values with differences of only 1-3 fold and the S2 pocket was able to accommodate bulky aromatic residues and long chains, which can be exploited for introducing fluorescent markers for experimental purposes. Furthermore, our crystallization studies show that inhibitors **1b** and **1c** bind to non-primed and primed-regions of the S2 pocket. Structural information obtained from this study holds significance for future drug design and to improve proteolytic stability. This is an ongoing study and we are currently undertaking crystallography studies for compounds **1f**, **2b**, **2c** and **2f** and conducting cross-reactivity assays for other proteases.

References

1. Bedford, L., et al., *Assembly, Structure and Function of the 26S proteasome*. Trends in cell biology, 2010. **20**(7): p. 391-401.
2. Adams, J., *The proteasome: structure, function, and role in the cell*. Cancer Treat Rev, 2003. **29 Suppl 1**: p. 3-9.
3. Kane, R.C., et al., *Velcade: U.S. FDA approval for the treatment of multiple myeloma progressing on prior therapy*. Oncologist, 2003. **8**(6): p. 508-13.
4. de la Puente, P. and A.K. Azab, *Contemporary drug therapies for multiple myeloma*. Drugs Today (Barc), 2013. **49**(9): p. 563-73.
5. Kumar, S.K., et al., *Phase 2 trial of ixazomib in patients with relapsed multiple myeloma not refractory to bortezomib*. Blood Cancer J, 2015. **5**: p. e338.
6. Groll, M., et al., *Crystal Structure of the Boronic Acid-Based Proteasome Inhibitor Bortezomib in Complex with the Yeast 20S Proteasome*. Structure, 2006. **14**(3): p. 451-456.
7. Kettner, C.A. and A.B. Shenvi, *Inhibition of the serine proteases leukocyte elastase, pancreatic elastase, cathepsin G, and chymotrypsin by peptide boronic acids*. J Biol Chem, 1984. **259**(24): p. 15106-14.
8. Gallastegui, N., et al., *Hydroxyureas as noncovalent proteasome inhibitors*. Angew Chem Int Ed Engl, 2012. **51**(1): p. 247-9.

9. Walker, B., et al., *Asymmetric Preference of Serine Proteases toward Phosphonate and Phosphinate Esters*. *Biochemical and Biophysical Research Communications*, 2000. **276**(3): p. 1235-1239.
10. Verdoes, M., et al., *A fluorescent broad-spectrum proteasome inhibitor for labeling proteasomes in vitro and in vivo*. *Chem Biol*, 2006. **13**(11): p. 1217-26.
11. Zhu, Y., et al., *Design, Synthesis, Biological Evaluation, and Structure–Activity Relationship (SAR) Discussion of Dipeptidyl Boronate Proteasome Inhibitors, Part I: Comprehensive Understanding of the SAR of α -Amino Acid Boronates*. *Journal of Medicinal Chemistry*, 2009. **52**(14): p. 4192-4199.

Methods and materials

Cell culture

Bortezomib (Selleckchem, Houston, TX, USA), Carfilzomib (Selleckchem, Houston, TX, USA), Ixazomib (Selleckchem, Houston, TX, USA) or in-house generated derivatives were dissolved in 10 mM DMSO and stored at -20°C . Human cell lines (WE-68, HCT116, MCF7, MDA-MB-468, MDA-MB-231, Hs578T, MCF-10A) were purchased from American Type Tissue Culture. Normal dermal fibroblasts (established from a normal individual) were a kind gift from A. Prof. Richard Sturm (Institute for Biomolecular Sciences, The University of Queensland, Brisbane, Australia). WE-68 and MCF7 cell lines were grown in RPMI-1640 media. RD-ES, MDA-MB-468, HCT116, MDA-MB-231, Hs578T and primary dermal fibroblast cell lines were grown in Dulbecco's Modified Eagle's Medium (DMEM). Both RPMI and DMEM media were supplemented with 10% FCS, 1% PSG and 10 mM HEPES. MCF-7 cells were supplemented with 1% insulin. MCF10A were cultured in DMEM/F12: (1:1) (Invitrogen) with 5% horse serum (Invitrogen), 10 $\mu\text{g}/\text{ml}$ insulin, 20 ng/ml human epidermal growth factor (Sigma-Aldrich, MO, USA), 100 ng/ml cholera toxin, and 500 ng/ml hydrocortisone (Sigma-Aldrich, MO, USA). All cells were maintained at 37°C in a humidified atmosphere of 5% CO_2 .

Determination of LD_{50}

Cells were seeded in 96-well microtiter plates at a density of 2×10^4 cells/well with varying concentrations of proteasome inhibitors. Cells were harvested 48 hours post treatment, centrifuged at $1,300 \times g$, washed in phosphate buffered saline (PBS) and stained with 7-amino-

actinomycin-D solution (2 $\mu\text{g}/\text{mL}$) (7AAD, Invitrogen) for 10 minutes at room temperature. Viable cells were determined with the use of a FACS Calibur flow cytometer (Becton Dickinson Immunocytometry Systems), and analyzed with the use of FLOWJO (Tree Star Inc.) and GraphPad Prism (GraphPad Software Inc. version 6).

***In Vitro* Proteasome Activity Assay**

Proteasome CT-L, C-L and T-L activities were determined using hydrolysis of specific short peptide substrates conjugated to the fluorescent tag 7-amido-4-methylcoumarin (AMC). Purified rabbit 20S proteasome and fluorogenic CT-L substrate (Suc-Leu-Leu-Val-Tyr-AMC) were purchased from Boston Biochem (Cambridge, MA, USA). The T-L and C-L fluorogenic substrates (Bz-Val-Gly-Arg-AMC and Ac-nLPnLD-AMC) were purchased from Enzo Life Sciences (Farmingdale, NY, USA). Purified 20S proteasome (Enzo Life Sciences, Farmingdale, NY, USA) (0-2 μg) was pre-incubated with the indicated concentrations of inhibitors at 37 °C for 15 minutes and subsequently added to the AMC-labelled substrate peptide (50 μM) in assay buffer (20 mM Tris-HCl, pH 7.5, 0.5 mM EDTA, and 0.001% SDS (w/v)) for a further 2 hours. Fluorescent substrate cleavage by the 20S proteasome was linear during this incubation period. Hydrolysed AMC was subsequently detected with the Synergy™ H4 Hybrid Multi-Mode Microplate Reader (BioTek, USA) at excitation/emission wavelengths of 390/460 nm. Hydrolysis activity was measured as relative fluorescence units allowing IC_{50} values to be calculated that represented half of the maximal inhibitory activity of the proteasome. A minimum of three biological replicates was performed for each data point.

SECTION II

Exploiting the p53 pathway as a targeted therapy to treat Ewing Sarcoma

Chapter 6

Exploiting the p53 pathway as a targeted therapy to treat Ewing Sarcoma

Introduction

Ewing sarcoma is a highly aggressive solid bone tumour that primarily afflicts children and young adults (peak incidence of 15 years) [1, 2]. The genetic change fundamental to the pathogenesis of Ewing sarcoma involves a chromosomal translocation between the EWS gene located on chromosome 22q12 and a member of the ETS transcription factor family. The majority of cases (85% to 90%), are associated with this t(11;22) where the amino terminal of the EWS gene is joined to the carboxyl terminus of FLI1 (chromosome 11) [3]. The resulting fusion protein is an oncogenic transcription factor that exerts its effect by altering cellular functions and signaling pathways leading to growth and proliferation of tumour cells [4, 5]. The development of a malignant neoplasm generally requires secondary genetic alterations, most frequently in oncogenes or tumour suppressors. P53 is one of the most frequently altered proteins in cancers, and this can occur via mutation of the TP53 gene (in 50% of all cancers) or overexpression of p53-regulatory proteins that suppress p53 activity e.g. MDM2 and MDM4 [6]. However, in Ewing sarcoma, TP53 mutations are rare with the majority of cases expressing a functional wild-type p53 [7, 8]. This feature is infrequent in cancer and is suggestive that Ewing sarcoma will be sensitive to p53-based targeted therapeutic strategies.

Tumour Suppressor p53

P53 is a transcription factor that governs major cellular tumour suppression pathways, inducing senescence, apoptosis and cell cycle arrest [9]. It has been long known that stabilization of p53 is pivotal for the cell to respond to cellular stresses (DNA damage, hypoxia etc.) and maintain cellular homeostasis. Protein levels of p53 within cells are tightly controlled and kept low primarily by its negative regulator MDM2, which binds to the amino terminus of p53, targeting it for ubiquitination and subsequent degradation [10].

Upon cellular or nucleolar stresses and depending on its cellular localization, p53 elicits various responses. Nuclear p53 up-regulates RNA polymerase II (Pol II) mediating transcription of cell cycle and apoptotic regulators (e.g. p21, BAX, PUMA) [11, 12], while cytoplasmic p53 induces activation of the mitochondrial apoptotic pathway [13]. In the nucleolus, p53 impairs ribosomal RNA (rRNA) synthesis by disrupting the binding of the upstream binding factor (UBF) to selectivity factor 1 (SL1) which then partially abrogates the assembly of the pre-initiation complex at rDNA promoters, thus repressing the transcription by RNA polymerase I (Pol I) [14]. With such a crucial role in cellular surveillance in response to stress, it is not surprising that p53 is often termed 'the guardian of the genome', and that mutations in the TP53 gene are commonly observed in diverse types of human cancer, making it an promising target for genetic or pharmacological intervention in cancer treatment.

History of Ewing sarcoma treatment

Despite decades of research Ewing sarcoma has retained the most unfavorable prognosis of all primary musculoskeletal tumours. Prior to the use of multi-drug chemotherapy, surgery alone cured less than 20% of patients with Ewing sarcoma, even if the disease was localized [15]. However, starting in the 1970s, introduction of chemotherapy as a critical component of Ewing sarcoma treatment has led to a remarkable increase in overall disease free survival, with survival rates for patients with localized Ewing sarcoma increasing to 70% [16]. In contrast, patients with metastatic Ewing sarcoma have <30% 5-year survival despite advances in treatment strategies including dose-intensification, use of multi-drug adjuvant therapy and stem cell transplantation. Failure to further manipulate or optimize the current chemotherapy treatment to increase overall survival has led to the development of new drugs that can specifically target the cancer cells. The idea is to use these targeted therapies in conjunction with traditional chemotherapy to achieve greater efficacy, and less toxicity to normal cells. To date, many targeted therapies are being explored in pre-clinical and clinical trials for Ewing sarcoma with some in advanced clinical stages (Table 1).

On the forefront of Ewing sarcoma targeted therapies are inhibitors of insulin-growth factor-receptor (IGF-R) and mammalian target of rapamycin (mTOR), signaling pathways involved in cell proliferation and resistance to apoptosis respectively. Patient trials show good tolerance and tumour regression, however the major challenges with these inhibitors are their brief response periods and rapid development of resistance (reviewed in [17]). Lack of response or partial response, pharmacokinetic properties and dose-limiting toxicities are some of the issues

that these targeted therapies currently face, thus prompting research into other potential biological targets and/or improved versions of current drugs.

Table 1. Molecular targets and current development of targeted therapies in Ewing sarcomas in advanced stage clinical trials.

Targets	Therapeutic agents	Stage	References
IGF1-R inhibitors	R1507; SCH 717454	Phase II paed	[18, 19]
mTOR inhibitors	Ridaforolimus	Phase III ad	[20]
Combination	Cixutumumab + temsirolimus	Phase II paed	[21]
Multi-agent inhibitors	Imatinib mesylate	Phase II paed	[22, 23]
Bone microenvironment	Zoledronic acid	Phase III paed/ad	[24]
Angiogenesis inhibitor	Bevacizumab	Phase I/II paed	[25]
HDAC inhibitors	Vorinostat, valproic acid	Phase I paed	[26, 27]
HSP90 inhibitors	17-AAG	Phase I paed	[28]

Abbreviations: ad, adult patients; HSP, heat shock protein; IGF, insulin-like

growth factor; Paed, paediatric patients; HDAC, histone deacetylase; mTOR, mammalian target of rapamycin.

Ribosomal RNA Polymerase as a therapeutic target

The nucleolus is the site of ribosomal synthesis and the assembly of nuclei depends on ongoing ribosomal DNA (rDNA) transcription and maturation. It is a dynamic region of the nucleus that is disassembled and reformed each cell cycle [29]. The major role for the nucleolus is the generation and assembly of the key components of the ribosome, the protein synthesis apparatus of the cell (Figure 1). Specifically, the 5.8S, 18S and 28S rRNAs are transcribed by ribosomal RNA polymerase (Pol I) as a single 47S rRNA precursor in the nucleolus that is subsequently processed and cleaved. These rRNAs, together with the 5S rRNA transcribed by Pol III in the nucleoplasm, form the nucleic acid backbone of functional ribosomes. The other major components of the ribosome, the Pol II transcribed ribosomal proteins, are transported from the cytoplasm into the nucleolus for assembly with the rRNAs (reviewed in [30]).

Though, traditionally viewed as a factory for ribosomal synthesis, 30% of nucleolar proteins do not participate in ribosomal biogenesis [31]. It is now clear that the nucleolus regulates a myriad of cellular functions, such as cell cycle control, stress response, protein degradation and mRNA modification and export suggesting a far greater role in cellular homeostasis than previously assumed [30].

Nucleolus in cancer

The relationship between the nucleolus and cancer has been the subject of study for many years. Abnormalities in the nucleolar morphology of cancer cells (enlarged and/or increased number of nucleoli) were first reported in late 19th century [32]. Since this initial report, a series of studies have been performed to clarify whether these nucleolar changes were a consequence of the cancerous state or if they might represent a cause of neoplastic transformation. In principle, the larger nucleoli associated with tumour cells could be attributed to greater levels of protein synthesis, and therefore ribosome biogenesis, required by rapidly dividing tumour cells. However, there is increasing evidence that nucleolar defects can be causative agents in the onset of cancer. Firstly, it was demonstrated that mammalian cells have a surveillance system for monitoring ribosomal biogenesis and nucleolar integrity and that disruption of these processes results in cell cycle arrest and programmed cell death at the G1 and G2 cellular checkpoints [33-35]. Of these, the best understood is the nucleolar stress pathway in which insults to the nucleolus lead to the accumulation of p53 [33].

The second critical observation was that the nucleolar stress pathway in tumour cells could be activated *in vivo* by a selective small molecule inhibitor (CX-5461) of Pol I transcription. This approach revealed that dysregulated rDNA transcription is necessary for the transformed phenotype induced by oncogenes such as MYC, and that targeting this dysregulated activity could be used as a therapeutic strategy to selectively kill malignant cells *in vivo* [36]. These findings shed light on an unappreciated role of dysregulated ribosome biogenesis and its

contribution to cellular transformation, and thus represent a novel strategy in the treatment of human cancers.

Dysregulation of Pol I transcription and ribosome biogenesis is universal in cancer. In general, this hyperactivation of rDNA transcription can be achieved by altered expression of upstream signaling pathways, or by oncogenic and tumour suppressive transcription factors such as p53 and MYC that interact directly with the rDNA promoter/transcription apparatus (reviewed in [37, 38]). These abundant and potent transcription factors regulate all three RNA polymerases, suggesting that, in addition to their traditional regulatory role in Pol II transcription, hijacking the control of Pol I and Pol III transcription may be essential for malignant transformation (reviewed in [36]). In addition to the core Pol I transcription apparatus, numerous other nucleolar proteins, some of which may also indirectly affect ribosome biogenesis, are modulated in cancer. The most prominent is nucleophosmin 1 (NPM1), which is overexpressed in various solid tumours including Ewing sarcoma [39, 40].

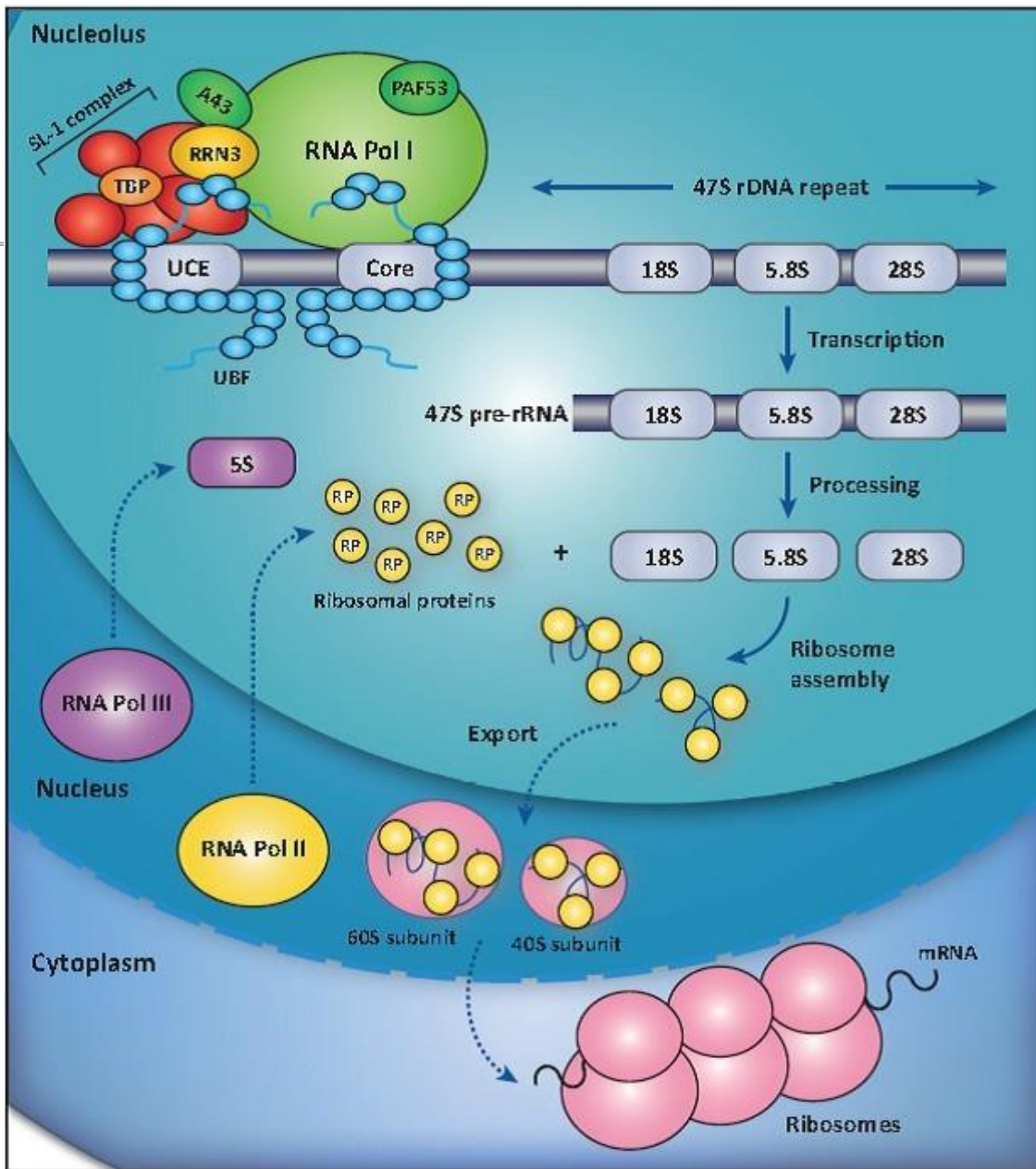


Figure 1. Schematic representation of ribosome biogenesis. Multiple coordinated steps are involved in ribosome biogenesis. Transcription of ribosomal genes exclusively by the Pol I transcriptional machinery in the nucleolus generates the 47S rRNA precursor which is rapidly processed into the 18S, 5.8S and 28S rRNAs. These three rRNAs will then assemble together with the 5S rRNA transcribed by Pol III, and with the ribosomal proteins transcribed by Pol II to form the 60S and 40S ribosomal subunit in the nucleus. These subunits further assemble into the mature 80S ribosome which is then exported to the cytoplasm [37]. From reference [37].

As yet, there is no clear evidence to support the notion that accelerated rDNA transcription in cancer is sufficient to initiate malignant transformation. This is in part due to the fact that rDNA transcription is a complex process that is tightly coupled to downstream processes, such as rRNA processing, ribosomal assembly, and transport. Therefore, modulation in any single rDNA transcription component will likely be counteracted by the rate-limiting step of the downstream processes. Although C-myc and oncogenic signaling pathways (PI3K/AKT/mTOR and RAS/RAF/ERK) can cause a robust increase in Pol I activity and subsequent acceleration of ribosomal synthesis, it is not possible to ascribe this function as causative for malignant transformation as these pathways and factors have pleiotropic effects on many aspects of malignant transformation in addition to their roles in ribosome biogenesis.

As one bottleneck limiting cancer cell proliferation is the rate of ribosomal synthesis, it is possible that tumour cells become 'addicted' to accelerated ribosome biogenesis and therefore are selectively vulnerable to therapeutics that inhibit rRNA synthesis. It is therefore not surprising that numerous anti-cancer drugs mediate their therapeutic effect, at least in part, through disrupting ribosome biogenesis. For example, cisplatin, doxorubicin, mitomycin C and low concentrations of actinomycin D (<10nM), all inhibit rRNA synthesis at the level of Pol I transcription, whereas camptothecin, flavopiridol, and roscovitine modulate early rRNA processing steps. In either case, inhibition of Pol I transcription or rRNA processing by these drugs leads to nucleolar disruption. In contrast to this, drugs including 5-fluorouracil and homoharringtonine, which impair late rRNA processing events, leave the nucleolus intact (reviewed in [37, 41]). The ellipticine family of planar alkaloid compounds, which were originally

identified in a screen for compounds that intercalate with DNA for use as anticancer agents, were recently found to selectively inhibit RNA Pol I by impairing SL-1 promoter binding and preinitiation complex assembly [42]. Various ellipticine derivatives have been evaluated in Phase I and II clinical trials, but failed further clinical development due to adverse side effects. Actinomycin D (FDA approved) which is currently used as a chemotherapeutic drug in Wilms and Ewing tumours. Unfortunately, none of these drugs are highly Pol I selective and therefore it is not possible to assign the proportion of therapeutic effect mediated via Pol I. Furthermore, these drugs are DNA damaging agents that are associated with off-target toxicity. By contrast, a new generation of drugs are currently being developed that selectively inhibit Pol I transcription for the specific purpose of cancer therapy.

CX-5461: a potent and selective rRNA polymerase inhibitor

CX-3543 (Cycle Pharmaceuticals) was the first chemotherapeutic agent developed that selectively targeted Pol I transcription (Pol I) *in vivo*. This drug selectively disrupts the nucleolin-rDNA G-quadruplex complex in the nucleolus. Similar to the functions of actinomycin D which intercalates into GC-rich duplex DNA, CX-3543 inhibits Pol I transcription at the site of RNA elongation and induces apoptosis in cancer cells. CX-3543 was shown to have clinical benefits for carcinoid/neuroendocrine tumours and is currently under phase I clinical trials [43].

CX-5461, is a next generation small molecule inhibitor, which impairs initiation of Pol I transcription by disrupting the interaction between Pol I transcription initiation factor SL-1 and the rDNA promoter [44]. CX-5461 has a 300–400 fold higher selectivity towards Pol I than either

Pol II or Pol III 44. *In vitro* studies have revealed that CX-5461 has a high anti-proliferative activity against a wide range of human cancer cell lines [45-48], however, the sensitivity towards Pol I inhibition varies widely between these cell lines (30 to 1000 fold). Interestingly, cell lines derived from p53 wild type hematological malignancies were the most sensitive. However the precise role of p53 status in conferring sensitivity to CX-5461 is an area of contention. CX5461 was shown to selectively kill B-cell lymphoma cells *in vivo*, but not normal B cells, by inducing p53-dependent apoptosis leading to the release of ribosomal proteins which bind MDM2, thus abrogating the p53–MDM2 interaction (Figure 2). Several other studies show efficacy of CX-5461 in *in vivo* models of acute myeloid leukemia and prostate cancer [48, 49]. In contrast, a study by Wang et al, demonstrated that low nanomolar concentrations of CX-5461 induce p53-independent autophagy in wild type, mutant and drug-resistant myeloma and pancreatic carcinoma cell lines [45] .

This type of non-genotoxic activation of p53 caused by CX- 5461 holds great promise in future cancer therapy. Whether selective targeting of ribosome biogenesis can be translated into anti-cancer treatment for different cancer types remains to be seen. Unfortunately, the majority of human cancers have lost wild type p53 functions, but recent results indicate that nucleolar stress can also be mediated independently of p53 function by other specific mechanisms, including inactivation of the E2F-1 transcription factor by MDM2 [35].

Summary

Ewing sarcoma is a childhood bone malignancy with alarmingly high mortality rate despite aggressive multi-modality treatment regimens. The majority of the Ewing sarcoma cases express a functional wild-type p53 suggesting that Ewing sarcoma will be sensitive to p53-based targeted therapeutic strategies.

Up-regulated rRNA transcription is a hallmark of cancer cells. To sustain rapid cell growth and proliferation, cancer cells become dependent on accelerated ribosome production which is controlled by Pol I. Previous studies show that selective inhibition of rRNA transcription by low concentration of actinomycin D results in rapid p53 stabilization and cancer cell apoptosis in Ewing sarcoma.

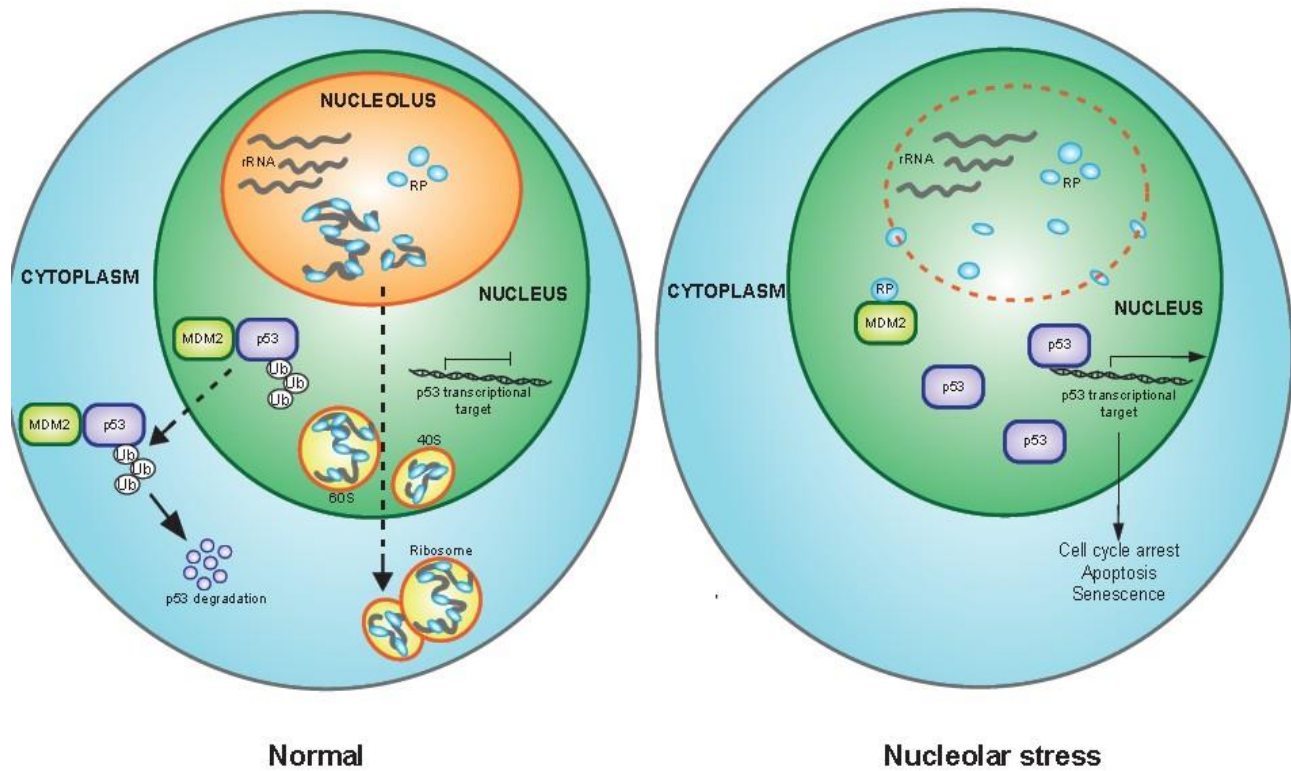


Figure 2. Overview of nucleolar stress related activation of the p53 pathway. Under normal conditions (left panel) the ribosomal proteins (RPs) are located within the nucleolus and exported to the cytoplasm where they assemble together with rRNA into functional ribosomes. MDM2 binds and ubiquitinates p53 which promotes p53 proteasomal degradation. Under nucleolar stress conditions (right panel) nucleolar disruption results in the release of RPs into the nucleoplasm where they bind MDM2 and abrogate its interaction with p53 leading to p53 stabilisation and activation of p53 downstream pathways, inducing cell cycle arrest, apoptosis, or senescence (adapted from 34).

CX-5461, a novel selective small-molecule inhibitor of RNA polymerase (pol) I, induces cell death in several human tumour types by both p53-dependent and independent mechanisms. However, *in vitro* results show that hematological cell lines with wild type p53 are the most sensitive to CX-5461 mediated cell death, suggesting that cancers with an intact p53 pathway will be sensitive to this drug.

Clinical Significance

Sarcomas represent 20% of malignancies in children and 10% of cancers in young adults. Despite aggressive multi-modal treatment regimens, the current mortality rate of approximately 50%, is amongst the worst of all cancer types in adolescents and young adults. The poor mortality rates have not improved over the past decade, suggesting an urgent need for more effective targeted treatment strategies.

RNA Pol I inhibition by CX-5461 is a promising approach for the treatment of Ewing sarcoma. Preliminary findings using Ewing sarcoma cell lines demonstrate low nanomolar drug activity providing a rationale for further research into CX-5461 as a potential therapeutic agent. Pre-clinical evaluation of the mechanism of CX5461 induced cellular death *in vitro* and in mouse models is paramount before translation of CX-5461 into the clinic. Furthermore, given that a considerable proportion of human cancers (~50%) exhibit mutations of the p53 gene, additional experiments are required to unequivocally address the role of p53 status in the sensitivity of cancers to RNA pol I inhibition.

References

1. Rodriguez-Galindo, C., S.L. Spunt, and A.S. Pappo, Treatment of Ewing sarcoma family of tumours: current status and outlook for the future. *Med Pediatr Oncol*, 2003. 40(5): p. 276-87.
2. Rosen, G., et al., Ewing's sarcoma: ten-year experience with adjuvant chemotherapy. *Cancer*, 1981. 47(9): p. 2204-13.
3. May, W.A., et al., The Ewing's sarcoma EWS/FLI-1 fusion gene encodes a more potent transcriptional activator and is a more powerful transforming gene than FLI-1. *Mol Cell Biol*, 1993. 13(12): p. 7393-8.
4. May, W.A. and C.T. Denny, Biology of EWS/FLI and related fusion genes in Ewing's sarcoma and primitive neuroectodermal tumour. *Curr Top Microbiol Immunol*, 1997. 220: p. 143-50.
5. Owen, L.A. and S.L. Lessnick, Identification of target genes in their native cellular context: an analysis of EWS/FLI in Ewing's sarcoma. *Cell Cycle*, 2006. 5(18): p. 2049-53.
6. Hollstein, M., et al., p53 mutations in human cancers. *Science*, 1991. 253(5015): p. 49-53.
7. Radig, K., et al., p53 and ras mutations in Ewing's sarcoma. *Pathol Res Pract*, 1998. 194(3): p. 157-62.
8. Komuro, H., et al., Mutations of the p53 gene are involved in Ewing's sarcomas but not in neuroblastomas. *Cancer Res*, 1993. 53(21): p. 5284-8.
9. Wei, C.L., et al., A global map of p53 transcription-factor binding sites in the human genome. *Cell*, 2006. 124(1): p. 207-19.
10. Honda, R. and H. Yasuda, Activity of MDM2, a ubiquitin ligase, toward p53 or itself is dependent on the RING finger domain of the ligase. *Oncogene*, 2000. 19(11): p. 1473-6.

11. el-Deiry, W.S., et al., WAF1, a potential mediator of p53 tumour suppression. *Cell*, 1993. 75(4): p. 817-25.
12. Jin, Z. and W.S. El-Deiry, Overview of cell death signaling pathways. *Cancer Biol Ther*, 2005. 4(2): p. 139-63.
13. Mihara, M., et al., p53 has a direct apoptogenic role at the mitochondria. *Mol Cell*, 2003. 11(3): p. 577-90.
14. Zhai, W. and L. Comai, Repression of RNA polymerase I transcription by the tumour suppressor p53. *Mol Cell Biol*, 2000. 20(16): p. 5930-8.
15. Ludwig, J.A., Ewing sarcoma: historical perspectives, current state-of-the-art, and opportunities for targeted therapy in the future. *Curr Opin Oncol*, 2008. 20(4): p. 412-8.
16. Thacker, M.M., H.T. Temple, and S.P. Scully, Current treatment for Ewing's sarcoma. *Expert Review of Anticancer Therapy*, 2005. 5(2): p. 319-331.
17. Scotlandi, K., Targeted Therapies in Ewing's Sarcoma, in *New trends in cancer for the 21st century*, A. Llombart-Bosch, V. Felipo, and J.A. López-Guerrero, Editors. 2006, Springer Netherlands: Dordrecht. p. 13-22.
18. Olmos, D., et al., Safety, pharmacokinetics, and preliminary activity of the anti-IGF-1R antibody figitumumab (CP-751,871) in patients with sarcoma and Ewing's sarcoma: a phase 1 expansion cohort study. *The Lancet Oncology*. 11(2): p. 129-135.
19. Pappo, A.S., et al., R1507, a monoclonal antibody to the insulin-like growth factor 1 receptor, in patients with recurrent or refractory Ewing sarcoma family of tumours: results of a phase II Sarcoma Alliance for Research through Collaboration study. *J Clin Oncol*, 2011. 29(34): p. 4541-7.

20. Demetri, G.D., et al., Results of an international randomized phase III trial of the mammalian target of rapamycin inhibitor ridaforolimus versus placebo to control metastatic sarcomas in patients after benefit from prior chemotherapy. *J Clin Oncol*, 2013. 31(19): p. 2485-92.
21. Schwartz, G.K., et al., Cixutumumab and temsirolimus for patients with bone and soft-tissue sarcoma: a multicentre, open-label, phase 2 trial. *The Lancet Oncology*, 2013 14(4): p. 371-382.
22. Chugh, R., et al., Phase II multicenter trial of imatinib in 10 histologic subtypes of sarcoma using a bayesian hierarchical statistical model. *J Clin Oncol*, 2009. 27(19): p. 3148-53.
23. CHAO, J., et al., Phase II Clinical Trial of Imatinib Mesylate in Therapy of KIT and/or PDGFR α -expressing Ewing Sarcoma Family of Tumours and Desmoplastic Small Round Cell Tumours. *Anticancer Research*, 2010. 30(2): p. 547-552.
24. Odri, G.A., et al., Zoledronic acid as a new adjuvant therapeutic strategy for Ewing's sarcoma patients. *Cancer Res*, 2010. 70(19): p. 7610-9.
25. Benesch, M., et al., Compassionate use of bevacizumab (Avastin[®]) in children and young adults with refractory or recurrent solid tumours. *Annals of Oncology*, 2008. 19(4): p. 807-813.
26. Fouladi, M., et al., Pediatric phase I trial and pharmacokinetic study of vorinostat: a Children's Oncology Group phase I consortium report. *J Clin Oncol*, 2010. 28(22): p. 3623-9.
27. Su, J.M., et al., Phase 1 study of valproic acid in pediatric patients with refractory solid or CNS tumours: a children's oncology group report. *Clin Cancer Res*, 2011. 17(3): p. 589-97.
28. Martins, A.S., et al., A pivotal role for heat shock protein 90 in Ewing sarcoma resistance to anti-insulin-like growth factor 1 receptor treatment: in vitro and in vivo study. *Cancer Res*, 2008. 68(15): p. 6260-70.

29. Boisvert, F.M., et al., The multifunctional nucleolus. *Nat Rev Mol Cell Biol*, 2007. 8(7): p. 574-85.
30. Scheer, U. and R. Hock, Structure and function of the nucleolus. *Curr Opin Cell Biol*, 1999. 11(3): p. 385-90.
31. Pederson, T. and R.Y.L. Tsai, In search of nonribosomal nucleolar protein function and regulation. *The Journal of Cell Biology*, 2009. 184(6): p. 771-776.
32. Montanaro, L., D. Treré, and M. Derenzini, Nucleolus, Ribosomes, and Cancer. *The American Journal of Pathology*, 2008. 173(2): p. 301-310.
33. Chakraborty, A., T. Uechi, and N. Kenmochi, Guarding the 'translation apparatus': defective ribosome biogenesis and the p53 signaling pathway. *Wiley Interdiscip Rev RNA*, 2011. 2(4): p. 507-22.
34. Iadevaia, V., et al., PIM1 kinase is destabilized by ribosomal stress causing inhibition of cell cycle progression. *Oncogene*, 2010. 29(40): p. 5490-9.
35. Donati, G., et al., Selective inhibition of rRNA transcription downregulates E2F-1: a new p53-independent mechanism linking cell growth to cell proliferation. *Journal of Cell Science*, 2011. 124(17): p. 3017-3028.
36. Bywater, M.J., et al., Inhibition of RNA polymerase I as a therapeutic strategy to promote cancer-specific activation of p53. *Cancer Cell*, 2012. 22(1): p. 51-65.
37. Bywater, M.J., et al., Dysregulation of the basal RNA polymerase transcription apparatus in cancer. *Nat Rev Cancer*, 2013. 13(5): p. 299-314.
38. Hannan, K.M., et al., Dysregulation of RNA polymerase I transcription during disease. *Biochim Biophys Acta*, 2013. 1829(3-4): p. 342-60.

39. Falini, B., et al., Translocations and mutations involving the nucleophosmin (NPM1) gene in lymphomas and leukemias. *Haematologica*, 2007. 92(4): p. 519-32.
40. Liu, Y., et al., Expression of Nucleophosmin/NPM1 correlates with migration and invasiveness of colon cancer cells. *Journal of Biomedical Science*, 2012. 19(1): p. 53.
41. Drygin, D., W.G. Rice, and I. Grummt, The RNA polymerase I transcription machinery: an emerging target for the treatment of cancer. *Annu Rev Pharmacol Toxicol*, 2010. 50: p. 131-56.
42. Andrews, W.J., et al., Old drug, new target. Ellipticines selectively inhibit RNA Polymerase I transcription. *Journal of Biological Chemistry*, 2013.
43. Drygin, D., et al., Anticancer activity of CX-3543: a direct inhibitor of rRNA biogenesis. *Cancer Res*, 2009. 69(19): p. 7653-61.
44. Drygin, D., et al., Targeting RNA polymerase I with an oral small molecule CX-5461 inhibits ribosomal RNA synthesis and solid tumour growth. *Cancer Res*, 2011. 71(4): p. 1418-30.
45. Wang, H., et al., CX-5461, a Novel RNA Polymerase I Inhibitor, Is Active Against Wild-Type and Mutant p53 Myeloma Models. *Blood*, 2013. 122(21): p. 4438-4438.
46. Yan, S., et al., The Potential of Targeting Ribosome Biogenesis in High-Grade Serous Ovarian Cancer. *International Journal of Molecular Sciences*, 2017. 18(1): p. 210.
47. Ye, Q., et al., Therapeutic Targeting of RNA Polymerase I With the Small-Molecule CX-5461 for Prevention of Arterial Injury–Induced Neointimal Hyperplasia. *Arteriosclerosis, Thrombosis, and Vascular Biology*, 2017. 37(3): p. 476-484.
48. Rebello, R.J., et al., The Dual Inhibition of RNA Pol I Transcription and PIM Kinase as a New Therapeutic Approach to Treat Advanced Prostate Cancer. *Clinical Cancer Research*, 2016. 22(22): p. 5539-5552.

49. Hein, N., et al., Inhibition of Pol I transcription treats murine and human AML by targeting the leukemia-initiating cell population. *Blood*, 2017.

CHAPTER 7

Dysregulating ribosomal biogenesis to treat Ewing sarcoma

Alaknanda Adwal¹, Kathleen I Pishas^{1,2}, Paul M Neilsen³, David F Callen¹

¹Centre for Personalised Cancer Medicine, Adelaide Medical School, The university of Adelaide, North Terrace, Adelaide, South Australia 5005, Australia

²Lessnick Sarcoma Laboratory, Centre for Childhood Cancer and Blood Disorders, 700 Children's Drive, Columbus Ohio, 43205, United States of America

³ School of Health, Medical and Applied Sciences. Central Queensland University, Bruce Highway, North Rockhampton, Queensland 4702, Australia

Statement of Authorship

Statement of Authorship

Title of Paper	Dysregulating ribosomal biogenesis to treat Ewing sarcoma		
Publication Status	<input type="checkbox"/> Published	<input type="checkbox"/> Accepted for Publication	
	<input type="checkbox"/> Submitted for Publication	<input checked="" type="checkbox"/> Unpublished and Unsubmitted work written in manuscript style	
Publication Details			

Principal Author

Name of Principal Author (Candidate)	Alaknanda Adwal		
Contribution to the Paper	Conducted majority of experiments, analysed and interpreted data and wrote manuscript.		
Overall percentage (%)	70%		
Certification:	This paper reports on original research I conducted during the period of my Higher Degree by Research candidature and is not subject to any obligations or contractual agreements with a third party that would constrain its inclusion in this thesis. I am the primary author of this paper.		
Signature		Date	6/3/2017

Co-Author Contributions

By signing the Statement of Authorship, each author certifies that:

- i. the candidate's stated contribution to the publication is accurate (as detailed above);
- ii. permission is granted for the candidate to include the publication in the thesis; and
- iii. the sum of all co-author contributions is equal to 100% less the candidate's stated contribution.



Name of Co-Author	Kathleen Irene Pishas		
Contribution to the Paper	Performed experimental work, interpreted data and wrote manuscript.		
Signature		Date	8 th March 2017



Name of Co-Author	Paul M Neilsen		
Contribution to the Paper	Contributed to conception, design and overall supervision of project, and data analysis and manuscript preparation.		
Signature		Date	10/03/17

Name of Co-Author	David F Callen		
Contribution to the Paper	Contributed to conception, design and overall supervision of project.		
Signature		Date	10/3/17

Prelude

This study has evaluated the molecular and cellular responses of cultured Ewing sarcoma cell lines following exposure to CX-5461, a recently discovered non-genotoxic specific RNA Polymerase I inhibitor. Our findings demonstrate that Ewing sarcoma cell lines are acutely sensitive to CX-5461. CX-5461 also displayed synergistic interactions with chemotherapeutic Actinomycin D that is currently used in treating Ewing sarcoma. Non-genotoxic cell death via CX-5461 provides a singular opportunity to overcome DNA damage associated with current treatments.

This chapter is presented as a manuscript in preparation for submission to a journal for publication.

Contribution by the candidate: Majority of biological experimental work and manuscript writing

Introduction

Ewing sarcoma is a highly aggressive bone and soft tissue cancer primarily diagnosed in children and young adolescents. It affects approximately 200,000 patients worldwide each year and has 10-20% long term survival in patients with metastatic, relapsed, or recurrent disease¹. Management of Ewing sarcoma is complicated by the use of genotoxic chemo-and radio-therapy that is associated with toxic bystander effects and secondary malignancies. The majority of the Ewing sarcoma patients retain functionally intact tumour suppressor p53 and downstream signalling pathways, hence exploiting p53-based therapies has been an attractive therapeutic approach. Inhibitors targeting MDM2 (e.g. Nutlin), the major negative regulator of p53, have demonstrated only modest benefits for patients harbouring wild-type p53. Recent sequencing studies demonstrate that Ewing sarcoma possesses one of the lowest mutation rates amongst all cancers (0.15 mutations/Mb)^{2, 3}, with recurrent mutation observed in EWS-FLI1 (85% cases) and STAG2. Targeted therapies for these proteins are in clinical and pre-clinical trials but thus far have no translational benefits.⁴⁻⁶ The constraints imposed by DNA damaging regimen and a combination of lack of recurrent driver mutations for this cancer require an alternative approach to evaluate non-genotoxic agents that broadly target cancer cell survival, either alone or in combination with traditional chemotherapies.

Dysregulating ribosome biogenesis is one such unexplored approach. Ribosomes are the primary protein synthesis apparatus of a cell and directly control cell growth and proliferation. Their synthesis is an intricately controlled process in which ribosomal RNA genes (rRNA 28S,

18S, 5.8S) transcribed by RNA polymerase I and assemble with ribosomal proteins and 5s rRNA transcribed by RNA Pol III and 5S RNA Pol II respectively to form functional ribosome. To maintain high proliferation rates, cancer cells need to increase their translational capacity and become addicted to high rates of ribosome biogenesis⁷⁻¹⁰, which can be exploited therapeutically. In fact, many clinically used chemotherapies that interfere with DNA metabolism also inhibit ribosome biogenesis¹¹ consequently preventing the transcription of rRNA, which leads to ribosomal stress and ultimately p53-dependent cell cycle arrest or apoptosis¹²⁻¹⁴. Actinomycin D, a commonly used chemotherapeutic for the treatment of Ewing sarcoma, also inhibits RNA Pol I. However, these multi-modal chemotherapy regimens have reached their full capacity now and further improvements to survival can only come from non-genotoxic approaches. Discovery of small molecule inhibitors that specifically inhibit ribosomal biogenesis has gained increased momentum in the last five years, with cell-based screens identifying several compounds that have minimal toxicity in non-malignant tissue^{15, 16}.

CX-5461 was the first non-genotoxic and selective inhibitor of ribosomal biogenesis to be reported¹⁵. CX-5461 selectively impairs initiation of Pol I transcription by disrupting the interaction between Pol I transcription initiation factor SL-1 to the rDNA promoter that leads to disruption in ribosome synthesis. CX-5461 elicits its anti-proliferative effects in a wide range of cell lines, including leukaemia, lymphoma, osteosarcoma, and prostate cancer cells. CX5461 was also shown to selectively kill B-cell lymphoma cells *in vivo*, but not normal B cells, by inducing p53-dependent apoptosis¹⁷. Currently, CX5461 is undergoing phase I clinical evaluation in patients with advanced hematologic malignancies and phase I/II evaluation

(NCT02719977) in patients with advanced/metastatic/recurrent solid tumours. The majority of sarcomas harbour wildtype p53^{18, 19}. This study assessed whether selective inhibition of RNA Pol I by CX-5461 represents a possible therapeutic approach for Ewing sarcoma both as a monotherapy and in combination with standard cytotoxic chemotherapeutic protocols..

Methods

Cell culture and reagents

CX-5461 and the ATM/ATR inhibitor KU-55933 were purchased from Selleck Chemicals (Houston, TX). WE-68 and VH-64 were kindly supplied by F. van Valen (Department of Orthopaedic Surgery, Westfälische-Wilhelms-University, Germany). TC-252 and TC-71 cell lines were kindly supplied by G. Hamilton (Department of Surgery, University of Vienna, Austria), STA-ET1 was sourced from P. Ambros (Children's Cancer Research Institute, St. Anna Children's Hospital, Vienna, Austria), and CADO-ES-1 was kindly supplied by J. Sonnemann (Department of Pediatric Haematology and Oncology, University Children's Hospital, Jena, Germany). MCF-10A, SK-ES-1, RD-ES, HCT116 were purchased from American Type Tissue Culture. YZ5 and pEBS were a kind gift from Prof. Kum Kum Khanna (Queensland Institute of Medical Research). Cell lines were cultured as previously described²⁰.

Western blot analysis

Western blot analysis was performed as previously described²¹. Whole protein lysates (5–20 µg) were resolved using SDS PAGE electrophoresis, and probed overnight at 4 °C with the following

primary antibodies Anti-E2F1 (C20, 1:500, Santa Cruz), p53 DO1 (1:1000, Santa Cruz Biotechnology), Phospho-p53 (Ser15) (1:500, Cell Signalling), Phospho-Histone H2A.X (Ser139) clone JBW301 (1:500, Millipore) and β -Actin (1:1000, AC-15, Sigma). Chemiluminescent detection of protein was achieved using appropriate secondary antibodies conjugated with horseradish peroxidase (Amersham) and the enhanced chemiluminescence kit according to the manufacturer's instructions (Amersham).

qPCR

Total RNA was extracted from cultured cells using RNeasy mini kits (Qiagen). One microgram of total RNA was reverse transcribed using MMLV reverse transcriptase (Life Technologies). qPCR was performed using SYBR Green mastermix and run on a CFX96 Bio-Rad real time PCR machine. Primer sequences are listed in the table below. Experiments were repeated three times. Results were normalized to GAPDH expression for each sample and plotted as relative to the expression of control samples.

18S pre-rRNA	CCGCGCTCTACCTTACCTACCT GCATGGCTTAATCTTTGAGACAAG
GAPDH	CGTCACCAACTGGGACGACA CTTCTCGCGGTTGGCCTTGG
ITAGV	TTGGAGCATCTGTGAGGTCG ACATGGAGCATACTCAACAGTCT
ITAG5	CGGGCTCCTTCTTCGGATTC CAGAGGTAGACAGCACCACC
ITGB1	CCGCGCGGAAAAGATGAATTT CCACAATTTGGCCCTGCTTG
ITGB3	CATCACCATCCACGACCGAA GTGCCCCGGTACGTGATATT

shRNA, siRNA and transfection

WE-68 and VH-64 shRNA stable cells were generated using retroviral transduction with pRetroSuper (pRS) vectors pRS-p53, which confers puromycin resistance. The pCMV-E2F1-HA (#24216) plasmid was purchased from Addgene, USA. Cells were transfected using lipofectamine 2000 or lipofectamine RNAimax according to the manufacturer's instructions.

Proliferation assay

Ewing sarcoma cells were seeded at 1×10^4 cells per well into 96-well plates, and treatments were administered. After the indicated time periods of incubation, medium was removed and cells were washed twice with PBS. 100 μ L of Cell-titre glo (1:1 ration with meduma, Promega) was added to each well and the cells were incubated for 10 mins in dark with shaking. Luminescence was measured on a LUMistar Omega Microplate Reader from BMG LABTECH (Carlsbad,, CA) with reactions normalised to vehicle control treated cells.

Cell viability assays

Cells were seeded in 96-well microtiter plates at a density of 2×10^4 cells/well in the presence of CX-5461 and chemotherapy drugs as indicated. For synergy experiments, cells were co-treated with indicated concentrations of CX-5461 and chemotherapies. Cells were harvested 48 hours post CX-5461 treatment, centrifuged at $1,300 \times g$, washed in phosphate buffered saline (PBS) and stained with 7-amino-actinomycin-D solution (2 μ g/mL) (7AAD, Invitrogen) for 10 minutes at room temperature. Viable cells were determined with the use of a FACS Calibur flow

cytometer (Becton Dickinson Immunocytometry Systems), and analyzed with the use of FLOWJO (Tree Star Inc.) and GraphPad Prism (GraphPad Software Inc. version 6).

Cell cycle analysis

Cells were harvested, collected by centrifugation, washed with PBS, fixed in cold 70% ethanol, and incubated overnight at 4°C. Cell pellets were washed twice with PBS and resuspended in PBS containing 25 mg/mL propidium iodide, RNase A, and Triton X-100 for 30 minutes at room temperature in the dark immediately before fluorescence-activated cell-sorting (FACS) analysis by FACSCalibur flow cytometer (Beckton Dickinson). DNA content was determined with the use of a FACS Calibur flow cytometer with cell cycle profiles analysed using MODFIT LT software (version 4.1.7). 50,000 cells were counted for DNA content.

Statistical analysis

Combination index (CI) values were calculated to determine the synergistic effects of CX-5461 on cell viability in the presence of cytotoxic agents. A CI value of <1, =1 and >1 indicates synergistic, additive and antagonistic effects respectively P values were calculated using Student's t-test with $P < 0.05$ considered statistically significant.

Results

Ewing sarcoma cells are hypersensitive to RNA Pol I inhibition

To investigate the utility of RNA Polymerase I inhibition for the treatment of Ewing sarcoma, the cytotoxic effects of CX-5461 (0-5000 nM) were assessed in a panel of nine Ewing sarcoma cell lines with varying *TP53* mutational status (Table 1). Cytotoxic sensitivity to CX-5461 varied widely across the cell lines (LD_{50} range 3-1176nM). Wild-type *TP53* cell lines VH-64 and WE-68 displayed the greatest sensitivity to CX-5461 with LD_{50} values of 3.0 nM and 3.4 nM respectively. In contrast, the mutant *TP53* cell line RD-ES was the most resistant to CX-5461 (LD_{50} 1120 nM), requiring greater than 300 fold CX5461 to achieve 50% cell death. However, there was no correlation observed between *TP53* status and CX-5461 sensitivity ($p = 0.29$) (supplementary figure 1).

A comparison of CX-5461 cytotoxic sensitivity (LD_{50s}) between Ewing sarcoma and previously reported solid cancers revealed Ewing sarcoma to be one of the most sensitive reported to date for all solid cancers tested with CX-5461 (supplementary figure 2). More importantly, these LD_{50} values mirror those displayed by haematological cell lines (supplementary figure 3) for which CX-5461 is in phase I or II clinical trials presently. Importantly, the viability of non-malignant breast (MCF-10A) and skin fibroblast (NDF) cell lines remained unaffected at these concentrations ($LD_{50} > 2500nM$) (Table 1).

Table 1. CX-5461 exhibits broad anti-cancer potency in a Ewing sarcoma cell panel.

Cell line	Histology	Patient gender/age	Origin	TP53 status	EWS rearrangement	CX-5461 LD ₅₀ (nM)
VH-64	ES	M/24	Relapse	Wildtype	t(11;22)	3.0 ± 6.3
WE-68	ES	F/19	Primary	Wildtype	t(11;22)	3.4 ± 8.7
SKES1	ES	M/18	Primary	Cys176Phe	t(11;22)	15± 12
TC71	ES	M/22	Primary	Truncation	t(11;22)	119±59
STA-ET1	pPNET	F/13	Relapse	Wildtype	t(11;22)	120±63
TC252	ES	Unknown	Relapse	Wildtype	t(11;22)	130±54
SK-N-MC	ES	F/14	Primary	Null	t(11;22)	132±67
CADO-ES1	ES	F/19	Relapse	Wildtype	t(21;22)	141±97
RD-ES	ES	M/19	Primary	Arg273Cys	t(11;22)	1176±284
MCF-10A	NM		Immortalized			>5000
NDF	Skin fibroblasts		Primary			>2500

ES, Ewing sarcoma; NM, Non-malignant; pPNET, peripheral primitive neuroectodermal tumour. Data represents mean ± SEM from three independent experiments. Representative dose-response curves and RNA Pol I inhibition are presented in supplementary figure 4.

Given this acute sensitivity of Ewing sarcoma cells to CX-5461, we next wanted to determine whether efficacy of current treatments for Ewing sarcoma could be increased in combination with CX-5461. Since current treatment is limited by toxicities, this combination approach provides a singular opportunity to both increase treatment efficacy as well as offer protection from DNA damage. The ability of CX-5461 to enhance the cytotoxic effects of four standard

Ewing sarcoma chemotherapeutic agents (vincristine, actinomycin D, doxorubicin or etoposide) was assessed in three Ewing sarcoma cell lines (WE-68, SK-ES1 and SK-N-MC). The synergistic, additive or antagonist drug interactions were calculated by combination index (CI) approach using Chou-Talalay method. CI values were then used to generate a heat map of drug interactions.

The combination results varied from additive to antagonistic for all chemotherapy agents tested. The most synergistic combination of CX-5461 was observed with Actinomycin D over a range of doses in both p53 wild-type WE-68 cells and p53 null SK-N-MC cells but conferred additive effect in SKES1 (Figure 1). We suspect similarity of synergy patterns of Actinomycin D and RNA polymerase I inhibitor CX-5461 might be due to their overlapping mechanisms of action, as previous studies report that Actinomycin D also inhibits ribosomal biosynthesis, albeit at low concentrations. A maximum of 40% and 20% increase in cell death was observed in SK-N-MC and WE-68 respectively, when the two agents were combined (48hr CX-5461 treatment). For doxorubicin, etoposide and vincristine, most combination doses with CX-5461 caused antagonistic effects in all cell lines tested (supplementary figure 5). Overall, the synergistic interaction between CX-5461 and Actinomycin D provides an attractive approach for treating Ewing sarcoma patients with drug combination over Actinomycin D treatment alone.

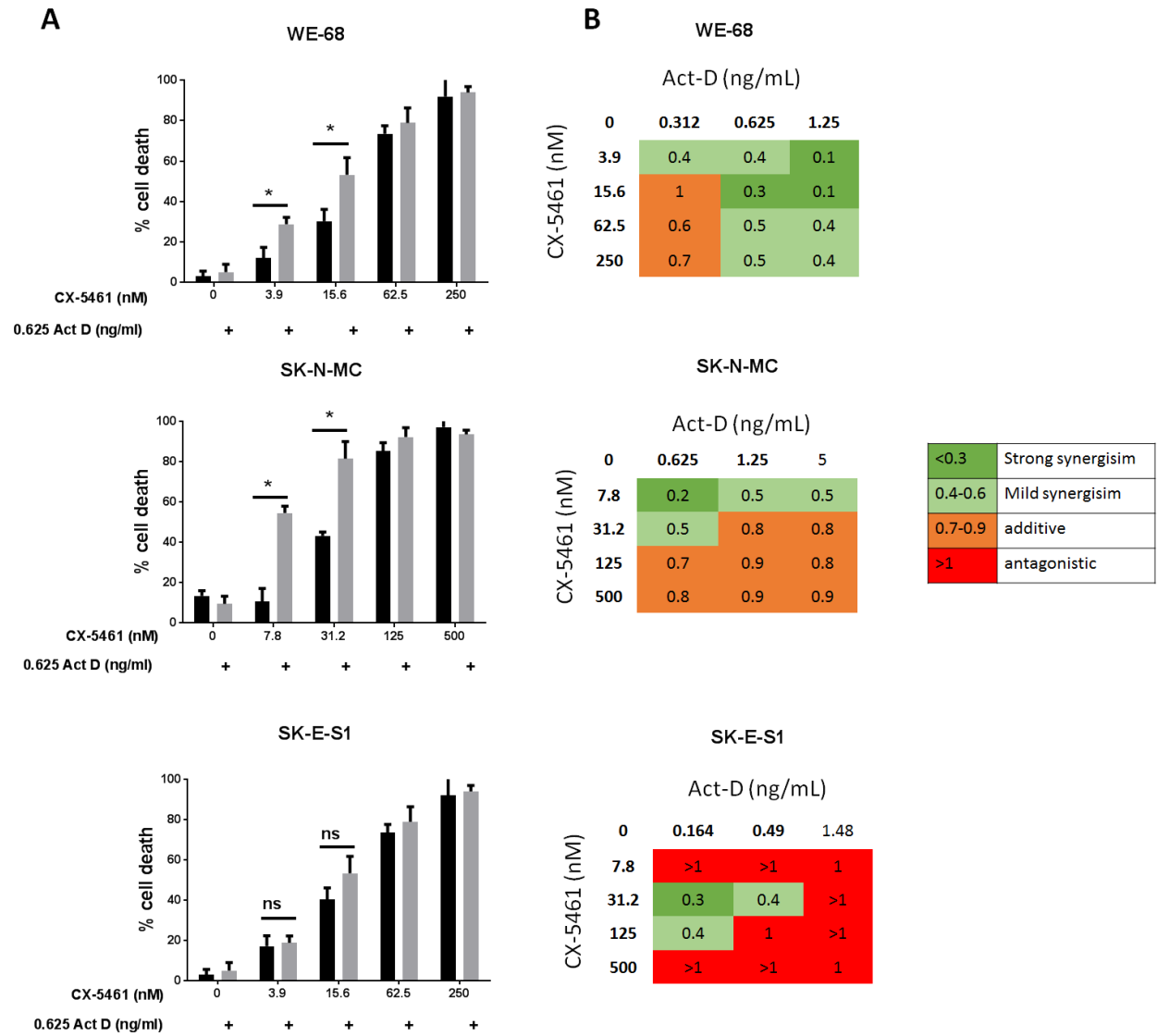


Figure 1. CX-5461 synergizes with Actinomycin D *in vitro*. A. Cells were treated for 48 h with the indicated concentrations of CX-5461 in the presence or absence of Actinomycin D (0.625 ng/ml). Cell viability was measured through 7AAD staining. B. Graphic heat-map representation of combination indices calculated for CX-5461 in combination with Actinomycin D using the Chou-Talalay method.

CX-5461 induces cell death and cell cycle arrest in Ewing sarcoma cell lines

Given the disparate sensitivity of cell lines to CX-5461, we initially examined the cellular outcome following CX-5461 treatment. Two highly sensitive (WE-68 and VH-64), a moderately sensitive (SK-N-MC) and a resistant (RD-ES) cell line were treated with CX-5461 for 24h or 48h and analysed for cell-cycle distribution using propidium iodide staining.

Treatment with CX-5461 for did not alter cell cycle profile of WE-68 and VH-64 compared to untreated controls (Figure 2A). However, as expected, these CX-5461 doses significantly increased cell death as shown by increase in sub-G1 peak (Figure 2B). In contrast, treatment with 200nM CX-5461 caused a significant G2/M arrest in SK-N-MC and RD-ES cell lines. In SK-M-C, the G2/M population of CX-5461 treated cells was 48% after 48 hr compared to 17% cells in untreated controls(Figure 2A). The most dramatic increase in G2/M cell population was observed for the CX-5461 resistant RD-ES cell line which displayed >300% increase in G2/M cell cycle arrest after 48h. The increase in G2 phase was found to be associated with a concomitant significant decrease in the S-phase populations. These data suggest that CX-5461 elicits different cellular outcomes on different Ewing sarcoma cell lines.

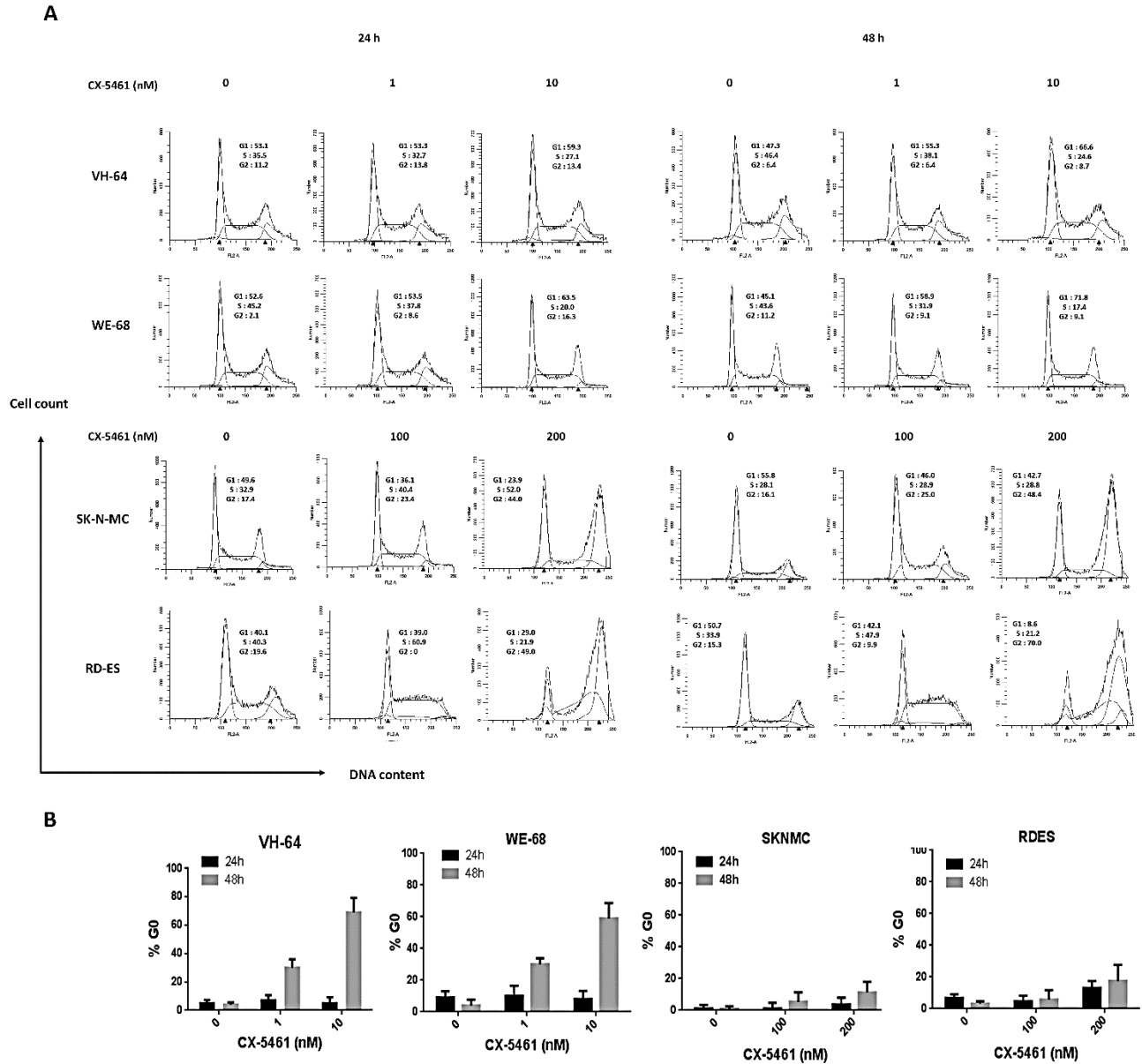


Figure 2. Anti-proliferative effects of CX-5461 in Ewing sarcoma cell lines. Cells were treated with indicated CX-5461 doses for either 24 or 48h and Cell cycle distribution was determined by flow cytometry analysis of propidium iodide stained cells for **A.** G1/S/G2/M population and **B.** Sub-G1 population as indicator cell death. One out of three biological replicate is shown.

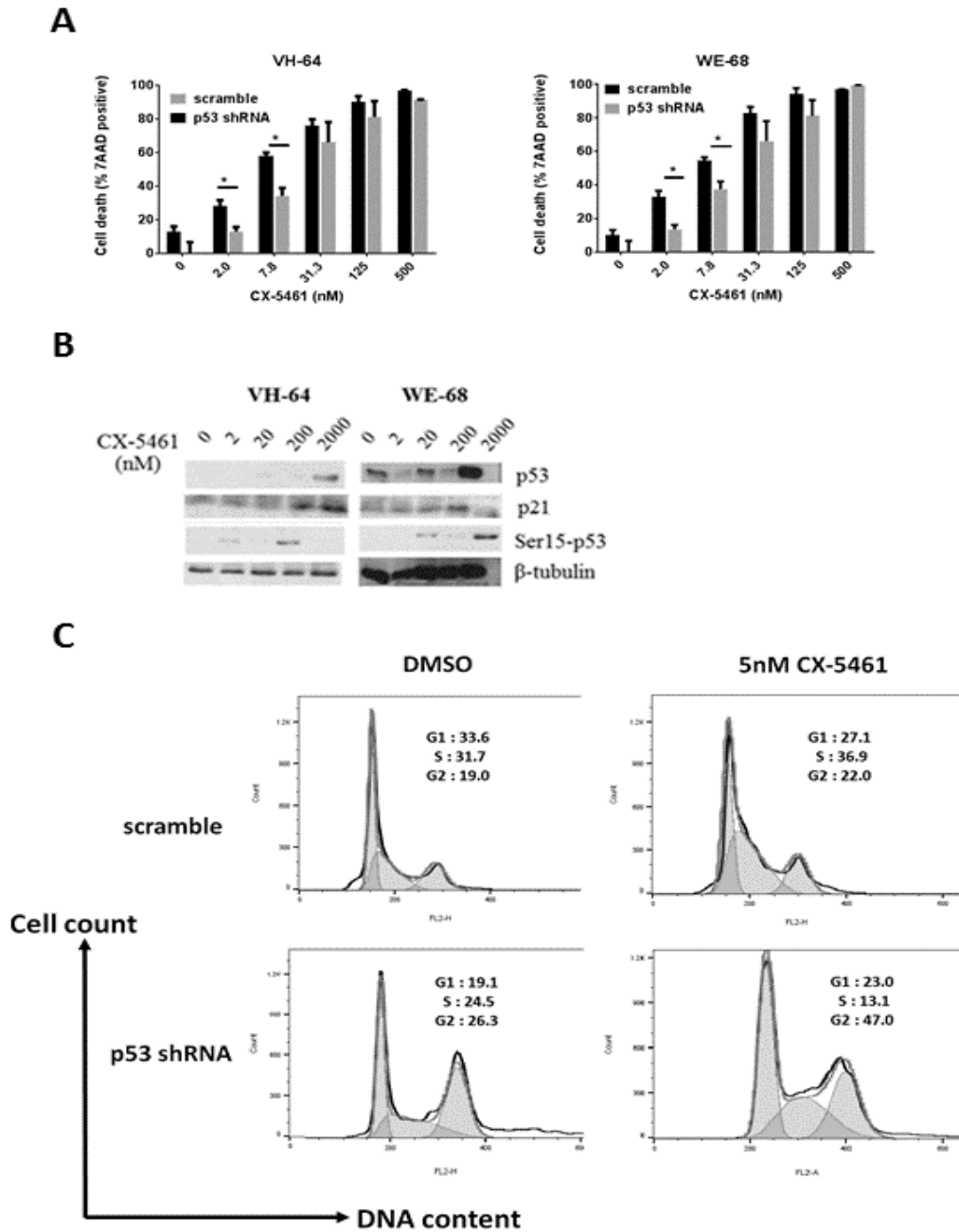
CX-5461 induced cell death in Ewing sarcoma cell lines is p53 dependent

A number of lines of evidence suggest that the anti-proliferative activity of CX-5461 is due to its ability to activate p53 signalling, an important tumour suppressor pathway that is commonly deactivated in >50% of cancers. Although there was no statistical difference between LD₅₀ values of p53 mutant and p53 wild-type cell lines (supplementary figure 1), two of the most CX-5461 sensitive cell lines had wild-type p53. Therefore, to determine whether sensitivity to CX-5461 is driven by p53 function in Ewing sarcoma, we used siRNAs to specifically knock down p53 expression in these two cell lines. Significant silencing of p53 protein (>80%) expression was confirmed in western blot analysis (supplementary figure 6).

Compared to cells transfected with control siRNA, WE-68 and VH-64 cell silenced for p53 activity exhibited a modest 15-20% decrease in cell death when exposed to CX-5461 (Figure 3A). This was not consistent with western blot analysis in which no appreciable increase was observed in either p53 or downstream target p21 protein expression except at the highest CX-5461 dose (Figure 3B). However, treatment with 200nM CX-5461 caused over 15 fold induction in p21 mRNA levels (supplementary figure 7).

Given the robust p21 induction and its role in p53 mediated cell cycle induction, we further assessed the inhibitory effect of CX-5461 on the cell cycle distribution in WE-68 cells silenced for p53 activity. Cell cycle profile of p53shRNA treated WE-68 cells showed that upon 24h treatment with 5nM CX-5461, these cells had a significantly higher proportion of G2/M cells compared to scramble controls (47% vs. 22%) (Figure 3C). These results suggested that in

response to CX-5461 treatment, in Ewing sarcoma cell lines both cell cycle and cell death



function of p53 are engaged.

Figure 3. CX-5461 induces anti-proliferative effect through a p53-dependent pathway. 7AAD uptake assay to determine the percentage (%) of dead cells of the **A.** WE-68 and WE-68 p53shRNA (n = 2) and VH-64 and VH-64 p53shRNA (n = 2) cell lines treated with CX-5461 as indicated. Error bars represent mean \pm s.d. after 48h CX-5461 treatment **B.** Western blot

analysis of p53, p21, p53(phospho- serine 15) and B-tubulin protein levels in VH-64 and WE-68 cell lines treated with increasing doses of CX-5461 for 24 h (representative of n = 2). C. Effect of CX-5461 on the cell cycle profile after p53 knock-down in WE-68 cells. Top, histograms of PI staining in WE-68 Ewing sarcoma cell line transfected with scrambled shRNA treated with vehicle control or 5nM CX-5461 for 48h. Bottom, same as above using WE-68 cells treated with TP53 shRNA.

CX-5461 induced ATM/ATR dependent G2/M arrest in resistant Ewing sarcoma cell lines

A possible mechanism driving the high CX-5461 sensitivity in sarcoma cells is the ATM/ATR pathway. Several previous studies report that in acute lymphoblastic leukaemia cell lines, CX-5461 treatment causes a non-canonical (non-genotoxic) ATM/ATR dependent G2/M cell cycle arrest^{22, 23}. The compounds KU-55933 and CGK733 have been reported as ATM and ATM/ATR dual inhibitors respectively. In WE-68 cells, pre-treatment with ATM or dual ATM/ATR inhibitor caused a 25% rescue in cell death caused by CX-5461 (Figure 4A). In contrast, pre-treatment with ATM or dual ATM/ATR inhibitor caused a significant 30% and 40% increase in cell death upon CX-5461 treatment compared to cells not pre-treated with ATM/ATR inhibitors. We expected that this observed increase in cell death was due to abrogation of G2/M arrest caused by CX-5461. Indeed, compared to 44.6% of RD-ES cells arrested in G2/M, 1hr pre-treatment with dual ATM/ATR inhibitor significantly down-regulated the G2/M arrested population to 16.4% (Figure 4B). As expected, there were no significant changes in the cell cycle profile of the WE-68 cells. Overall, these results suggest that in CX-5461 resistant Ewing sarcoma cell lines, treatment with CX-5461 induces a G2/M arrest that can be abrogated with co-treatment with checkpoint kinase inhibitors.

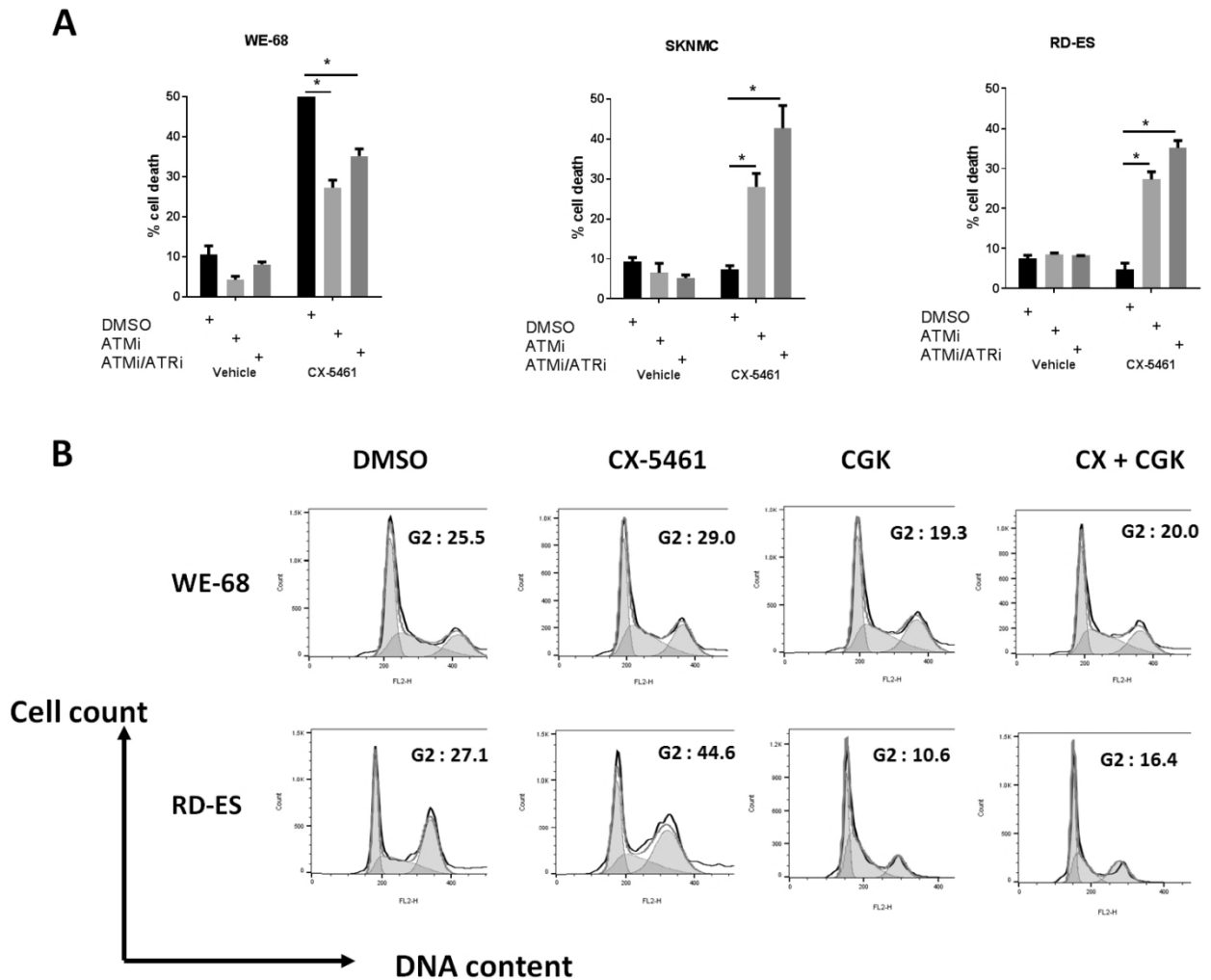


Figure 4. CX-5461 induces ATM/ATR driven cell cycle arrest in Ewing sarcoma cells. **A.** Sarcoma cell lines pre-treated with 200nM ATM and ATM/ATR inhibitors for 2 h and subsequently incubated in the absence or presence of CX-5461. Cell death was measured using 7AAD staining after 48h. **B.** Cell cycle analysis in WE-68 and RD-ES cells pre-treated with ATM inhibitor or ATM/ATR inhibitor for 2h and subsequently treated with CX-5461 (10 nM and 1000 nM for WE-68 and RD-ES respectively). Cell cycle analysis using propidium iodide staining and flow cytometry.

E2F1 protein levels predict response to CX-5461

Regarding the mechanism by which CX-5461 might induce its anti-tumourigenic effects in the absence of p53 function, we focused our attention on the expression of E2F-1, a transcription factor that is engaged upon ribosomal stress. E2F1 has been shown to stabilize following rRNA transcription inhibition using low levels of actinomycin D. Therefore, we measured the expression of E2F-1 protein in the Ewing sarcoma panel exposed to CX-5461 for 16h. Although 16h exposure to CX-5461 did not modify E2F1 expression compared with untreated cells, basal E2F1 protein levels significantly correlated with sensitivity to CX-5461 (Figure 5A and 5B). Sensitive cell lines WE-68, TC-71, SK-E-S1 expressed significantly higher levels of E2F1 compared to the moderately sensitive SKNMC or resistant RD-ES cell lines.

Next, we assessed the effect of E2F-1 overexpression on the sensitivity to CX-5461. When RD-ES were transfected with E2F1 overexpression plasmid pCMV-E2F1-HA, >60% of cells lost viability. Similar results were obtained from SK-N-MC cell lines overexpressing E2F1 through transfection of pCMV-E2F1-HA plasmid (Figure 5C).

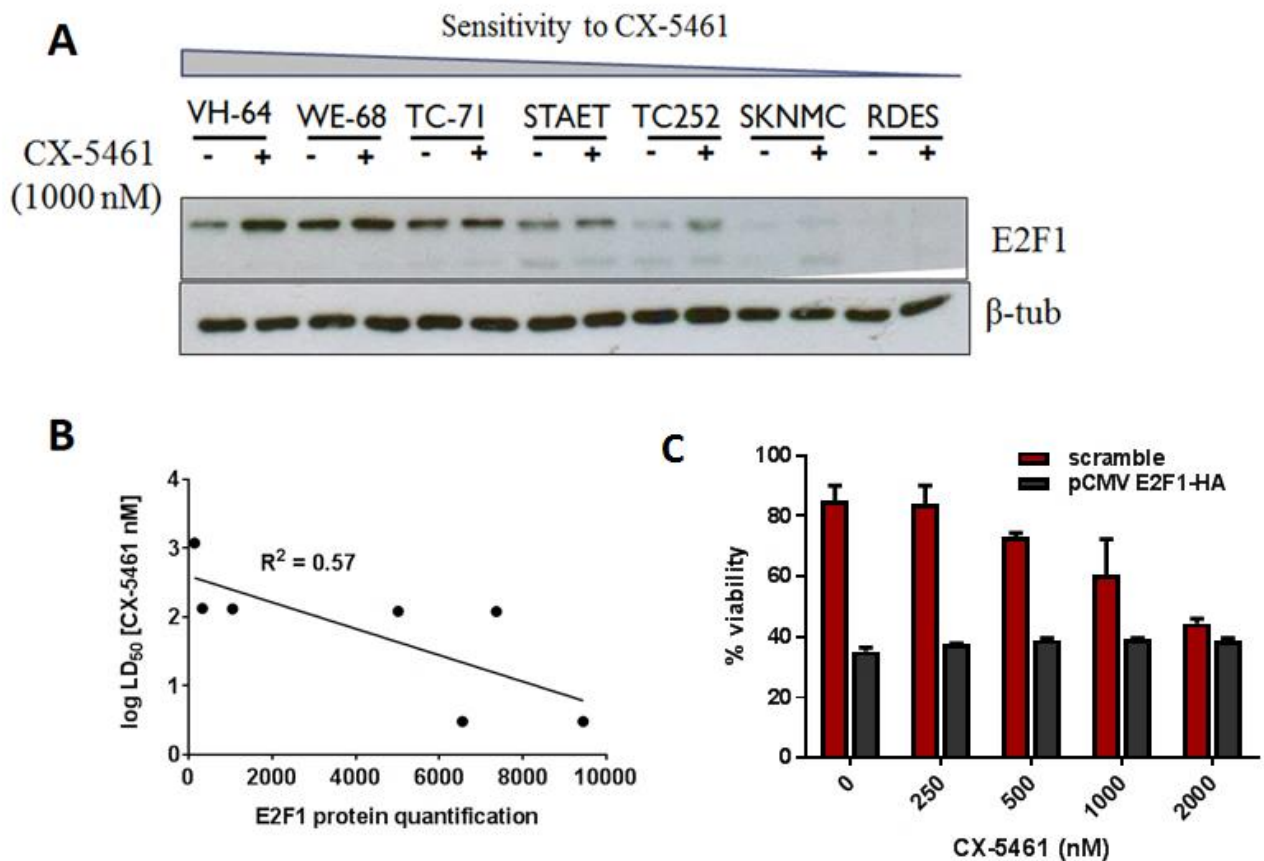


Figure 5. E2F1 protein levels correlate with CX-5461 sensitivity in Ewing sarcoma cell lines. A. E2F1 protein expression was determined by western blot analysis, 16h after CX-5461 treatment. **B.** Correlation between cytotoxic sensitivity to CX-5461 and E2F1 protein expression (quantified using ImageJ program). **C.** 7AAD cell viability after 48h in RD-ES cells transfected with pCMV-E2F1-HA overexpression construct.

Discussion

Overall survival for patients with metastatic Ewing sarcoma is less than 30% with multi-agent chemotherapy²⁴. Current multi-modal chemo regimens have made a big impact in improving Ewing sarcoma survival rates over the past decades, but they have reached their full capacity now and further improvements to survival can only come from non-genotoxic approaches. CX-5461 is a novel non-genotoxic RNA polymerase I inhibitor that has demonstrated its anti-proliferative effects in a vast panel of hematological and solid tumour cell lines. Encouraging results from initial *in vitro* and *in vivo* evaluations demonstrated hematological cell lines with wild-type p53 to be acutely sensitive to CX-5461, which has led to Phase I/II clinical evaluations of CX-5461 in advanced hematological malignancies. Given that approximately 90% of Ewing sarcomas retain a functional wild-type p53, we hypothesized that activation of the p53 pathway via CX-5461 has potential for Ewing sarcoma treatment.

Here, we show that Ewing sarcoma cell lines are exquisitely sensitive to CX-5461, with a subset (WE-68, VH-64 and SKES-1) undergoing cell death at extremely low CX-5461 doses (LD₅₀ <15nM; 48h). Comparison of LD₅₀ values from previously published studies revealed Ewing sarcoma is by far the most responsive solid tumour to CX-5461 that has been tested to date. In particular, VH-64 and WE-68 Ewing sarcoma cell lines showed sensitivities lower than any ever reported in the literature for solid tumours and parallel some of the most potent responses observed in blood cancers. In both VH-64 and WE-68, the anti-tumorigenic response to CX-5461 was p53 dependent. Silencing of p53 activity in WE-68 and VH-64 markedly decreased cytotoxic

sensitivity to CX-5461. Furthermore, cell cycle analysis of WE-68 cells silenced for p53 activity showed a significant G2/M arrest compared to scramble controls. Combination drug experiments revealed synergistic interaction with Actinomycin D in both wild-type p53 WE-68 and p53 null SK-N-MC cell lines. Previous studies have reported that at low nM doses Actinomycin D causes p53 stabilization and subsequent cell death suggesting that CX-5461 may be effective in Ewing sarcoma cases that do not retain functional p53 ²⁵.

p53 mutant RD-ES and p53 null SK-N-MC cell lines that were inherently resistant to CX-5461, underwent a G2/M arrest. We demonstrate that this G2/M cell cycle arrest is driven via checkpoint kinases ATM/ATR in Ewing sarcoma cells. Furthermore, pre-treatment with ATM/ATR inhibitor CGK733 abrogates CX-5461 mediated G2/M arrest and results in cell death. This observation is consistent with previous studies that show that CX-5461 treatment induces an ATM/ATR dependent G2/M cell cycle arrest in both hematological cell and solid cancer cell lines in a p53-independent manner ^{22, 26-28}.

The fact that CX-5461 was able to induce cell death in mutant p53 cell lines (SK-ES-1 and TC-71) implies the involvement of p53-independent mechanisms. Apart from inducing p53-dependent signaling, ribosomal stress is also known to induce p53-independent signaling through E2F1 (reviewed in²⁹). Indeed, our results strongly indicate that cell line sensitivity to CX-5461 was reflected in E2F1 protein expression in Ewing sarcoma cell panel. This is in line with a previous study that shows that in response to low doses of Actinomycin D, p53 deficient neuroblastoma cell lines undergo cell death by upregulating E2F1 protein expression ²⁵. Previous studies show

that CHK1 and CHK2 promote E2F1 stabilization and activity after ribosomal stress in a p73-dependent manner as a backup when p53 is defective to ensure that damaged cells can undergo cell death ³⁰. Role of E2F1 in CX-5461 mediated cell death is also consistent with the observation that autophagy is the mechanism of CX-5461 mediated cell death in solid cancers (ref). It is likely that cellular outcome following CX-5461 treatment is determined by a complex interplay and cross-talk between E2F1- ATM/ATR and E2F1-p53 determine cellular outcome and warrants further experimentation.

In conclusion, we show that Ewing sarcoma cell lines are exquisitely sensitive to CX-5461. Amongst all cancers screened to date, Ewing sarcoma are by far the most responsive solid tumour. Sensitivity to CX-5461 is driven by both p53 dependent and p53-independent mechanisms, and likely through the E2F1 pathway. Furthermore, combination of CX-5461 with chemotherapeutic Actinomycin D produces synergistic interaction and causes potent cell death. Taken together, our study provides encouraging pre-clinical results for the application of CX-5461 as a single agent and/or alongside chemotherapies for Ewing sarcoma treatment.

References

- 1 Jemal A, Siegel R, Xu J, Ward E. Cancer statistics, 2010. *CA Cancer J Clin* 2010; 60: 277-300.
- 2 Brohl AS, Solomon DA, Chang W, Wang J, Song Y, Sindiri S *et al.* The genomic landscape of the Ewing Sarcoma family of tumours reveals recurrent STAG2 mutation. *PLoS Genet* 2014; 10: e1004475.
- 3 Crompton BD, Stewart C, Taylor-Weiner A, Alexe G, Kurek KC, Calicchio ML *et al.* The genomic landscape of pediatric Ewing sarcoma. *Cancer Discov* 2014; 4: 1326-1341.
- 4 Erkizan HV, Kong Y, Merchant M, Schlottmann S, Barber-Rotenberg JS, Yuan L *et al.* A small molecule blocking oncogenic protein EWS-FLI1 interaction with RNA helicase A inhibits growth of Ewing's sarcoma. *Nat Med* 2009; 15: 750-756.
- 5 Kovar H, Ban J, Pospisilova S. Potentials for RNAi in sarcoma research and therapy: Ewing's sarcoma as a model. *Semin Cancer Biol* 2003; 13: 275-281.
- 6 Tanaka K, Iwakuma T, Harimaya K, Sato H, Iwamoto Y. EWS-FlI1 antisense oligodeoxynucleotide inhibits proliferation of human Ewing's sarcoma and primitive neuroectodermal tumour cells. *J Clin Invest* 1997; 99: 239-247.
- 7 Gentilella A, Kozma SC, Thomas G. A liaison between mTOR signaling, ribosome biogenesis and cancer. *Biochim Biophys Acta* 2015; 1849: 812-820.
- 8 Ruggero D, Pandolfi PP. Does the ribosome translate cancer? *Nat Rev Cancer* 2003; 3: 179-192.

- 9 Ruggiero D. Revisiting the nucleolus: from marker to dynamic integrator of cancer signaling. *Sci Signal* 2012; 5: pe38.
- 10 Thomas G. An encore for ribosome biogenesis in the control of cell proliferation. *Nat Cell Biol* 2000; 2: E71-72.
- 11 Burger K, Mühl B, Harasim T, Rohmoser M, Malamoussi A, Orban M *et al.* Chemotherapeutic Drugs Inhibit Ribosome Biogenesis at Various Levels. *The Journal of Biological Chemistry* 2010; 285: 12416-12425.
- 12 Perry RP, Kelley DE. Inhibition of RNA synthesis by actinomycin D: characteristic dose-response of different RNA species. *J Cell Physiol* 1970; 76: 127-139.
- 13 Donati G, Peddigari S, Mercer CA, Thomas G. 5S ribosomal RNA is an essential component of a nascent ribosomal precursor complex that regulates the Hdm2-p53 checkpoint. *Cell Rep* 2013; 4: 87-98.
- 14 Merkel O, Wacht N, Sifft E, Melchardt T, Hamacher F, Kocher T *et al.* Actinomycin D induces p53-independent cell death and prolongs survival in high-risk chronic lymphocytic leukemia. *Leukemia* 2012; 26: 2508-2516.
- 15 Drygin D, Lin A, Bliesath J, Ho CB, O'Brien SE, Proffitt C *et al.* Targeting RNA polymerase I with an oral small molecule CX-5461 inhibits ribosomal RNA synthesis and solid tumour growth. *Cancer research* 2011; 71: 1418-1430.
- 16 Peltonen K, Colis L, Liu H, Trivedi R, Moubarek Michael S, Moore Henna M *et al.* A Targeting Modality for Destruction of RNA Polymerase I that Possesses Anticancer Activity. *Cancer Cell* 25: 77-90.

- 17 O'Brien S, Drygin D, Harrison SJ, Khot A, Cullinane C, Geoff M *et al.* Inhibition Of RNA Polymerase I Transcription By CX-5461 As a Therapeutic Strategy For The Cancer-Specific Activation Of p53 In Highly Refractory Haematological Malignancies. *Blood* 2013; 122: 3941-3941.
- 18 Kovar H, Auinger A, Jug G, Aryee D, Zoubek A, Salzer-Kuntschik M *et al.* Narrow spectrum of infrequent p53 mutations and absence of MDM2 amplification in Ewing tumours. *Oncogene* 1993; 8: 2683-2690.
- 19 Kovar H, Pospisilova S, Jug G, Printz D, Gardner H. Response of Ewing tumour cells to forced and activated p53 expression. *Oncogene* 0000; 22: 3193-3204.
- 20 Pishas KI, Al-Ejeh F, Zinonos I, Kumar R, Evdokiou A, Brown MP *et al.* Nutlin-3a is a potential therapeutic for ewing sarcoma. *Clin Cancer Res* 2011; 17: 494-504.
- 21 Pishas KI, Adwal A, Neuhaus SJ, Clayer MT, Farshid G, Staudacher AH *et al.* XI-006 induces potent p53-independent apoptosis in Ewing sarcoma. *Scientific Reports* 2015; 5: 11465.
- 22 Negi SS, Brown P. rRNA synthesis inhibitor, CX-5461, activates ATM/ATR pathway in acute lymphoblastic leukemia, arrests cells in G2 phase and induces apoptosis. *Oncotarget* 2015; 6: 18094-18104.
- 23 Quin J, Chan KT, Devlin JR, Cameron DP, Diesch J, Cullinane C *et al.* Inhibition of RNA polymerase I transcription initiation by CX-5461 activates non-canonical ATM/ATR signaling. *Oncotarget* 2016.
- 24 Leavey PJ, Mascarenhas L, Marina N, Chen Z, Krailo M, Miser J *et al.* Prognostic Factors for Patients with Ewing sarcoma (EWS) at First Recurrence Following Multimodality

- Therapy – A Report from the Children’s Oncology Group. *Pediatric blood & cancer* 2008; 51: 334-338.
- 25 Cortes CL, Veiga SR, Almacellas E, Hernández-Losa J, Ferreres JC, Kozma SC *et al.* Effect of low doses of actinomycin D on neuroblastoma cell lines. *Molecular Cancer* 2016; 15: 1.
- 26 Ye Q, Pang S, Zhang W, Guo X, Wang J, Zhang Y *et al.* Therapeutic Targeting of RNA Polymerase I With the Small-Molecule CX-5461 for Prevention of Arterial Injury–Induced Neointimal Hyperplasia. *Arteriosclerosis, Thrombosis, and Vascular Biology* 2017.
- 27 Negi SS, Brown P. Transient rRNA synthesis inhibition with CX-5461 is sufficient to elicit growth arrest and cell death in acute lymphoblastic leukemia cells. *Oncotarget* 2015; 6: 34846-34858.
- 28 Li L, Li Y, Zhao J, Fan S, Wang L, Li X. CX-5461 induces autophagy and inhibits tumour growth via mammalian target of rapamycin-related signaling pathways in osteosarcoma. *OncoTargets and therapy* 2016; 9: 5985-5997.
- 29 Olausson KH, Nistér M, Lindström MS. p53 -Dependent and -Independent Nucleolar Stress Responses. *Cells* 2012; 1: 774-798.
- 30 Urist M, Tanaka T, Poyurovsky MV, Prives C. p73 induction after DNA damage is regulated by checkpoint kinases Chk1 and Chk2. *Genes & development* 2004; 18: 3041-3054.

Supplementary material

Supplementary results

Figure 1. Correlation between p53 status and CX-5461 cytotoxic LD₅₀ values.

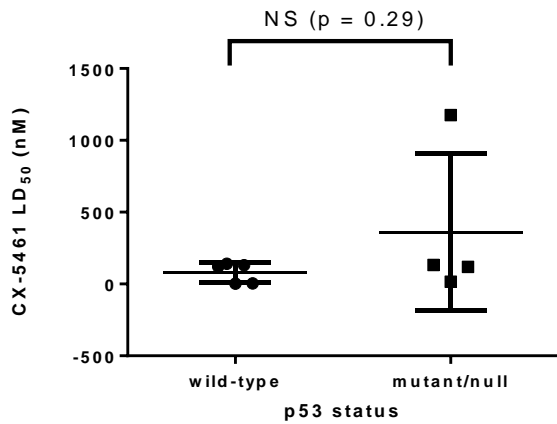


Figure 2. Relative LD₅₀ of all solid tumour cell lines published. Ewing sarcoma cell lines (in red) VH-64, WE-68 and SK-E1 are three of the most sensitive cell lines to CX-5461.

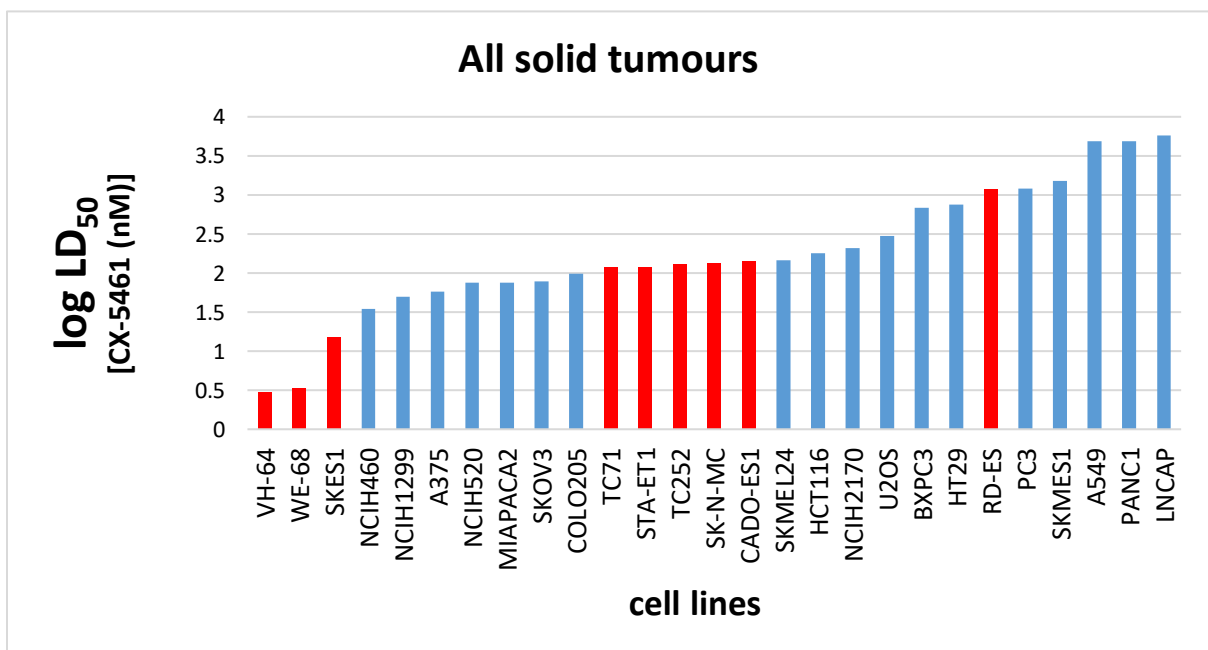


Figure 3. Relative LD₅₀ of all blood cancer cell lines published. Ewing sarcoma cell lines in red.

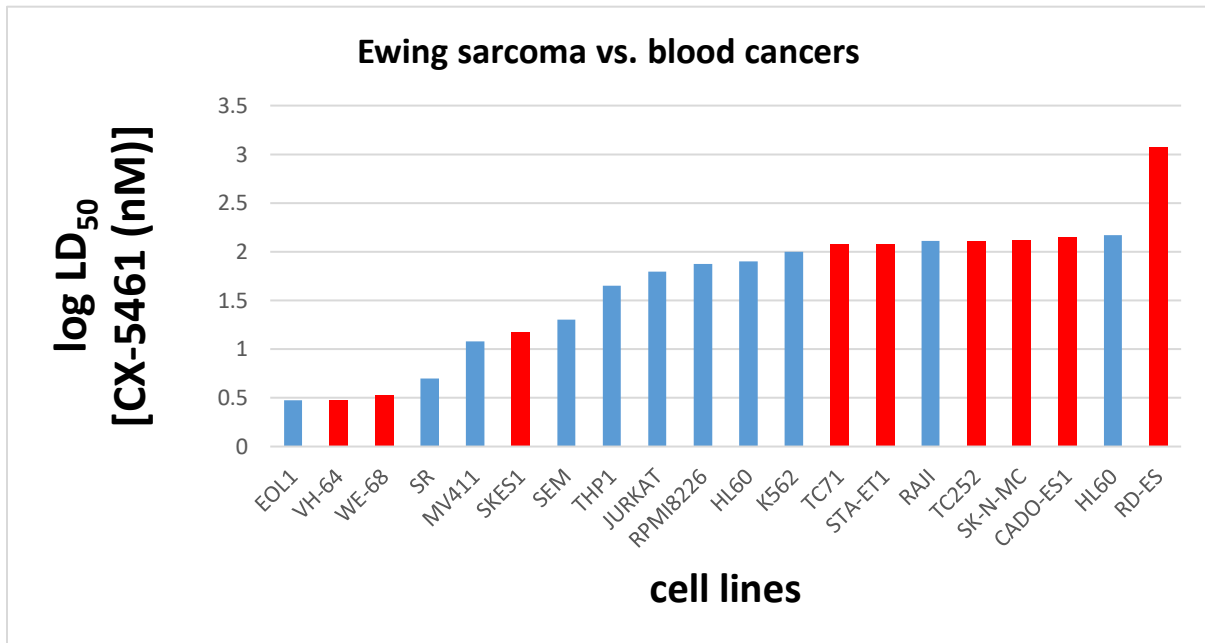


Figure 4. Representative LD₅₀ and IC₅₀ inhibition.

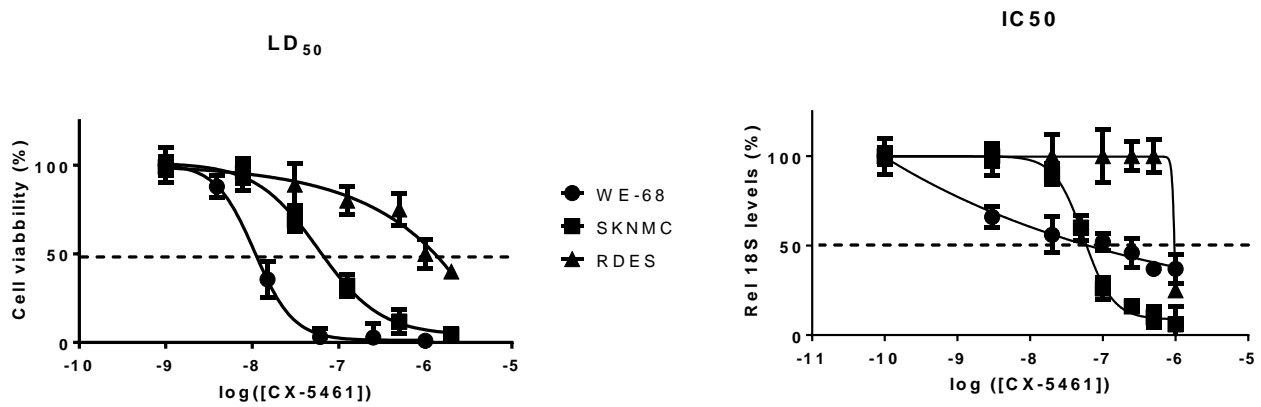
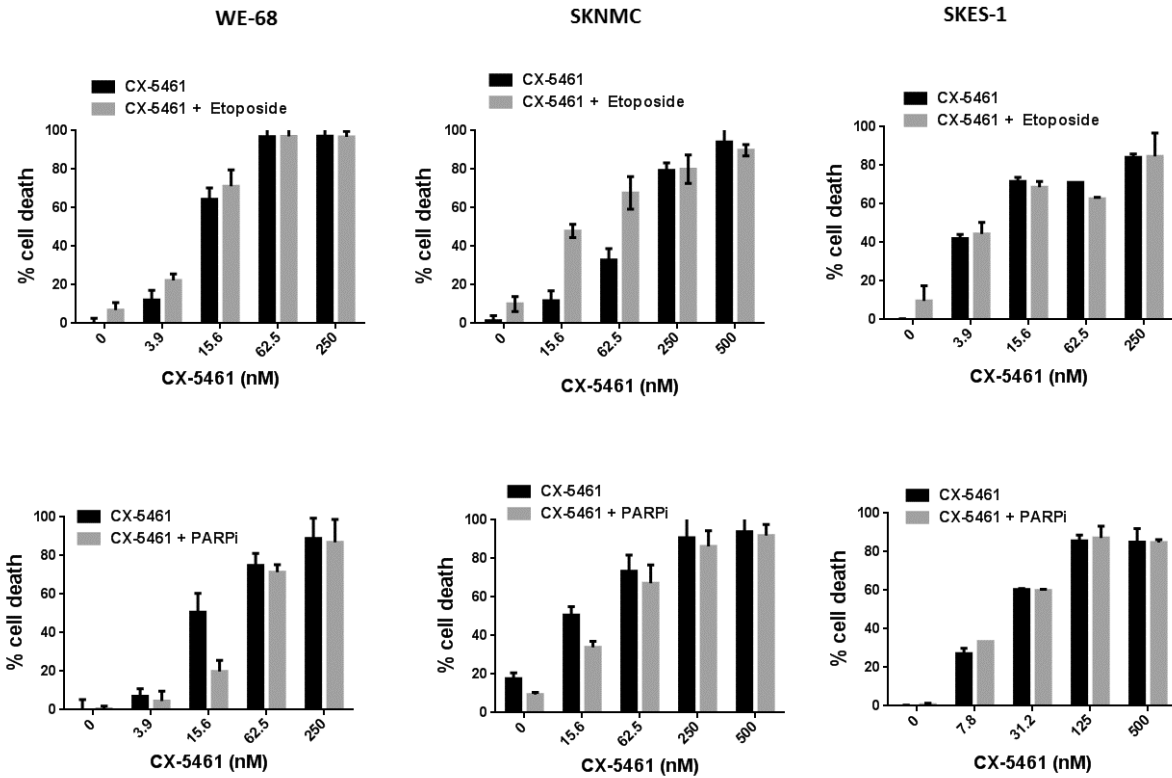


Figure 5. CX-5461 combination charts and heat map with various chemotherapies. Combination indices show that combination with most chemotherapies (Doxorubicin, Vincristine, and Etoposide) were either antagonistic or additive in all three cell lines for most concentrations tested. One exception was the combination with Nutlin (a p53 activator) in WE-68 cell line, where drug combinations were almost invariably synergistic at all concentrations tested.



WE-68

		Dox (ng/mL)			
		0	2.5	5	20
CX-5461 (nM)	3.9	1	>1	1	
	15.6	0.8	0.2	0.9	
	62.5	0.9	0.6	0.7	
	250	0.6	0.8	0.4	

		Etop (ng/mL)			
		0	156	312	625
CX-5461 (nM)	3.9	1	>1	0.8	
	15.6	0.8	>1	0.6	
	62.5	0.2	>1	0.5	
	250	0.1	>1	1	

		Vinc (ng/mL)			
		0	0.312	0.625	1.25
CX-5461 (nM)	7.8	1	1	1	
	31.2	0.4	0.6	0.7	
	125	0.4	0.5	0.5	
	500	1	1	0.4	

		Nut (ng/mL)			
		0	0.082	0.625	1.25
CX-5461 (nM)	7.8	0.9	0.09	0.08	
	31.2	0.02	0.01	0.04	
	125	0.06	0.01	0.07	
	500	0.04	0.05	0.03	

SKNMC

		Dox (ng/mL)			
		0	9	18	37
CX-5461 (nM)	3.9	>1	>1	1	
	15.6	0.9	0.9	0.8	
	62.5	0.9	1	1	
	250	1	1	1	

		Etop (ng/mL)			
		0	156	312	625
CX-5461 (nM)	3.9	0.2	>1	>1	
	15.6	0.2	>1	>1	
	62.5	0.3	>1	>1	
	250	1	>1	>1	

		Vinc (ng/mL)			
		0	0.039	0.078	0.156
CX-5461 (nM)	7.8	1	>1	1	
	31.2	0.7	>1	0.9	
	125	0.5	>1	0.9	
	500	0.9	>1	1	

		Nut (ng/mL)			
		0	0.312	0.625	1.25
CX-5461 (nM)	7.8	1	1	1	
	31.2	0.4	0.6	0.7	
	125	0.4	0.5	0.5	
	500	1	1	0.4	

SKES-1

		Dox (ng/mL)			
		0	2.5	0.2	2.2
CX-5461 (nM)	3.9	1	>1	>1	
	15.6	>1	>1	>1	
	62.5	0.3	0.3	0.3	
	250	0.2	0.7	0.9	

		Etop (ng/mL)			
		0	6.1	18.5	55.5
CX-5461 (nM)	3.9	0.8	0.7	0.8	
	15.6	0.6	0.6	0.5	
	62.5	>1	>1	>1	
	250	>1	>1	>1	

		Vinc (ng/mL)			
		0	0.0008	0.002	0.007
CX-5461 (nM)	7.8	>1	0.7	1	
	31.2	0.6	0.6	0.6	
	125	>1	1	>1	
	500	>1	>1	1	

		Nut (ng/mL)			
		0	0.082	0.247	0.74
CX-5461 (nM)	7.8	>1	>1	1	
	31.2	0.4	0.5	0.3	
	125	1	1	0.6	
	500	>1	>1	>1	

<0.3	Strong synergisim
0.4-0.6	Mild synergisim
0.7-0.9	additive
>1	antagonistic

Figure 6. p53 protein knockdown in WE-68 and VH-64 cell lines using shRNA pRS-p53.

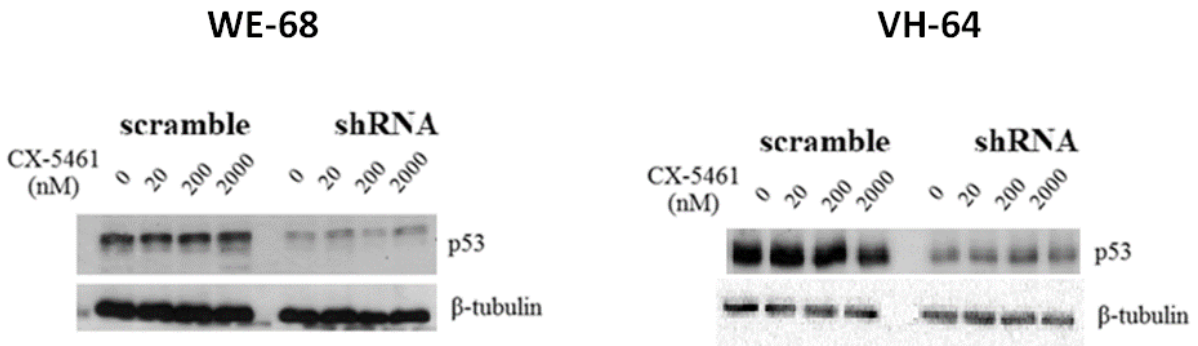
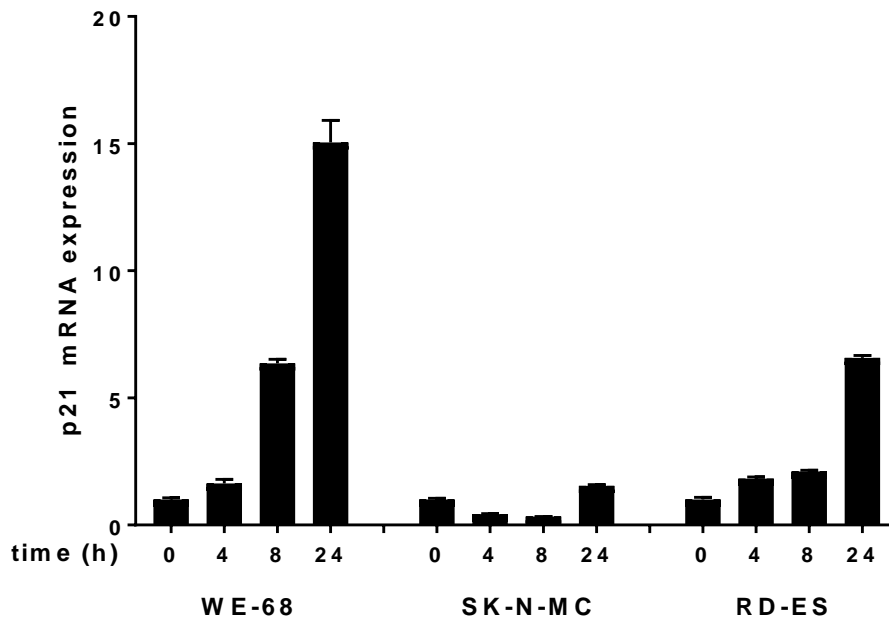


Figure 7. mRNA expression levels of p21 in cell lines treated with 200nM CX-5461. Error bars represent mean \pm s.d of three biological replicates.



Chapter 8

XI-006 induces potent p53-independent apoptosis in Ewing sarcoma

Kathleen I. Pishas^{1,2}, **Alaknanda Adwal**^{1,2}, Susan J. Neuhaus³, Mark T. Clayer⁴, Gelareh Farshid⁵,
Alexander H. Staudacher⁶, David F. Callen^{1,2}

¹Sarcoma Research Group, Adelaide Medical School, University of Adelaide, Adelaide, Australia

²Cancer Therapeutics Laboratory, Adelaide Medical School, University of Adelaide, Adelaide,
Australia

³Department of Surgery, Royal Adelaide Hospital and University of Adelaide, Adelaide, Australia

⁴Department of Orthopaedics and Trauma, Royal Adelaide Hospital, Adelaide, Australia

⁵Division of Tissue Pathology, SA Pathology, Adelaide, Australia

⁶Translational Oncology Laboratory, Centre for Cancer Biology, SA Pathology, Adelaide,
Australia

Statement of Authorship

Statement of Authorship

Title of Paper	XI-006 induces potent p53-independent apoptosis in Ewing sarcoma		
Publication Status	<input checked="" type="checkbox"/> Published	<input type="checkbox"/> Accepted for Publication	
	<input type="checkbox"/> Submitted for Publication	<input type="checkbox"/> Unpublished and Unsubmitted work written in manuscript style	
Publication Details	<i>Scientific Reports</i> 5, Article number: 11465 (2015)		

Principal Author

Name of Principal Author (Candidate)	Alaknanda Adwal		
Contribution to the Paper	Conducted all experiments requested by reviewers for publication.		
Overall percentage (%)	10%		
Certification:	This paper reports on original research I conducted during the period of my Higher Degree by Research candidature and is not subject to any obligations or contractual agreements with a third party that would constrain its inclusion in this thesis. I am the primary author of this paper.		
Signature		Date	6/3/2017

Co-Author Contributions

By signing the Statement of Authorship, each author certifies that:

- i. the candidate's stated contribution to the publication is accurate (as detailed above);
- ii. permission is granted for the candidate to include the publication in the thesis; and
- iii. the sum of all co-author contributions is equal to 100% less the candidate's stated contribution.

Name of Co-Author	Kathleen Irene Eijsbas		
Contribution to the Paper	Performed majority of experimental work, interpreted data and wrote manuscript.		
Signature		Date	8 th March 2017

Name of Co-Author	Susan J Neuhaus.		
Contribution to the Paper	Contributed to patient recruitment, surgical resection of human sarcoma samples and manuscript preparation		
Signature		Date	4/4/17

Please cut and paste additional co-author panels here as required.

Name of Co-Author	Mark T Clayer.		
Contribution to the Paper	Contributed to patient recruitment, surgical resection of human sarcoma samples and manuscript preparation.		
Signature		Date	3/4/17

Name of Co-Author	Gelareh Farshid		
Contribution to the Paper	Clinical pathologist responsible for confirmation of sarcoma histology		
Signature		Date	3/4/2017

Name of Co-Author	Alex H. Staudacher		
Contribution to the Paper	Contributed to manuscript preparation.		
Signature		Date	10/03/17

Name of Co-Author	David F Callen		
Contribution to the Paper	Contributed to conception, design and overall supervision of project, experimental work, data analysis. Also, acted as corresponding author.		
Signature		Date	10/3/17

Prelude

This study has evaluated the molecular and cellular responses of cultured Ewing sarcoma cell lines following exposure to XI-006, a MDM2 inhibitor. Treatment with XI-006 results in potent p53-independent apoptosis at non-DNA damaging concentrations in Ewing sarcoma cell lines. Notably, strong synergy was observed with olaparib, a PARP inhibitor that is gaining significant interest for the treatment of solid cancers and thus represents a novel therapeutic intervention for the treatment of Ewing sarcoma.

This research has been published in Scientific Reports. (Dec, 2016) and this chapter is the published version of the manuscript.

Contribution by the candidate: Conducted all experiments requested by reviewers for publication).

Abstract

There is an imperious need for the development of novel therapeutics for the treatment of Ewing sarcoma, the second most prevalent solid bone tumour observed in children and young adolescents. Recently, a 4-nitrobenzofuroxan derivative, XI-006 (NSC207895) was shown to diminish MDM4 promoter activity in breast cancer cell lines. As amplification of MDM4 is frequently observed in sarcomas, this study examined the therapeutic potential of XI-006 for the treatment of Ewing and osteosarcoma. XI-006 treatment of Ewing and osteosarcoma cell lines (n = 11) resulted in rapid and potent apoptosis at low micro-molar concentrations specifically in Ewing sarcoma cell lines (48 hr IC₅₀ 0.099–1.61 μM). Unexpectedly, apoptotic response was not dependent on MDM4 mRNA/protein levels or TP53 status. Alkaline/neutral comet and γH2AX immunofluorescence assays revealed that the cytotoxic effects of XI-006 could not be attributed to the induction of DNA damage. RNA expression analysis revealed that the mechanism of action of XI-006 could be accredited to the inhibition of cell division and cycle regulators such as KIF20A and GPSM2. Finally, potent synergy between XI-006 and olaparib (PARP inhibitor) were observed due to the down-regulation of Mre11. Our findings suggest that XI-006 represents a novel therapeutic intervention for the treatment of Ewing sarcoma.

Introduction

Sarcomas are a group of rare malignancies that affect approximately 200,000 individuals worldwide each year¹. Exemplifying the heterogeneous nature of this malignancy type, approximately 50 distinct histological subtypes of sarcoma have been identified to date, ranging from indolent to highly invasive and metastatic². The introduction of cytotoxic chemotherapeutic agents such as doxorubicin in the 1960's for chemo-sensitive subtypes was a paradigm shift in oncology practice, however current multi-agent chemotherapeutic regimens are associated with significant cumulative and late toxicities. With the exception of gastrointestinal stromal tumours (GIST), limited progress in the management of sarcomas has been achieved over the past few decades years. For this reason, the advent of novel and targeted therapeutics with favourable efficacy and toxicity profiles are eagerly awaited, especially for those 20–40% of patients with non-responding, unresectable or metastatic disease.

Cancer is a multifaceted process that can arise due to the activation of proto-oncogenes and/or inactivation of tumour suppressor genes. The development of novel anti-cancer agents, specifically those focused on targeting oncogene addiction has undergone a dramatic renaissance over the past decade. One particular oncogene which has gained significant interest is MDM4 (Mouse Double Minute 4), a structural homologue of MDM2, thought to promote tumourigenesis via its ability to inhibit the tumour suppressor function of TP53³. In keeping with this hypothesis, amplification and/or overexpression of MDM4 has been documented across a wide spectrum of tumours including cutaneous melanoma (68.5%)⁴,

retinoblastoma (65%)⁵, head and neck squamous carcinoma (50%)⁶ , breast (19%)³ and sarcoma (17%)^{7,8}. In particular, MDM4 copy number gain was documented in 54% of conventional, intramedullary, high-grade osteosarcomas and 33% of parosteal osteosarcomas⁹. Furthermore, amplification of MDM4 defined as >3 fold was shown to be a distinctive attribute of Ewing, synovial and osteosarcomas, with amplification observed in 50%, 44% and 35% of tumour samples respectively⁸. Prevailing evidence suggests that MDM4 primarily represses the transcriptional activity of p53 by binding its trans-activation domain. However, although displaying no intrinsic E3 ubiquitin ligase activity, MDM4 can also regulate p53 stability by promoting MDM2-mediated degradation^{10,11}.

Owing to the prevalence of MDM4 genomic amplification/mRNA overexpression in human cancers, several strategies aimed at inhibiting the oncogenic activity of MDM4 have been explored. Although a selective MDM4 small-molecule inhibitor does not currently exist, the first reported p53-MDM4 antagonist, SJ-172550, did exhibit cytotoxicity in retinoblastoma cells¹². However, the thiol reactivity of SJ-172550 precludes its chemical scaffold from further development¹³. Recently, a peptide antagonist of the p53-MDM4 interaction, designated SAH-p53-8 has been developed. This stapled peptide possesses substantially improved pharmacokinetic profiles compared to non-stapled peptide counterparts, and has nano-molar binding affinity to the N-terminal p53-binding pocket of both MDM2 and MDM4¹⁴. However, the bioavailability of stapled peptides and their potential as therapeutic agents has been questioned. Small molecules are considered more desirable for cancer therapy as their cellular uptake is dependent on passive diffusion, whereas stapled peptides such as SAH-p53-8 require

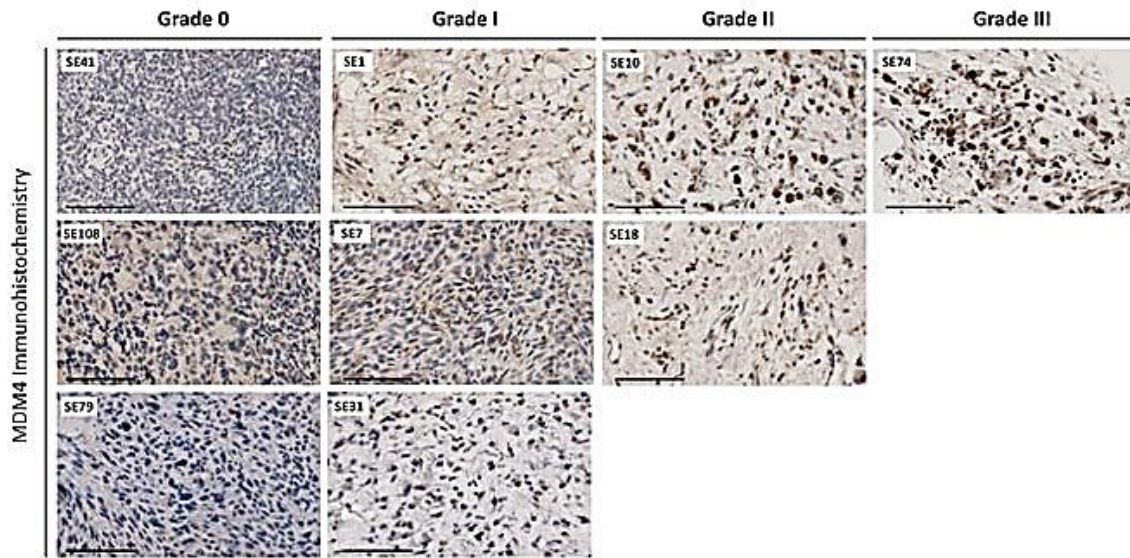
pinocytosis, which is less effective¹⁵. Indeed, this is highlighted by the fact that high concentrations of SAH-p53-8 (15–30 μ M) were required to induce significant cytotoxicity in melanoma cells *in vitro*, uptake was attenuated in the presence of serum, and complete regression of xenograft tumours was not achieved^{4,16}. Given that aberrant transcription of MDM4 can be attributed to its overexpression in cancer¹⁷, Wang and colleagues employed a high-throughput drug screening strategy to identify small molecules that could mitigate MDM4 promoter activity. A 4-nitrobenzofuroxan derivative, designated XI-006 (NSC207895) was identified and was shown to repress MDM4 promoter activity resulting in decreased MDM4 mRNA and protein expression and cell viability in MDM4 amplified breast cancer cell lines¹⁸. To our knowledge, no studies have hitherto directly addressed whether repression of MDM4 activity can represent a novel therapeutic strategy for the treatment of sarcomas. In particular, as MDM4 amplification is a characteristic of both Ewing and osteosarcoma, this study has examined the biological effects of XI-006 both as a single agent and in combination with standard chemotherapeutic agents and olaparib (PARP inhibitor) in a comprehensive panel of Ewing and osteosarcoma cell lines *in vitro*. Specifically, treatment of Ewing sarcoma cell lines resulted in potent apoptosis that was remarkably not dependent on MDM4 mRNA or protein levels or TP53 status.

Results

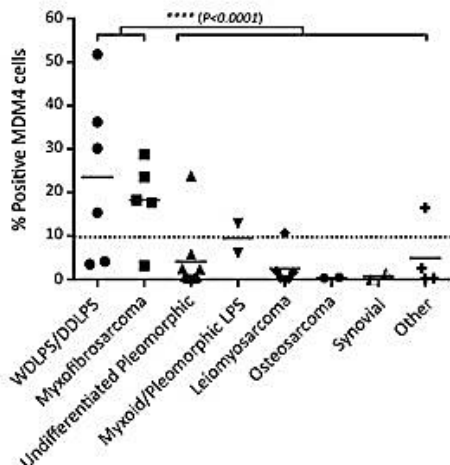
MDM4 protein is overexpressed in sarcomas

The majority of studies that have evaluated sarcoma MDM4 expression levels have done so through quantification of mRNA. As MDM4 mRNA expression was recently shown not to correlate with protein expression in freshly isolated human melanomas⁴, these previous studies may have grossly underestimated the frequency of MDM4 protein expression in sarcomas. Indeed, MDM4 mRNA overexpression was not observed in our previous cohort of 24 sarcoma tissues¹⁹. As such, MDM4 protein expression in a cohort of 36 sarcoma samples of varying histopathology was determined through immunohistochemical analysis (IHC). Although MDM4 expression was very low to undetectable (<10% MDM4 positive cells) in 24/36 (66.7%) of tumour samples, strong positive staining was observed in 12/36 (33.3%) cases ([Fig. 1a](#), [Table 1](#)). Grade III staining (>51% positive MDM4 cells) was only observed in one de-differentiated liposarcoma (Tumour SE74). Interestingly, well/de-differentiated liposarcomas and myxofibrosarcomas exhibited significantly higher levels of MDM4 protein expression compared to the rest of the sarcoma cohort ($p < 0.0001$) ([Fig. 1b](#)).

a



b



c

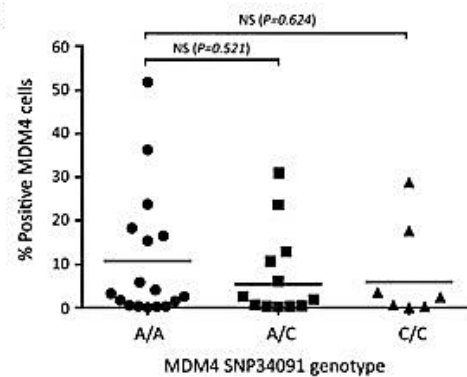


Figure 1: MDM4 protein is overexpressed in sarcomas

a) Representative images of sarcoma MDM4 immunohistochemical staining. MDM4 grading determined from the average number of MDM4 positive cells from four fields of view, Grade 0 (<10% positive cells), Grade I (11–25% positive cells), Grade II (26–50% positive cells), Grade III (>51% positive cells) Scale bar=100uM. (b) Correlation between sarcoma pathology and percentage positive MDM4 cells determined from immunohistochemical analysis. Asterisk denotes statistical significance in MDM4 expression (****P < 0.0001). (c) Lack of correlation between MDM4 SNP34091 genotype (AA, AC, CC) and percentage positive MDM4 cells determined from immunohistochemical analysis.

Table 1: Clinical characteristics and MDM4 SNP34091 genotype of the sarcoma cohort.

Sarcoma ID	Patient Gender	Pathology	% Positive MDM4 cells	MDM4 IHC Grade	MDM4 SNP34091
SE74*	M	De-differentiated liposarcoma	51.8 ± 2.3	3	A/A
SE73	M	Well-differentiated liposarcoma	36.2 ± 5.4	2	A/A
SE10*	M	Well-differentiated liposarcoma	30.2 ± 1.8	2	A/C
SE18*	M	Myxofibrosacroma	28.8 ± 2.5	2	C/C
SE31	F	Undifferentiated pleomorphic sarcoma	23.8 ± 5.1	1	A/A
SE13*	F	Myxofibrosacroma	23.6 ± 3.7	1	A/C
SE15*	F	Myxofibrosacroma	18.3 ± 1.7	1	A/A
SE1	M	Myxofibrosacroma	17.7 ± 2.0	1	C/C
SE27*	F	Radiation induced sarcoma	16.5 ± 1.9	1	A/A
SE61*	M	Well-differentiated liposarcoma	15.4 ± 2.6	1	A/A
SE7*	M	Pleomorphic liposarcoma	12.9 ± 2.8	1	A/C
SE24*	M	Leiomyosarcoma	10.7 ± 4.0	1	A/C
SE35*	M	Myxoid liposarcoma	6.1 ± 1.5	0	A/C
SE72*	M	Undifferentiated pleomorphic sarcoma	5.8 ± 2.3	0	A/A
SE39*	M	De-differentiated liposarcoma	4.1 ± 2.3	0	A/A

SE54	M	Well-differentiated liposarcoma	3.5 ± 1.0	0	C/C
SE58*	F	Myxofibrosacroma	3.2 ± 1.4	0	A/A
SE100	M	Chondrosarcoma	2.6 ± 0.6	0	A/C
SE43*	F	Undifferentiated pleomorphic sarcoma	2.5 ± 1.3	0	A/A
SE108	F	Undifferentiated pleomorphic sarcoma	2.4 ± 2.0	0	C/C
SE66	F	Leiomyosarcoma	1.9 ± 1.0	0	A/C
SE115	F	Leiomyosarcoma	1.7 ± 1.0	0	A/A
SE105	M	Synovial Sarcoma	1.5 ± 0.8	0	A/A
SE69*	M	Undifferentiated pleomorphic sarcoma	0.7 ± 0.7	0	A/C
SE79*	F	Undifferentiated pleomorphic sarcoma	0.6 ± 0.0	0	C/C
SE51*	F	Osteosarcoma	0.5 ± 0.5	0	A/A
SE52*	F	Leiomyosarcoma	0.4 ± 0.2	0	A/C
SE41*	M	Ewing sarcoma	0.3 ± 0.2	0	A/C
SE104	M	Undifferentiated pleomorphic sarcoma	0.3 ± 0.3	0	A/C
SE88	M	Osteosarcoma	0.3 ± 0.2	0	A/A
SE86	F	Undifferentiated pleomorphic sarcoma	0.3 ± 0.2	0	A/A
SE3	F	Undifferentiated pleomorphic sarcoma	0.2 ± 0.2	0	C/C
SE83	M	Leiomyosarcoma	0.2 ± 0.2	0	A/C
SE47*	M	Angiosarcoma	0.2 ± 0.2	0	A/A
SE77	M	Synovial sarcoma	0.0 ± 0.0	0	C/C

SE45	M	Leiomyosarcoma	0.0 ± 0.0	0	A/A
-------------	---	----------------	-----------	---	-----

MDM4 IHC Grade 0 (<10% positive cells), Grade I (11–25% positive cells), Grade II (26–50% positive cells), Grade III (>51% positive cells). * Denotes sarcoma samples previously described in Pishas et al., 2014.

Recently, Wynendaele and colleagues reported that presence of a single nucleotide polymorphism (SNP34091, rs4245739) located 32 nucleotides downstream of the stop codon in the 3'UTR of MDM4 was associated with statistically significant increased MDM4 protein expression in high-grade ovarian carcinomas²⁰. This A>C transversion was reported to create a putative illegitimate target site for hsa-miR-191, which only recognised the 3'UTR of the MDM4-C allele resulting in decreased MDM4 mRNA and protein expression. To determine whether SNP34091 regulates MDM4 protein expression in sarcomas, the 3'UTR of MDM4 was sequenced. Genotypes were as follows, 17 (47.2%) were homozygous for the wild-type allele (A/A), 12 (33.3%) were heterozygous (A/C) and 7 (19.4%) were homozygous for SNP34091 (C/C) (Table 1). Presence of the C allele was not significantly associated with decreased MDM4 protein expression within our sarcoma cohort (AA vs AC: P = 0.521) (AA vs CC: P = 0.624) (Fig. 1c).

XI-006 induces potent apoptosis in Ewing sarcoma cell lines.

As amplification of MDM4 is frequently observed in Ewing and osteosarcomas⁸, the anti-tumour activity of XI-006 was evaluated in a panel of eleven Ewing and osteosarcoma cell lines. Sarcoma cell lines were exposed to escalating concentrations of XI-006 (0–10 µM), with the

degree of apoptosis determined after 24 and 48 hrs of treatment through 7AAD staining and flow cytometry. A pronounced reduction in cell viability was observed specifically in Ewing sarcoma cell lines at low micro-molar concentrations ([Table 2](#), [Fig. 2a](#)). Following treatment, concentrations of XI-006 required to induce 50% apoptosis (IC_{50}) in Ewing sarcoma cell lines ranged from 0.376–2.46 μ M and 0.099–1.61 μ M, 24 and 48 hr treatment respectively. In contrast, osteosarcoma cell lines required significantly higher levels of XI-006 ($P = 0.008$) to achieve an IC_{50} , range of 3.60–>10 μ M and 2.14–5.41 μ M, 24 and 48 hr treatment respectively ([Fig. 2b](#)). Importantly, the viability of normal human fibroblasts (IMR90) remained unaffected at these low micro-molar concentrations, IC_{50} of 8.35 μ M and 6.80 μ M (24 and 48 hr treatment respectively) ([Table 2](#)). Colony formation assays were performed to investigate the long term effect of XI-006 on cellular proliferation. Following 10 days of XI-006 treatment, no colonies were observed at any XI-006 concentration exceeding 0.03 μ M in TC252 and RD-ES Ewing sarcoma cell lines, and 0.11 μ M in U2OS and SJSA osteosarcoma cell lines ([Supplementary Fig. S1a,b](#)). In contrast, numerous colonies were observed at the maximum XI-006 concentration tested (3 μ M) in IMR90 fibroblasts ([Supplementary Fig. S1c](#)), highlighting the tumour specific effect of XI-006.

Table 2: XI-006 IC₅₀ values of the sarcoma cell line cohort.

Cell line	Histol ogy	TP53 status	MDM4 expression	mRNA	XI-006 IC ₅₀ (nM, 24 hr)	XI-006 IC ₅₀ (nM, 48 hr)
STA-ET-1	ES	Wild-type	1.68 ± 0.03		376.3 ± 26.9	98.9 ± 19.5
TC252	ES	Wild-type	2.74 ± 0.04		390.2 ± 106.6	115.6 ± 6.6
SK-N-MC	ES	Truncation	0.61 ± 0.00		472.3 ± 176.4	121.8 ± 31.7
SK-ES-1	ES	Cys176Phe	0.70 ± 0.01		442.4 ± 57.5	236.0 ± 15.0
RD-ES	ES	Arg273Cys	0.32 ± 0.00		638.9 ± 142.4	299.7 ± 68.5
TC71	ES	Truncation	0.40 ± 0.02		567.9 ± 150.8	396.1 ± 78.8
WE-68	ES	Wild-type	1.09 ± 0.04		2089.3 ± 20.4	1475.7 ± 222.6
VH-64	ES	Wild-type	1.07 ± 0.01		2456.4 ± 315.1	1613.1 ± 274.4
Saos-2	OS	Null	0.17 ± 0.00		3600.2 ± 525.7	2143.0 ± 34.9
SJSA	OS	Wild-type	0.15 ± 0.01		6257.1 ± 366.5	3690.5 ± 270.2
U20S	OS	Wild-type	1.94 ± 0.04		>10 000	5416.8 ± 255.7
IMR90	LFB	Wild-type	—		8348.0 ± 231.0	6802.1 ± 696.5

ES: Ewing sarcoma, OS: Osteosarcoma, LFB: Lung fibroblast

IC₅₀: Concentration of XI-006 required to induce 50% apoptosis (mean ± STDEV from two independent experiments).MDM4 mRNA expression determined through real-time qPCR analysis (mean ± SE from triplicate reactions).

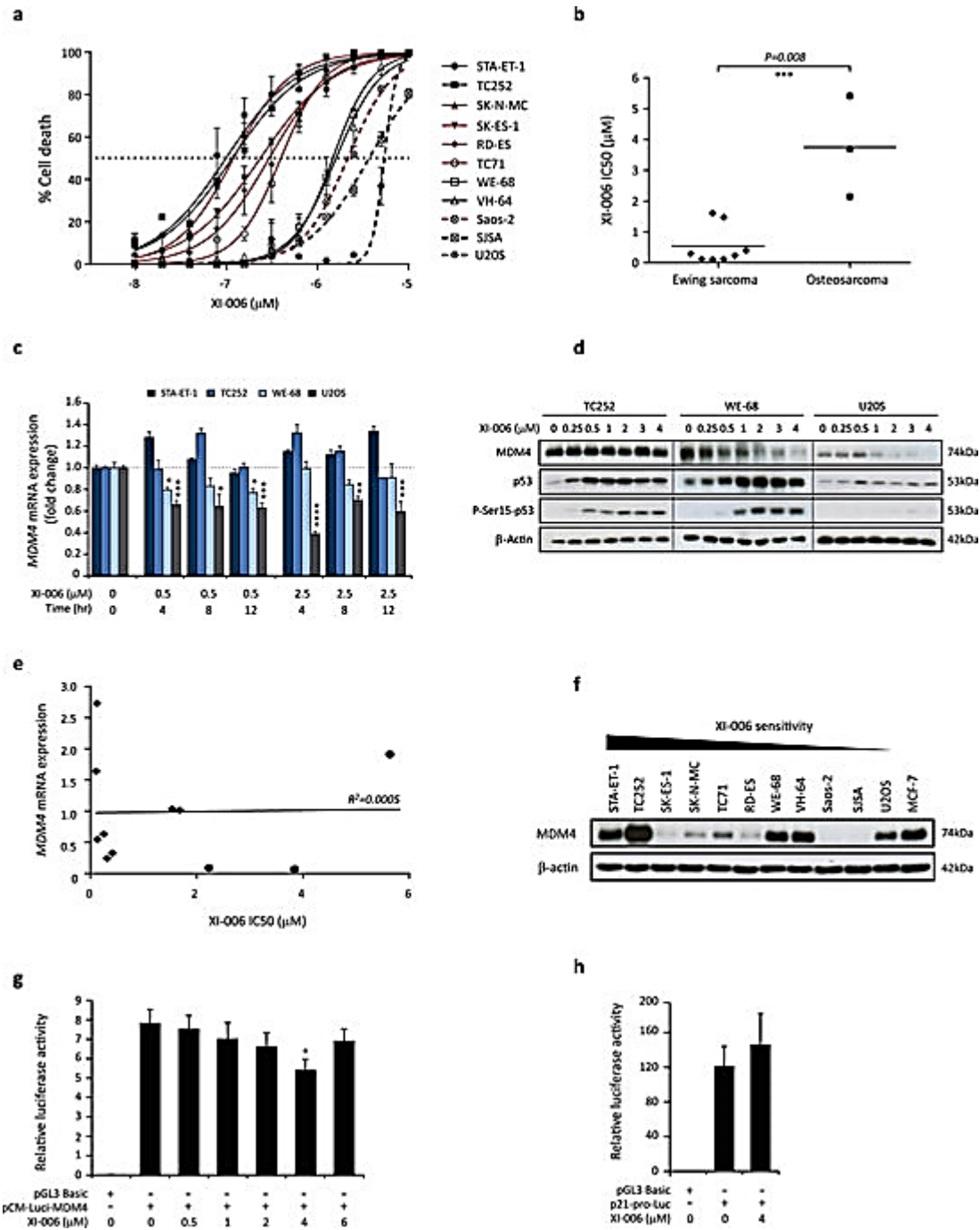


Figure 2: MDM4 mRNA and protein levels do not confer XI-006 sensitivity

(a) XI-006 apoptotic dose response curves of all sarcoma cell lines following 48 hrs of XI-006 treatment. Dashed and red lines denote osteosarcoma and mutant TP53/null cell lines respectively. Data represents mean \pm STDEV from two independent experiments, duplicate

reactions. (b) Correlation between XI-006 apoptotic 48 hr IC₅₀ values determined from 7AAD staining and sarcoma pathology. (c) STA-ET-1, TC252, WE-68 and U2OS cells were treated with XI-006 (0, 2.5 and 5 μM) for the indicated times with mRNA expression levels of MDM4 determined through real-time qPCR analysis. Data represents mean expression (fold change) ± SE from triplicate reactions. (d) TC252, WE-68 and U2OS cell lines were treated for 4 hrs with the indicated concentrations of XI-006. MDM4, p53, and phosphorylated p53 (serine 15) protein levels were detected through western blot analysis. β-Actin was used a loading control. (e) Lack of correlation between XI-006 apoptotic 48 hr IC₅₀ values and basal MDM4 mRNA expression levels. ♦• Denotes Ewing sarcoma and osteosarcoma cell lines respectively. (f) Western blot analysis of basal MDM4 protein levels of the cell line cohort. Cell lines ranked in order of XI-006 sensitivity. MCF-7 (MDM4 amplified breast cancer cell line) was used as a positive control. Luciferase assay of (g) MDM4 and (h) p21 promoter activity from U2OS cells treated with XI-006 for 6 hrs. Data represents mean ± SE from 3 independent experiments. Asterisk denotes statistical significance (*P < 0.05, **P < 0.01, ***P < 0.001, ****P < 0.0001).

To examine the cellular outcome following XI-006 treatment, cell lines were treated with XI-006 for 48 hrs, with cell cycle distribution determined through propidium iodide (PI) staining ([Supplementary Fig. S2](#)). In the Ewing sarcoma cell lines TC252 and RD-ES, XI-006 induced a dose-dependent decrease in the number of G1-phase cells, and accumulation of cells in SubG1. In contrast, XI-006 effectively arrested cell cycle progression in osteosarcoma cell lines (U2OS, Saos-2), depleting the G1 compartment to 18.6–19.9% and increasing the G2 compartment to 45.7–61.5% (3 μM treatment).

MDM4 mRNA and protein levels do not confer sensitivity to XI-006

As XI-006 was shown to decrease MDM4 expression in breast cancer cell lines¹⁸, we investigated the effects of XI-006 on both MDM4 mRNA and protein levels in cell lines with varying MDM4 genomic²¹, mRNA and protein expression levels (Table 2, Fig. 2f). A maximum 61.2% reduction in MDM4 mRNA expression was observed in U2OS cells (2.5 μ M, 4 hrs) following XI-006 treatment; however U2OS cells were the least sensitive cell line to XI-006 (Fig. 2c). Although XI-006 did not attenuate MDM4 mRNA levels in the sensitive Ewing sarcoma cell line TC252, a 23.1% reduction was observed in WE-68 cells (0.5 μ M, 12 hrs), the least sensitive Ewing sarcoma cell line. Consistent with these findings, a dose-dependent reduction in MDM4 protein levels following XI-006 treatment was only observed in U2OS and WE-68 cells, but not TC252 cells (Fig. 2d). We next determined whether basal MDM4 mRNA and protein levels in our cohort of cell lines confers sensitivity to XI-006. Unexpectedly, no correlation between MDM4 mRNA or protein levels and XI-006 sensitivity was observed ($R^2 = 0.0005$) (Table 2, Fig. 2e,f). To confirm whether XI-006 can repress MDM4 promoter activity, luciferase assays of U2OS cells treated with escalating concentrations of XI-006 for 6 hrs were performed. A significant decrease in MDM4 promoter activity was only observed at 4 μ M ($P = 0.05$), equating to a 30.5% reduction in activity (Fig. 2g). No effect on p21 promoter activity was observed at this dose ($P = 0.491$) (Fig. 2h). As XI-006 had no effect on MDM4 promoter activity or mRNA/protein levels at concentrations required to induce 50% apoptosis in the most sensitive Ewing sarcoma cell lines (<0.5 μ M), this suggest that the ability of XI-006 to impart apoptosis occurs independently of MDM4.

XI-006 cytotoxicity occurs independently of TP53

We next examined whether XI-006 can induce expression of TP53 target genes implicated in apoptosis (BAX, PUMA), cell cycle arrest (CDKN1A) and p53 regulation (MDM2). Wild-type TP53 Ewing (TC252, STA-ET-1, WE-68) and osteosarcoma (U2OS, SJSA) cell lines were treated with XI-006 (0.5, 2.5 μ M), with target gene expression assessed through real-time qPCR assays ([Supplementary Fig. S3a](#)). XI-006 dramatically increased mRNA expression levels of all TP53 target genes in Ewing sarcoma cell lines in a dose and time dependent manner. A maximum 63 fold increase in BBC3 levels was observed in STA-ET-1 cells (2.5 μ M, 4 hrs). In contrast, induction of these target genes was significantly lower in all osteosarcoma cell lines, in particular BAX and CDKN1A, where no induction was observed for all time points and XI-006 concentrations.

To determine whether induction of p53 target genes specifically in Ewing sarcoma cells could be attributed to activation and stabilisation of p53, p53 protein levels following XI-006 treatment were examined. Activation and stabilisation of p53 protein levels was only observed in TC252 and WE-68 Ewing sarcoma cell lines but not U2OS cells following 4 hrs of XI-006 treatment ([Fig. 2d](#)). Furthermore, phosphorylation of p53 at serine 15 which is synonymous with ATM dependent activation of the DNA damage pathway²² was observed at XI-006 concentrations exceeding 0.5 μ M. Although XI-006 induced expression of TP53 target genes, the cytotoxic effects of XI-006 were shown to be TP53 independent, as XI-006 sensitivity was not correlated with TP53 status ($P = 0.190$) ([Supplementary Fig. S3b](#)). Indeed, the least sensitive Ewing (WE-68, VH-64) and osteosarcoma (U2OS, SJSA) cell lines harboured wild-type p53 ([Table 2](#)). To further examine the role of TP53 in XI-006 cytotoxicity, TP53 wild-type and null HCT116

isogenic cell lines were treated with XI-006 (0–10 μ M) ([Supplementary Fig. S3c](#)). No significant difference in both XI-006 IC₅₀ values (24 hr: P = 0.230, 48 hr: P = 0.505) or relative viability at any concentration tested was observed, endorsing the p53-independent cytotoxic effects of XI-006.

Low micro-molar concentrations of XI-006 do not induce DNA damage

Previous reports proposed that XI-006 activates the DNA damage response pathway leading to a delay in cell cycle progression²³. As XI-006 cytotoxicity occurs independently of MDM4, we sought to address whether XI-006 drives apoptosis through DNA damage. Clustering of phosphorylated H2AX moieties (γ H2AX foci) at the site of double-strand breaks (DSBs) is one of the earliest events indicative of DNA damage²⁴. Indeed a dose dependent increase in γ H2AX foci was detected through immunofluorescence analysis following 4 hrs of XI-006 treatment in TC252 and U20S cells ([Fig. 3a](#)). At 4 μ M 64.7–79.3% of cells (TC252 and U20S respectively) displayed >5 positive γ H2AX foci. However at low doses required to induce apoptosis in the most sensitive Ewing sarcoma cell lines (0.5 μ M), positive γ H2AX foci were only detected in 9.9–17.4% of cells ([Fig. 3b](#)). In agreement with these findings XI-006 induced γ H2AX foci formation was correlated with H2AX phosphorylation ([Fig. 3c](#)). Neutral comet assays were also employed to determine whether low dose XI-006 (0.075, 0.150, 0.300 μ M) induces DSB's following long term exposure (20 hrs) in TC252 and RD-ES cells ([Fig. 3d](#)). No significant difference in comet tail length was observed in comparison to vehicle control treated cells at any XI-006 concentration tested ([Fig. 3e](#)).

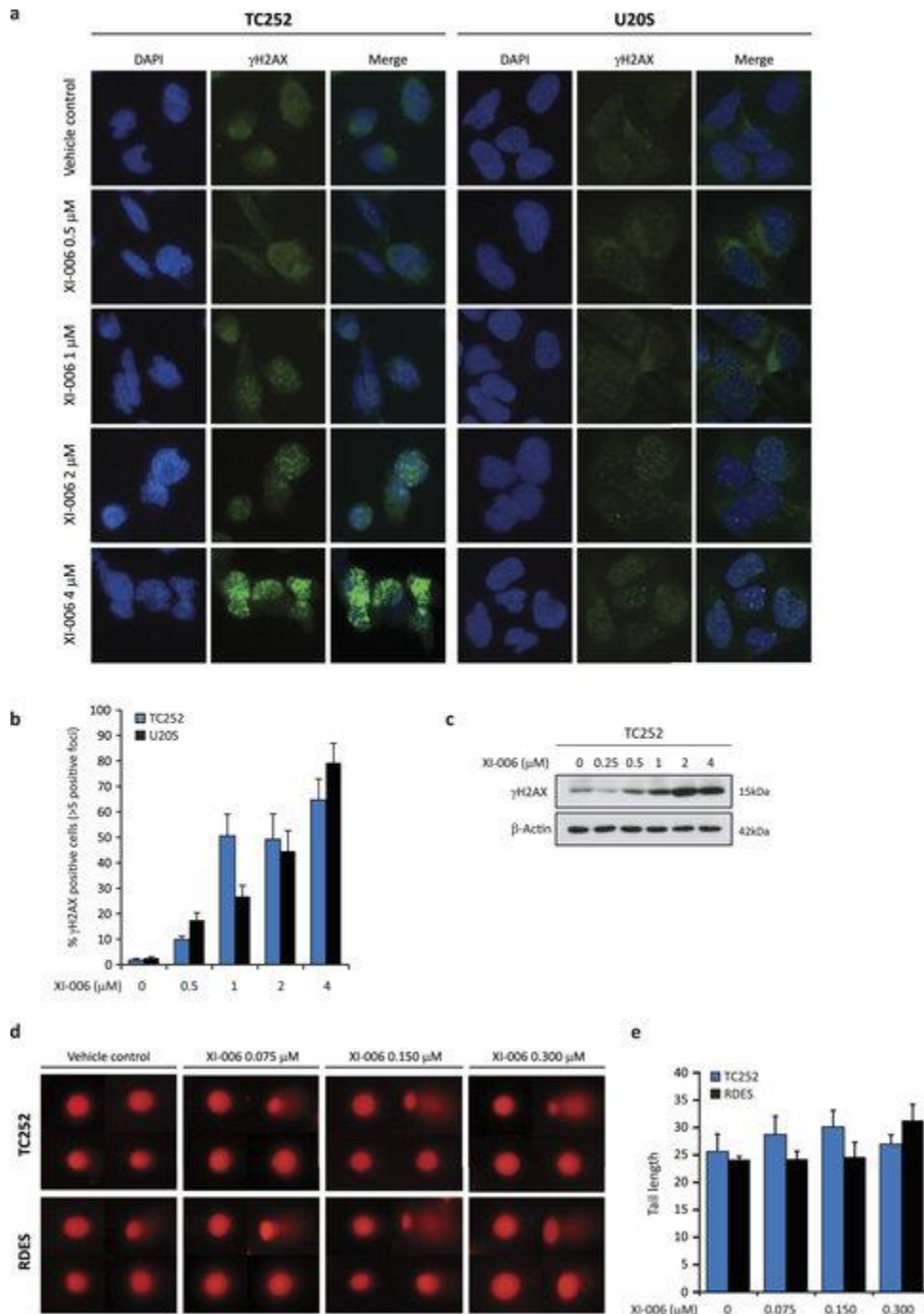


Figure 3: XI-006 does not induce double-strand break DNA damage at low micro-molar concentrations. (a) Representative images of γ H2AX foci formation (immunofluorescence) from TC252 and U20S cells treated with the indicated concentrations of XI-006 for 4 hrs. Cells were stained with DAPI (blue) and γ H2AX (green). (b) Percent nuclei positive for γ H2AX foci (>5) from

cells treated as in (a) (mean \pm STDEV from duplicate wells). (c) Western blot analysis of γ H2AX protein levels in TC252 cells treated as in (a). β -Actin was used as the loading control. (d) Representative images of neutral comet assays from TC252 and RDES cells treated with low dose XI-006 (0.075, 0.150, 0.300 μ M) for 20 hrs. (e) Quantification of tail length from cells treated as in (d), mean \pm SE.

The serine/threonine protein kinase ATM (ataxia telangiectasia mutated) is critical for sensing and co-ordinating repair of DNA DSBs. To further confirm that the cytotoxic effects of XI-006 was not due to DNA damage at low concentrations, Ewing cells (TC252, RD-ES and WE-68) were pre-treated with the ATM inhibitor KU-55933, before the addition of XI-006 (0.02–5 μ M). A significant reduction in both ATM and ATR mRNA expression (82.0% and 87.5% respectively) was observed following monotherapy KU-55933 treatment (5 μ M) ([Supplementary Fig. S4a,b](#)). No significant difference in XI-006 apoptotic IC₅₀ values (24 and 48 hr treatment) was observed following ATM inhibition across all cell lines tested ([Supplementary Fig. S4c](#)).

Previous chemogenomic profiling studies suggested that XI-006 imparts its cytotoxic effect through the activation of the DNA-damage-response pathway. Phosphorylation of the N-terminal domain of EWS-FLI1, the hallmark gene fusion of Ewing sarcoma, at Thr₂₅ has been reported in response to mitogen or DNA alkylating agent induced DNA damage²⁶. This post-translational modification was found to be catalysed by p38 α /p38 β mitogen-activated protein kinases (MAPKs). As all Ewing sarcoma cell lines utilised in this study harbour the EWS-FLI1 fusion, we examined the role p38 α /p38 β MAPKs in XI-006 sensitivity. TC252 and RD-ES cells

were pre-treated with the p38 α /p38 β MAPK inhibitor BIRB 796 (0.1, 1 and 10 μ M) before the addition of XI-006 (0–2.5 μ M) for 24 and 48 hrs. BIRB 796 was previously shown to inhibit p38 α /p38 β MAPKs specifically at 0.1 μ M, p38 γ /p38 δ MAPKs at 1 μ M and completely suppress the activation and activity of all JNKs at 10 μ M²⁶ in Ewing cell lines. Treatment with BIRB 796 had no effect on XI-006 induced cytotoxicity (24 and 48 hrs), as a significant reduction in apoptosis (>30%) was not observed at any BIRB 796 concentration ([Supplementary Fig. S5](#)).

Finally, alkaline comet assays were employed to investigate whether XI-006 induces single-strand break DNA damage. Following 4 hrs of XI-006 treatment, a significant increase in comet tail and length was only observed at concentrations exceeding 2 μ M ([Fig. 4](#)). Collectively these results suggest that XI-006 concentrations (<0.5 μ M) required to induce apoptosis in sensitive Ewing sarcoma cells lines cannot be attributed to a DNA damage mechanism of action

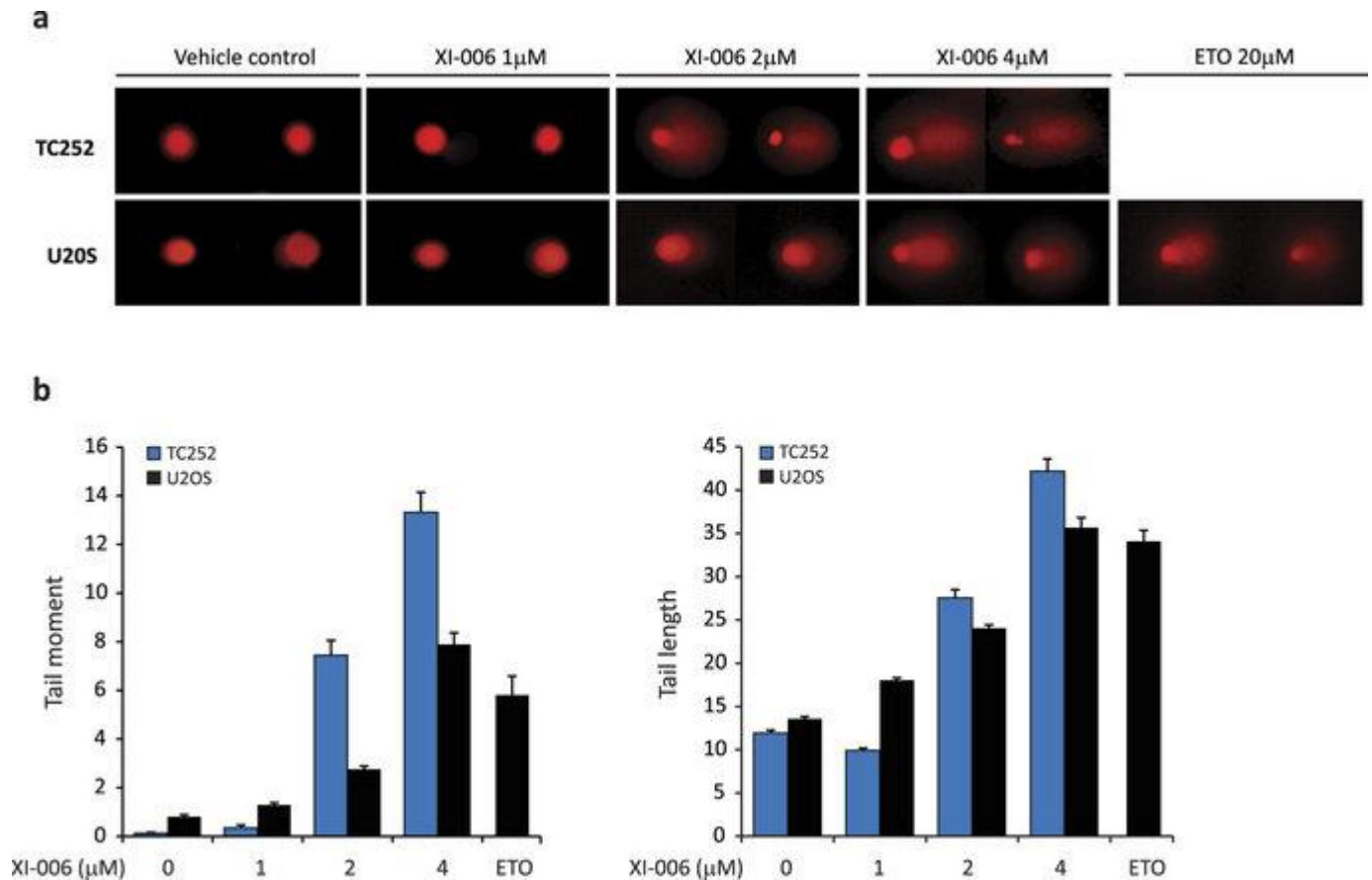


Figure 4: XI-006 does not induce single-strand break DNA damage at low micro-molar concentrations. a) Representative images of alkaline comet assays from TC252 and U20S cells treated with XI-006 (1, 2, 4 μM) for 4 hrs. Etoposide (ETO) was used as a positive control (b) Quantification of tail length and tail moment from cells treated as in (a) mean \pm SE.

XI-006 synergises with olaparib, actinomycin D, doxorubicin and etoposide

As conventional single-agent cancer therapy increases the likelihood of the emergence of resistant cancer cell clones, combination therapies are required to achieve maximal therapeutic response. As such, the ability of XI-006 to enhance the cytotoxic effects of four standard Ewing sarcoma chemotherapeutic agents (vincristine, actinomycin D, doxorubicin or etoposide) was assessed in five Ewing sarcoma cell lines (TC252, STA-ET-1, WE-68, RD-ES, and SK-N-MC).

Modest synergistic combination indexes ($CI < 1$) were observed in 4/5 cell lines for actinomycin and doxorubicin and 3/5 cell lines tested for etoposide (CI range 0.753–0.989) over multiple chemotherapeutic doses ([Supplementary Table S2](#), [Supplementary Fig. S6](#)). Although antagonistic CI values were obtained between XI-006 and vincristine (inhibitor of microtubule assembly), a strong correlation ($R^2 = 0.722$) was observed between XI-006 and vincristine IC_{50} values in all Ewing sarcoma cell lines, suggesting that these two agents may have a similar mechanism of action ([Supplementary Fig. S7](#)).

The EWS-FLI fusion protein has been shown to drive expression of PARP1 (poly-ADP-ribose polymerase), which subsequently further promotes transcriptional activation by EWS-FLI²⁷. The primary function of PARP is to sense and mediate repair of DNA single strand breaks (SSB). Therefore we determined if XI-006 can synergise with olaparib (PARP inhibitor) in EWS-FLI positive Ewing sarcoma cell lines. TC252, RD-ES and WE-68 cells were pre-treated with olaparib prior to addition of XI-006 (0–5 μ M). Potent synergy between these two agents was observed in all cell lines tested and across multiple XI-006 concentrations, 24 and 48 hrs post XI-006 treatment. A maximum 51.9% increase in apoptosis was observed in RD-ES cells when these two agents were combined (48 hr XI-006 treatment) ([Fig. 5a](#)). Olaparib did not abrogate the cytotoxic effects of XI-006 at any concentration tested, suggesting that XI-006 does not induce DNA damage via single stranded breaks at low doses.

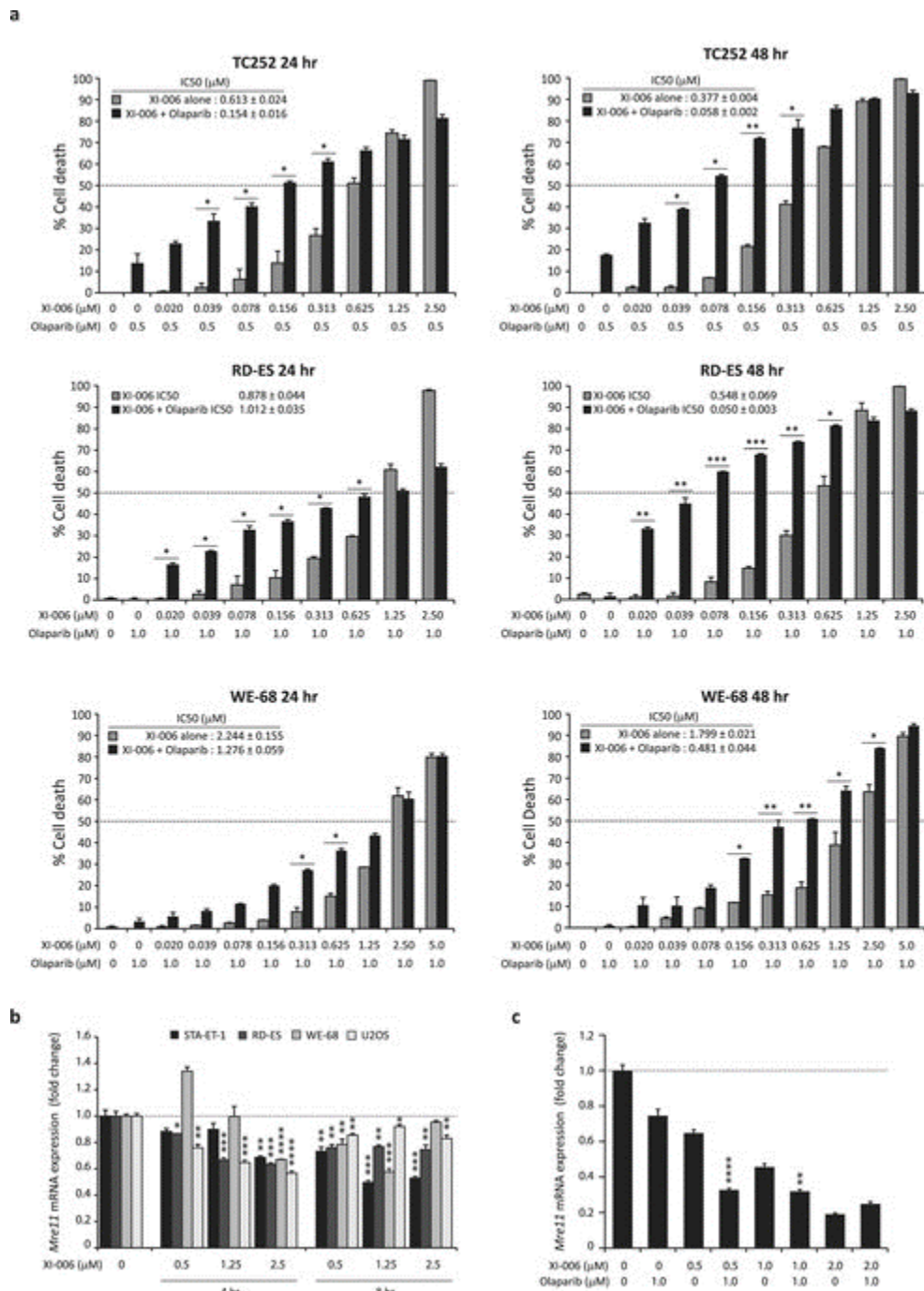


Figure 5: Inhibition of PARP potentiates the cytotoxic effects of XI-006

a) TC252, RD-ES and WE-68 were pre-treated with olaparib (0.5 or 1 μM) or vehicle control (DMSO) for 2 hrs, prior to the addition of XI-006 (0–5 μM). Cell viability was determined through 7AAD staining (24 and 48 hrs post XI-006 treatment) and analysed by flow cytometry. Data represents average percentage cell death \pm STDEV from duplicate reactions. Asterisk

denotes significant increase in apoptosis compared to XI-006 alone (*15–30%, **31–45%, ***>46% increase). (b) STA-ET-1, RDES, WE-68 and U2OS cells were treated with XI-006 (0.5, 1.25, 2.5 μ M) for 4 and 8 hrs. mRNA expression levels of Mre11 were determined through real-time qPCR analysis. Data represents mean expression (fold change) \pm SE from triplicate reactions. (c) RD-ES cells were pre-treated with Olaparib for 2 hrs prior to the addition of XI-006 (0.5, 1, 2 μ M) for an additional 4 hrs. Mre11 mRNA expression levels determined as in (b). Asterisk denotes statistical significant reduction in expression compared to either vehicle control (b) or XI-006 treatment alone (c) (*P < 0.05, **P < 0.01, ***P < 0.001, ****P < 0.0001).

In addition to repair of SSB, PARP detects stalled replication forks and attracts Mre11 (meiotic recombination 11) for end processing to facilitate replication restart and recombination repair²⁸. As XI-006 was previously shown to induce a significant delay in replication²³, Mre11 mRNA expression levels following XI-006 treatment was assessed. A decrease in Mre11 mRNA expression was observed across all cell lines tested, with a maximum 50.1% reduction observed in STA-ET-1 cells (8 hr treatment) ([Fig. 5b](#), [Supplementary Fig. S8](#)). As PARP mediates the recruitment Mre11 to stalled replication forks, Mre11 expression in RD-ES pre-treated with olaparib (1 μ M) before the addition of XI-006 was assessed. Olaparib treatment alone resulted in a significant 25% decrease in Mre11 mRNA expression ([Fig. 5c](#)). Co-treatment with XI-006 (0.5 and 1 μ M) further repressed Mre11 mRNA expression levels, maximum 50.4% reduction compared to XI-006 treatment alone observed. Together, these findings indicate that in the absence of DNA damage low micro-molar concentrations of XI-006 can potentiate the cytotoxic effects of olaparib due to down-regulation of Mre11 expression.

HEG1, FLOT1, UTRN and EDIL3 are differentially expressed in Ewing and osteosarcoma cells following XI-006 treatment.

mRNA sequencing of XI-006 treated and untreated cell lines was employed to identify genes responsible for XI-006 cytotoxicity. Across all Ewing and osteosarcoma cell lines eleven genes were found to be either significantly ($P < 0.05$, Bonferroni correction) repressed (KIF20A, IDH1, SCD, GPSM2, EIF2AK4, HIBCH) or induced (STK19, DNAJC24, MTG2, FAM175B, CYB5D1) following non DNA-damaging XI-006 treatment ($0.5 \mu\text{M}$) ([Table 3](#)). Real-time qPCR analyses confirmed that KIF20A which is required for normal cleavage furrow ingression and cytokinesis during cell division²⁹ and IDH1 (cytosolic NADP dependent enzyme) were repressed on average by 51.2% and 41.3% respectively across all cell lines following XI-006 treatment ([Supplementary Fig. S9](#)).

We next sought to identify genes that were differentially expressed between Ewing and osteosarcoma cell lines following XI-006 treatment. Four genes (UTRN, HEG1, FLOT1, EDIL3) were identified and validated through real-time qPCR analysis ([Table 3](#), [Supplementary Fig. S10](#)). Of particular interest UTRN which mediates several mitochondria dependent apoptosis pathways, was found to be significantly up-regulated in Ewing cell lines (average 22.7% increase) which undergo apoptosis following XI-006 treatment, and repressed in osteosarcoma cell lines (average 31.9% decrease) ($P = 0.025$) which undergo cell-cycle arrest following XI-006 treatment.

Table 3: Genes identified from RNA expression profiling of Ewing and osteosarcoma cell lines treated with XI-006.

Genes significantly induced or repressed following XI-006 across all sarcoma cell lines					
Accession Number	Gene	Location	Full Name	% Change	P value
NM_005733	KIF20A	5q31	Kinesin family member 20A	-44.49	0.0214
NM_005063	SCD	10q24.31	Stearoyl-CoA desaturase (delta-9-desaturase)	-38.01	0.0076
NM_005896	IDH1	2q33.3	Isocitrate dehydrogenase 1 (NADP+), soluble	-37.14	0.0040
NM_013296	GPSM2	1p13.3	G-protein signalling modulator	-33.34	0.0401
NM_001013703	EIF2AK4	15q15.1	Eukaryotic translation initiation factor 2 alpha kinase	-24.35	0.0034
NM_014362	HIBCH	2q32.2	3-hydroxyisobutyryl-CoA hydrolase	-16.66	0.0134
NM_004197	STK19	6p21.3	Serine/threonine kinase 19	31.43	0.0433
NM_181706	DNAJC24	11p13	DnaJ (Hsp40) homolog, superfamily C, member 24	25.99	0.0181
NM_015666	MTG2	20q13.33	Mitochondrial ribosome-associated GTPase 2	25.18	0.0040
NM_032182	FAM175B	10q26.13	Family with sequence similarity 175, member B	24.37	0.0459
NM_144607	CYB5D1	17p13.1	Cytochrome b5 domain containing 1	20.32	0.0311

Genes differentially expressed in Ewing and osteosarcoma cell lines following XI-006 treatment

Accession Number	Gene	Location	Full Name	% Change Ewing sarcoma	% Change Osteosarcoma	P value
NM_020733	HEG1	3q21.2	Heart development protein with EGF-like domains 1	4.77	-73.76	0.00001
NM_005803	FLOT1	6p21.3	Flotillin	-5.44	-98.73	0.0007
NM_007124	UTRN	6q24	Utrophin	2.65	-53.96	0.0128
NM_005711	EDIL3	5q14	EGF-like repeats and discoidin I-like domains 3	-1.01	-110.0	0.0269

Discussion

Despite the use of aggressive multi-modal therapeutic strategies, five year survival rates for relapsed Ewing sarcoma patients is <30% and in such cases no standard therapy currently exists for second line treatment. Despite the emerging role of MDM4 (structural homologue of MDM2) in the pathogenesis, maintenance, and chemo-resistance of human cancer, there are currently no selective MDM4 antagonists undergoing clinical trial evaluation. As MDM4 gene amplification is a characteristic of both Ewing and osteosarcoma⁸, this study assessed the therapeutic potential of XI-006, a small molecule thought to attenuate MDM4 promoter activity, for the treatment of sarcoma. Indeed, MDM4 IHC analysis of our sarcoma cohort detected MDM4 protein expression (>10 positive cells) in 33.3% (12/36) of cases and was highly prevalent in well/de-differentiated liposarcomas and myxofibrosarcomas (Fig. 1).

Low micro-molar concentrations of XI-006 induced rapid apoptosis specifically in Ewing sarcoma cell lines (IC_{50} 0.099–1.61 μ M) in the absence of both observable DNA damage and effect on MDM4 expression levels (Table 1, Fig. 2). Cell line sensitivity to XI-006 was not correlated with MDM4 mRNA or protein levels, and reduction of MDM4 mRNA and protein levels were only observed in the least sensitive Ewing sarcoma and osteosarcoma cell lines at high XI-006 concentrations (>1 μ M) that also induced DNA damage (Figs 3 and 4). It is known that DNA damage induces ATM/Chk2 dependent phosphorylation of several MDM4 C-terminal residues (S342, S367, S403), resulting in degradation of MDM4 and activation of p53²⁵. Indeed, ATM mediated phosphorylation of serine 15 in p53 was observed in Ewing sarcoma cell lines

following treatment with double-strand break inducing concentrations of XI-006 (>0.5 μ M). As only a maximum 30.5% reduction in MDM4 promoter activity was observed following 4 μ M XI-006 treatment ([Fig. 2](#)), our findings suggest that XI-006 cytotoxicity in Ewing sarcoma cell lines cannot be attributed to repression of MDM4 activity.

The introduction of systemic chemotherapy in the 1960's greatly improved survival rates for patients with localised Ewing sarcoma³⁰, hence it is imperative that XI-006 can synergise with current chemotherapeutic protocols as well as novel agents. In addition to synergising with doxorubicin, etoposide and actinomycin D (CI range 0.753–0.989), a maximum 51.9% increase in apoptosis was observed when XI-006 was combined with the PARP inhibitor olaparib ([Fig. 5](#)).

PARP-1 is a member of the base excision repair pathway that sensors and modulates the spatial and temporal organization of single-strand break repair³¹. Inhibition of PARP-1, results in the accumulation of persistent single-strand breaks which are converted to lethal double-strand breaks upon replication. Since the 1990's it has been known that Ewing sarcomas express high levels of PARP-1³², and the premise of PARP inhibition as a therapeutic avenue for the treatment of Ewing sarcoma has been furthered strengthened by several key studies. Firstly, large-scale drug screening (130 compounds) in >600 human cancer cell lines identified a highly significant association between EWS-FLI1, the hallmark translocation of Ewing sarcoma, and sensitivity to the olaparib. Indeed, FLI1 expression levels in Ewing sarcoma cell lines were highly correlated with olaparib sensitivity³³. This study was complemented by Brenner and colleagues, who demonstrated that the EWS-FLI1 fusion acted in a positive feedback loop to maintain the expression of PARP1 which was required for EWS-FLI1-mediated transcription²⁷.

Furthermore, DNA damage induced by expression of EWS-FLI1 was potentiated by PARP1 inhibition *in vitro*. As PARP1 inhibitors have exhibited promising activity in early clinical trials³⁴, phase I/II trials of PARP inhibitors (olaparib and BMN-673) are currently undergoing investigations in adults with recurrent and metastatic Ewing sarcoma (NCT01583543), and patients with locally advanced or metastatic solid tumours (NCT02049593).

Previous chemogenomic profiling studies suggested that XI-006 (referred to as NSC-207895) activates the DNA-damage-response pathway through an indirect mechanism leading to a significant delay in replication and cell cycle progression²³. Replication stress, defined as the slowing or stalling of replication fork progression and/or DNA synthesis, has severe implications for genome stability and cell survival³⁵. Several studies have implicated that PARP binds to and is activated at stalled replication forks that contain small gaps (<4 nucleotides) or short ssDNA regions, and mediates the recruitment of Mre11²⁸. Mre11 is a key component of the MRN (Mre11-Rad50-Nbs1) complex, which is vital for double-strand break (DSB) recognition, replication fork stabilization, ATM/ATR activation and the initiation of end resection required for replication restart and homologous recombination (HR)³⁶. Inhibition or loss of PARP impairs Mre11 localisation to stalled forks, RPA and RAD51 foci formation, HR and replication restart. Indeed numerous studies have shown that due to impaired HR DNA repair, loss of Mre11 expression sensitizes breast³⁷, colorectal^{38,39}, endometrial⁴⁰, and haematological cancers⁴¹ to PARP-inhibitors. In the absence of DNA damage, our findings demonstrate that low dose XI-006 rapidly down regulates the expression of Mre11 (Fig. 5) and this repression is further enhanced in the presence of olaparib (Fig. 5), resulting in potent apoptosis. As such, these

findings provide a strong rationale for further investigations into the combinatorial approach of PARP inhibitors with XI-006.

To elucidate the genes specifically responsible for Ewing sarcoma apoptotic XI-006 sensitivity, mRNA sequencing was employed and identified four genes significantly differentially expressed between Ewing and osteosarcoma cell lines following XI-006 treatment ([Table 3](#)). Of particular relevance, UTRN (Utrophin) was significantly up-regulated in Ewing sarcoma cell lines but repressed in osteosarcoma cell lines ($P = 0.025$). The GTPase UTRN also known as Drip1, mediates outer mitochondrial membrane fission and is essential for the normal progression of several mitochondria dependent apoptosis pathways⁴². Upon induction of apoptosis, UTRN is recruited from the cytosol to the mitochondrial outer membrane, where it colocalizes with Bax at fission sites and mediates the release of apoptotic regulatory proteins including cytochrome c prior to caspase activation^{43,44}. The expression of FLOT1 (flotillin) was also significantly repressed in osteosarcoma cell lines ($P = 0.044$) compared to Ewing. The flotillin family of proteins have been implicated in numerous cellular processes such as actin-cytoskeleton reorganization, endocytosis, adhesion and transduction of cellular signals⁴⁵. Knockdown of FLOT1 has been shown to significantly impair cell proliferation and tumorigenicity of breast and esophageal squamous cell carcinoma cells *in vitro* and *in vivo* through the Akt/FOXO3a pathways^{46,47}. Indeed, silencing of FLOT1 induced G1-S-phase arrest of breast cancer cells due to up-regulated expression of the CDK inhibitors p21Cip1 and p27Kip1. Following XI-006 treatment, both UTRN and FLOT1 were strongly repressed in osteosarcoma cell lines (31.9% and 33.8% decrease in mRNA expression respectively) but not in Ewing cell lines. This may be

the basis of the finding that XI-006 induces apoptosis in Ewing sarcoma cell lines but cell cycle arrest in osteosarcoma cell lines ([Supplementary Fig. S2](#)).

Expression profiling also revealed that following XI-006 treatment, eleven genes were globally repressed or induced across all Ewing and osteosarcoma cell lines. Three of these genes which were downregulated, KIF20A, IDH1 and GPSM2 (44.49%, 37.14% and 33.34% reduction respectively), have been implicated in cell proliferation. KIF20A belongs to the family of kinesin microtubule-dependent motor proteins, which are required for bipolar spindle assembly, chromosome alignment, chromosome segregation, and cytokinesis⁴⁸. Similarly GPSM2 is required for spindle cell orientation towards the interphase long-axis⁴⁹. Several studies have demonstrated the essential role of KIF20A in cytokinesis and maintenance of cell viability. Microinjection of anti-KIF20A antibody was shown to induce multi-nucleation in HeLa cells⁵⁰ and knockdown of endogenous KIF20A expression markedly attenuated the growth of pancreatic and gastric cancer cells^{51,52}. As sensitivity to XI-006 was strongly correlated with vincristine sensitivity ($R^2 = 0.722$) ([Supplementary Fig. S7](#)), a widely used chemotherapeutic that inhibits microtubule assembly and induces tubulin self-association into coiled spiral aggregates⁵³, this supports that the mechanism of action of XI-006 at low, micro-molar concentrations ($<0.5 \mu\text{M}$) can be attributed to inhibition of cell division and cycle regulators and not DNA damage.

In summary, our findings demonstrate that XI-006 is a promising new potential therapeutic for the treatment of Ewing sarcoma as it induced potent p53-independent apoptosis at non-DNA

damaging concentrations specifically in Ewing sarcoma cell lines. Notably, strong synergy was observed with olaparib, a PARP inhibitor that is gaining significant interest for the treatment of solid cancers. As such, our preclinical findings warrant further pharmacokinetic and pharmacodynamic investigations of XI-006 in vivo.

Methods

Cell lines and reagents

Ewing sarcoma cell lines were cultured as previously described²¹ and supplied by G. Hamilton (University of Vienna, Austria) (TC252, TC71), F. van Valen (Westfälische-Wilhelms-University, Germany) (WE-68, VH-64), P. Ambros (St. Anna Children's Hospital, Austria) (STA-ET-1) and V. Russo (Murdoch Children's Research Institute, Australia) (SK-N-MC). SK-ES-1, RD-ES cell lines were purchased from American Type Tissue Culture. Osteosarcoma cells (SJSA, U2OS and Soas-2) were supplied by A. Evdokiou (University of Adelaide, Australia).

XI-006 and BIRB 796 were purchased from Merck Millipore, KU-55933 and olaparib (AZD2281) were purchased from Selleck. Vincristine sulfate (Hospira), doxorubicin HCl (Pfizer), actinomycin D/Cosmegen (Lundbeck) and etoposide (Royal Adelaide Hospital, Australia) were supplied by M.P Brown (Centre for Cancer Biology, Australia).

Sarcoma tissue cohort

Chemotherapy/radiotherapy naïve tumour specimens were collected from thirty-six patients with sarcoma (22 males, 14 females) undergoing surgical resection/core biopsy at three clinical institutions; Royal Adelaide Hospital (RAH), Calvary Wakefield Hospital, and St Andrew's Hospital between 2010 and 2013. Patient consent was obtained for accrual of surgically excised tissue. Study was approved by the Royal Adelaide Hospital Human Ethics Committee (RAH Protocol #100505). The different morphological subtypes were represented by nine undifferentiated pleomorphic sarcomas, eight liposarcomas (four well-differentiated, two de-differentiated, one pleomorphic and myxoid), six leiomyosarcomas, five myxofibrosarcomas,

two osteosarcomas, two synovial and one Ewing sarcoma, angiosarcoma, chondrosarcoma and radiation induced sarcoma. Twenty patients were previously described¹⁹. All methods were carried out in accordance with National Health and Medical Research (NHMRC) approved guidelines.

Immunohistochemistry

MDM4 immunohistochemical protocol was adapted from⁵⁴. Briefly, FFPE (4 µm thickness) were deparaffinised by serial immersion in a xylene-to-ethanol solvent gradient. After citrate buffer (0.001 mol/L, pH 6.0) antigen retrieval, slides were quenched in 3% hydrogen peroxide for 5 mins to eliminate endogenous peroxidase activity. Sections were blocked with normal goat serum (30 mins) and immuno-labelled with rabbit HdmX/MDM4 (1:250, IHC-00108, Bethyl Laboratories) overnight at 4 °C. Digital images were acquired using a Nanozoomer Digital Pathology Scanner, at x40 magnification. To determine the percentage of positive MDM4 cells, a minimum of 80 cells per field of view (four) were assessed.

MDM4 SNP34091 genotype analysis

DNA from sarcoma tissues was isolated using the DNeasy Blood and Tissue Kit (Qiagen) according to the manufacturer's instructions. The 3'UTR region of MDM4 was amplified using the following primer pair⁵⁵ forward: 5'ACGGGCCATCTTGTCACCTTGTT 3' and reverse: 5'ACCTGACTGCT GCATAAAGTAATCCAT 3', to amplify a 355 base pair (bp) product. PCR was performed using 100 ng of genomic DNA and FastStart Taq DNA Polymerase (Roche) using the following parameters, enzyme activation 95 °C 3 mins, followed by 45 cycles of denaturation at 95 °C 30 secs, annealing at 57 °C 15 secs, and extension at 72 °C 60 secs, followed by 1 cycle of

final extension at 72 °C 10 mins. Reactions were processed on an ABI Hitachi 3730 DNA analyser.

Apoptosis and Cell cycle analysis

For viability assays, cell were seeded in 96-well micro-titer plates at a density of 3×10^4 cells/well and treated with XI-006 alone or in combination with chemotherapeutics agents. For inhibitor studies, cells were pre-treated with olaparib, KU-55933 or BIRB 796 for 2 hrs prior to the addition of XI-006. Following treatment for 24 and/or 48 hrs, cells were centrifuged at 2500 rpm for 5 mins, washed in phosphate buffered saline (PBS) and stained with 7-amino-actinomycin-D solution (7AAD, 2 mg/mL, Invitrogen) for 10 mins at room temperature.

For cell cycle analysis, XI-006 and vehicle control treated cells were permeabilized with cold 70% ethanol overnight, and stained with a solution containing 50 µg/ml propidium iodide (PI, Sigma Aldrich), 0.05% Triton-X and 100 µg/ml RNase A at 37 °C for 40 mins. Cell viability and DNA content was determined through the use of a FACS Calibur flow cytometer (Becton-Dickinson Immunocytometry Systems) with cell cycle profiles and viability analyzed using FLOWJO software (V7.6.5).

Luciferase Assay

U2OS cells (3.2×10^4) were seeded overnight in 24-well plates (triplicate wells per treatment) and transfected with 200 ng of pCM-luci-MDM4 or p21-pro-Luc reporter constructs and 25 ng of pRL-TK plasmid (Promega) using Lipofectamine LTX (Invitrogen) according to the manufacturers' instructions. pCM-Luci-MDM4 was kindly supplied by C. Yan (GRU Cancer Center). Cells were treated with vehicle control or XI-006 for 6 hrs with Dual-luciferase reporter assays (Promega) performed according to the manufacturer's instructions.

Real-time qPCR analysis

Total RNA was extracted using RNeasy mini kit (Qiagen), using on-column RNase-free DNase digestion according to the manufacturer's instructions. cDNA was synthesized by reverse transcribing 600 ng of total RNA using random primers (Promega) and Moloney murine leukemia virus reverse transcriptase (H₂O; Promega). Real-time qPCR reactions were performed using iTaq Universal Sybr Green Supermix (BIORAD) and processed on a CFX Real-Time PCR detection system (BIORAD). Cycling parameters were as follows: 95 °C for 3 mins, followed by 45 cycles of denaturation at 95 °C for 10 secs, annealing at 59–63 °C for 15 secs, and extension at 72 °C for 30 secs. Relative target mRNA expression was determined using the Δ CT method from triplicate reactions, with the levels of gene expression normalized to the relative average Ct value of Peptidylprolyl Isomerase-G (PPIG). Primer sequences and annealing temperatures are listed in [Supplementary Table S1](#).

Western blot

Western blot analysis was performed as previously described²¹. Whole protein lysates (5–20 μ g) were resolved using SDS PAGE electrophoresis, and probed overnight at 4 °C with the following primary antibodies MDM4 (1:500; A300-287A, Bethyl Laboratories), p53 DO1 (1:1000, Santa Cruz Biotechnology), Phospho-p53 (Ser15) (1:500, Cell Signalling), Phospho-Histone H2A.X (Ser139) clone JBW301 (1:500, Millipore) and β -Actin (1:1000, AC-15, Sigma).

Immunofluorescence

TC252 and U2OS cells (1.5×10^4 cells per 6 well chamber) were seeded on microscope slides and treated with XI-006 (0.5, 1, 2 and 4 μ M) or vehicle control (DMSO) for 4 hrs. Cells were fixed with 10% neutral-buffered formalin, washed with PBS and blocked with 5% bovine albumin

serum with 0.3% Triton-X 100 (Sigma-Aldrich). Slides were washed in PBS (3 × 5 min), then incubated with 1 µg/ml biotinylated mouse anti-human anti-phospho-histone H2AX (ser139) (JBW301, Millipore) overnight at 4 °C. After further washing, samples were incubated with 5 µg/ml streptavidin-Alexa Fluor 488 (Life Technologies) followed by counterstaining with 1 µg/ml DAPI. Slides were examined using an Olympus IX71 microscope (x40 magnification) with CellSens Standard (v1.6) software. Images were analysed using ImageJ (v1.45) (National Institute of Health).

Comet Assay

Neutral and alkaline comet assays were performed with the Trevigen CometAssay kit according to the manufacturer's protocol. Briefly, 3.5×10^5 cells were plated in 6 well plates and treated with XI-006 or vehicle control for 4 or 20 hrs. Lysed cells were subjected to electrophoresis for 40 mins at 30 V (300 mA) at 4 °C. Cells were stained with 2.5 µg/ml PI for 15 mins and visualised with an Olympus IX71 microscope (x20 magnification) with CellSens Standard (v1.6) software. Tail length and moment were assessed using AutoComet software (TriTek) from a minimum of 60 cells.

mRNA sequencing

Ewing and osteosarcoma cell lines (n = 11) were treated with XI-006 (0.5 µM) or vehicle control for 4 hrs. One µg of RNA was used for polyA selection and library construction with NEBNext UltraT RNA Library Prep Kits for Illumina sequencing, according to the manufacturer's instructions (E7530 Version 2). The mRNA library size was validated with the Agilent BioAnalyzer on High Sensitivity chips, with yield determined with a Life Technologies Qubit 2.0 Fluorometer. The mRNA libraries were pooled and sequenced across five lanes of an Illumina

HiSeq 2500 flowcell (1 × 50 bp reads) at the Australian Cancer Research Foundation Cancer Genomics Facility (Adelaide, Australia). Reads were trimmed for the NEB single end adapter “AGATCGGAAGAGCACACGTCTGAACTCCAG TCAC” with Cutadapt v1.3, requiring a minimum overlap of 5, allowing a 20% error rate and discarding trimmed sequences shorter than 18 bases. Reads were mapped to the UCSC hg19 genome and GTF annotations with Tophat 2.0.9 using default parameters. Gene counts were performed with HTSeq-count v0.6.1p1 using gene_id as the GTF feature ID.

Statistics

Combination Index (CI) values were used to determine synergy between XI-006 and cytotoxic agents. A CI value of <1, =1 and >1 indicates synergistic, additive and antagonistic effects respectively⁵⁶. P values were calculated using Student t test using Graph Pad Prism Version 6.

References

1. Jemal, A., Siegel, R., Xu, J. & Ward, E. Cancer statistics, 2010. *CA Cancer J Clin* 60, 277–300 (2010).
2. Fletcher CDM, B. J., Hogendoorn, P. C. W. & Mertens, F. World Health Organization Classification of tumours and soft tissue of bone. 4th, IARC Press (Lyon 2013).
3. Danovi, D. et al. Amplification of Mdmx (or Mdm4) directly contributes to tumour formation by inhibiting p53 tumour suppressor activity. *Mol Cell Biol* 24, 5835–5843 (2004).
4. Gembarska, A. et al. MDM4 is a key therapeutic target in cutaneous melanoma. *Nat Med* 18, 1239–1247 (2012).
5. Laurie, N. A. et al. Inactivation of the p53 pathway in retinoblastoma. *Nature* 444, 61–66 (2006).
6. Valentin-Vega, Y. A., Barboza, J. A., Chau, G. P., El-Naggar, A. K. & Lozano, G. High levels of the p53 inhibitor MDM4 in head and neck squamous carcinomas. *Hum Pathol* 38, 1553–1562 (2007).
7. Bartel, F. et al. Significance of HDMX-S (or MDM4) mRNA splice variant overexpression and HDMX gene amplification on primary soft tissue sarcoma prognosis. *Int J Cancer* 117, 469–475 (2005).
8. Ito, M. et al. Comprehensive mapping of p53 pathway alterations reveals an apparent role for both SNP309 and MDM2 amplification in sarcomagenesis. *Clin Cancer Res* 17, 416–426 (2011).

9. Duhamel, L. A. et al. Frequency of Mouse Double Minute 2 (MDM2) and Mouse Double Minute 4 (MDM4) amplification in parosteal and conventional osteosarcoma subtypes. *Histopathology* 60, 357–359 (2012).
10. Linares, L. K., Hengstermann, A., Ciechanover, A., Muller, S. & Scheffner, M. HdmX stimulates Hdm2-mediated ubiquitination and degradation of p53. *Proc Natl Acad Sci USA* 100, 12009–12014 (2003).
11. Migliorini, D. et al. Hdmx recruitment into the nucleus by Hdm2 is essential for its ability to regulate p53 stability and transactivation. *J Biol Chem* 277, 7318–7323 (2002).
12. Reed, D. et al. Identification and characterization of the first small molecule inhibitor of MDMX. *J Biol Chem* 285, 10786–10796 (2010).
13. Bista, M. et al. On the mechanism of action of SJ-172550 in inhibiting the interaction of MDM4 and p53. *PLoS One* 7, e37518 (2012).
14. Bernal, F. et al. A stapled p53 helix overcomes HDMX-mediated suppression of p53. *Cancer Cell* 18, 411–422 (2010).
15. Verdine, G. L. & Hilinski, G. J. Stapled peptides for intracellular drug targets. *Methods Enzymol* 503, 3–33 (2012).
16. Wade, M., Li, Y. C. & Wahl, G. M. MDM2, MDMX and p53 in oncogenesis and cancer therapy. *Nat Rev Cancer* 13, 83–96 (2013).
17. Gilkes, D. M. et al. Regulation of MDMX expression by mitogenic signaling. *Mol Cell Biol* 28, 1999–2010 (2008).
18. Wang, H., Ma, X., Ren, S., Buolamwini, J. K. & Yan, C. A small-molecule inhibitor of MDMX activates p53 and induces apoptosis. *Mol Cancer Ther* 10, 69–79 (2011).

19. Pishas, K. I. et al. Nutlin-3a efficacy in sarcoma predicted by transcriptomic and epigenetic profiling. *Cancer Res* 74, 921–31 (2014).
20. Wynendaele, J. et al. An illegitimate microRNA target site within the 3' UTR of MDM4 affects ovarian cancer progression and chemosensitivity. *Cancer Res* 70, 9641–9649 (2010).
21. Pishas, K. I. et al. Nutlin-3a is a potential therapeutic for ewing sarcoma. *Clin Cancer Res* 17, 494–504 (2011).
22. Banin, S. et al. Enhanced phosphorylation of p53 by ATM in response to DNA damage. *Science* 281, 1674–1677 (1998).
23. Kapitzky, L. et al. Cross-species chemogenomic profiling reveals evolutionarily conserved drug mode of action. *Molecular systems biology* 6, 451 (2010).
24. Rogakou, E. P., Pilch, D. R., Orr, A. H., Ivanova, V. S. & Bonner, W. M. DNA double-stranded breaks induce histone H2AX phosphorylation on serine 139. *J Biol Chem* 273, 5858–5868 (1998).
25. Chen, L., Gilkes, D. M., Pan, Y., Lane, W. S. & Chen, J. ATM and Chk2-dependent phosphorylation of MDMX contribute to p53 activation after DNA damage. *Embo J* 24, 3411–3422 (2005).
26. Klevernic, I. V., Morton, S., Davis, R. J. & Cohen, P. Phosphorylation of Ewing's sarcoma protein (EWS) and EWS-Fli1 in response to DNA damage. *Biochem J* 418, 625–634 (2009).
27. Brenner, J. C. et al. PARP-1 inhibition as a targeted strategy to treat Ewing's sarcoma. *Cancer Res* 72, 1608–1613 (2012).
28. Bryant, H. E. et al. PARP is activated at stalled forks to mediate Mre11-dependent replication restart and recombination. *Embo J* 28, 2601–2615 (2009).

29. Neef, R. et al. Phosphorylation of mitotic kinesin-like protein 2 by polo-like kinase 1 is required for cytokinesis. *The Journal of cell biology* 162, 863–875 (2003).
30. Balamuth, N. J. & Womer, R. B. Ewing's sarcoma. *Lancet Oncol* 11, 184–192 (2010).
31. Yelamos, J., Farres, J., Llacuna, L., Ampurdanes, C. & Martin-Caballero, J. PARP-1 and PARP-2: New players in tumour development. *American journal of cancer research* 1, 328–346 (2011).
32. Prasad, S. C., Thraves, P. J., Bhatia, K. G., Smulson, M. E. & Dritschilo, A. Enhanced poly(adenosine diphosphate ribose) polymerase activity and gene expression in Ewing's sarcoma cells. *Cancer Res* 50, 38–43 (1990).
33. Garnett, M. J. et al. Systematic identification of genomic markers of drug sensitivity in cancer cells. *Nature* 483, 570–575 (2012).
34. Fong, P. C. et al. Inhibition of poly(ADP-ribose) polymerase in tumours from BRCA mutation carriers. *N Engl J Med* 361, 123–134 (2009).
35. Zeman, M. K. & Cimprich, K. A. Causes and consequences of replication stress. *Nat Cell Biol* 16, 2–9 (2014).
36. Stracker, T. H. & Petrini, J. H. The MRE11 complex: starting from the ends. *Nat Rev Mol Cell Biol* 12, 90–103 (2011).
37. Daemen, A. et al. Cross-platform pathway-based analysis identifies markers of response to the PARP inhibitor olaparib. *Breast Cancer Res Treat* 135, 505–517 (2012).
38. McPherson, L. A., Shen, Y. & Ford, J. M. Poly (ADP-ribose) polymerase inhibitor LT-626: Sensitivity correlates with MRE11 mutations and synergizes with platinum and irinotecan in colorectal cancer cells. *Cancer Lett* 343, 217–223 (2014).

39. Vilar, E. et al. MRE11 deficiency increases sensitivity to poly(ADP-ribose) polymerase inhibition in microsatellite unstable colorectal cancers. *Cancer Res* 71, 2632–2642 (2011).
40. Koppensteiner, R. et al. Effect of MRE11 loss on PARP-inhibitor sensitivity in endometrial cancer in vitro. *PLoS One* 9, e100041 (2014).
41. Gaymes, T. J. et al. Microsatellite instability induced mutations in DNA repair genes CtIP and MRE11 confer hypersensitivity to poly (ADP-ribose) polymerase inhibitors in myeloid malignancies. *Haematologica* 98, 1397–1406 (2013).
42. Suen, D. F., Norris, K. L. & Youle, R. J. Mitochondrial dynamics and apoptosis. *Genes Dev* 22, 1577–1590 (2008).
43. Frank, S. et al. The role of dynamin-related protein 1, a mediator of mitochondrial fission, in apoptosis. *Developmental cell* 1, 515–525 (2001).
44. Karbowski, M. et al. Spatial and temporal association of Bax with mitochondrial fission sites, Drp1, and Mfn2 during apoptosis. *The Journal of cell biology* 159, 931–938 (2002).
45. Langhorst, M. F., Reuter, A. & Stuermer, C. A. Scaffolding microdomains and beyond: the function of reggie/flotillin proteins. *Cell Mol Life Sci* 62, 2228–2240 (2005).
46. Lin, C. et al. Knockdown of FLOT1 impairs cell proliferation and tumourigenicity in breast cancer through upregulation of FOXO3a. *Clin Cancer Res* 17, 3089–3099 (2011).
47. Song, L. et al. Flotillin-1 promotes tumour necrosis factor-alpha receptor signaling and activation of NF-kappaB in esophageal squamous cell carcinoma cells. *Gastroenterology* 143, 995–1005 e1012 (2012).
48. Daire, V. & Pous, C. Kinesins and protein kinases: key players in the regulation of microtubule dynamics and organization. *ArchBiochem Biophys* 510, 83–92 (2011).

49. Corrigan, A. M. et al. Automated tracking of mitotic spindle pole positions shows that LGN is required for spindle rotation but not orientation maintenance. *Cell Cycle* 12, 2643–2655 (2013).
50. Hill, E., Clarke, M. & Barr, F. A. The Rab6-binding kinesin, Rab6-KIFL, is required for cytokinesis. *Embo J* 19, 5711–5719 (2000).
51. Taniuchi, K. et al. Down-regulation of RAB6KIFL/KIF20A, a kinesin involved with membrane trafficking of discs large homologue 5, can attenuate growth of pancreatic cancer cell. *Cancer Res* 65, 105–112 (2005).
52. Yan, G. R. et al. Genistein-induced mitotic arrest of gastric cancer cells by downregulating KIF20A, a proteomics study. *Proteomics* 12, 2391–2399 (2012).
53. Lobert, S., Vulevic, B. & Correia, J. J. Interaction of vinca alkaloids with tubulin: a comparison of vinblastine, vincristine, and vinorelbine. *Biochemistry* 35, 6806–6814 (1996).
54. Touqan, N. et al. An observational study on the expression levels of MDM2 and MDMX proteins, and associated effects on P53 in a series of human liposarcomas. *BMC clinical pathology* 13, 32 (2013).
55. McEvoy, J. et al. Analysis of MDM2 and MDM4 single nucleotide polymorphisms, mRNA splicing and protein expression in retinoblastoma. *PLoS One* 7, e42739 (2012).
56. Zhao, L., Wientjes, M. G. & Au, J. L. Evaluation of combination chemotherapy: integration of nonlinear regression, curve shift, isobologram, and combination index analyses. *Clin Cancer Res* 10, 7994–8004 (2004).

Supplementary materials

Supplementary Table S1: Primer sequences utilised in this study.

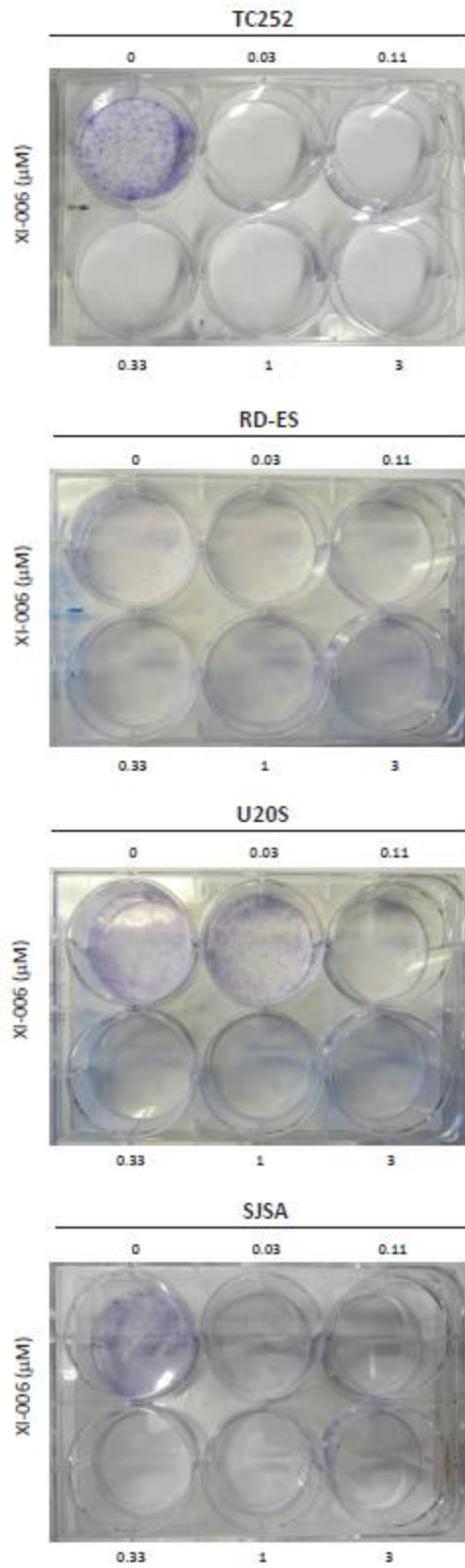
Target	Primer sequence 5' to 3'		Annealing Temperature
	Forward	Reverse	
<i>ATM</i>	TGGTTTGAGAAGCGATTGGC	TTCAACACCCGTAATGCCCA	65°C
<i>ATR</i>	CTGATGCGTGATCAGCGAGA	ACGGCAGTCCTGTCCTCTA	65°C
<i>EDIL3</i>	GAACCAACTTCAGCAGGTCCC	TAAATTCGCCTGGGCACTCA	61°C
<i>FLOT1</i>	ACTGGCATTGCCAGGTAAA	AGGGCAATGTGGCAATCTC	63°C
<i>HEG1</i>	TCCCAGAGTGGCAACTTAGC	ATCTCCGAGGTTCCACT	61°C
<i>IDH1</i>	TTGGCTGCTTGCAATAAAGGTT	GTTTGGCCTGAGCTAGTTTGA	61°C
<i>KIF20A</i>	CTACAAGCACCCAAGGACTCT	AGATGGAGAAGCGAATGTTT	61°C
<i>MDM2</i>	TCTACAGGGACGCCATCGA	CTGATCCAACCAATCACCTGAA	61°C
<i>MDM4</i>	TCTCGCTCTCGCACAGGATCACA	AACCACCAAGGCAGGCCAGCTA	61°C
<i>Mre11</i>	TGCCCAGGAAAATGAAGTGGA	CAGGCCGATCACCCATACAA	61°C
<i>p21 (CDKN1A)</i>	TGGACCTGGAGACTCTCAGGGTCCG	TTAGGGCTTCCTCTTGGAGAAGATC	61°C
<i>PARP-1</i>	AGCGAGAGCATCCCCAAGG	TCAAACATGGGCGACTGCAC	61°C
<i>PPIG</i>	CAGATGCAGCTAGCAAACCGTTTG	CTCTTCAGTAGCACTTTCGGAATCAGAGG	61°C
<i>PUMA (BBC3)</i>	ACGACCTCAACGCACAGTACG	TCCCATGATGAGATTGTACAGGAC	61°C
<i>UTRN</i>	TTGCACTGGCAGGTGAAAGA	ACGTTGACTTGGCTGTAGGG	59°C

Supplementary Table 2: Combination Index (CI) values obtained from XI-006/chemotherapeutic agent synergy studies

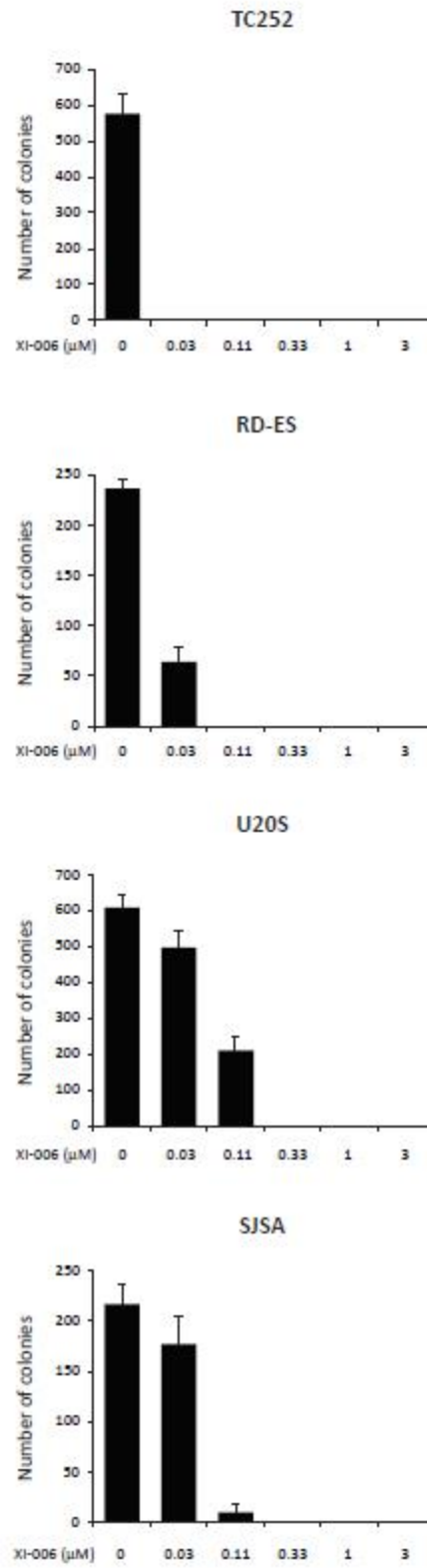
Sarcoma Cell Line	VIN IC ₅₀ (ng/ml)	VIN Dose (ng/ml)	VIN + XI-006 Combination Index	ActD IC ₅₀ (ng/ml)	ActD Dose (ng/ml)	ActD + XI-006 Combination Index	DOX IC ₅₀ (ng/ml)	DOX Dose (ng/ml)	DOX + XI-006 Combination Index	ETO IC ₅₀ (ng/ml)	ETO Dose (ng/ml)	ETO + XI-006 Combination Index
STA-ET-1	3.13 ± 0.70	0.098	1.078	3.80 ± 0.32	0.195	1.029	28.2 ± 1.30	1.17	1.195	592 ± 45.7	31.3	0.936
		0.195	1.112		0.391	0.879		2.34	1.190		62.5	0.861
		0.391	1.144		0.781	0.794		4.69	0.994		125	0.891
		0.781	1.271		1.563	0.800		9.38	1.009		250	0.778
		0.156	1.208		3.125	1.041		18.8	0.889		500	0.913
TC252	2.73 ± 0.00	0.098	0.927	1.74 ± 0.16	0.195	1.209	8.61 ± 0.87	0.59	0.989	285 ± 9.85	7.81	0.961
		0.195	1.026		0.391	1.513		1.17	1.025		15.6	1.078
		0.391	1.076		0.781	1.383		2.34	1.057		31.3	0.961
		0.781	1.157		1.563	1.034		4.69	1.007		62.5	0.961
		1.563	1.200		3.125			125			125	0.875
RD-ES	1.06 ± 0.06	0.049	1.093	8.76 ± 0.05	0.195	1.000	36.7 ± 3.81	2.34	0.997	870 ± 40.1	31.3	1.726
		0.098	1.069		0.390	0.876		4.69	0.904		62.5	1.802
		0.195	1.118		0.781	0.902		9.38	0.980		125	1.486
		0.391	1.182		1.56	1.057		18.8	0.860		250	1.404
		0.781	1.262		3.12	1.171		37.5	1.093		500	1.295
SK-N-MC	0.87 ± 0.04	0.024	1.061	8.72 ± 0.57	0.195	1.142	19.6 ± 1.15	1.17	1.053	559 ± 23.8	15.6	0.985
		0.049	1.091		0.390	0.998		2.34	1.092		31.3	0.976
		0.098	1.103		0.781	0.979		4.69	1.112		62.5	0.932
		0.195	1.172		1.56	0.950		9.38	1.063		125	0.835
		0.391	1.235		3.12	1.034		18.8	1.060		250	0.753
WE-68	2.31 ± 0.02	0.049	1.063	1.72 ± 0.02	0.049	0.899	23.7 ± 0.27	0.59	1.050	1000 ± 115	31.3	1.066
		0.098	1.084		0.098	0.969		1.17	0.864		62.5	1.051
		0.195	1.151		0.195	1.026		2.34	0.972		125	1.048
		0.391	1.076		0.391	1.161		4.69	0.976		250	1.035
		0.781	1.333		0.781	0.945		9.38	0.898		500	1.007
		1.563	1.063	1.563	1.512	18.8	0.965	1000	1.624			

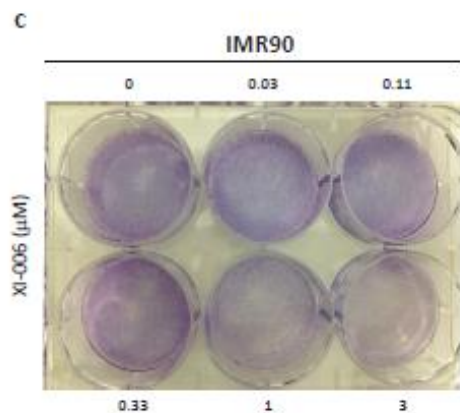
VIN: Vincristine, ActD: Actinomycin D, DOX: Doxorubicin, ETO: Etoposide. CI value of <1, =1 and >1 indicates synergistic, additive and antagonistic effects respectively. CI numbers in bold denote synergism.

a



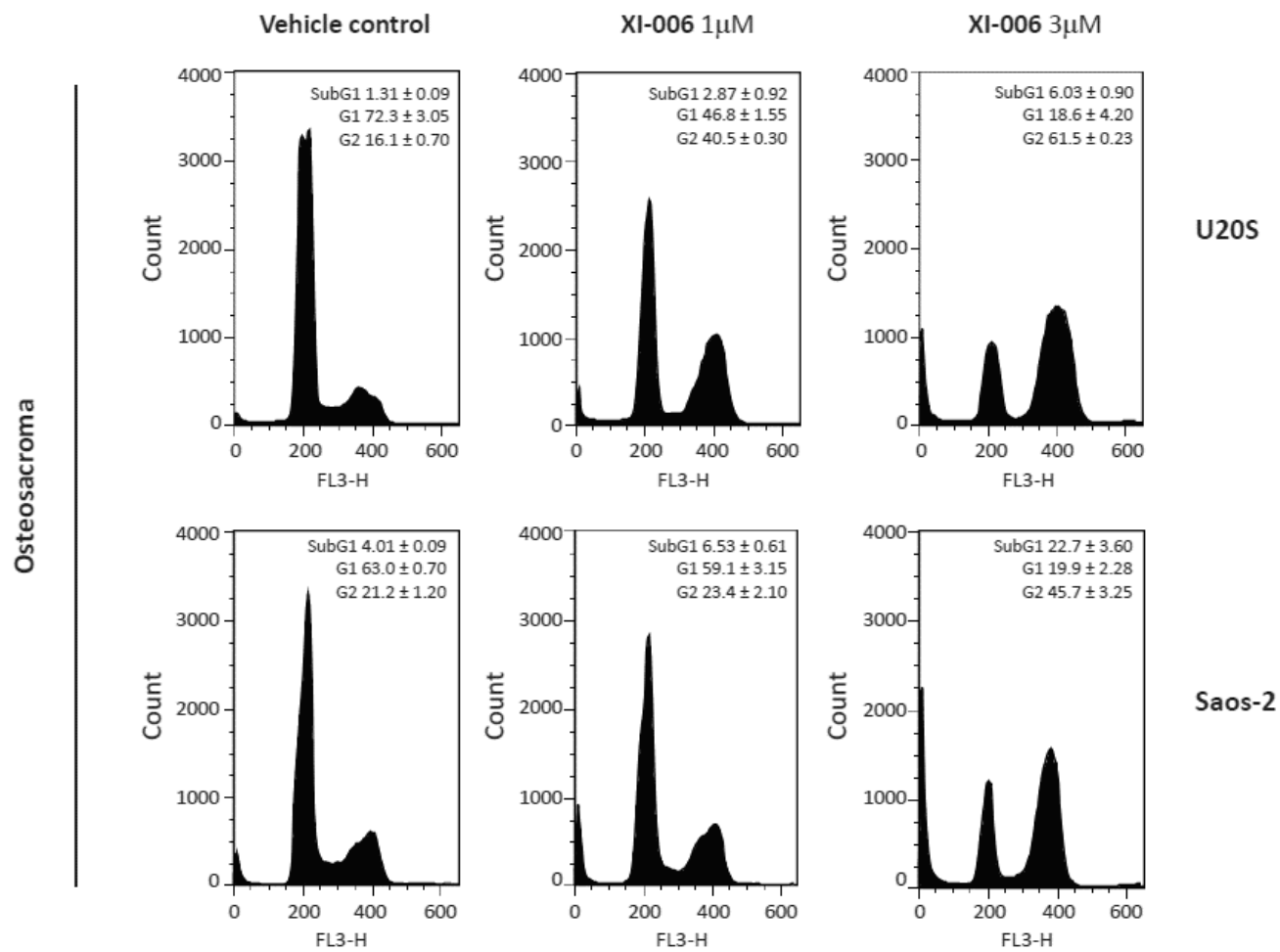
b

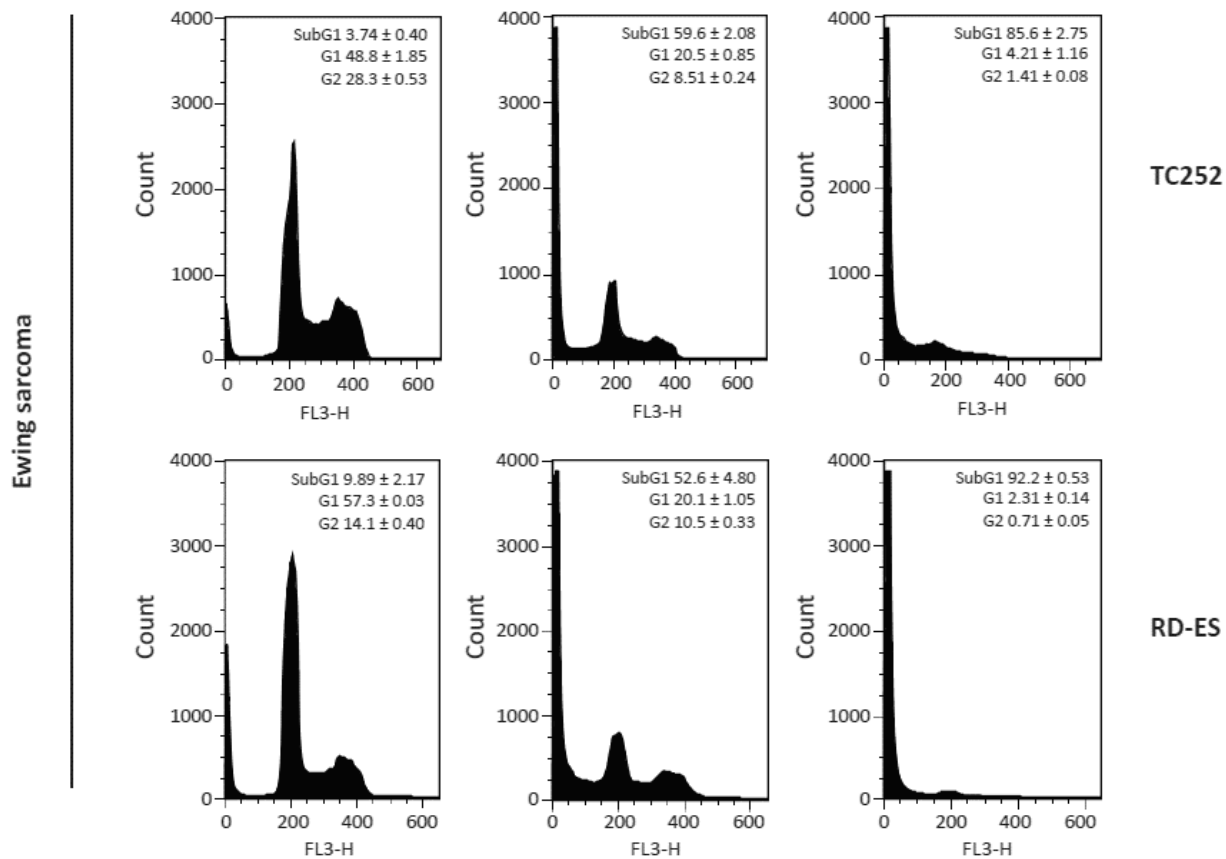




Supplementary Figure 1: XI-006 reduces cellular proliferation specifically in cancer cell lines (a) Ewing (TC252, RD-ES) and osteosarcoma (U2OS and SJSA) cell lines were seeded (3×10^3 cells/well) in 6-well plates in the presence or absence of XI-006 (0.03, 0.11, 0.33, 1, $3 \mu\text{M}$). Cells were fixed in methanol (5mins) and stained with giemsa (Sigma) (50 mins) 10 days post seeding. (b) Quantification of colonies from cells treated as in (a). Data represents mean \pm STDEV from two independent experiments. (c) Representative image of IMR90 cells (normal human fibroblasts) treated as in (a).

Supplementary Figure 2

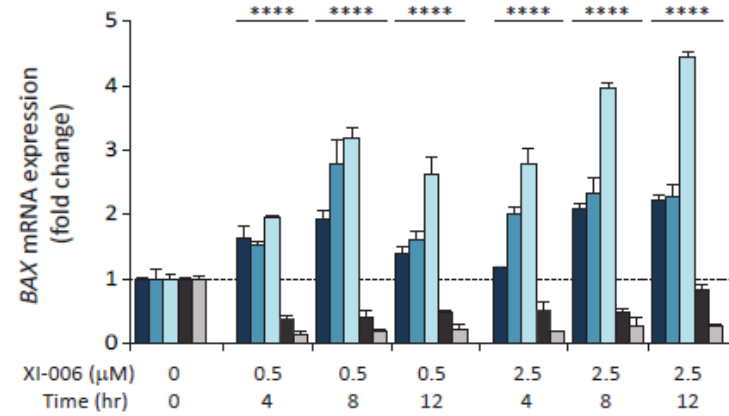
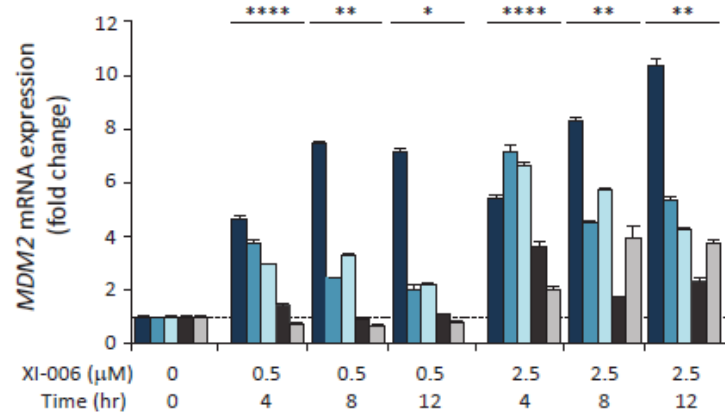
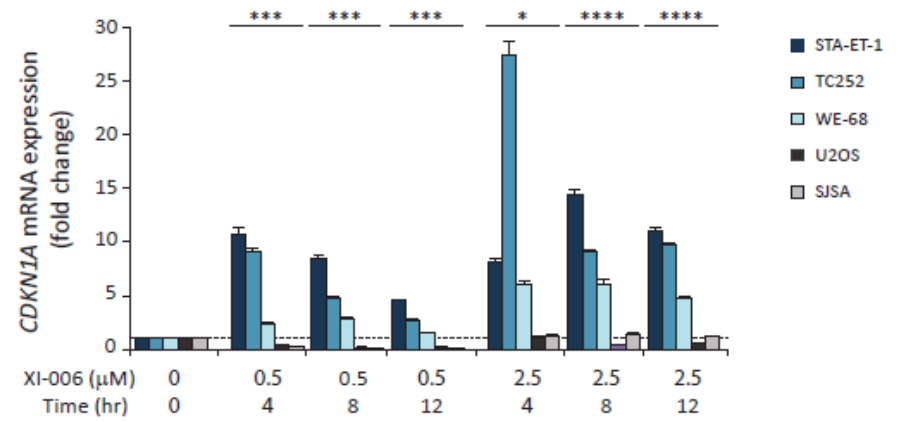
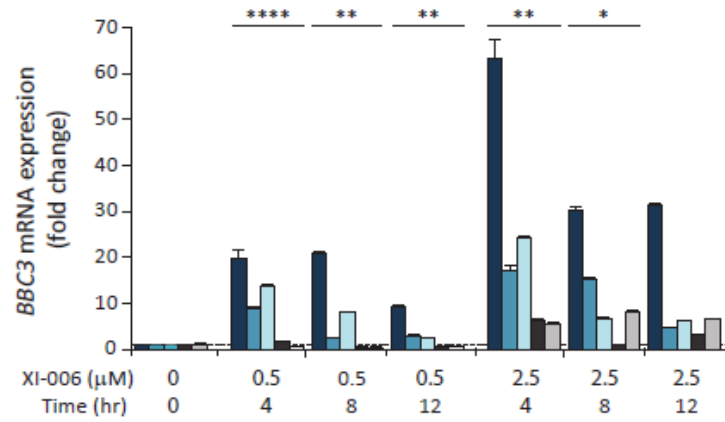


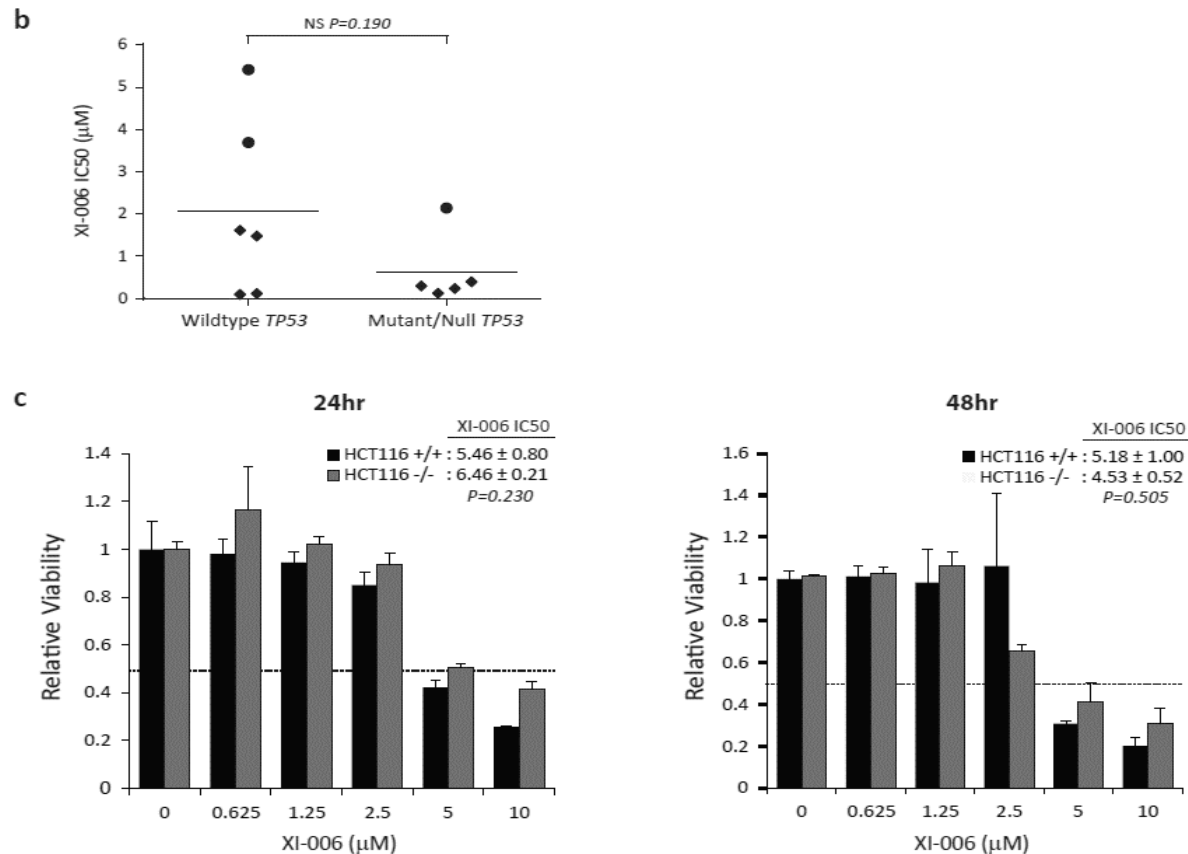


Supplementary Figure 2. XI-006 induces apoptosis specifically in Ewing sarcoma cells. Ewing (TC252, RD-ES) and osteosarcoma (U2OS, Soas-2) cells were treated with XI-006 (1 μ M, 3 μ M) or vehicle control for 48hrs. Cells were fixed, stained with propidium iodide, and analyzed by flow cytometry for DNA content. Numbers inserted in graphs indicate percentage of cells at different stages of the cell cycle (mean \pm STDEV from two independent experiments). 60,000 PI stained cells were analysed for DNA content.

Supplementary Figure 3

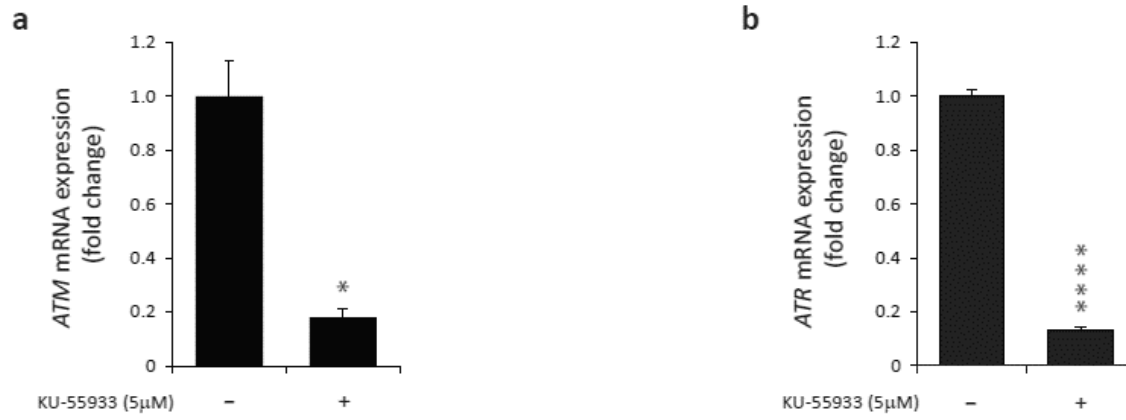
a



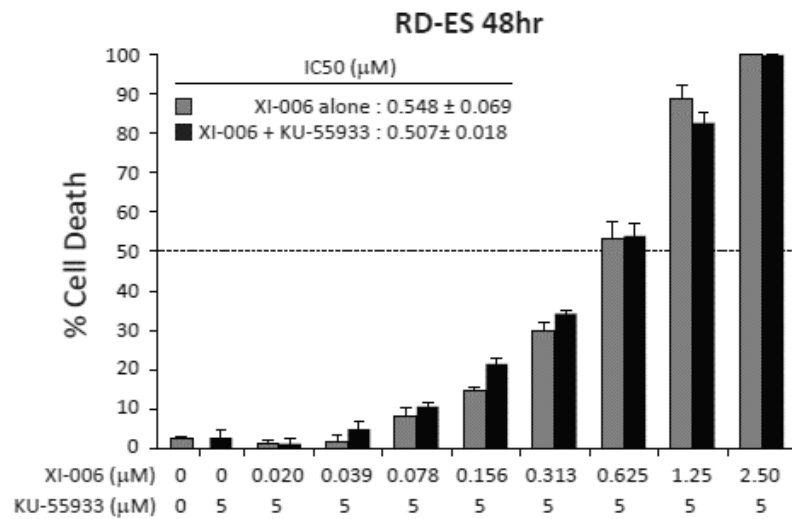
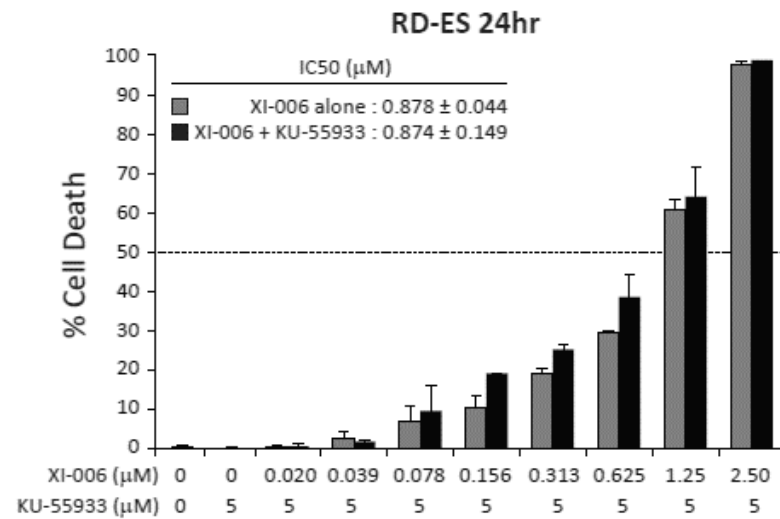
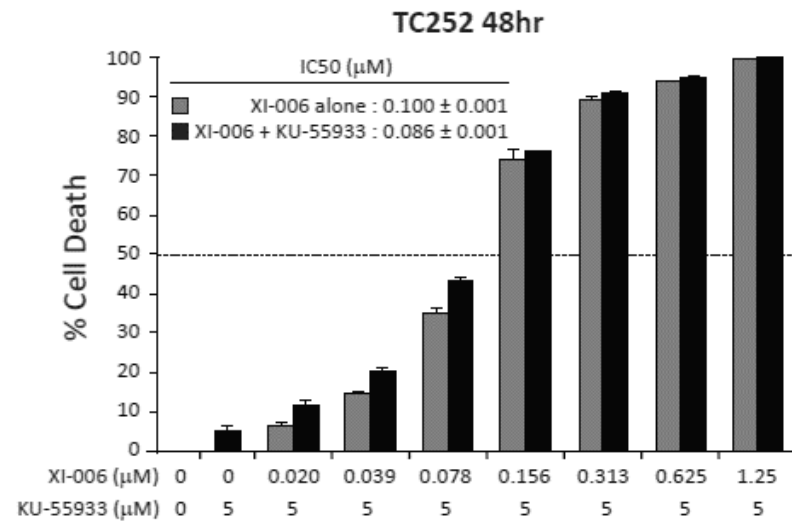
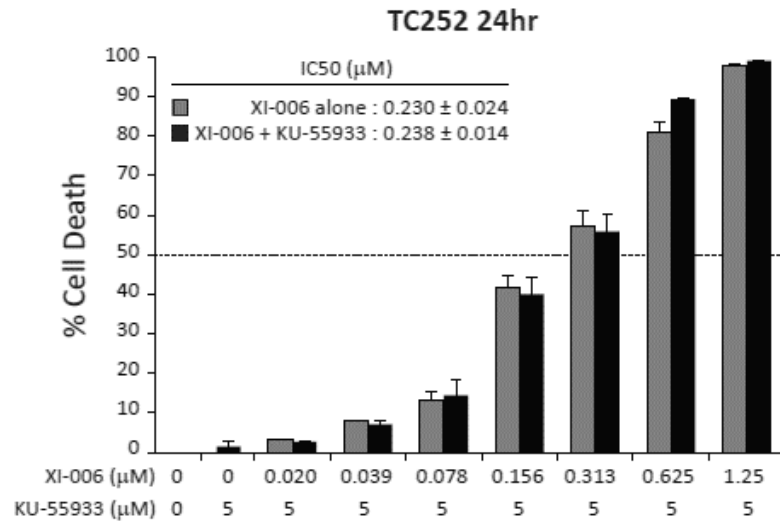


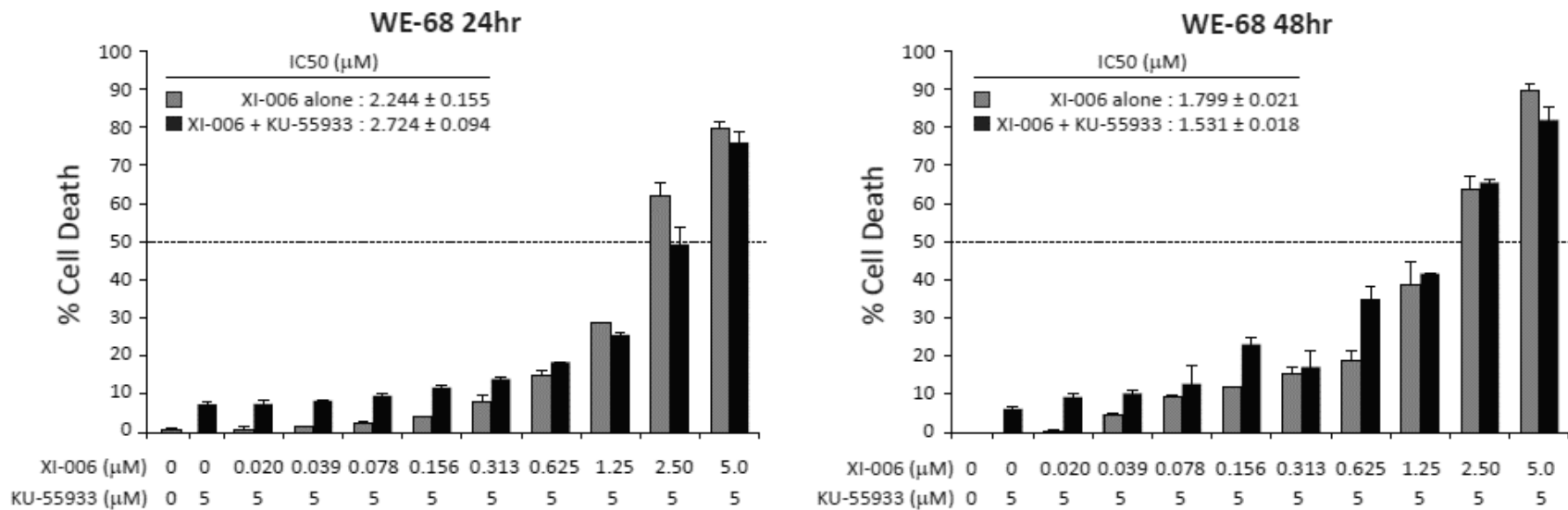
Supplementary Figure 3: XI-006 induces expression of p3 target genes specifically in Ewing sarcoma cell lines (a) Wild-type Ewing (STA-ET-1, TC252, WE -68) and osteosarcoma (U20S, SJSA) cell lines were treated with XI-006 (0, 2.5 and 5 μM) for the indicated times. mRNA expression levels of TP53 target genes (BBC3, CDKN1A, MDM2, BAX) was determined through real-time (qPCR) analysis. Data represents mean expression (fold change) \pm SE from triplicate reactions. Asterisk denotes statistical significance in target gene expression (Ewing versus osteosarcoma cell lines) (* $P < 0.05$, ** $P < 0.01$, *** $P < 0.001$, **** $P < 0.0001$). (b) Lack of correlation between XI-006 apoptotic 48hr IC50 values and TP53 status (wild-type versus mutant/null). \blacklozenge Denotes Ewing sarcoma and osteosarcoma cell lines respectively. (c) Relative viability of TP53 wild-type (+/+) and null (-/-) HCT116 isogenic cell lines following treatment with XI-006 for 24 and 48hrs. Data represents mean \pm STDEV from duplicate reactions. Viability determined through Cell Titer-Glo assays.

Supplementary Figure 4:

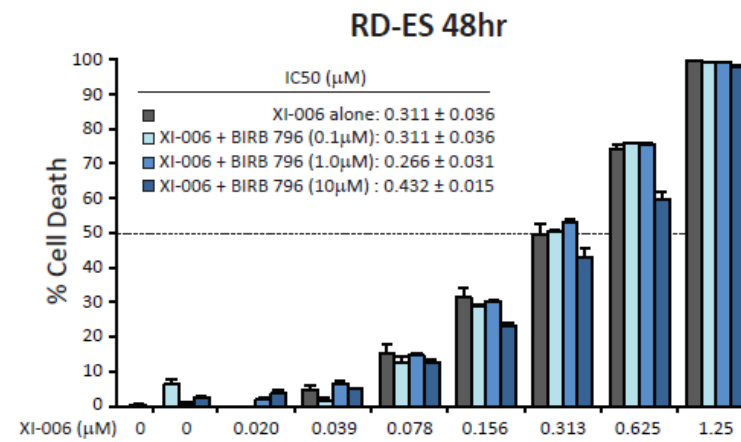
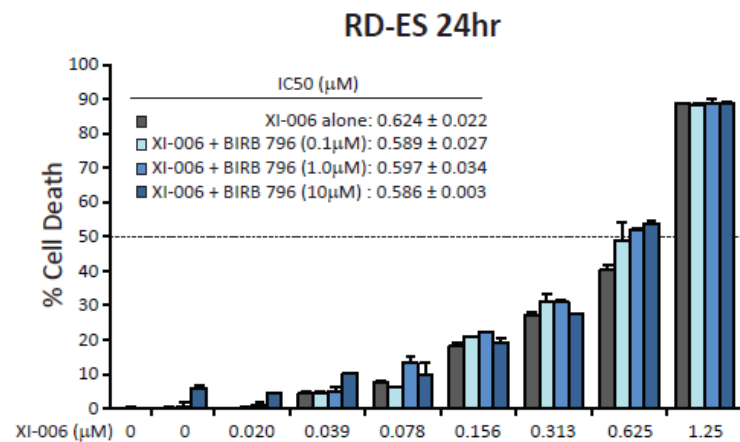
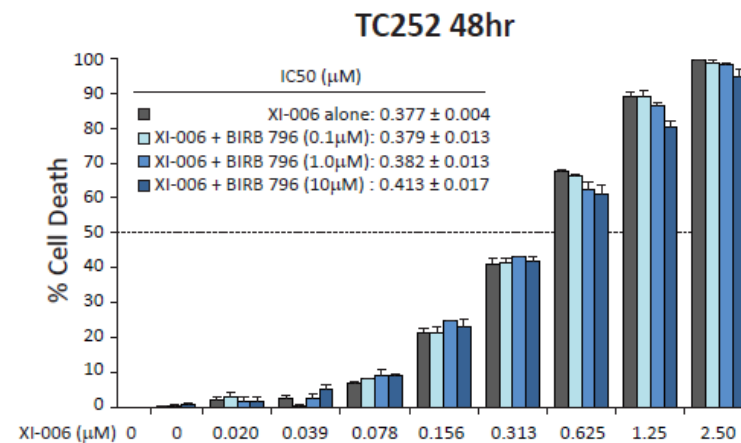
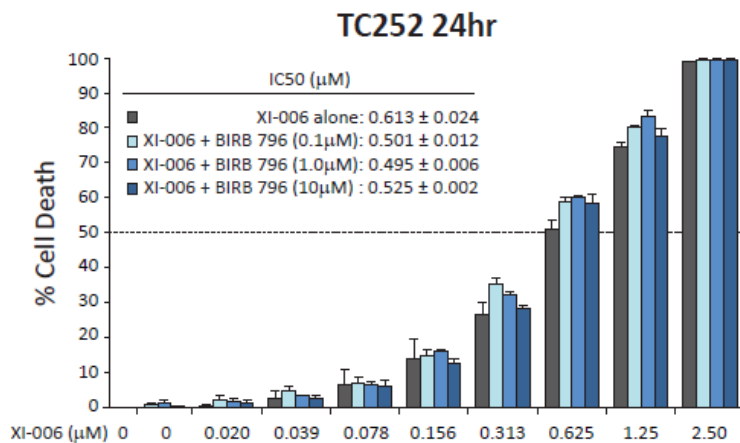


C



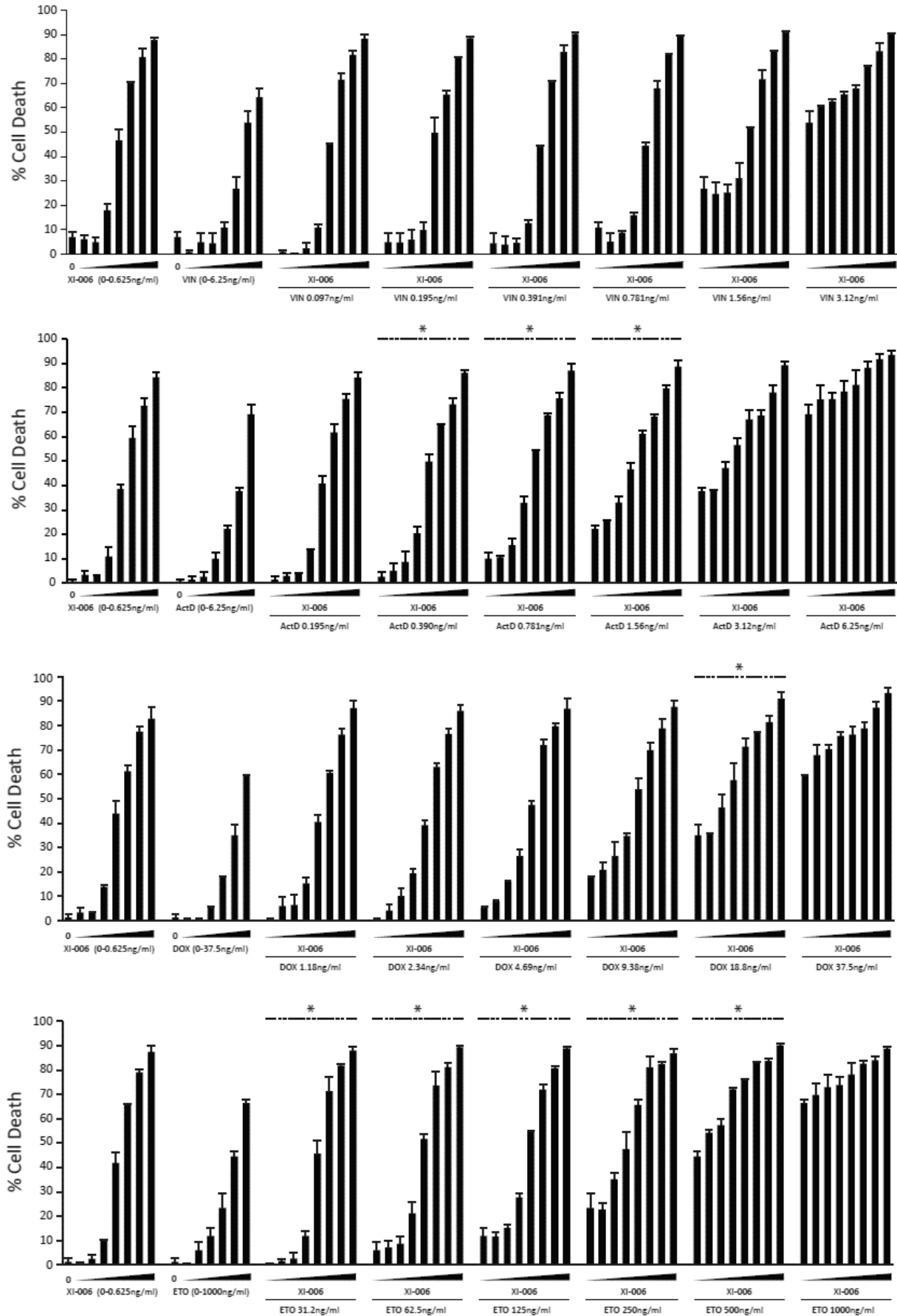


Supplementary Figure 4: Inhibition of ATM does not suppress XI-006 cytotoxicity. Real-time qPCR analysis of (a) ATM and (b) ATR mRNA expression following treatment with the ATM inhibitor KU-55933 (5 μM) for 6hrs. Data represents mean expression (fold change) \pm SE from triplicate reactions. Asterisk denotes statistically difference compared to vehicle control treated cells (* $P < 0.05$, **** $P < 0.0001$). (c) TC252, RDES and WE-68 were pretreated with KU-55933 (5 μM) or vehicle control (DMSO) for 2hrs, prior to the addition of XI-006 (0-5 μM). Cell viability was determined through 7AAD staining (24 and 48hrs post XI-006 treatment) and analysed by flow cytometry. Data represents average percentage cell death \pm STDEV from duplicate reactions.

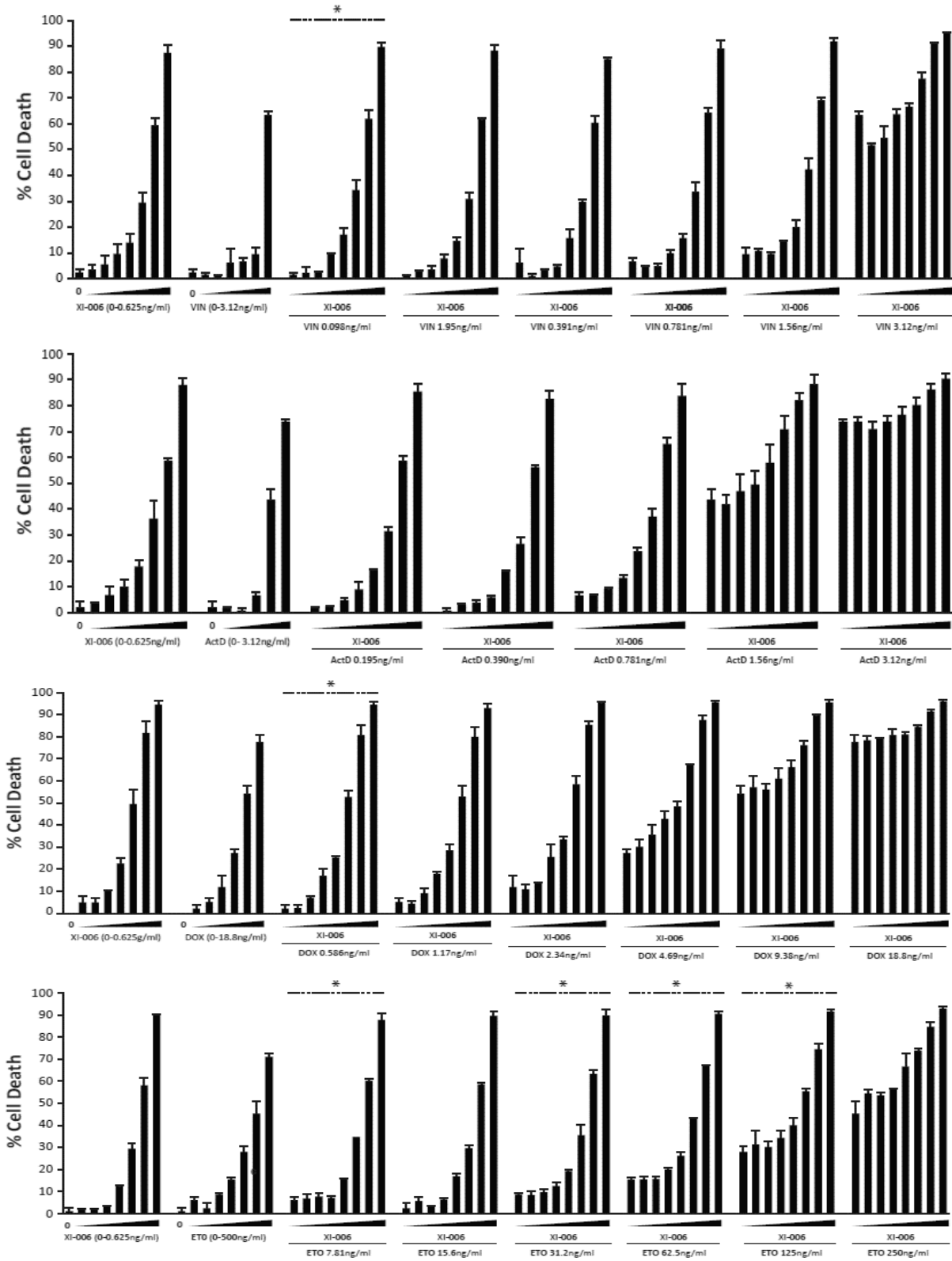


Supplementary Figure 5: Inhibition of p38 MAPKs has no effect on XI -006 sensitivity. TC252 and RD-ES cells were pre-treated with BIRB 796 (0.1 μM, 1 μM and 10 μM) or vehicle control (DMSO) for 2hrs, prior to the addition of XI-006 (0-2.5 μM). Percentage cell death was determined through 7AAD staining (24 and 48hrs post XI-006 treatment) and analysed by flow cytometry. Data represents average percentage cell death ± STDEV from duplicate reactions.

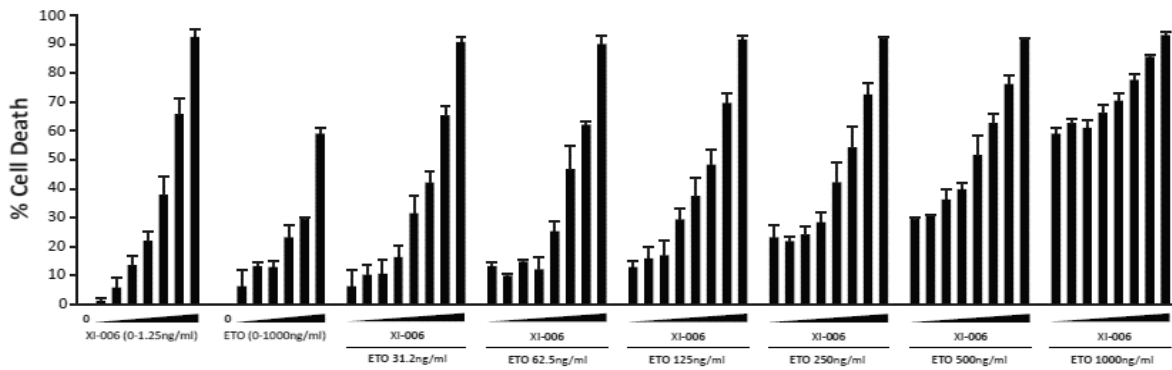
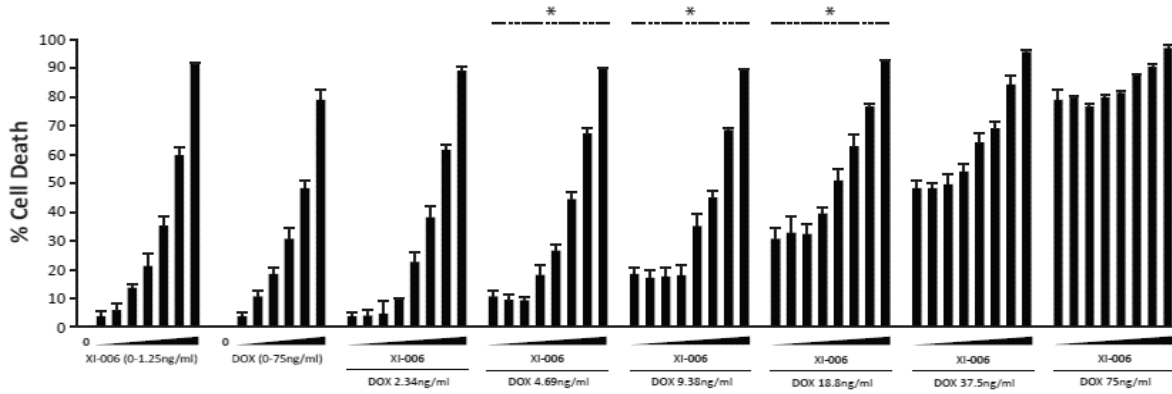
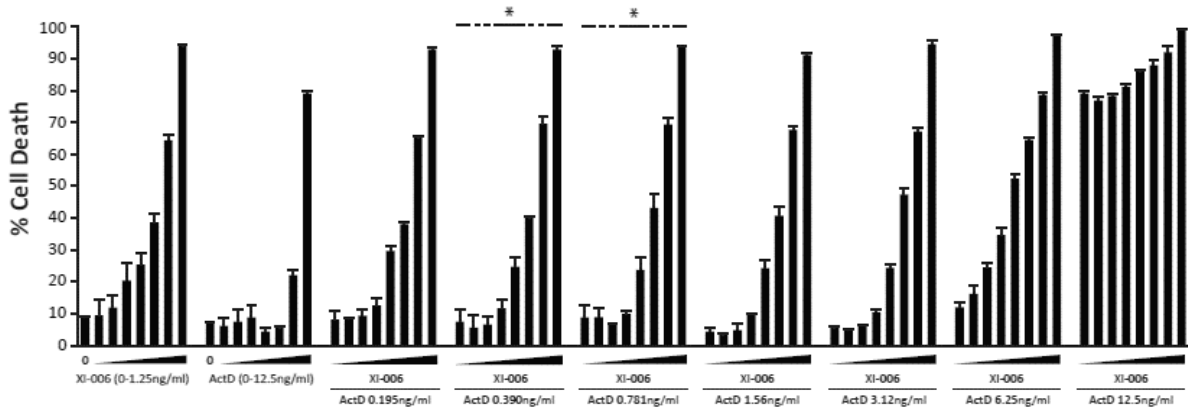
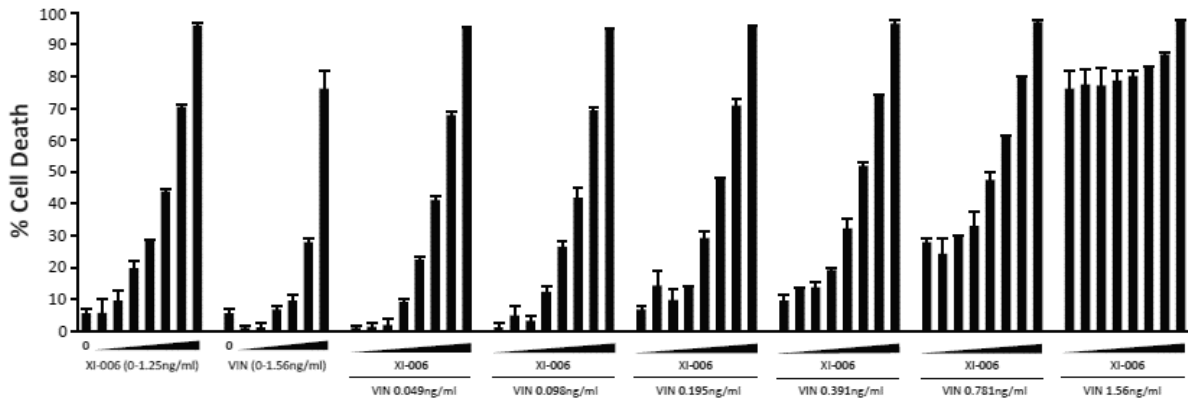
STA-ET-1



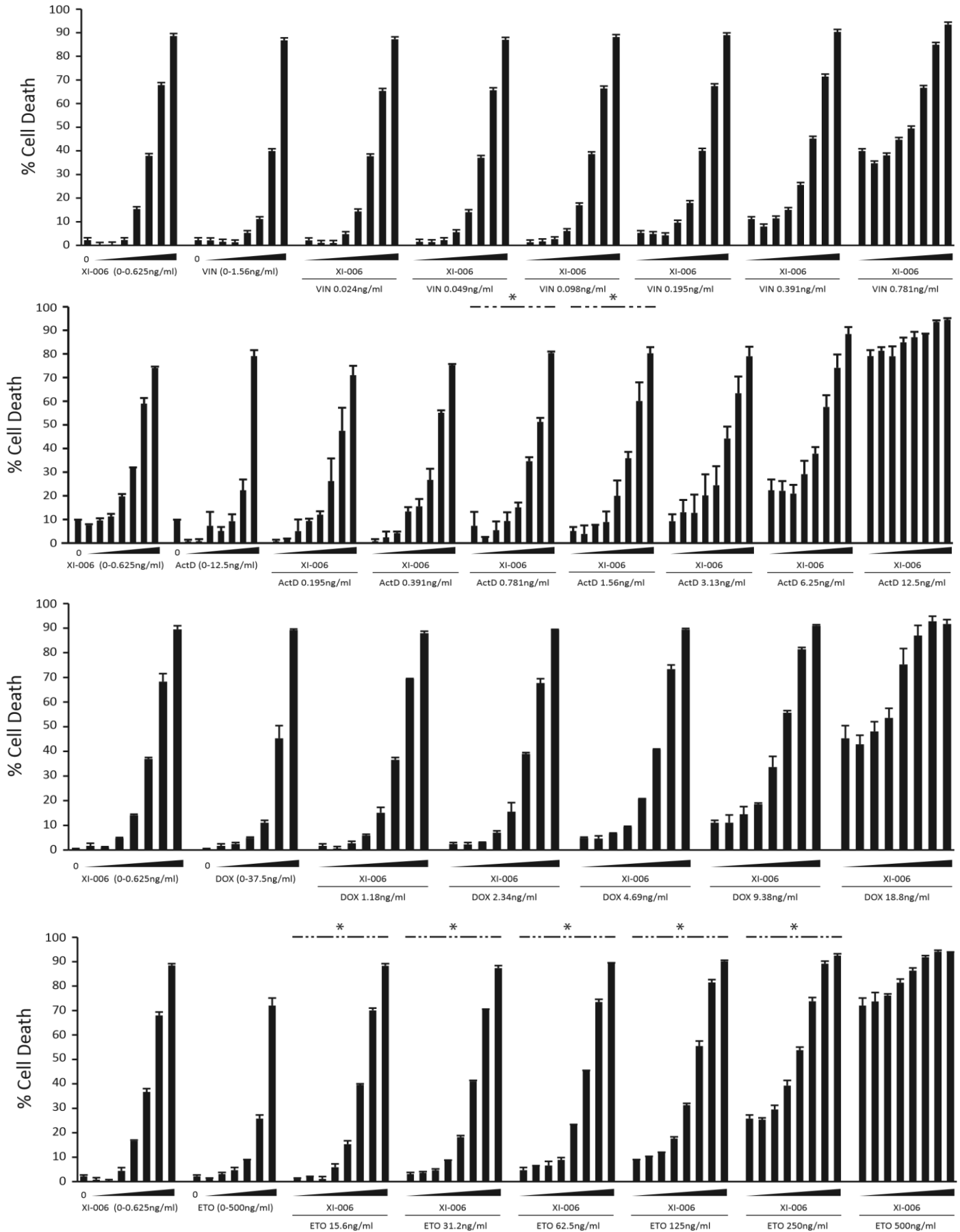
TC252



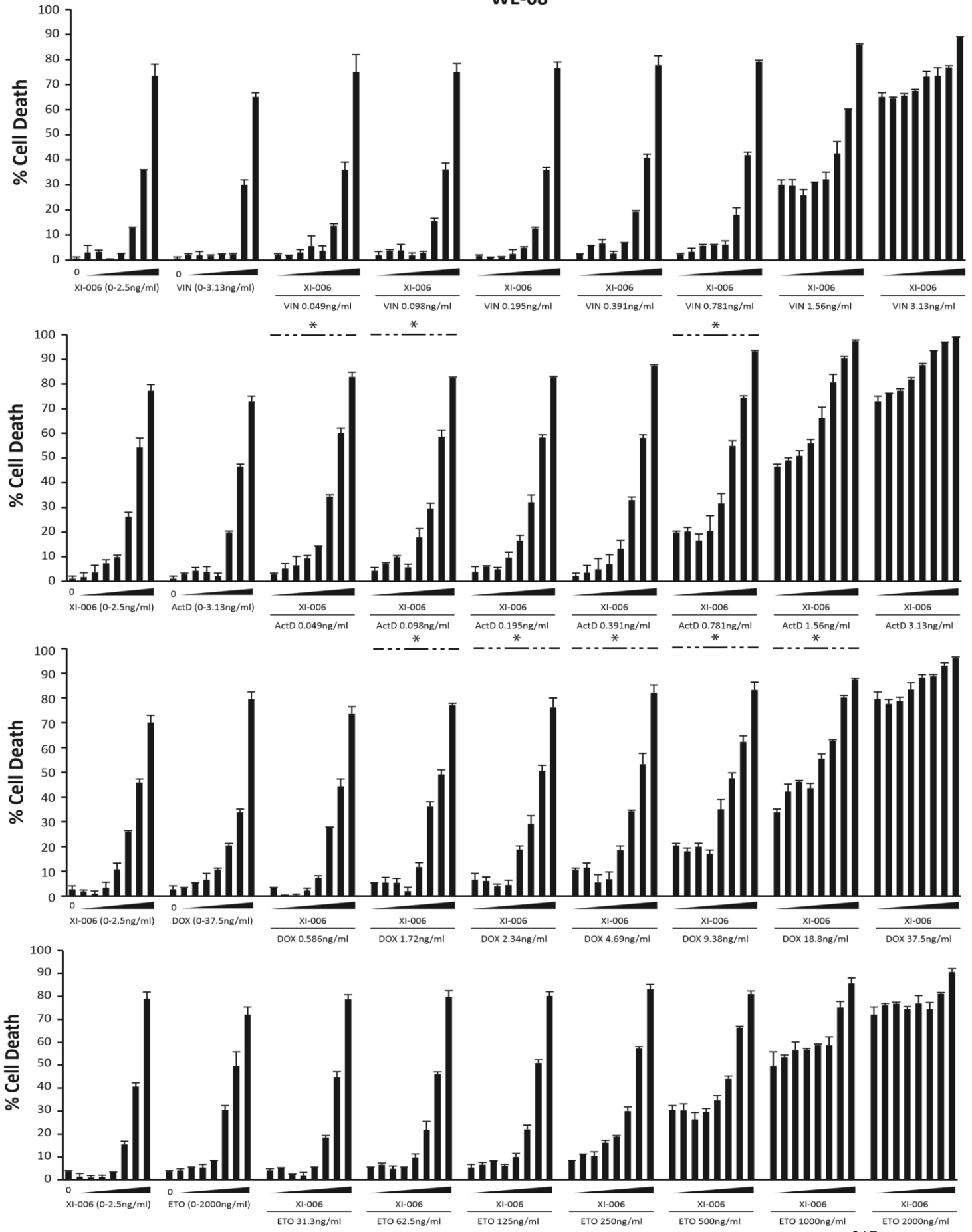
RD-ES



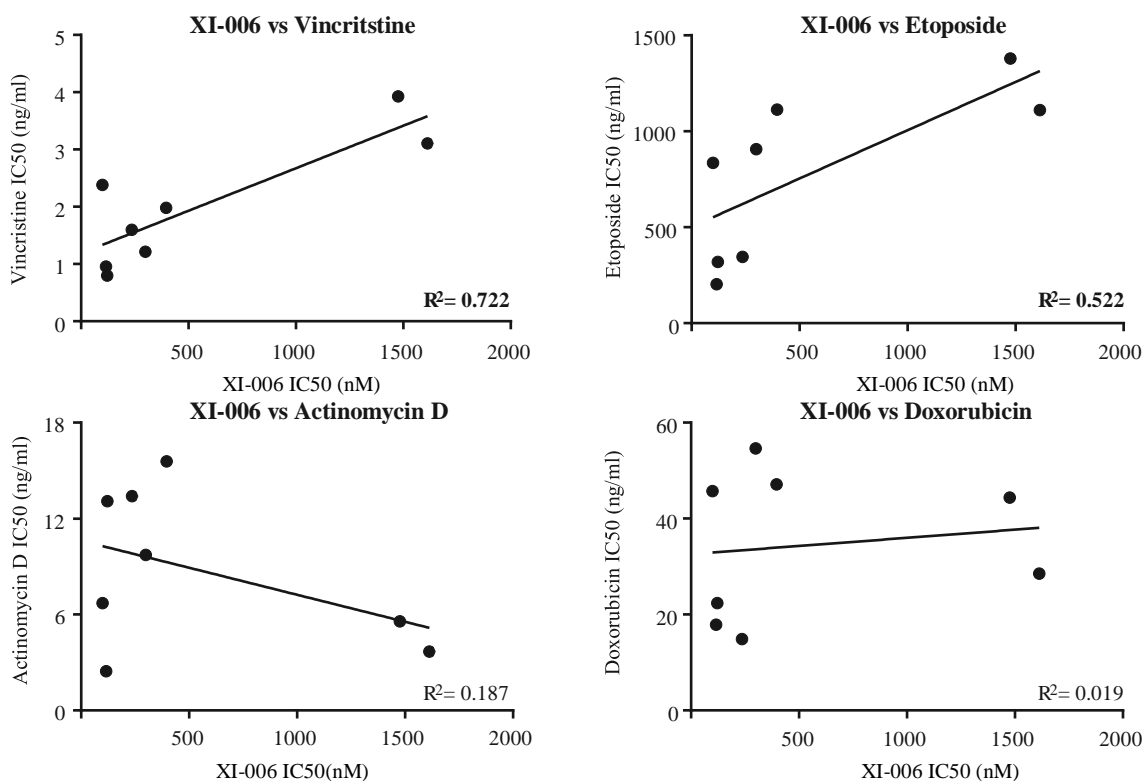
SK-N-MC



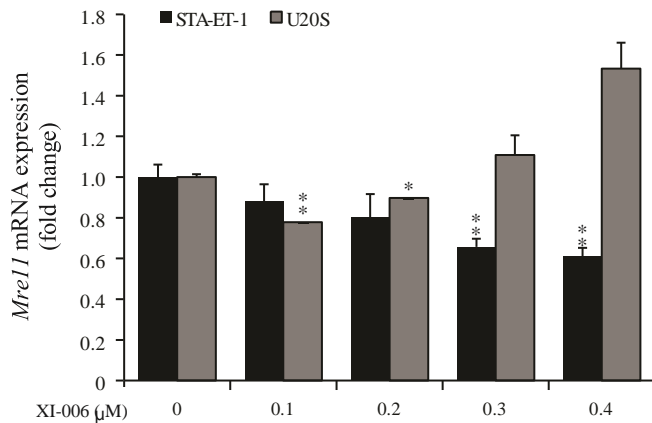
WE-68



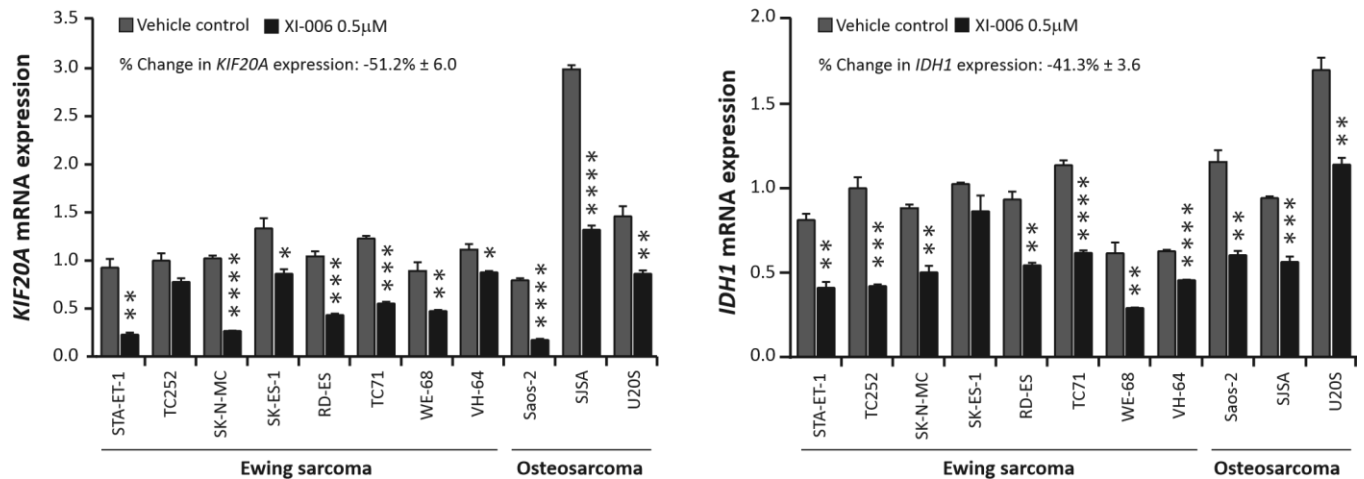
Supplementary Figure. 6: XI-006 synergises with etoposide, doxorubicin, and actinomycin D but not vincristine STA-ET-1, TC252, RD-ES, SK-N-MC and WE-68 cells were treated with the chemotherapeutic agents vincristine (VIN), actinomycin D (ActD), doxorubicin (DOX) and Etoposide (ETO) alone or in the presence of XI-006 (indicated concentrations) for 48hrs. Cell viability was determined through 7AAD staining and analysed by flow cytometry. Data represents average percentage cell death \pm STDEV from duplicate reactions. Asterisk denotes a Combination Index (CI) of <1 , indicating synergy.



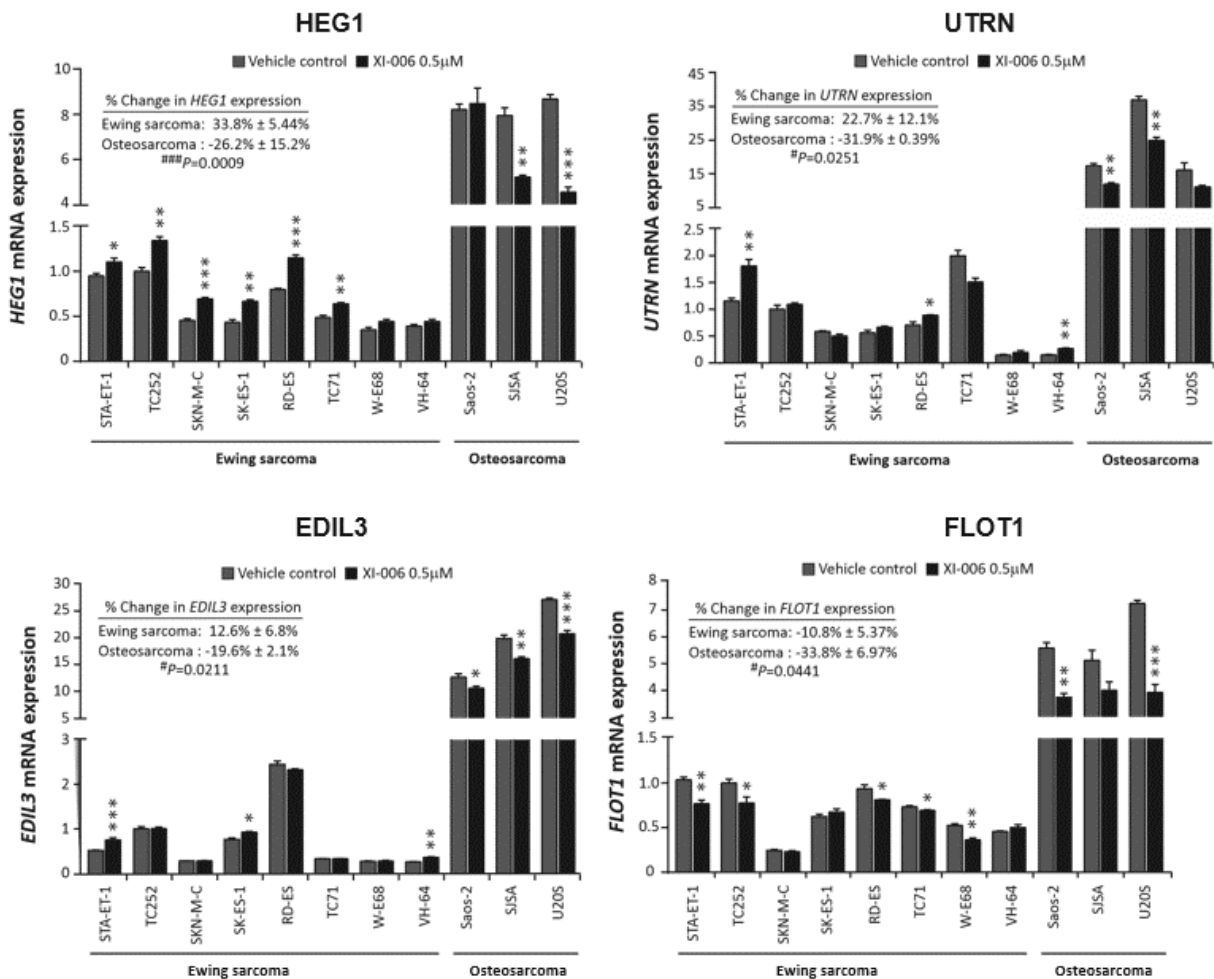
Supplementary Figure 7: XI-006 sensitivity correlates with vincristine sensitivity in Ewing sarcoma cell lines. Correlation between XI-006 IC50 values and chemotherapeutic (vincristine, actinomycin D, doxorubicin, etoposide) IC50 values. All Ewing sarcoma cell lines (n=8) were treated with chemotherapeutic agents or XI-006 for 48hrs. Cell viability was determined through 7AAD staining and analysed by flow cytometry. Data represents mean apoptotic IC50 values (duplicate wells).



Supplementary Figure 8: Lowmicro-molar doses of XI-006 reduces Mre11 mRNA expression. Mre11 mRNA expression levels were determined through real-time qPCR analysis from STA-ET-1 and U20S cells treated with XI-006 (0.1, 0.2, 0.3 and 0.4μM) or vehicle control for 6hrs. Data represents mean expression (fold change) ± SE from triplicate reactions. Asterisk denotes statistical significant reduction in expression compared to vehicle control (*P<0.05, **P<0.01)



Supplementary Figure 9: KIF20A and IDH1 are repressed following XI-006 treatment. Real-time qPCR analysis of KIF20A and IDH1 expression levels following 4hr XI-006 (0.5μM) or vehicle control treatment. Data represents mean ± SE from triplicate reactions. Asterisk denotes statistical significance compared to vehicle control (*P<0.05, **P<0.01, ***P<0.001, ****P<0.0001).



Supplementary Figure 10: *EDIL3*, *UTRN*, *HEG1* and *FLOT1* expression levels following XI-006 treatment. Real-time qPCR analysis of *EDIL3*, *UTRN*, *HEG1* and *FLOT1* expression levels following 4hr XI-006 treatment (0.5µM). Data represents mean ± SE from triplicate reactions. (*) denotes statistical significance in expression compared to vehicle control (*P<0.05, **P<0.01, ***P<0.001). (#) denotes significant difference in % change in expression, Ewing sarcoma cell lines versus osteosarcoma cell lines (# P<0.05, ###P<0.001)

Conclusion

Over the past decade, deeper understanding of molecular mechanisms underlying cancer progression have led to development of new compounds that target specific pathways involved in tumorigenesis. Incorporation of these targeted therapies alongside chemotherapies has drastically improved patient survival in many cancers. However, for basal-like (triple-negative) breast cancers and metastatic sarcomas, the survival rates are less than 30%. Although research continues to reveal critical targetable pathways, there are currently no targeted treatments available for these cancers. This research is intended to highlight the potential for exploiting two relatively unexplored molecular targets, ribosomal RNA Polymerase I and the proteasome, for the treatment of Ewing sarcoma and breast carcinomas, respectively. These findings will provide the basis for future clinical studies and have the potential to provide new therapies for patients.

Basal-like (triple negative) breast cancers accounts for 15-20% of all breast cancers and have the poorest survival amongst breast cancer subgroups. The current lack of targeted therapy for this subgroup stems from the fact that there are no recognized targets. Here, we have investigated whether the proteasome has utility as a therapeutic target in the treatment of breast cancers. Although breast cancers patients did not respond to bortezomib in the limited early clinical trials, these studies did not assess proteasome levels/activity. Detailed characterization of the proteasome in breast cancers utilizing the TCGA RNA sequencing data from breast cancer patients revealed that the basal-like and HER2⁺ breast cancer subgroups have high expression of the immuno-proteasome variant. This was surprising as immuno-

proteasome expression is classically associated with cells of the immune lineage. As multiple myeloma cells that express high levels of immuno-proteasome are extremely sensitive to proteasome inhibitor based therapy, we hypothesized that breast cancer cell lines with high levels of immuno-proteasome will likely respond to bortezomib. Indeed, cytotoxic sensitivity of breast cancer cell lines to the proteasome inhibitor bortezomib was significantly correlated with immuno-proteasome expression. A limited number of studies have shown immuno-proteasome overexpression in solid cancer tissues, but to the best of our knowledge this is the first report that characterizes proteasome expression and evaluates proteasome inhibitory effects in the breast cancer subgroups in detail. In addition, we provide an overarching hypothesis that encapsulates cross-talk between immuno-proteasomes, immune surveillance and superior prognosis in breast cancer patients. Overall, our results provide convincing preliminary evidence for the utility of immuno-proteasomes both as a prognostic and predictive biomarker for proteasome inhibitor based therapy for the targeted treatment of basal-like and HER2⁺ breast cancers.

The limited use of proteasome inhibitors for the treatment of cancers has been attributed to their dose-limiting toxicities and instability. Since the late 1990s, bortezomib has been assessed in several clinical trials in various solid cancers both as monotherapy and in combination with chemotherapies. Unfortunately, almost invariably patients did not respond and further research into proteasome inhibitor drug-development and assessment in solid cancer treatment was abandoned. Instead, the major focus for drug-design veered into developing second-generation proteasome inhibitors that have superior potency and less toxicity

specifically for multiple myeloma treatment. However, like bortezomib, these second generation proteasome inhibitors share similar structural characteristics and were marred by dose-limiting toxicities and drug delivery issues. Here, we have conceptualized and developed second-generation proteasome inhibitors by modifying peptide backbones using non-natural peptides and by attaching photo-switches for specific activation. Overall, *in vitro* analyses of some of these new compounds revealed significantly less toxicities and better efficacies compared to benchmark drugs.

In second part of the thesis we investigated the utility of activating p53 signaling using two different approaches for the treatment of Ewing sarcoma. Overall survival for patients with metastatic Ewing sarcoma is less than 30% with multi-agent chemotherapy. Activation of the p53 pathway has been a primary focus for Ewing sarcoma treatment as approximately 90% of Ewing sarcomas retain a functional wild-type p53. CX-5461 is a novel non-genotoxic RNA polymerase I inhibitor that has demonstrated its anti-proliferative effects in a vast panel of hematological and solid tumour cell lines. Encouraging results from initial *in vitro* and *in vivo* evaluations demonstrated hematological cell lines with wild-type p53 to be acutely sensitive to CX-5461, which led to Phase I/II clinical evaluations of CX-5461 in advanced hematological malignancies. Here, we show that Ewing sarcoma is by far the most responsive solid tumour to CX-5461 that has been tested to date. In particular, two of the Ewing sarcoma cell lines show sensitivities lower than any ever reported in the literature for solid tumours and parallel some of the most potent responses observed in blood cancers. While some Ewing sarcoma cell lines were inherently resistant to CX-5461, in the sensitive subgroup, the anti-tumorigenic response

was p53 dependent. In our second approach to exploit p53 signaling for Ewing sarcoma treatment, we found that while XI-006 caused rapid apoptosis in cancer cell lines, its effect was independent of p53 activation. However, in addition to being non-genotoxic, both CX-5461 and XI-006 were synergistic in combinations with chemotherapies, highlighting tremendous therapeutic potential that warrants further pre-clinical studies.

There are currently 77 FDA approved anti-cancer targeted therapies and few hundred more in clinical trials. However, these targeted therapies are effective only in limited number of cancers, and within those cancers for only a proportion of patients. It is now becoming increasingly clear that cancer is a highly heterogeneous disease and that moving forward it is crucial to identify those patients who will respond to these targeted therapies. In this regard, this research provides excellent leads and highlights how immuno-proteasome expression can serve as a biomarker for stratifying patients who will respond to proteasome inhibitor based therapy in breast cancer and perhaps, in other solid cancers.
